

LONG TERM DEFLECTIONS OF REINFORCED
CONCRETE BEAMS

LONG TERM DEFLECTIONS OF REINFORCED
CONCRETE BEAMS

by

JEFFREY DOUGLAS WALKER, B.Eng.

A Thesis

Submitted to the School of Graduate Studies
in Partial Fulfilment of the Requirements
for the Degree
Master of Engineering

McMaster University

April, 1987

MASTER OF ENGINEERING (1987)

McMASTER UNIVERSITY

(Civil Engineering)

Hamilton, Ontario

TITLE: Long Term Deflections of Reinforced Concrete Beams

AUTHOR: JEFFREY DOUGLAS WALKER, B.Eng. (McMaster University)

SUPERVISOR: Dr. R. G. Drysdale

NUMBER OF PAGES: xii 284

Abstract

A study of long term deflections in reinforced concrete beams is presented in this thesis. Two simply supported beams and four continuous beams were tested under sustained loads for periods of about 1 1/2 years. When the deflections were compiled it was observed that all beams had long term to short term deflection ratios that exceeded ACI and CAN3-A23.3 Code limits.

A finite element program was developed to model concrete behaviour for short term and long term loading. When compared with experimental data, the model predictions were almost always within the normal variability limits for deflections.

A parametric study using the Factorial Design Method was undertaken to develop an accurate long term deflection prediction method using deflections generated by the finite element model. The ACI and CAN3-A23.3 Code approach of using a long term to short term deflection ratio was adopted in this study. The resulting relationship had mixed results which raises questions about the advisability of using the deflection ratio approach for predicting long term deflections.

Acknowledgements

I would like to thank my supervisor, Dr. R. G. Drysdale, for his assistance and guidance throughout the course of this thesis.

I am also indebted to Dr. F. A. Mirza for his assistance with the finite element modelling and for the use of his creep program, and to Mr. Ugur Polat for his help in the development of the parametric study.

Finally, I would like to express my appreciation to the Canada Mortgage and Housing Corporation, McMaster University, and the Natural Science and Engineering Research Council for their financial support.

TABLE OF CONTENTS

	PAGE
ABSTRACT	iii
ACKNOWLEDGEMENTS	iv
TABLE OF CONTENTS	v
LIST OF FIGURES	vii
CHAPTER 1 INTRODUCTION	
1.1 Introduction	1
1.2 Objectives	3
1.3 Literature Review	3
1.4 Thesis Outline	13
CHAPTER 2 EXPERIMENTAL PROGRAM	
2.1 Introduction	14
2.2 Design of Experiment	15
2.2.1 Concrete Mix Design	15
2.2.2 Batching and Curing	16
2.3 Concrete Properties	17
2.3.1 Compressive Strength	17
2.3.2 Stress-strain Relationship	18
2.3.3 Shrinkage	20
2.3.4 Creep	20
2.4 Beam Tests	25
2.4.1 Description of Test Beams	25
2.4.2 Beam Test Setup	25
2.4.3 Applied Loads	33
2.4.4 Summary	45
CHAPTER 3 FINITE ELEMENT MODEL	
3.1 Constitutive Relationships	47
3.1.1 Strength and Elastic Relationships	47
3.1.2 Shrinkage	54
3.1.3 Creep	60
3.1.4 Creep Under Variable Stresses	67
3.1.5 Bond Stress and Bond Slip	76

	<u>PAGE</u>
3.2 Finite Element Modelling	85
3.2.1 Literature Review	85
3.2.2 Concrete Elements	94
3.2.3 Cracked Concrete Elements	99
3.2.4 Steel Elements	103
3.2.5 Bond Elements	106
3.2.6 Creep and Shrinkage Formulation	110
3.3 Sensitivity	115
3.3.1 Higher Stress Case	117
3.3.2 Lower Stress Case	130
3.4 Evaluation of Model for Short Term Loads	147
3.5 Evaluation of Model for Long Term Loads	180
CHAPTER 4 PARAMETRIC STUDY	
4.1 Introduction	215
4.2 Design of Experiment	216
4.3 Test Conditions	220
4.4 Results	226
4.5 Summary	246
CHAPTER 5 CONCLUSIONS	
5.1 General	248
5.2 Experimental Work	248
5.3 Finite Element Model	250
5.4 Parametric Study	251
5.5 Recommendations for Future Research	252
BIBLIOGRAPHY	254
APPENDIX A Computer Program Listing	259

LIST OF FIGURES

FIGURE	TITLES	<u>PAGE</u>
2.1	CONCRETE SHRINKAGE MEASUREMENTS	21
2.2	CONCRETE CREEP EQUIPMENT	23
2.3	CONCRETE CREEP MEASUREMENTS	24
2.4	BEAM A DETAILS	26
2.5	BEAM B DETAILS	27
2.6	BEAM C, E DETAILS	28
2.7	BEAM D, F DETAILS	29
2.8	BEAM TEST SETUP	30
2.9	INITIAL AND FINAL LOADS ON BEAM C AND BEAM D	35
2.10	BEAM A LONG TERM DEFLECTIONS	37
2.11	BEAM B LONG TERM DEFLECTIONS	38
2.12	BEAM C LONG TERM DEFLECTIONS	39
2.13	BEAM D LONG TERM DEFLECTIONS	40
2.14	CRACK PATTERNS FOR BEAM C AND BEAM D	42
2.15	BEAM E LONG TERM DEFLECTIONS	43
2.16	BEAM F LONG TERM DEFLECTIONS	44
3.1	3 NODE CONCRETE ELEMENT	96
3.2	CRACKED CONCRETE ELEMENT	96
3.3	2 NODE BAR ELEMENT	105
3.4	4 NODE GOODMAN JOINT ELEMENT	105
3.5	INFLUENCE OF TENSILE STRENGTH ON SHORT TERM DEFLECTIONS AT HIGH LOADS	119
3.6	INFLUENCE OF TENSILE STRENGTH ON LONG TERM DEFLECTIONS AT HIGH LOADS	120

FIGURE	TITLES	<u>PAGE</u>
3.7	INFLUENCE OF E_c ON SHORT TERM DEFLECTIONS AT HIGH LOADS	122
3.8	INFLUENCE OF E_c ON LONG TERM DEFLECTIONS AT HIGH LOADS	123
3.9	INFLUENCE OF SHRINKAGE ON LONG TERM DEFLECTIONS AT HIGH LOADS	125
3.10	INFLUENCE OF CREEP ON LONG TERM DEFLECTIONS AT HIGH LOADS	127
3.11	INFLUENCE OF DOUBLE THE NUMBER OF ELEMENTS ALONG THE LENGTH ON SHORT TERM DEFLECTIONS AT HIGH LOADS	128
3.12	INFLUENCE OF DOUBLE THE NUMBER OF ELEMENTS ALONG THE LENGTH ON LONG TERM DEFLECTIONS AT HIGH LOADS	129
3.13	INFLUENCE OF TENSILE STRENGTH ON SHORT TERM DEFLECTIONS AT LOADS NEAR CRACKING	132
3.14	INFLUENCE OF TENSILE STRENGTH ON LONG TERM DEFLECTIONS AT LOADS NEAR CRACKING	133
3.15	INFLUENCE OF E_c ON SHORT TERM DEFLECTIONS AT LOADS NEAR CRACKING	135
3.16	INFLUENCE OF E_c ON LONG TERM DEFLECTIONS AT LOADS NEAR CRACKING	136
3.17	INFLUENCE OF SHRINKAGE ON LONG TERM DEFLECTIONS AT LOADS NEAR CRACKING	138
3.18	INFLUENCE OF CREEP ON LONG TERM DEFLECTIONS AT LOADS NEAR CRACKING	139
3.19	INFLUENCE OF DOUBLE THE NUMBER OF ELEMENTS ALONG THE LENGTH ON SHORT TERM DEFLECTIONS AT LOADS NEAR CRACKING	141
3.20	INFLUENCE OF DOUBLE THE NUMBER OF ELEMENTS ALONG THE LENGTH ON LONG TERM DEFLECTIONS AT LOADS NEAR CRACKING	142

FIGURE	TITLES	<u>PAGE</u>
3.21	INFLUENCE OF DOUBLE THE NUMBER OF ELEMENTS ALONG THE LENGTH ON LONG TERM DEFLECTIONS AT LOADS NEAR CRACKING	143
3.22	INFLUENCE OF DOUBLE THE NUMBER OF ELEMENTS ALONG THE DEPTH ON LONG TERM DEFLECTIONS AT LOADS NEAR CRACKING	145
3.23	DETAILS OF BEAM 7/1	149
3.24	EXPERIMENTAL AND FINITE ELEMENT DEFLECTIONS FOR BEAM 7/1	150
3.25	DETAILS OF BEAM OA-2	153
3.26	EXPERIMENTAL AND FINITE ELEMENT DEFLECTIONS FOR BEAM OA-2	154
3.27	EXPERIMENTAL AND FINITE ELEMENT CRACK PATTERNS FOR BEAM OA-2	155
3.28	DETAILS OF BEAM DR10	157
3.29	EXPERIMENTAL AND FINITE ELEMENT DEFLECTIONS FOR BEAM DR10	159
3.30	DETAILS FOR BEAM E3A1	161
3.31	EXPERIMENTAL AND FINITE ELEMENT DEFLECTIONS FOR BEAM E3A1	162
3.32	DETAILS FOR BEAM E5A	164
3.33	EXPERIMENTAL AND FINITE ELEMENT DEFLECTIONS FOR BEAM E5A	165
3.34	DETAILS FOR BEAM A	167
3.35	DETAILS FOR BEAM B	168
3.36	DETAILS FOR BEAM C	169
3.37	DETAILS FOR BEAM D	170
3.38	DETAILS FOR BEAM E	174
3.39	EXPERIMENTAL AND FINITE ELEMENT DEFLECTIONS FOR BEAM E	175

FIGURE	TITLES	<u>PAGE</u>
3.40	DETAILS OF BEAM F	176
3.41	EXPERIMENTAL, STANDARD FINITE ELEMENT, AND 50% REDUCED TENSILE STRENGTH FINITE ELEMENT DEFLECTIONS	178
3.42	DETAILS OF BEAM C1	182
3.43	EXPERIMENTAL AND FINITE ELEMENT DEFLECTIONS FOR BEAM C1	183
3.44	EXPERIMENTAL AND FINITE ELEMENT CRACK PATTERNS FOR BEAM C1 AND BEAM C3	184
3.45	SHORT TERM AND LONG TERM STRAIN PROFILES FOR BEAM C1	186
3.46	DETAILS FOR BEAM C3	188
3.47	EXPERIMENTAL AND FINITE ELEMENT DEFLECTIONS FOR BEAM C3	190
3.48	SHORT TERM AND LONG TERM STRAIN PROFILES FOR BEAM C3	191
3.49	DETAILS FOR BEAM C4	193
3.50	EXPERIMENTAL AND FINITE ELEMENT DEFLECTIONS FOR BEAM C4	194
3.51	EXPERIMENTAL AND FINITE ELEMENT CRACK PATTERN FOR BEAM C4	196
3.52	SHORT TERM AND LONG TERM STRAIN PROFILES FOR BEAM C4	197
3.53	DETAILS FOR DILGER ET AL. BEAM	199
3.54	EXPERIMENTAL AND FINITE ELEMENT DEFLECTIONS FOR DILGER ET AL. BEAM	201
3.55	EXPERIMENTAL AND FINITE ELEMENT DEFLECTIONS FOR BEAM A	203
3.56	EXPERIMENTAL AND FINITE ELEMENT CRACK PATTERNS FOR BEAM A AND BEAM B	205
3.57	EXPERIMENTAL AND FINITE ELEMENT DEFLECTIONS FOR BEAM B	206

FIGURE	TITLES	<u>PAGE</u>
3.58	EXPERIMENTAL AND FINITE ELEMENT DEFLECTIONS FOR BEAM E	209
3.59	EXPERIMENTAL AND FINITE ELEMENT CRACK PATTERNS FOR BEAM E AND BEAM F	210
3.60	EXPERIMENTAL, STANDARD FINITE ELEMENT, AND 50% REDUCED TENSILE STRENGTH FINITE ELEMENT DEFLECTIONS	212
4.1	DETAILS FOR BEAM USED IN PARAMETRIC STUDY	223

CHAPTER 1

INTRODUCTION

1.1 Introduction

Long term deflections in reinforced concrete beams are an important serviceability consideration that has not yet received the attention it deserves. The introduction of Ultimate Strength Design methods has increased the importance of deflection criteria because it has led to the use of more slender members that are sensitive to deflections. Unfortunately the ability to predict the long term deflections of reinforced concrete beams has not kept pace with advances in predicting their ultimate strengths. This has led to the increased likelihood of deflection problems, and the possibility of serviceability failures.

The ability to accurately predict deflections is a difficult problem that has been impeded in the past by many different factors. Among these were a general lack of concern about serviceability considerations in general, the length of time required for long term testing, the large number of influencing variables, the effect of load history, and the variability of the material. Factors that are difficult to

quantify like tension stiffening, bond breakdown, initial stresses due to shrinkage, and degree of cracking have also contributed to the problem. To make the task of deflection prediction even more formidable is the fact that test results on identical beams often produce deflections which vary significantly.

Currently accepted techniques for calculating long term deflections were derived from a limited supply of experimental data, and consequently their general applicability may be open to question. The recent and current ACI approaches for computing long term deflections (2), which were also used in the Canadian Code (12), was to apply the following multipliers to the instantaneous deflection.

$$k_r = 2 - 1.2 A's/As \quad (1.1)$$

and now

$$\lambda = \frac{2.0}{(1 + 50\rho')} \quad (\text{for loads sustained beyond 5 years})$$

These equations were formulated by Branson (8) and were based primarily on the data of Washa and Fluck (53)(54) and Yu and Winter (56). While these equations may provide a reasonable approximation for the deflections from these tests, it is difficult to assess their applicability for general use. The very simplicity of the approach is evidence of their approximate nature. Since the adoption of these approaches there have been very few concentrated attempts to verify their accuracy or to suggest alternatives. Through experimental work and the use of a finite element model, this thesis is dedicated to discovering whether the current approach is the best solution, or whether some alternative should be proposed.

1.2 Objectives

The major objectives of this thesis were threefold:

- 1) To provide long term deflection results from beams loaded for a substantial period.
- 2) To develop an accurate finite element model to simulate long term deflections in reinforced concrete beams.
- 3) To provide a long term deflection prediction method using an organized parametric study.

Each of these objectives alone could be the subject of a separate study, but it was felt that an exhaustive study addressing all three objectives would be more useful in contributing to the knowledge of long term deflections. The final objective is the ultimate goal of this thesis but it was necessary to fulfill the other two before this one could be addressed. To meet the objectives it was necessary to delve into the way concrete properties are treated and to assess the methods that are used to predict them. This effort may be considered a minor objective that complemented the others.

1.3 Literature Review

Research into long term deflections of reinforced concrete members is still in its infancy, and very little attention seems to have been focused on this subject. This may be due to the relatively recent interest in serviceability, which has only lately emerged as an impor-

tant design consideration. [This may reflect increasing concern arising from more frequent serviceability problems.] The prime thrust of research work to date has been in estimating the effects of sustained loads on deflections. Previous investigations have provided useful insights into the magnitudes of long term deflections, but a relative scarcity of reliable experimental data has impeded a complete understanding of this phenomenon and has hindered the development of an accurate prediction method. This lack of complete data may explain the general lack of consensus on even a general technique for controlling long term deflections. A brief review of some of the important work that has been done in this area is now presented.

Washa and Fluck (54) provided the experimental data which has served as the basis for most of the empirical design methods currently available. In their first study, they observed the effect of compression reinforcement on time dependent deformations. Thirty-four full size beams with various dimensions and reinforcement details were tested for a period of two and a half years. Many of these specimens were more characteristic of slabs than they were of beams, so the collected data was really a mixture of both conditions. The main conclusion from this study was that compression reinforcement had a beneficial effect on reducing deflections because it decreased curvatures due to shrinkage.

In a second study, Washa and Fluck (53) furnished the only readily available data on long term deformations of statically indeterminate beams. Eighteen full scale beams, representing three different sizes and three different reinforcement patterns were tested for two

and a half years. The inclusion of compression reinforcement reduced time dependent deformations for these beams, but the effect was not as pronounced as for the simply supported beams from their earlier study. Washa and Fluck concluded that although the plastic flow generally tended to relieve the maximum stresses, inelastic deformations in one region of a beam induced an increase in the maximum stresses elsewhere.

Miller (34) was one of the first researchers to investigate and report on the warping of concrete beams due to shrinkage. Shrinkage deflections were measured for sixteen small uncracked reinforced concrete beams. A major conclusion from this study was that shrinkage deflections were strictly a geometrical phenomenon and therefore the elastic properties of the materials were not governing factors. Using his experimental data, Miller suggested a prediction method whereby the shrinkage curvature was dependent on the shrinkage strain and on the depth of the section.

In 1960, Yu and Winter (56) presented experimental data on T-beams, and proposed prediction methods for instantaneous and long term deflections. Twelve T-beams were tested over a five to six month period to determine their deflections. From these and other tests, (53)(54) two simplified methods were developed to estimate time dependent deflections. In the first method, an effective modulus of elasticity was used in the usual elastic deflection formulas to account for the time dependent effects. The long term deflection in the second method was found by multiplying the instantaneous deflection by a factor which depended on the duration of loading and on the reinforcement details. A compar

ison of the two methods indicated that although they both showed fair agreement with test data, the deflection multiplier method produced the best results. In addition, the effective modulus method did not perform well for beams with both tension and compression reinforcement.

In 1962, Gesund (20) published one of the first theoretical studies on the effects of creep and shrinkage on deflections. His analysis showed that because of shrinkage, the plane of zero stress was not the plane of zero strain. He also derived a simple model from normal beam theory using an effective modulus of elasticity to account for the long term effects. Deflections for both statically determinate and indeterminate beams were calculated by evaluating separately the influence of the elastic, creep and shrinkage strains. Gesund concluded that, in a prediction method, the deflection should be divided into two parts, one part due to elastic and creep strains, dependent on the moment, and the other part due to shrinkage, dependent on the geometry.

In 1963, Hajnal-Konyi (23) conducted an experimental program to check the effects of concrete strengths, steel strengths, steel percentages, and various span to depth ratios on long term deflections. Six pairs of small beams loaded under service load were observed for four and three quarter years. Probably the most striking result from Hajnal-Konyi's tests was that even those beams with small span to depth ratios had high long term to short term deflection ratios. In fact, all of the twelve beams tested had deflection ratios which exceeded the upper limit of 2.0 specified in the ACI Code equations (Eq. 1.1). The average long term to short term deflection ratio for the beams reinforced with mild

steel was 2.69, and 2.36 for those reinforced with high strength steel. Hajnal-Konyi's results also showed that although beams made with stronger concrete generally had lower time dependent deflections than those made with weaker concrete, the differences were relatively small.

Hajnal-Konyi compared his test data with deflections calculated by various analytical methods. The ACI method of factoring the initial deflection was compared with a method using an effective modulus. The method using an effective modulus of elasticity showed better agreement with the experimental results than the ACI method of using a factored initial deflection. (This is the reverse to what Yu and Winter found). Hajnal-Konyi also noted that methods which took into account the contribution of the concrete tensile strength performed better than those which did not.

Hajnal-Konyi examined the use of limiting span-to-depth ratios as a means of limiting long term deflections. He concluded that since reinforced concrete design is based on the assumption that there are no tensile stresses in the concrete, the slenderness of beams should be related to the effective depth and not to the overall depth. In addition, he suggested that the limiting slenderness ratios should depend on the stresses in the steel and the concrete.

Corley and Sozen (17) tested four beams for a two year period, and using this plus previous data (23)(53)(54)(56) proposed a simple method for estimating long term deflections. The variables in their tests were the amount of tension steel and the depth of the section.

The six foot long and three inch wide test beams were smaller than those generally found in service so the results need to be viewed objectively. An interesting point which emerged during the test was that even though the total deflections of the beams were different, the ratio of the total to the instantaneous deflection was always about the same.

A simple method for calculating long term deflections was proposed by Corley and Sozen in which the curvatures due to creep and shrinkage were determined separately. The creep curvature was computed as a percentage of the instantaneous curvature, where the factor was dependent on the amount of steel and the depth to the neutral axis. The shrinkage curvature was estimated from the reinforcement details and the depth of the section. Good agreement was reported between the proposed equations and the experimental data. Finally, Corley and Sozen noted that the influence of the tension in the concrete was significant for lightly reinforced sections.

In 1972, Stevens (50) conducted a series of sustained loading tests on reinforced concrete beams and then discussed simple methods to predict strain and deflections. Twenty-nine full scale beams were subjected to sustained loads for a two year period. The concrete cover, amount of reinforcement, type of environment, type of concrete, and overall dimensions were varied to determine their influences. A number of conclusions were reached from these sustained loading tests. One of these was that for cracked beams, the contribution of the concrete in tension decreased considerably with time. Another observation was that although beams made with lightweight concrete has larger initial

deflections than those made with normal concrete, the subsequent changes were quite similar. Stevens also determined that for analysis purposes, using an average relative humidity gave a good analytical approximation for beams exposed to variable humidities.

Stevens proposed two different methods for predicting the total strains due to long term loading. In the first method a normal elastic analysis was used to calculate the elastic strains, and an effective modulus of elasticity was used to account for the creep effects. In the second method the curvature was calculated by assuming that the strain in the steel could be found from an elastic analysis, and the compressive strain could be found in terms of the initial strain, the creep coefficient, and the shrinkage strain. In both cases the time dependent properties of the concrete were needed as input variables.

An extensive examination of the long term properties of concrete and a comparison and discussion of available prediction methods was compiled by Branson (8). In this study he stated that long term deflections were affected by the following effects:

- a. Creep of concrete in compression and tension, including bond creep
- b. Shrinkage of concrete
- c. Formation of new cracks and the widening of earlier cracks
- d. Relaxation of tensile stresses in concrete
- e. Movement of the neutral axis

- f. Compression steel
- g. Repeated load cycles
- h. Moment redistribution in statically indeterminate elements

After examining the experimental work of previous investigators, Branson proposed a number of methods for predicting long term deflections. For calculating shrinkage curvatures alone, Branson suggested an empirical method based on a modification of Miller's method (34). They both assumed that the shrinkage curvature was a direct function of the free shrinkage and the steel content and an inverse function of the depth of the section. Using the full thickness rather than the effective depth was observed to give the best results. Branson also concluded that the effect of cracking could be ignored in a simple shrinkage analysis.

Branson also proposed a method for calculating creep deflections, where the initial deflection was multiplied by a factor which depended on the compression steel ratio. Branson concluded that the compression steel ratio rather than the ratio of tension to compression steel gave the best representation of the effect of compression reinforcement. The same method was proposed for combined creep plus shrinkage deflections, but the constants in the basic equation were modified. Branson preferred factoring the initial deflection to using an effective modulus of elasticity, because he felt that it was easier to use, more adaptable, and seemed to give better results.

In 1982, Hobbs (26) did a theoretical analysis of shrinkage curvatures using the Equivalent Tensile Force Method. This method was later expanded to include creep curvature, but a comparison with experimental results showed only fair agreement.

It is obvious from the preceding review that although some research work has been done in the area of long term deflections of reinforced concrete beams, there is still no general agreement on the best method of prediction. Even though over 100 beams have been tested to date, there is no complete statistical sample of deflections available. This is probably due to a lack of coordination between researchers. This lack of coordination seems to have prevented the methodical development of a prediction method from all of the available collected data. Compared to most other areas of concrete research, the amount of experimental data which is available on this subject is not very large. This is perhaps understandable considering the amount of time which is required for testing and the high cost of full scale experiments. It is also unfortunate because there is a very high variability associated with long term deflections, and significant trends may not be readily apparent where the number of tests are limited. One problem with the long term deflection tests which have been conducted is that there is very little available data on the deflections of continuous beams. This is surprising considering their prevalence in practice. In addition, information of the deflection characteristics of beams with compression reinforcement also seems lacking.

The prediction methods and Building Code equations that are currently in use are very simple and therefore probably relatively inaccurate. Washa and Fluck's data provided most of the experimental data which has been used to develop almost all of the currently available prediction methods. This is regrettable because the influence of their particular material and storage parameters has tended to overshadow the results of other researchers.

Since long term deflection prediction methods are necessarily empirical in nature, an important issue must be raised. When the experimental data that was used to develop a prediction method is also used to verify it, the results are favourably biased and the empirical equations may appear to be better than they actually are. In almost all cases this is what has been done with current prediction methods.

In the available literature, two major approaches have been proposed for predicting time dependent deflections. These have been identified as the Effective Modulus of Elasticity Method and the Factored Initial Deflection Approach. Very little attention seems to have been paid to any other approaches, so it may be advantageous for future researchers to examine alternatives. The one difficult requirement which all useful design equations must satisfy is that they can only make use of information which is readily available to designers. The necessity for simplicity and accuracy are difficult requirements to deal with, and until an extensive parametric study is completed, or a fundamental analytical technique is developed, the accurate prediction of long term deflections may be an elusive goal.

1.4 Thesis Outline

An outline of the organization of this thesis is provided to aid the reader. Chapter 2 contains the experimental work which was done in this study. There is a lack of experimental data on long term deflections, and the six beams tested, four of which were continuous, should add to the current supply. These beams were also tested to provide some means for verifying the finite element model. In Chapter 3 the development of the finite element model is discussed. First the constitutive relationships necessary for accurately specifying the material properties are chosen. Then the finite element modelling of reinforced concrete is examined and the proposed model is derived. It is hoped that this model will provide a workable compromise between efficiency and accuracy. The short term and long term accuracy of the proposed model is also checked using available experimental data to ensure that the model may be used confidently to simulate reinforced concrete behaviour. In Chapter 4 a parametric study using the Factorial Design Method to develop a long term deflection prediction method is presented. Results generated by the proposed model are used to provide the necessary data. Finally, the general conclusions and recommendations are contained in Chapter 5.

CHAPTER 2

EXPERIMENTAL PROGRAM

2.1 Introduction

The examination of the existing literature reported in Section 1.3 indicated that there was a serious shortage of varied experimental data on long term deflections. This was particularly the case for full size beams and continuous members. The number and range of parameters which have been tested seemed very limited, and this has very likely had a significant impact on the accuracy of current design equations. In most cases the available experimental data tends to be incomplete, and this makes it extremely difficult to develop empirical design methods, and to verify analytical models. Obviously the acquisition of more experimental information would greatly improve the situation. With these factors in mind an experimental program was undertaken with the dual purpose of assessing the accuracy of the proposed finite element model, and providing usable experimental data for future researchers. This information may also be useful for evaluating the design methods currently in use. The material properties, test set-up, beam specifications, and results from the experimental program are presented in this chapter.

2.2 Design of Experiment

Six simply supported beams, of which four were continuous, were designed, constructed, and tested under controlled conditions. The testing program was not intended to be a complete statistical study of the factors which influence long term deflections, but rather a brief examination of some of the more important parameters. The main elements of interest included the section depth, the tension steel ratio, the compression steel ratio, the age of loading, the level of sustained load as a percentage of ultimate load, and the existence of negative and positive moments. The experimental program was designed so that the beam sizes and test conditions were realistic. Problems such as scaling effects, unusual concrete properties, unusual support conditions, and uncommon span lengths were therefore eliminated. All of the beams were full sized, and had span-to-depth ratios which were large enough to minimize shear effects. The loads which were applied to the beams were well within the service load range, and the resulting bending moment diagrams resembled those of uniformly loaded beams. All of the beams were simply supported and determinate, which meant that the reactions, and therefore the bending moment diagrams, were always known. It was hoped that these considerations would ensure that the experimental program produced results that were both useful and reliable.

2.2.1 Concrete Mix Design

A concrete mix was designed to produce a 28 day compressive strength of 4000 psi. This strength was chosen because it is represen-

tative of concretes generally used in reinforced concrete structures. The mix proportions, given by weight, are shown in Table 2.1. The concrete produced by this mix is slightly "pasty", and the subsequent creep and shrinkage strains, although well within normal limits, should be slightly higher than usual. The same carefully controlled concrete mix was used throughout the test so that differences due to changing mix parameters could be eliminated.

2.2.2 Batching and Curing

The experimental program was divided into three distinct series of two beams per series. This was done because of time limitations in the mixing and placing of the concrete in each set of beams. In addition, staggering the casting days made the scheduling of the preparation and loading of the beams easier. On each mixing day, before the first batch was prepared, the nine cubic foot horizontal drum concrete mixer was conditioned with a "butter batch" of approximately one quarter of the mixer capacity. This concrete was thrown out and the regular batches were then prepared. A slump test was taken after each batch was mixed to ensure that the concrete met the required specifications. A Standard 12 Inch High Slump Cone was used to measure the slump and in all cases the value was within $3/4$ of an inch of the specified slump of 2 $1/2$ inches. All of the aggregate was air dried, but in the third series it was observed that the sand on this day was slightly damp, and therefore it was necessary to make some minor adjustments in the mix to get the correct slump. Mixing and pouring proceeded quickly so that neither the mixer nor the concrete was allowed to dry out.

The concrete for the beams was placed in wooden forms and vibrated internally using a poker type vibrator. Three 12 in. high cylinders were poured from every batch, and one 22 × 6 × 6 in. prism was poured from nearly every second batch. The cylinders were placed and vibrated in three layers, and the prisms were placed and vibrated in two layers. Nine batches was the maximum needed to make all of the beams, cylinders, and prisms required for any series.

When the concrete had begun to harden, approximately four to five hours after pouring, wet burlap was placed over the beams, cylinders and prisms. The burlap was kept moist throughout the seven day curing period. When this period was over, the specimens were taken from the laboratory floor and placed in a humidity controlled environment. Further details about the tent used to control the humidity are mentioned later in this chapter.

2.3 Concrete Properties

2.3.1 Compressive Strength

Cylinders from different batches for each beam series were tested at ages of 7 days, 28 days, and after the end of the test. The reason for determining the uniaxial compressive strength was to ensure that the concrete satisfied the specified strength of 4000 psi, and because information was needed for the prediction of other material properties which were not tested separately. The compressive strength

test was conducted in accordance with ASTM specifications, and the results are shown in Table 2.2.

2.3.2 Stress-Strain Relationship

The modulus of elasticity is a very important material property, especially for a finite element analysis, and is found from the stress-strain diagram. The concrete stress-strain relationship in this test was measured by one of two methods. In the first method, a compressometer was used in accordance with ASTM specifications to plot the stress-strain diagram until failure. In the second method, a mechanical strain indicator called a Demec gauge was used. This indicator has an 8" gauge length. To use the Demec gauge it was necessary to equip the cylinders with two sets of gauge points which were mounted on opposite sides of the cylinders. During the loading sequence, readings were taken with the Demec gauge at regular intervals until failure and the strains were calculated by averaging the results on both sides of the cylinders. The compressometer was used more often than the Demec setup because the compressometer was easier to use and it eliminated the need for halting the loading procedure to take readings. The results from the modulus of elasticity test for various concrete ages are shown in Table 2.3.

Table 2.1 Concrete Mix Data

Component	Percent by Weight	Weight in pcf
Portland Type 1 Cement	14.0	21.2
Water	9.1	13.8
Sand	46.6	70.6
Gravel	30.3	45.9

Table 2.2 Compressive Strength
(psi)

	Series 1	Series 2	Series 3
7 days	3310	3336	3370
28 days	3966	4280	4433
761 days		4191	
803 days	3866		4776

Table 2.3 Modulus of Elasticity ($\text{psi} \times 10^6$)

	Series 2	Series 3
7 days	-	3.292
28 days	3.375	3.957

2.3.3 Shrinkage

The shrinkage properties of the concrete were determined from 22 × 6 × 6 in. prisms which were cast at the same time as the beams and cylinders. One pair of Demec gauge points were mounted on each of the four sides of the prisms, near the middle of each side. Strains were measured with the Demec Strain Indicator and the total shrinkage was calculated by averaging the four results from each prism. All of the prisms were initially moist cured for seven days after which they were stored in the controlled environment. The relative humidity was maintained at 50% ± 5% and the temperature ranged between 70°F and 75°F. Shrinkage results for all three series are presented in Figure 2.1. It should be noted that the age of the concrete when the initial readings were taken is different for each series.

2.3.4. Creep

The creep properties of the concrete were evaluated with prisms which were identical to those used for shrinkage. The Demec gauge points were also the same, as were the conditions of storage, and the measurement of the strains. The creep specimens were subjected to different load levels and loading ages to provide a general representation of the creep properties of this concrete. Since the analysis was exclusively concerned with the service load state, where creep is nearly linear with stress (38), the prisms were subjected to constant loads of either 15%, or 30%, of f'_c . It was felt that this range would give a good overall picture of the service load creep for this concrete.

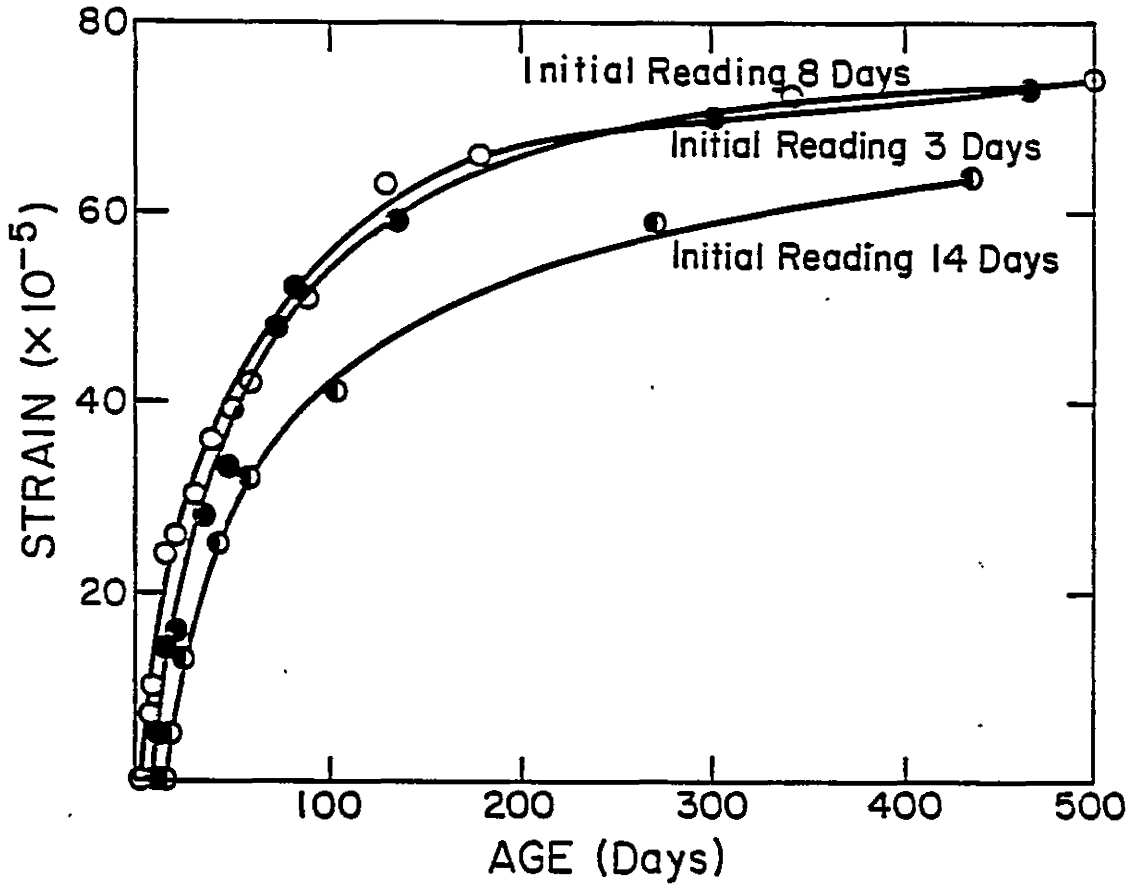


FIGURE 2.1 CONCRETE SHRINKAGE MEASUREMENTS

The creep specimens were tested using the setup illustrated in Figure 2.2. Before the prisms were loaded, 2" thick notched metal plates were plastered to the top and bottom of each specimen. A ball or roller was then placed between this plate and another identical plate. A compression load cell was then added to the top of this arrangement and the specimen was centered in the spring-loaded creep frame.

The load was applied with a hydraulic jack by jacking between the top plate of the frame and the plate above the springs. This force compressed the springs and loaded the specimen. When the specified load level was reached the nuts on top of the plate covering the springs were tightened, and the jack was released. The load level was monitored and adjusted at regular intervals throughout the test to ensure that the applied load remained constant. The springs were included in the apparatus to moderate the reduction in the load produced by the creep and shrinkage strains.

Creep results from all three concrete series are shown in Figure 2.3. The creep strains in this figure were calculated by subtracting the shrinkage strains of Figure 2.1 from the total long term strains which were measured with the creep specimens. Any long term changes in the elastic strain were included as part of the creep.

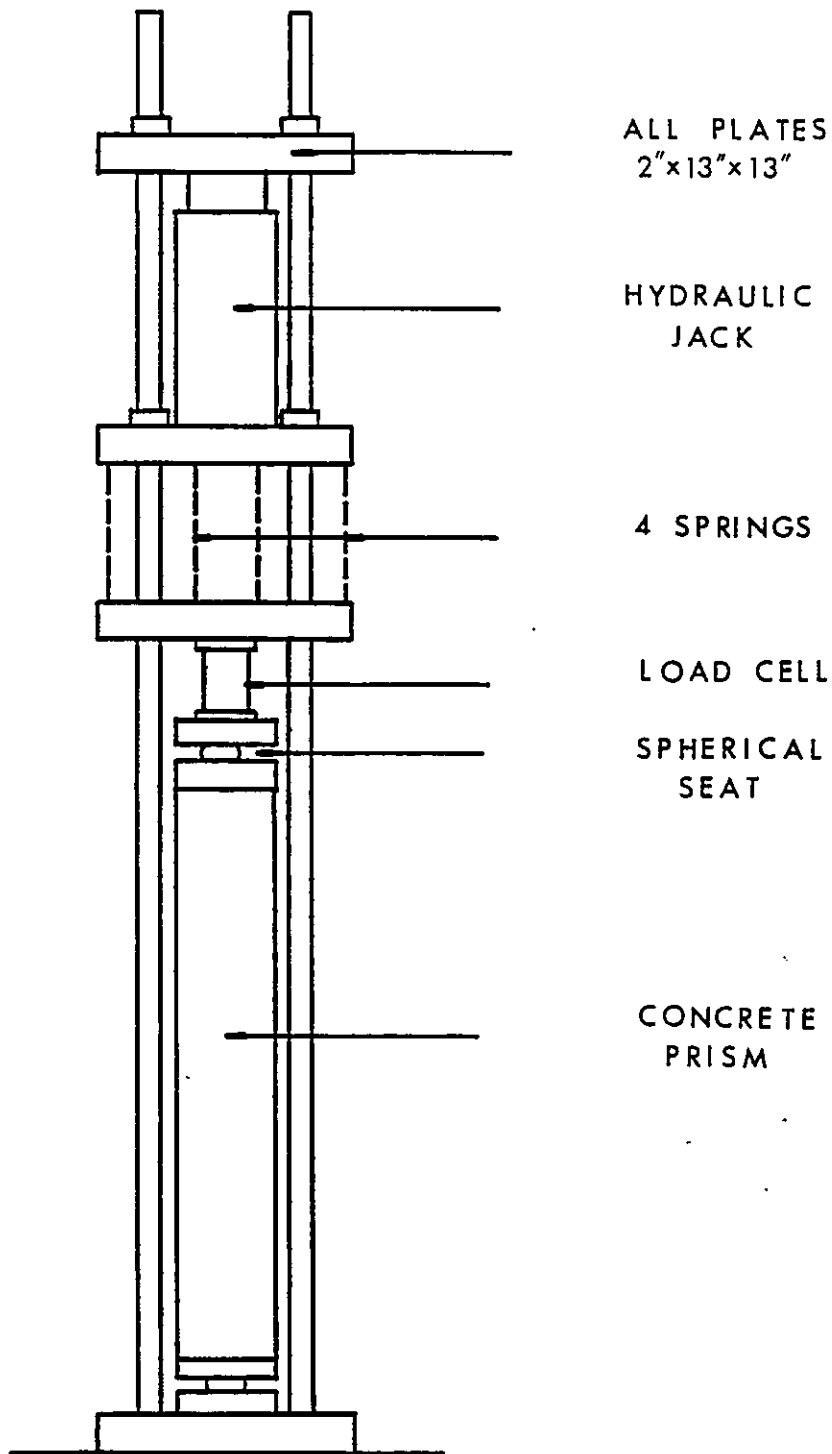


FIGURE 2.2

CONCRETE CREEP EQUIPMENT

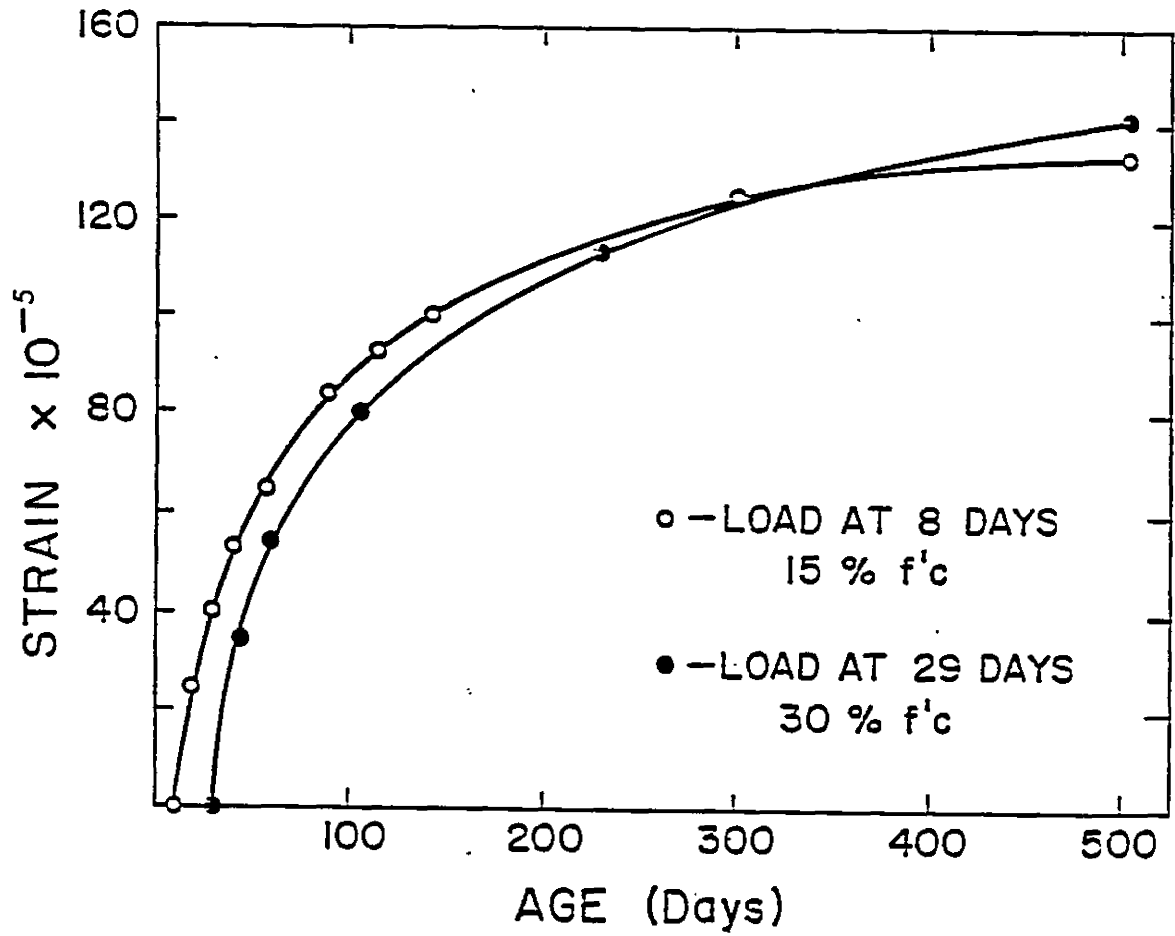


FIGURE 2.3 CONCRETE CREEP MEASUREMENTS

2.4 Beam Tests

2.4.1 Description of Test Beams

The cross-sectional properties and reinforcement details of the four different beam designs are shown in Figures 2.4 to 2.7. A total of six beams were designed and all of the beams had a common width of 6 inches, a concrete cover of 2 1/2 inches, and a side cover of 1 inch. There were two different lengths, two different depths, three different steel areas, and two different support conditions. Two 16 foot beams and four 24 foot beams were produced. Minimum shear reinforcement was provided for all of the beams even though they were not loaded to failure. Plain 1/4 inch diameter closed stirrups were used in all cases. All beams had maximum stirrup spacings corresponding to the Code limitation of one half the depth of the section.

All of the beams contained either two or four vertical 1 1/2 inch diameter hollow tubes through which threaded rods could be passed to apply the loads and to tie the beams together. This will be discussed further in the next section.

2.4.2 Beam Test Setup

One or two days before the beams were loaded, the two beams of each series were arranged as shown in Figure 2.8. The beams were placed back-to-back so that the two beams could be loaded at the same time using only one set of load cells, supports, and loading apparatus. It

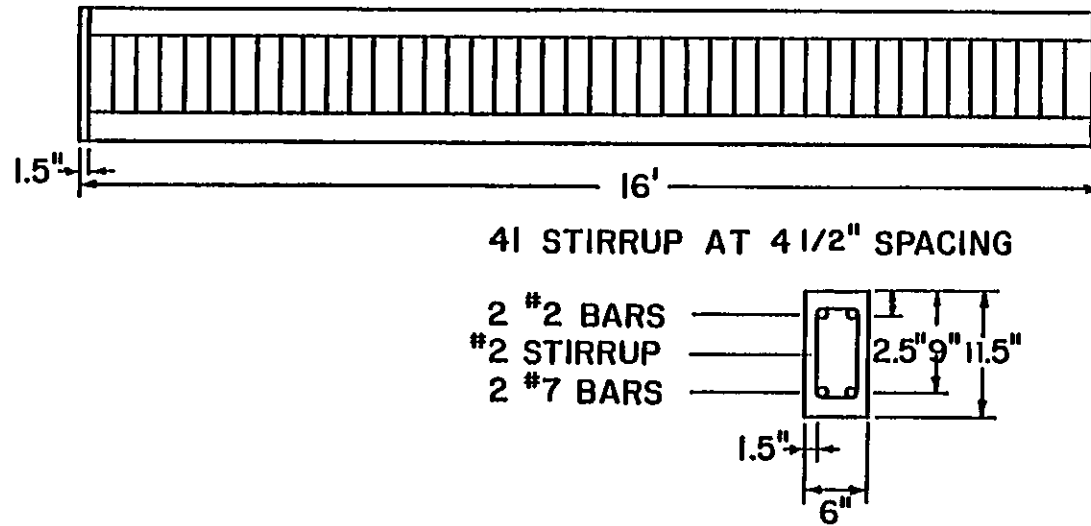


FIGURE 2.4 BEAM A DETAILS

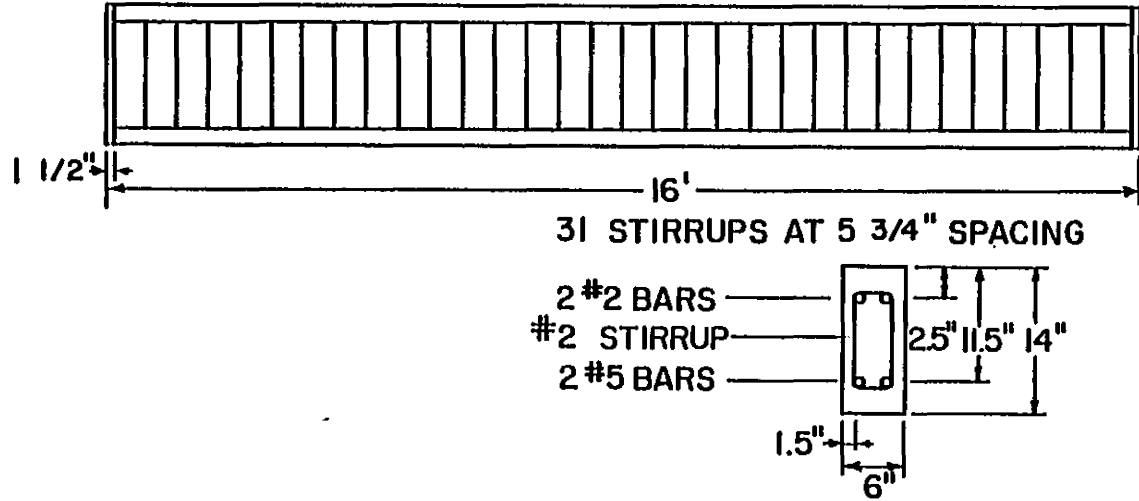


FIGURE 2.5 BEAM B DETAILS

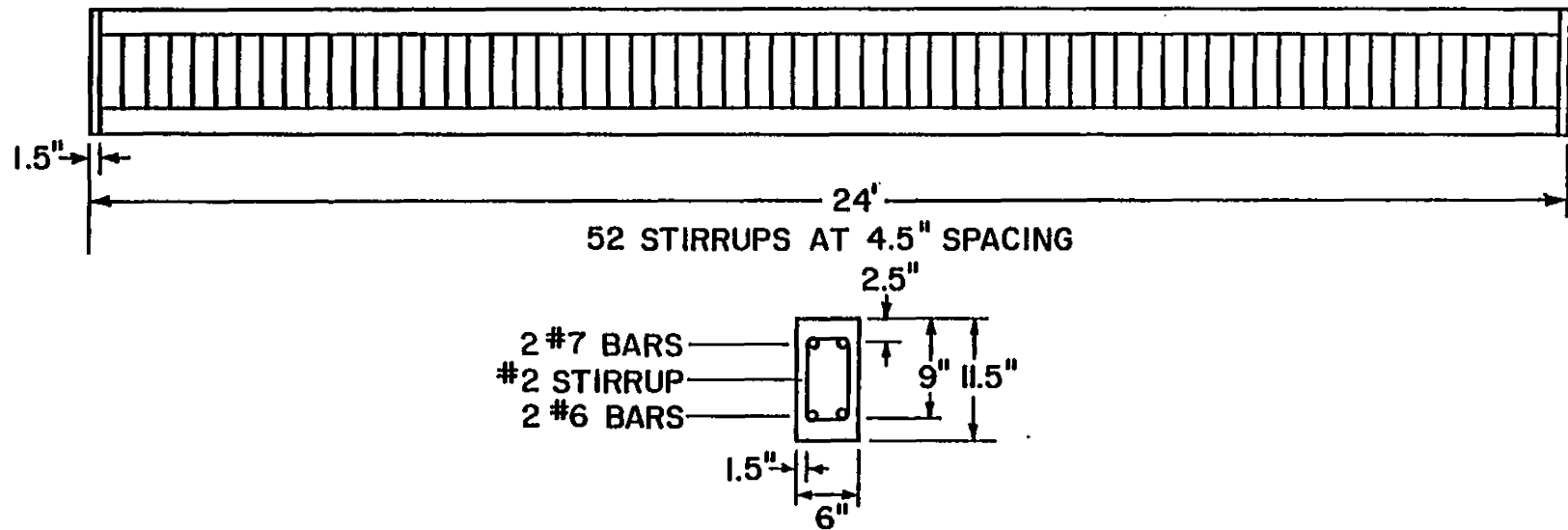


FIGURE 2.6 BEAM C, E DETAILS

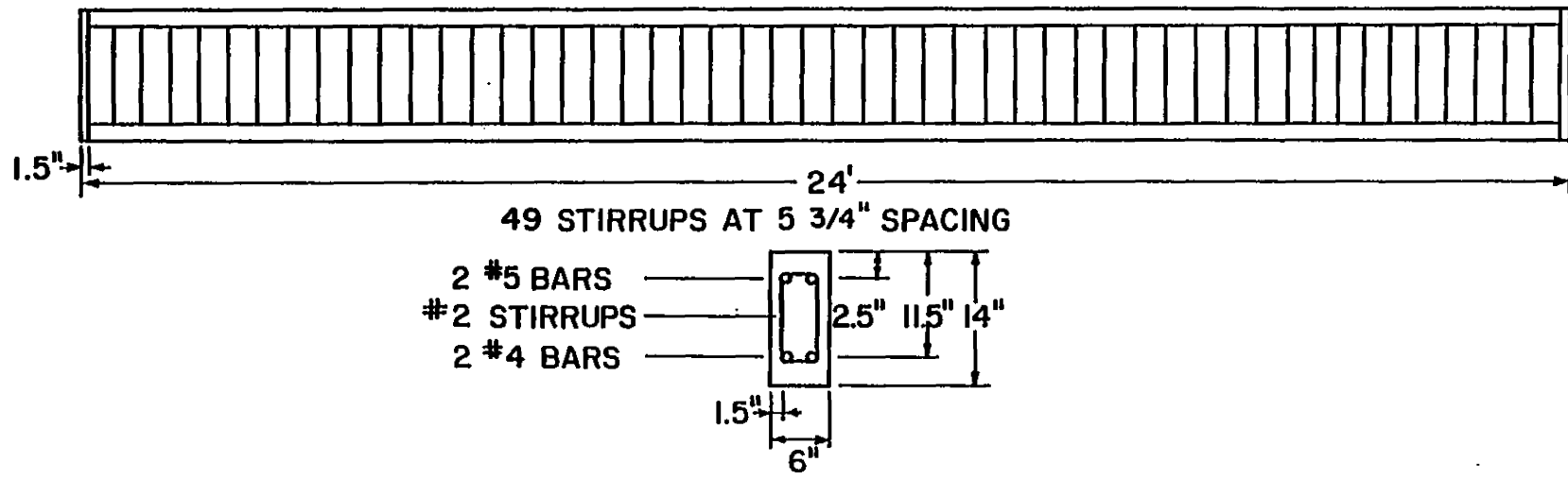
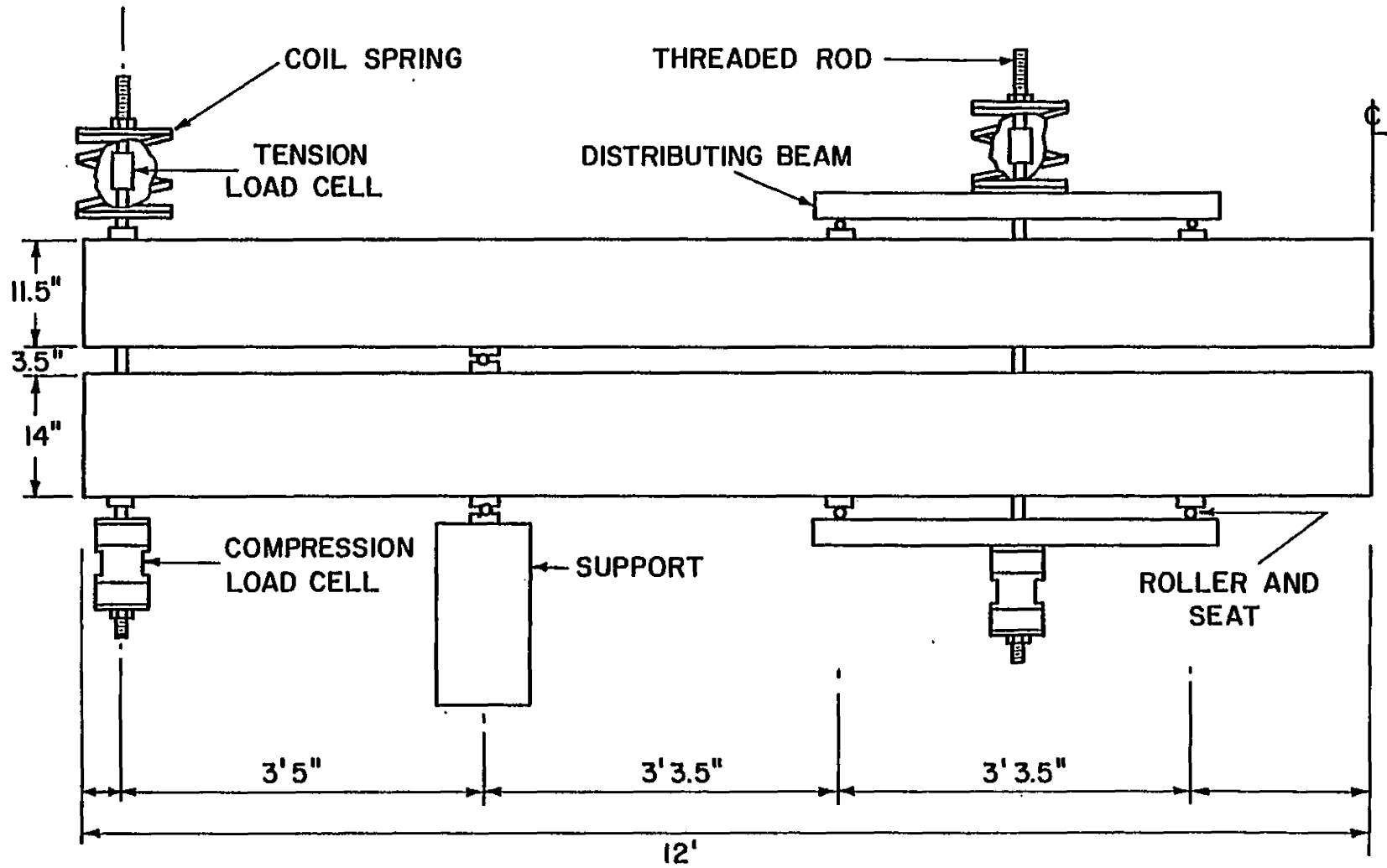


FIGURE 2.7 BEAM D, F DETAILS

FIGURE 2.8 BEAM TEST SETUP



also reduced the amount of laboratory space needed for the testing period. The one drawback to this kind of setup is that the direction of the gravity load for the bottom beam is in the opposite direction to the applied loads. This is not usually observed in practice. Each pair of beams in the setup consisted of one 14 inch deep beam and one 11 1/2 inch deep beam. The 14 inch beam was placed on the bottom because it had a lower ultimate load than the 11 1/2 inch beam. If the 14 inch beam had been placed on top, the additional gravity load would have caused the beam's total load to be outside of the service range.

To arrange the beams as shown in Figure 2.8, the 14 inch thick beam was placed upside down on blocks. Roller bearings were located at the support points and the 11 1/2 inch thick beam was placed on top. The position of the roller bearings coincided with the position of the blocks so that the weight of the top beam would not affect the load distribution of the bottom beam. The load points were positioned at the quarter points for all beams, and also at the ends of the continuous beams. It was thought that this loading arrangement would give moment distributions which were reasonably close to those for uniformly loaded beams, and would therefore give a more accurate representation of design loads. Threaded rods were passed through the hollow tubes which were embedded in both beams, and the load was applied at these locations by tightening the nuts located near the top of the threaded rods. Spreader beams were positioned along the center span to distribute the load from the threaded rod locations to the load points. Helical springs were placed on top of the spreader beams, and at the ends for the continuous beams, to moderate the changes in the load that occurred because of the

time dependent deflections. A compression load cell was placed near the bottom of every threaded rod, and for the continuous beams a tension load cell was inserted near the top of the rods between threaded rod portions.

In most cases the applied loads were measured in more than one way. Compression load cells were the primary means of measuring the loads for the 16 foot beams, and the secondary method for measuring the loads for the 24 foot beams. The compression cells were compressed between two 6" x 6" x 1/2" plates and two 3" diameter x 2" thick plates. The thick plates were put in to decrease stress concentrations on the load cells. Unfortunately, difficulties were discovered with the accuracy of the compression load cells. The readings from these cells were not always repeatable and seemed very sensitive to slight load eccentricities. For this reason, tension load cells were added to the instrumentation for the 24 foot beams. The tension load cells seemed to produce more reliable and repeatable readings. For the 24 foot beams, the tension load cells were considered as the primary means of measuring the applied loads, and the compression cells acted as a backup. The deformation of the springs acted as a further backup, but these results were not very reliable because the springs deflected slightly out of their vertical plane.

The main aim of the experimental work was to obtain deflection data and this was done with dial gauges. Deflection measurements were taken at the center of every beam and also at the ends of the continuous beams. A metal bar was glued to the bottom of the beams at the

designated locations, and the dial gauges were fixed against these. The dial gauges were marked in divisions of .001 inches, which was considered more than enough accuracy for the expected deflections.

When the beams, cylinders, and prisms were fully cured, they were placed in a humidity controlled tent. A 29 foot long, by 15.5 foot wide, by 8.5 foot high polyethelene covered frame was constructed to house the test specimens. A relative humidity of $50\% \pm 5\%$ was maintained in this tent using a humidifier-dehumidifier tandem. A temperature of 70°F to 75°F was maintained in the laboratory. Two oscillating fans were positioned at opposite ends of the tent to eliminate any air stratification.

2.4.3 Applied Loads

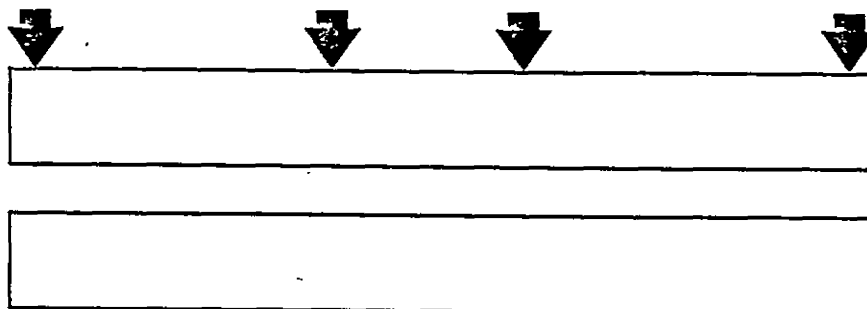
Two simply supported beams, designated A and B, were tested in Series 1. Beam A was the top beam and Beam B was the lower beam. Initially the loads applied to the quarter points of the two beams were set at 1400 pounds. This was well within the service load range for these beams. As mentioned earlier there was some difficulty with the load cells of this series, and towards the end of the test it became apparent that the loads had varied with time. Therefore the test was ended, the final deflection readings were taken, and the beam was unloaded. To determine what loads were actually present at the end of the test, accurate tension load cells were installed in the setup and the beam was immediately reloaded until the previously recorded final deflections were duplicated. The load at this point was 1050 pounds,

which represented a drop of 27% from the initial load. This load was then assumed to represent the final load applied to the beams. This may not be exactly correct because the loads on the two load cells at the end of the test were not necessarily the same, but it was felt that this was probably a reasonably accurate representation of the true situation.

Series 2 and 3 both consisted of two continuous beams, designated C and D for the 8 day loading, and E and F for the 28 day loading. The loads initially applied to the quarter points of the interior spans were 1800 pounds and the loads at the ends were 2700 pounds. Unfortunately as was the case for Series 1, there was some variance in the applied loads on these beams. At the end of the test period the load cells were recalibrated and it was discovered that while the loads at the ends of the beams of Series 2 and all of the loads of Series 3 had changed by less than 14%, and usually much less, the load measured by one of the interior load cells of series 2 had increased by 50%. Figure 2.9 shows the initial and final loads applied to the continuous beams.

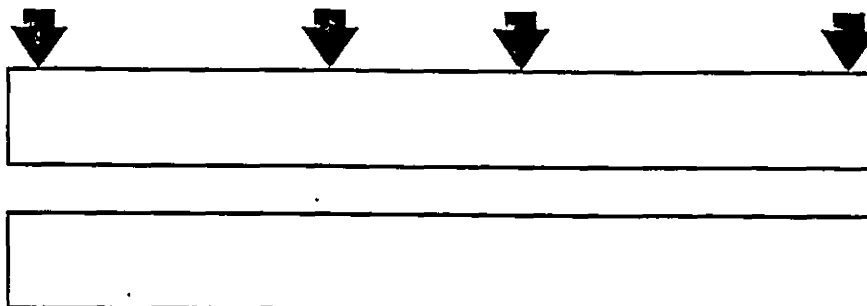
An inspection of the time-deflection curves that follow shows that there were no abrupt changes in their slopes. This suggests that the load changes were gradual rather than sudden. Through logic and further study of the deflection curves it was postulated that the change in load was probably logarithmic in nature, and this was the assumption that was made for the model verification described later in Section 3.4.

INITIAL	2700	3600	3600	2700
FINAL	2434	5283	2990	2540



SERIES 2

INITIAL	2700	3600	3600	2700
FINAL	2361	3620	3283	2657



SERIES 3

FIGURE 2.9 INITIAL AND FINAL LOADS ON BEAM C AND BEAM D

Series 1

The crack patterns for Beam A and Beam B are not contained in this Chapter but are shown later in Section 3.5, where they are compared with finite element simulations. The long term deflection curves for these two beams are presented in Figure 2.10 and Figure 2.11. The immediate deflection of Beam A was .220 inches and the additional long term deflection was .662 inches, which gave a ratio of long term to short term deflection of 3.0. The immediate deflection of Beam B was .166 inches, the additional long term deflection was .352 inches, and the ratio of long term deflection to short term deflection was 2.1. The deflection ratio of Beam B was not much higher than the Code (12)(58) approximation of 1.8, but the ratio for Beam A was much higher than the Code approximation of 1.9. Had the load not dropped with time the tested deflection ratios would have been even higher, which perhaps emphasizes the inadequacy of the current code approach.

Series 2

Beam C and Beam D were continuous beams loaded to an age of eight days. Beams C and D were loaded in stages so that all loads increased at the same rate. This meant that the final loads on the load cells at the ends of the beams were reached before the final loads on the load cells in the interior span. The midspan deflection of Beam C, the top beam, was .199 inches, while the deflection at the midspan of Beam D was .067 inches. The long term deflection curves for these beams are shown in Figures 2.12 and 2.13. The total long term deflection for

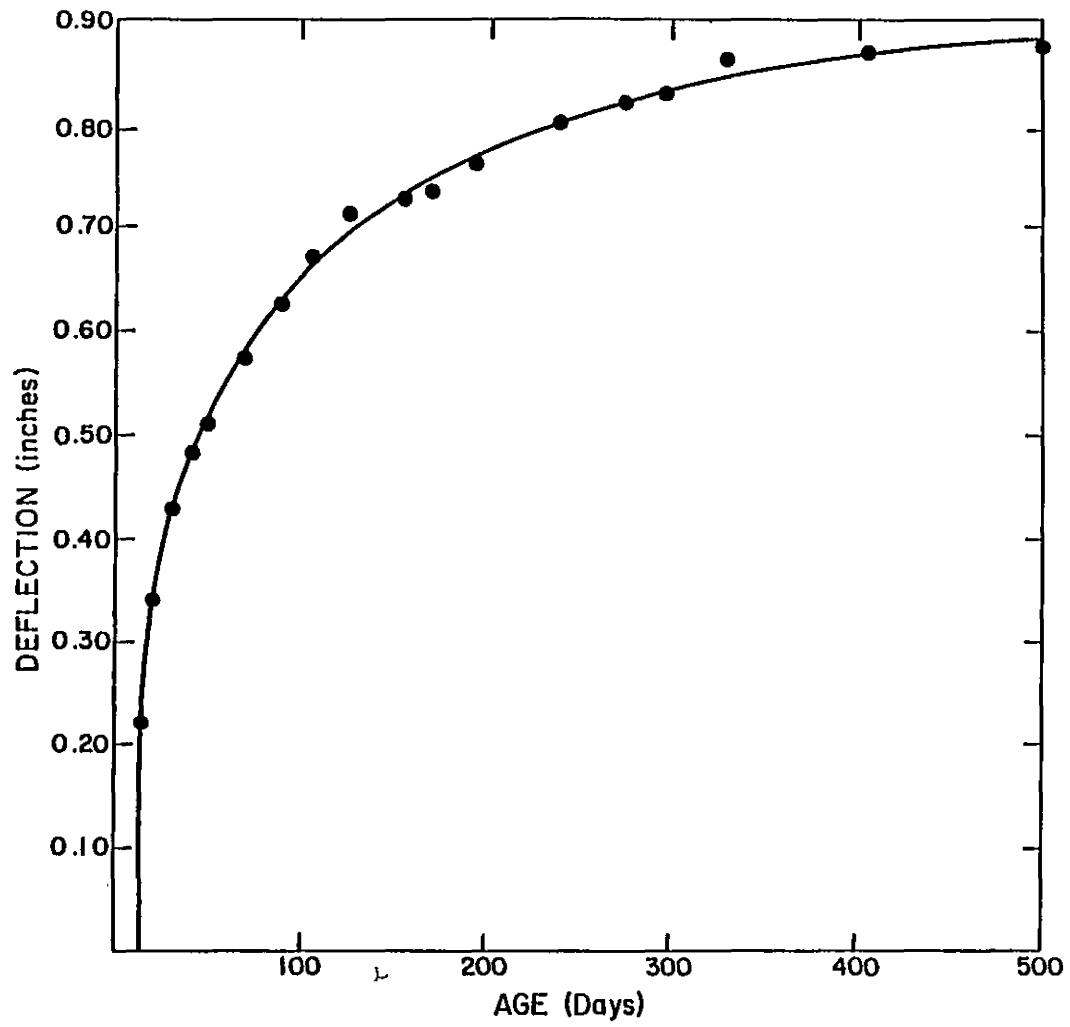


FIGURE 2.10 BEAM A LONG TERM DEFLECTIONS

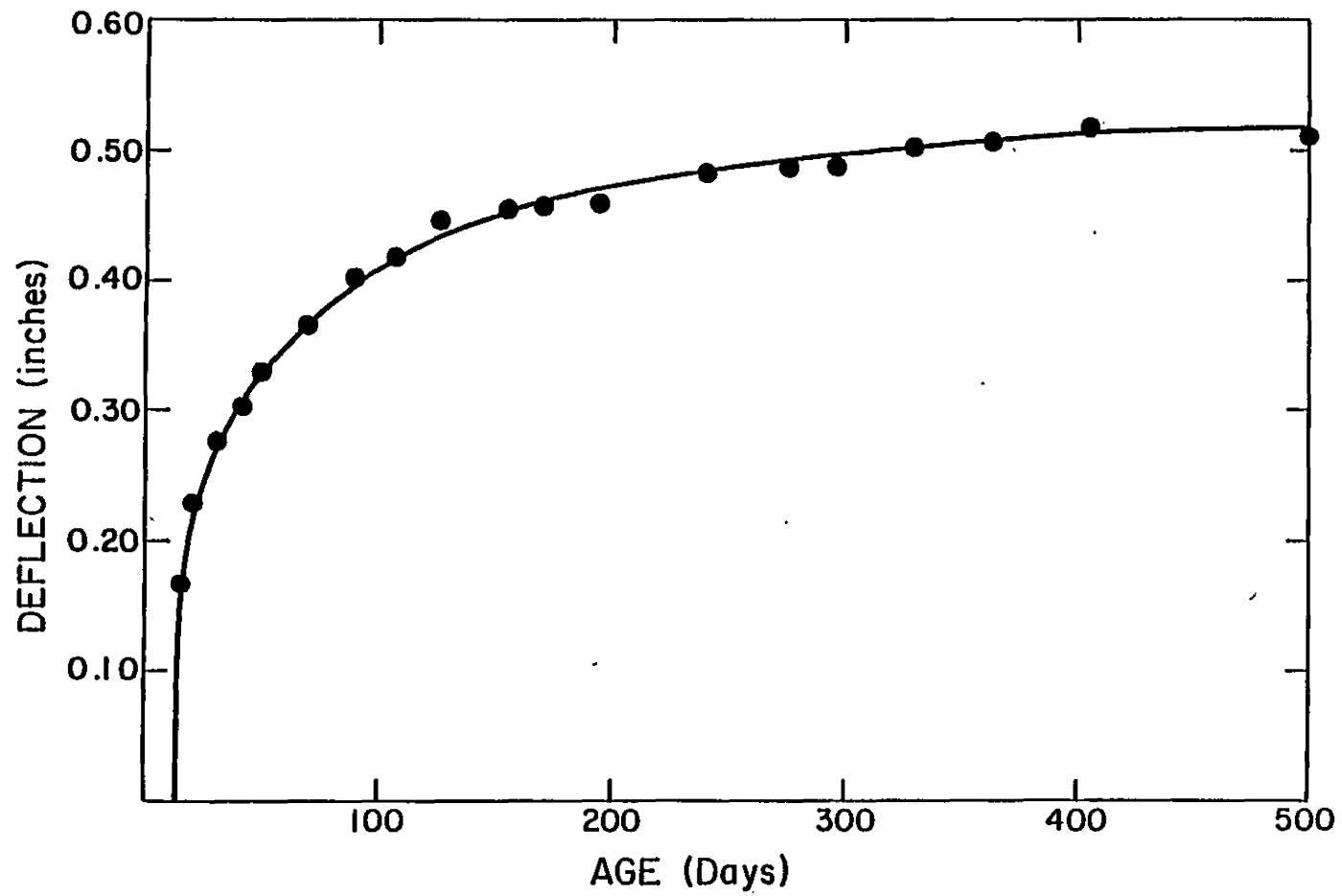


FIGURE 2.11 BEAM B LONG TERM DEFLECTIONS

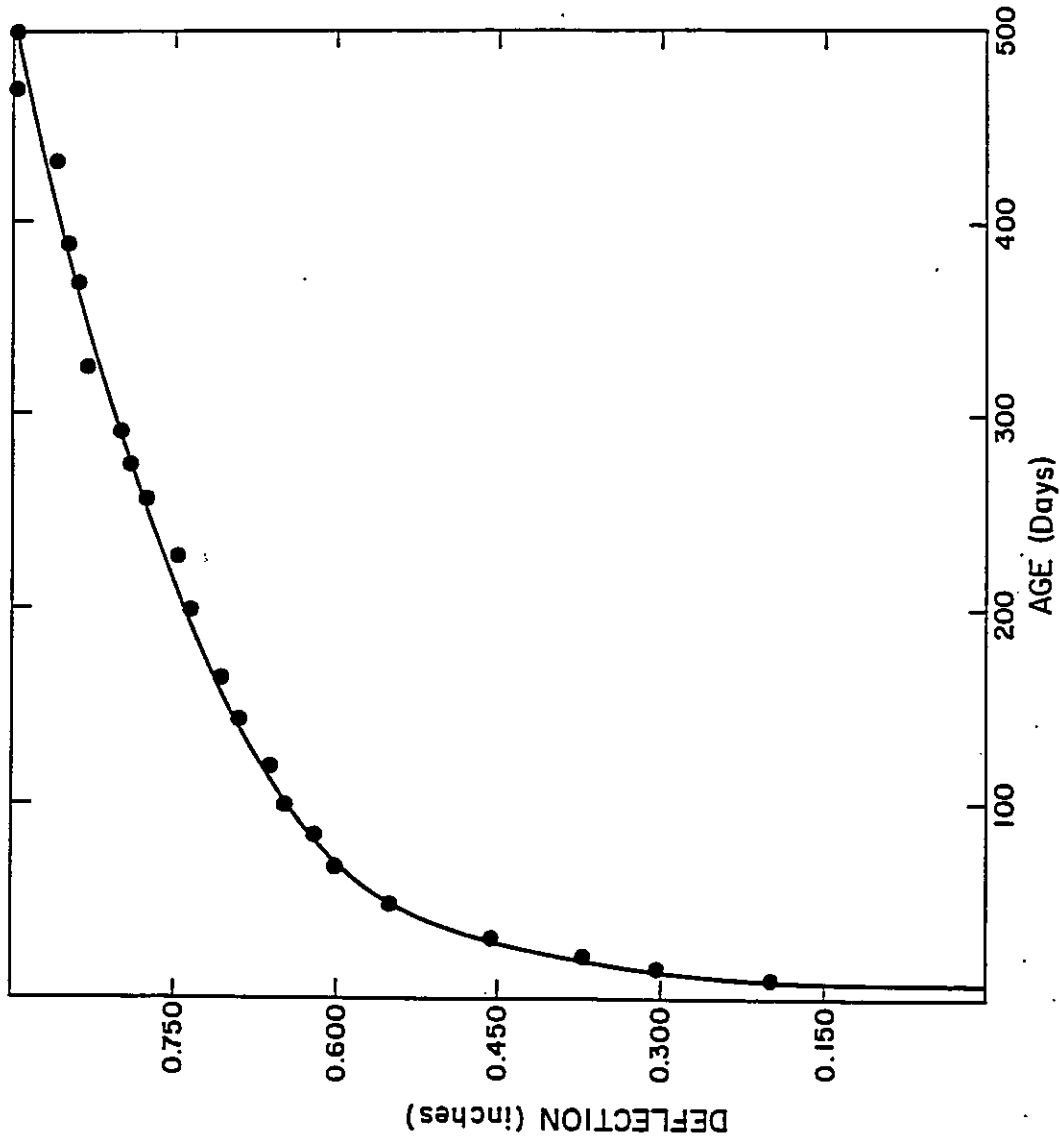


FIGURE 2.12 BEAM C LONG TERM DEFLECTIONS

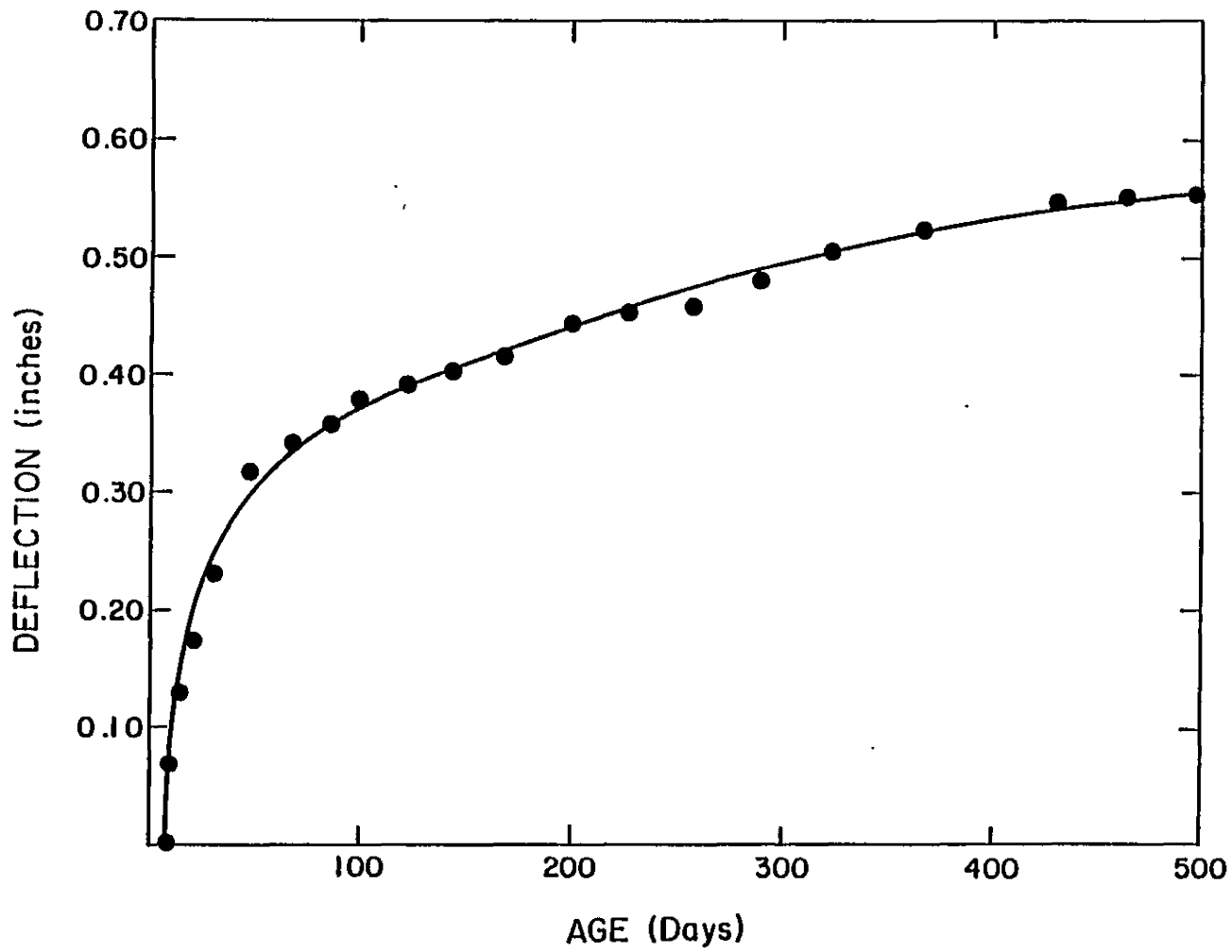


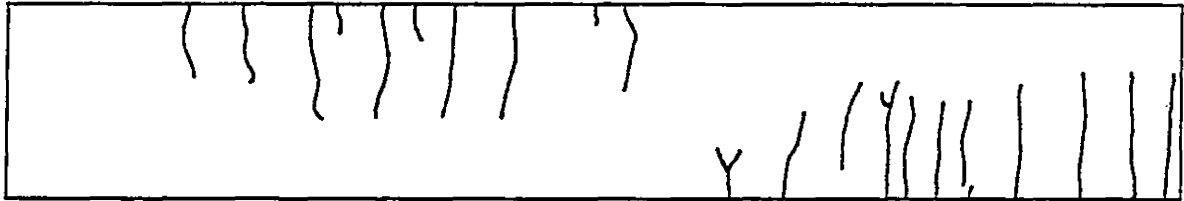
FIGURE 2.13 BEAM D LONG TERM DEFLECTIONS

Beam C was .670 inches, and .487 inches for Beam D. These values represented the combined effects of shrinkage, creep, and increased loads. Crack patterns for the two beams can be found in Figure 2.14.

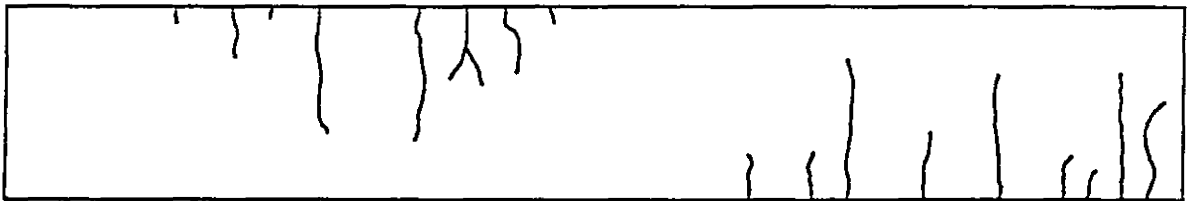
Series 3

The results of Series 3 gave a much better picture of the behaviour of a beam under constant loads than did the other two series. Although there was some change in the applied loads with time, the mid-span moments of these beams changed very little. It is therefore reasonable to assume that the measured deflections represented the constant load condition very well. The load deflection curves for Beams E and F are presented in Section 3.5. The loading procedure used with Beams E and F was somewhat different from that used for Beams C and D. The loads of E and F were applied proportionally so that the final loads at all locations were reached at the same time. This meant that the loads on the load cells in the center span increased at a faster rate than those at the ends. This scheme was easier to monitor and was easier to simulate in a finite element model than the previous scheme. Beam E had a short term deflection of .143 inches and Beam F had a short term deflection of .070 inches.

The long term deflection curve for Beam E is shown in Figure 2.15. The time dependent deflection for this beam was .316 inches, which meant that the long term to short term deflection ratio was 2.2. Figure 2.16 shows the long term deflection curve for Beam F, where the time dependent deflection was .202 inches, and the ratio of long term to



BEAM C



BEAM D

FIGURE 2.14 CRACK PATTERNS FOR BEAM
C AND BEAM D

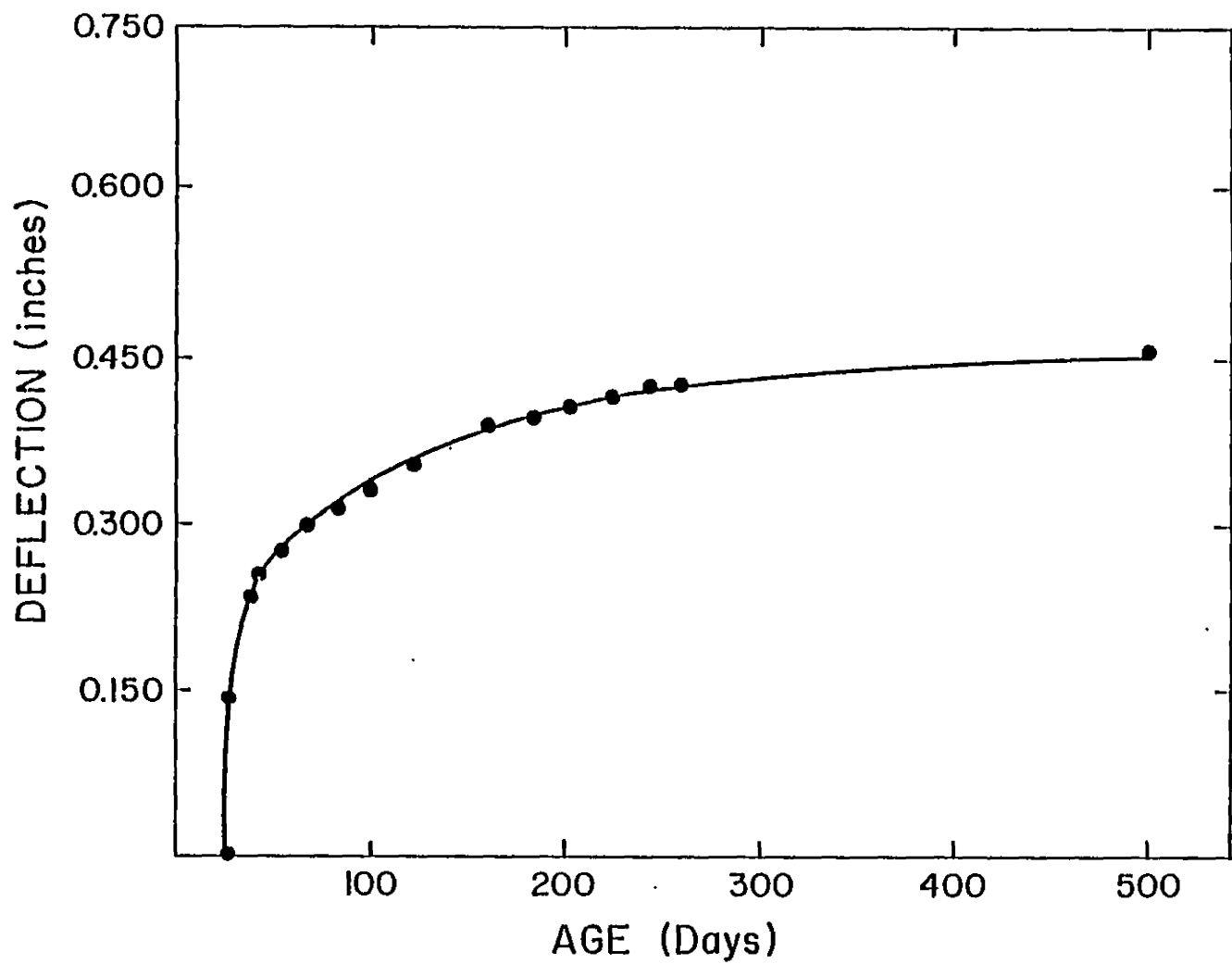


FIGURE 2.15 BEAM E LONG TERM DEFLECTION

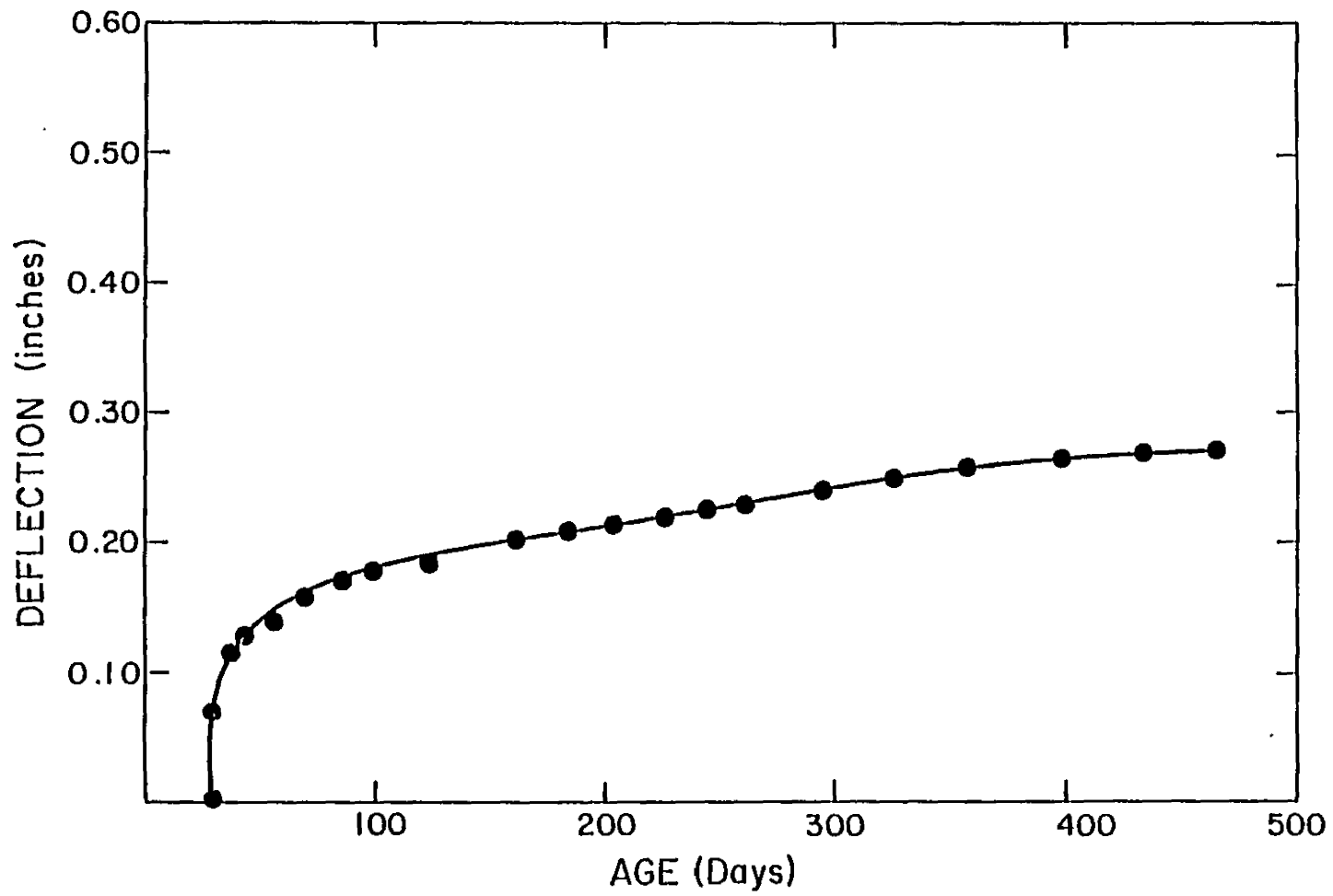


FIGURE 2.16 BEAM F LONG TERM DEFLECTION

short term deflection was 2.9. These ratios are again significantly higher than the Code predictions and would have been even higher had the test continued for a longer period of time.

2.4.4 Summary

The most significant fact which emerged from the long term test results was the evidence that the ACI Code approach for predicting long term deflections is not always very accurate. In addition, based on the values observed from these tests, there does not seem to be any conservatism built into it. The long term deflections from Series 1 and Series 3, which represented constant and slightly dropping load conditions, were all higher than the Code predictions. In a deflection sensitive structure this could cause damage and inconvenience. The results also gave some indication that the Code approach of treating simply supported beams and continuous beams the same way may not be advisable. The continuous beams tested in this program had high compression steel ratios, and yet their deflection ratios were also very high. This may be due to the fact that the action in one high moment region of a beam may significantly affect the long term deflections in another. While recognizing that the Code equations need to be simple, there is obviously a need for a more accurate approach, or, failing that a more conservative approach. Unlike Series 1 and Series 3, Series 2 did not provide much of an insight into the performance of the Code equation, but it did show how deflections are affected by changing loads. Structural members are rarely subjected to constant loads throughout their design lives, and deflections may vary between high and

low extremes. Designers must keep this fact in mind when assessing the influence of deflections. Another fact that surfaced during the test was the apparent long term sensitivity of the test equipment. Durability is a key element because equipment which appears to be perfectly acceptable in a short term test may fail over the long term.

The experimental data presented in this chapter served other purposes besides testing the accuracy of the present ACI Code prediction method. It was also used to check the accuracy of the finite element model detailed in Chapter 3, and will provide long term deflection data for future researchers. Hopefully the data will help further the knowledge of long term deflection behaviour and aid in the development of a successful method for treating deflections in design.

CHAPTER 3

FINITE ELEMENT MODEL

3.1 Constitutive Relationships

3.1.1 Strength and Elastic Relationships

Accurate constitutive stress and stress-strain relationships are very important for the overall accuracy of finite element solutions. This is not a major problem when all of the necessary experimental data is readily available, but often this is not the case. When experimental values have not been provided it becomes necessary to use empirical prediction equations to fill in the missing information. Although these prediction methods may be very useful, it must be remembered that they are really only approximations of the correct values. This section contains a review of the established prediction methods which have been developed for the tensile strength of concrete, the modulus of elasticity of steel and concrete, the compressive strength of concrete, and the changes of these values with time. Also their proposed use in the finite element model presented later in this chapter will be examined.

Modulus of Elasticity of Concrete

The modulus of elasticity is probably the most important material property used in a finite element analysis. It represents the stiffness of the material and is found from the stress-strain diagram. In the case of concrete, the calculation of the elastic modulus is complicated by its nonlinear nature. Fortunately the concrete stress-strain relationship is approximately linear up to maximum stresses of about 75% of ultimate (38), and an average value, usually defined as a secant modulus, can acceptably represent the behaviour in this range. Since this study was mainly concerned with the service load state, it was possible to use the secant modulus exclusively to represent the stiffness of the concrete.

Predicting the modulus of elasticity of concrete is very difficult and has not yet reached a very high level of sophistication. It is generally accepted that the modulus of elasticity can be approximated by an equation which is a function of the compressive strength and the unit weight of concrete (8). Most of the prediction methods now available relate the elastic modulus to these two quantities. Because the actual relationship is much more complicated than this, current equations are not very accurate (8). Other factors which influence the modulus of elasticity include, the condition of the specimen when tested, the properties of the aggregate, the mix proportions, the age of the specimen, and the curing conditions.

The modulus of elasticity prediction method chosen for use with the proposed finite element model was suggested by Branson (8) and is as follows:

$$E_c = (39.0 - .0015 f'_c) \sqrt[3]{w f'_c} \quad (3.1)$$

where E_c = modulus of elasticity (psi)

f'_c = compressive strength (psi)

w = unit weight (pcf)

Branson reported that in a comparison with 274 experimental values, about 62% of the data fell within 10% of the values calculated by this equation, 83% fell within 20% of the calculated results, and 95% were within 30%.

Most of the preceding discussion was concerned with the stress-strain relationship of concrete in compression, but concrete exhibits a different behaviour in tension. Houde (27) reported that the stress-strain curve in tension was nearly linear up to 90% of the ultimate strength, and a straight line could be used to represent its behaviour without any significant loss of accuracy. It was therefore assumed in this study that concrete was linearly elastic in tension until failure. Information on the tensile modulus of elasticity of concrete is very rare and there are no readily recognized prediction methods that can be used in the absence of experimental data. Therefore, it was necessary to assume that the modulus of elasticity in tension was the same as that in compression, although this is only approximately correct.

Modulus of Elasticity of Steel

The modulus of elasticity for steel is a much easier property to predict than the corresponding value for concrete. When more exact information is not available, ACI Standard 318 (2) has suggested that a value of 29,000,000 psi can be used as the modulus of elasticity for reinforcing steel. Since steel is not a highly variable material, this value should always be reasonably close to the correct one. In the range of stresses which were considered in this study, steel is linearly elastic, and failure is not a factor. Therefore incorporating the reinforcement properties into the finite element model was relatively simple and accurate.

Tensile Strength

The tensile strength of concrete is not usually a very significant design parameter, but in a finite analysis which must predict the onset and progression of cracking, this parameter is extremely important. Unfortunately experimental tensile strength is rarely reported in the literature, and it is usually necessary to use a prediction formula to determine it. Towards this end, researchers have developed a few relatively simple equations which relate the tensile strength to the compressive strength. The tensile strength of concrete is an extremely difficult quantity to measure, but it is generally thought that the modulus of rupture gives a fair representation of the cracking behaviour in beams (38). Therefore, in this study, whenever a reference is made

to the tensile strength of concrete, it will actually be the modulus of rupture that is being discussed.

Researchers have discovered that many of the factors which affect the compressive strength also affect the tensile strength (8), and prediction formulas have been designed to reflect this relationship. Unfortunately the relationship between tensile strength and compressive strength is very complex and is also affected by the age and strength of the concrete, the type of curing, the degree of compaction, and the methods used to measure the two strengths. This, and the fact that the tensile strength is normally a highly variable quantity makes its prediction extremely difficult.

In the finite element model of this study, the following prediction equation suggested in the ACI Code (2) was used to represent the tensile strength when reliable experimental data was not available.

$$f_r = 7.5\sqrt{f'_c} \quad (3.2)$$

where f_r = modulus of rupture (psi)

f'_c = compressive strength (psi)

It should be noted that this equation is very approximate, and values between $7.5\sqrt{f'_c}$ and $12\sqrt{f'_c}$ have been reported (8) for normal weight concrete.

Compressive Strength and Time

This study was primarily concerned with the service load state, so the compressive strength of concrete ($f'c$) was not itself an important material property. However, $f'c$ was one of the major variables in the prediction equations for the tensile strength of concrete, the modulus of elasticity of concrete, and the bond properties. Since these values were important, the compressive strength was needed for the analysis.

The compressive strength at the time of a test is usually specified so it is rarely necessary to use prediction equations to estimate it. However, equations may be necessary when a prediction of the change in compressive strength with time is required. In this study predictions of changes in compressive strength with time were necessary because the tensile strength, modulus of elasticity, and bond properties were all time variant, and their prediction was dependent on $f'c$. Branson (8) proposed the following hyperbolic design equation which was used in this study to define the gain in the compressive strength with time. For moist cured, normal cement:

$$(f'c)_t = \frac{t}{4.00 + .85t} (f'c)_{28d} \quad (3.3)$$

where $(f'c)_{28d}$ = 28 day compressive strength

t = time (days)

Similar equations were suggested for moist cured high-early strength cement, steam cured normal cement, and steam cured high-early strength

cement. These equations imply that the development of strength is dependent on the type of cement and the curing conditions, but obviously there are also other factors. When testing his equations, Branson found that in a comparison with 253 test specimens, 62% of the data fell within 10% of the values calculated by his formulas, and 93% were within 20% of the calculated values.

Discussion

The accurate prediction and representation of the elastic and strength properties of concrete and steel have significant effects on the ultimate accuracy of finite element solutions. Unfortunately, it is not always possible to rely on empirical prediction methods for missing information. Prediction methods have been developed for the tensile strength of concrete, the modulus of elasticity of steel and concrete, and the changes in the compressive strength with time. Some of these equations have been presented in this section. In nearly every case the compressive strength is the only unknown variable in the prediction equations. Unfortunately the material relationships are much more complicated than this, and the formulas are usually not very accurate. This situation may have arisen because researchers in the past seemed willing to sacrifice accuracy for simplicity. Although this may be acceptable for design purposes, it significantly limits the effectiveness of analytical models which rely on these equations. More accurate relationships are required to improve the situation, but for now it is necessary to use the methods that are currently available. If the limitations of these prediction methods are properly understood, they

can still be extremely useful because they usually give a fair estimation of otherwise unknown material properties.

3.1.2 Shrinkage

Introduction

It is well known that concrete changes its volume when it is subjected to variations in moisture content. When it gains water it expands, and when it loses water it shrinks. Concrete is seldom continuously saturated so shrinkage is the moisture change which is usually most important to engineers. This study is concerned with the time dependent behaviour of reinforced concrete, and therefore it is necessary to accurately model concrete shrinkage. The fact that shrinkage is highly variable and not uniform throughout a specimen, means that it is difficult to simulate it analytically. When experimental data is not available, the problem is even more difficult because prediction methods are needed to determine shrinkage strains. Since these strains are often not reported in the literature, the prediction of shrinkage formed a necessary part of this study.

The currently accepted technique for predicting shrinkage is to relate it to material and storage parameters. This approach of predicting shrinkage has been examined in many studies (3)(4)(8) and many empirical prediction methods have been proposed. Unfortunately there is no universal agreement on the identity of all of the important factors that influence the shrinkage behaviour, and the empirical methods which

have been developed are very dissimilar in form and give widely differing solutions. Hence the objective of the following discussion is to examine the prediction of shrinkage strains and to select the prediction method best suited for inclusion in a finite element model.

Prediction Methods

The shrinkage mechanism, and thus the parameters affecting shrinkage are not completely understood. Since a rational theory for shrinkage is not available, prediction methods have been developed empirically by studying the influencing parameters and assuming their effects. As mentioned earlier, researchers have attempted to identify these factors experimentally, but there is little agreement on which factors should be included in an equation. Complicating the problem is the difficulty in identifying any interdependence between parameters. The cement paste parameters which have been identified include the water/cement ratio, cement content, cement composition, air content, and moisture content. The aggregate parameters have been reported to consist of the aggregate stiffness, the total aggregate content, and the gradation. Other factors such as the relative humidity, temperature, time of drying, and member size have also been identified (3)(4)(8)(37)(38). The quantitative effects of those parameters on the shrinkage curve are difficult to determine, and to properly develop an accurate empirical design method, it is necessary to use a very large and well organized statistical sample. This does not seem to have been done yet.

Numerous prediction methods have been developed over the years. These vary from very simple equations to quite complex relationships. All of the methods can be separated into two main groups. In the first group, a shrinkage curve is defined for a set of standard conditions which can be modified for nonstandard conditions. In the second category, the entire shrinkage curve is derived from empirically based equations. It should be noted that these prediction methods have very little theoretical basis and are almost entirely empirical in nature. None are capable of predicting shrinkage strains exactly and they can never really replace the acquisition of reliable experimental data. In the next few paragraphs the available shrinkage prediction methods are examined, and the specific ways in which they predict shrinkage are detailed. From this review a method was selected for use with the finite element model.

Schorer, 1943 (8)

Schorer introduced one of the first shrinkage prediction equations, shown below. This simple relationship highlighted the importance of the relative humidity on the ultimate shrinkage strain. It did not however give the complete shrinkage curve.

$$E_{shu} = 12.4 \cdot 10^{-6} (90-H)$$

Naturally this equation is not very accurate because it depends exclusively on the relative humidity, and there are many more factors involved. It has been reported that the strains predicted by this

equation are usually much less than the actual values (8), nevertheless, this equation did provide an important first step towards the development of more accurate methods.

Jones, Hirsch, and Stephenson, 1959 (8)

Jones, Hirsch, and Stephenson proposed a method for predicting shrinkage of lightweight concrete using standard curves. A single curve was derived empirically for specific concrete mix and storage conditions. When the cement content, slump, air content, percent fines, relative humidity, or size differed from the standard conditions, the shrinkage curve was modified with empirically derived correction curves. Although this method was developed specifically for lightweight concrete, it does not appear to be any less accurate for normal concrete (8).

Meyers, Branson, Schumann, and Christiason, 1970 (33)

Meyers, Branson, Schumann, and Christiason proposed a shrinkage prediction method that was very similar to the method suggested by Jones et al. A hyperbolic equation was used to characterize the time dependence of concrete shrinkage, and a standard curve was introduced for a set of fixed mix and storage parameters. Correction factors were applied to the standard shrinkage curve when other conditions were present, and these factors were determined from test data for which the only variable was the parameter under consideration. This technique effectively eliminated the possibility of detecting any interdependence

between the variables. The important parameters which were used in the analysis were the relative humidity, the age, the dimensions, the slump, the percent fines, the cement content, and the air content. These factors are essentially the same as those suggested by Jones et al. This method was later adopted in the ACI Code for the prediction of concrete shrinkage in the absence of experimental data.

CEB 1978 (13)

The CEB adopted a simplified empirical prediction method for the calculation of shrinkage which used a standard shrinkage curve. This curve was related to the specimen dimensions and was modified for the effects of relative humidity, cement type, and temperature. The modification factors were presented in tables and graphs, and although this is useful for design purposes, it is not directly applicable to computer programs. A potential weakness of the CEB procedure is the fact that there is no provision for the effect of mix parameters. It has been noted that this could have a serious impact on the accuracy of its solutions because these factors are actually very important (4). The method seems to be an updated version of the one introduced in 1970, but the 1970 CEB (8) method also included the effects of the water/cement ratio and the cement content. It is possible that simplifications may have been made in the current procedure to accommodate designers. Designers do not usually have access to mix properties and would not be able to use a more complex relationship.

Bazant and Panula 1978 (3) (4)

Bazant and Panula proposed a square root hyperbolic prediction method for shrinkage in which the entire shrinkage curve was calculated from empirically based equations. This prediction method was developed exclusively for normal concrete and there is no provision for the treatment of lightweight concrete. Although the formulas were empirically derived, there was a certain theoretical basis in their development. Diffusion theory was used to determine the effect of specimen size and shape on the shrinkage curve. The other parameters in the relationship, whose effects were found empirically, included relative humidity, temperature, water/cement ratio, cement content, the aggregate/cement ratio, gravel/sand ratio, sand/cement ratio, modulus of elasticity, and 28 day compressive strength. A wide range of experimental data was used to develop the empirical formulas, and computer optimization techniques were used to determine the constants and coefficients. In this way it was possible to include the interdependence that may have existed between variables. This capacity for including interdependence is this method's greatest advantage.

Summary

Bazant and Panula's method was chosen in this study as having the greatest potential for accurately predicting shrinkage strains in a finite element model. Shrinkage data from 11 different sources were used to develop these formulas, which seems to be more than was used for the other methods reviewed. It is also the most complicated method, and

although complexity does not always improve accuracy, the added complexity allows for the inclusion of more effects. In assessing their approach, Bazant and Panula used all of the experimental data they could find to compare their equations with the CEB and ACI methods. This comparison indicated that their equations performed best. This evidence seems to support the selection of this method.

3.1.3 Creep

Introduction

The time dependent behaviour of concrete is influenced by two main properties, shrinkage and creep. Both of these phenomena have significant effects on the long term deflections of reinforced concrete beams and an accurate finite element model requires a good representation of both of them. Although there appears to be some interdependence between shrinkage and creep, it is normal to treat them separately. This section will examine the inclusion of creep.

Creep can be defined simply as the time dependent deformation of concrete due to applied stresses. Like shrinkage, the inclusion of creep strains in an analytical model is not a simple task, even when reliable experimental data is available. If data has not been provided, an empirically based prediction method is required to generate creep strains. Numerous studies have been devoted to creep prediction but none of them have so far been completely successful in developing a method that is always reasonably accurate. It is the object of this

section to review creep and creep prediction, and to provide the rationale for choosing a method for use with the finite element model.

Various hypotheses have been developed to explain creep but no agreement has yet been reached on which explanation is the correct one. Most of the creep mechanisms that have been proposed so far can be grouped into a few general theories. Viscous and visco-elastic flow, solid solution, thermodynamic, deferred elasticity, and seepage theories have all gained some acceptance (37). None of these theories completely explains the causes of creep, so the true mechanism may be some combination of them. There is some evidence (3)(37) that there are two distinct components of creep. One takes place in the absence of moisture movement between the concrete and the atmosphere and is called basic creep, and the other is affected by the drying process and is called drying creep. An accurate prediction method must consider both parts. The difficulty in measuring and separating creep and shrinkage, basic creep and drying creep, and the uncertainty surrounding the creep mechanism, may account for the relative inaccuracy which is evident in current creep prediction methods.

Prediction Methods

Since there is no general theory for creep, researchers have had to rely on experimental data to identify and quantify the influencing parameters in a creep relationship. There is no overall agreement between researchers about which variables should be included in a creep relationship and this has led to the development of widely differing

prediction methods. The prediction of creep from material and environmental parameters has developed in much the same way as for shrinkage. More research work has been done with creep than with shrinkage, but this does not seem to have made its prediction any more accurate. All of the available prediction methods can again be separated into two main groups. The creep curve in the first group is specified for a certain set of standard conditions which can be modified for nonstandard conditions. In the second group the entire creep curve is calculated uniquely from empirical relationships. Unless otherwise specified, the prediction methods reviewed in this section have combined basic and drying creep together, implying that the time shapes of the two curves are the same. Care must be taken when using methods employing this simplification because there is some evidence that this assumption may not be exactly correct (3). The following section will review the prediction of creep and explain the choice of the method used in the finite element model presented later.

Ross 1937 (37)

Ross provided some of the earliest work on creep and creep prediction. He suggested that the creep time curve was best represented by a hyperbolic function, and this contention has generally been supported by subsequent researchers (33). Ross used an empirically based prediction chart to estimate the effects of mix and storage parameters on the creep curve. He assumed that creep strains were dependent on the stress level, the water/cement ratio, the relative humidity, the age of loading, and the diameter of the specimen. Although this method is

mainly of historical interest now, Ross' work formed the foundation of many subsequent investigations.

Wagner 1958 (8)

Wagner was one of the first researchers to use standard curves and correction factors for creep prediction. He suggested that the ultimate specific creep of a normal weight concrete was related to age of loading, type of cement, relative humidity, cement paste content, water/cement ratio, and the minimum dimension. A standard creep coefficient was presented for fixed mix and storage properties which was used as a reference point in the creep analysis. Empirically derived correction factors were used to modify the standard creep coefficient when nonstandard conditions were present. Unlike most current prediction methods, only the ultimate specific creep was calculated by this method. Since many researchers have found that the creep of lightweight concrete is not significantly different from the creep of normal concrete (8)(37), this method would probably be valid for both cases.

Jones, Hirsch, and Stephenson 1959 (8)

The procedure that was developed for creep by Jones, Hirsch, and Stephenson is very similar to their method for shrinkage. A creep curve

for lightweight concrete was presented for standard conditions of cement content, slump, air content, percent fines, stress level, size, relative humidity, and age of loading. The standard creep curve was modified with empirically developed correction factors when nonstandard conditions existed. Apparently the authors thought that the factors that influence shrinkage were essentially the same as the factors which affected creep since the parameters they chose were the same for both relationships. This method was developed from data on lightweight concrete. As mentioned earlier, the creep of lightweight concrete is probably similar to the creep of normal concrete, so this method is probably applicable for both cases.

Meyers, Branson, Schumann, and Christiason 1970 (33)

Meyers, Branson, Schumann, and Christiason proposed a prediction method for creep which is also very similar to their method for shrinkage. This method might be considered an updated version of Jones et al's creep method because the important parameters in both instances are essentially the same. The hyperbolic specific creep curve was used by the authors to represent the creep time curve for concrete. Standard conditions of relative humidity, size, age of loading, slump, air content, cement content, and percent fines, were defined for a particular concrete and a reference creep curve was presented. This curve was modified with empirical correction factors when any other conditions were present. The correction factors and the standard creep curve were developed from mixed experimental data for normal and lightweight concretes, and for Type I and Type III cements. This method was adopted by the ACI (1) as a suggested creep prediction approach.

CEB 1978 (13)

The creep prediction method introduced by the CEB in 1978 is a major departure from the formulation they suggested in 1970 (8). In the 1978 version, creep was divided into two parts consisting of a reversible (delayed elastic) part and an irreversible part. The irreversible creep was also divided into two parts. The first represented the irreversible component of the deformation which develops during the first few days after loading, and the second represented the irreversible delayed deformation (flow) which is primarily affected by the age of the concrete when loaded. From this theoretical basis, an empirical prediction method was developed. The total creep coefficient was assumed to depend on relative humidity, composition of the concrete, dimensions of the specimen, temperature, and rate of hardening of the concrete. The creep curves for the reversible and irreversible components were calculated separately and later combined to represent the total creep. The recoverable part of the delayed deformation was assumed to be independent of aging in its development, and a single creep time curve applicable for all conditions was defined. The irreversible creep was calculated from the concrete strength, the relative humidity, the dimensions, the age of loading, and the temperature. The fact that the composition of the concrete was not included in the analysis may mean that this method was primarily intended for designers. If this is the case, it may not be accurate enough for analytical models. The method is also not directly adaptable to computer modelling because the creep curves and coefficients are presented in charts and tables which do not readily lend themselves to computer programming.

Bazant and Panula 1978 (3) (4)

Bazant and Panula proposed a unique creep prediction method that is more complex than any of the other methods which have been presented. In their formulation the total creep was separated into a basic creep component and a drying creep component, and both were evaluated separately. The authors felt that this was necessary because the basic and drying creep time curves did not have the same shape. By examining a wide range of experimental data, Bazant and Panula developed an empirical creep prediction method by using computer optimization techniques. They related the basic creep to water/cement ratio, age when loaded, compressive strength, aggregate/cement ratio, sand/cement ratio, aggregate/gravel ratio, and type of cement. The drying creep was related to relative humidity, age when loaded, compressive strength, sand/aggregate ratio, water/cement ratio, gravel/sand ratio, final shrinkage strain, and member dimensions. The presence of a shrinkage-type function in the drying creep equations seems to indicate that Bazant and Panula did not simply assume that shrinkage and creep were additive. This agrees with experimental evidence. Although these prediction equations were almost entirely empirical, they did have some theoretical justification because diffusion theory was used to analyze the effect of member size and shape on the drying creep. The authors stated that their prediction method was applicable to all creep periods including very long time creep and very short time creep. Most other methods cannot make this claim.

Summary

After careful consideration the creep prediction method chosen as the most appropriate for use with the finite element model presented later in this chapter was the one proposed by Bazant and Panula. Bazant and Panula used experimental data from 36 sources to derive their equations, and this appears to be more than was used to derive the other methods which were reviewed. Their method had some theoretical basis and their statistical analysis seemed reasonably detailed. In addition the equations used in their method were easily incorporated into a computer program. For these reasons the Bazant Panula method was selected for use in this study.

3.1.4 Creep Under Variable Stresses

Most research work on creep has been devoted to the effects of constant stresses, but since concrete structures are rarely subjected to constant stresses throughout their design lives, it is important to understand the influence of variable stresses on creep. Even when the applied loads on a member are kept constant there can be significant variations in stress due to indeterminacy or the movement of the neutral axis. A proper representation of creep must include some provision for this condition.

A number of theories have been proposed to treat the effect of variable stresses on creep, but all have problems with accuracy and adaptability. This is not surprising because there is a limited supply

of experimental data available on this subject and researchers have had to draw their conclusions from small statistical samples. The analysis is further complicated by the high variability normally associated with long term properties.

Four main methods have been proposed for computing creep under varying stresses and these have been identified as the Effective Modulus Method, the Rate of Creep Method, the Method of Superposition, and the Rate of Flow Method. This section will examine the techniques which have been proposed for treating the effects of variable stresses on concrete creep and discuss how the phenomenon was considered in the finite element model to be presented later in Chapter 3.

Effective Modulus Method

The Effective Modulus Method is the least sophisticated proposal for considering the influence of variable stresses on creep. In this method a normal elastic analysis is used to determine the short term behaviour of concrete, but the modulus of elasticity is replaced by an effective modulus when the effect of creep is considered. The effective modulus is a reduced modulus of elasticity which represents the sum of elastic and creep strains. The effective modulus can be defined as:

$$E'_c = \frac{E_c}{1 + C_1 E_c}$$

where $E'c$ = effective modulus

E_c = elastic modulus

C_1 = specific creep (creep strain/unit of stress)

This method is the easiest one to apply to an analytical model because it only requires the replacement of the modulus of elasticity. In this regard it can be very useful in some cases.

Rate of Creep Method

The Rate of Creep Method is a little more theoretically complex than the Effective Modulus Method but it does seem to give better results. This method assumes that the rate of creep is independent of the age of loading and the previous stress history. The rate of creep for a certain stress in an interval of time is known, and by differentiating the specific creep curve, the creep under a variable stress can be defined as:

$$c = \int_0^t f\left(\frac{dc_1}{dt}\right)dt$$

where c = creep

$\frac{dc_1}{dt}$ = rate of creep

dt = time increment

f = stress during time increment

The Rate of Creep Method is reasonably simple to apply and in many instances gives acceptable results. The method generally overestimates creep under a decreasing stress (18).

Method of Superposition

The Method of Superposition is probably the most tedious method to apply numerically to a creep problem but it also has some significant theoretical advantages over the other methods mentioned. The principal advantage of this approach is that it allows for the consideration of stress history. Variable stresses are treated in this method by superimposing the creep curves for each applied stress, where stress decrements are considered as increments of negative stress. Strains produced in the concrete by a stress increment at any time are considered to be independent of the effects of stresses applied at any other time.

Rate of Flow Method

The Rate of Flow Method is the latest creep formulation which allows for the consideration of the effect of variable stresses. In this method the total creep is divided into a reversible (delayed elastic) part and an irreversible (flow) part. The implication is that reversible and irreversible creep are caused by different mechanisms and variable stresses only affect the delayed elastic component. This assumption tends to contradict the superposition principle which assumes that creep is a single reversible phenomenon. The effect of stress history and creep recovery are implied in the Rate of Flow Method and there is some theoretical justification in its development. This method is not generally applicable to all creep problems because the separation of the reversible and irreversible components means that only the 1978

CEB creep prediction method, or specific experimental data, can be used to analyze creep.

Discussion

For this study it was anticipated that concrete would be subjected to some variations in stress and it was therefore necessary to account for this effect in the creep formulation. None of the methods which have been described are consistently accurate for variable stresses and there is no general consensus as to which is the best one to use. It has been stated that all of the suggested methods give an adequate representation of creep for small or gradual changes of stress, and when this occurs the simplest method is probably the best (37). However, when large or sudden changes in stress are experienced, the methods can give very different solutions.

In this study the Rate of Creep Method was chosen to represent the creep for variable stresses because this method provided the best combination of generality, computational efficiency, and accuracy. Theoretically and numerically this may not be the most accurate method available, but the following examination of some of the practical difficulties associated with the other methods, and creep analysis in general, should explain the choice.

The Effective Modulus Method suffers from a number of serious weaknesses and is not usually appropriate for a creep analysis unless it is substantially modified (46). In its normal form this method predicts

complete strain recovery when the stresses in the concrete are removed. In actual fact concrete does not exhibit this kind of behaviour. In addition, since the effective modulus does not have the same value as the modulus of elasticity, it does not give the correct solution for an instantaneous change of strain due to a changing stress. With decreasing stresses the strains are generally underestimated and with increasing stresses the strains are usually overestimated (18). These deficiencies combined with the omission of the effect of stress history, effectively eliminates this method for all but the simplest creep analyses.

The Rate of Flow Method has some theoretical justification but the validity of dividing the creep into reversible and irreversible components is still open to question (3). There is a major difficulty with applying this method to concrete creep because if the 1978 CEB creep prediction method is not used, specific experimental data is required to determine the reversible and irreversible strains. This information is rarely available and the 1978 CEB prediction method seems overly simplified for a detailed analysis.

The superposition method also has some theoretical justification but the required computational effort is substantial because the creep equations need to be modified at each load level. Although this method is often fairly accurate for increasing stresses (18), researchers have found that the principle of superposition may give erroneous results, particularly where changes in load cause a decrease in the total concrete strain (44). In addition the superposition method cannot be

applied to all creep analyses because a creep curve needs to be defined at the age of each load change. This is possible when prediction equations are used to determine the creep relationship but is usually unrealistic when experimental data is used. This is particularly true for a constantly changing load. Even when the use of the Method of Superposition is possible, the computational effort can be substantial.

It is generally recognized that Rate of Creep Method is not the most accurate one available for treating the effects of variable stresses but unavoidable sources of error tend to reduce the superiority of the more complex methods. Whether the creep strains are determined experimentally or with prediction equations, significant inaccuracies are inevitable. For example, the creep strains in the parametric study were generated with the Bazant-Panula prediction method and this method has an expected error range of about $\pm 20\%$. An error of this magnitude virtually eliminates the benefits of using a more exact and complex formulation for variable stresses. The increased costs cannot be justified. When experimental data is used to determine the creep strains, the high variability which is normally observed in long term tests reduces the accuracy of the results. In addition, the conditions under which creep tests are conducted are not exactly the same as those experienced in beams. It is therefore unrealistic to expect the creep curves to be the same. In particular the effect of size must be recognized as a factor that affects the curves for creep specimens and beams differently.

There are some simplifications usually made for creep which also affect the accuracy of creep analyses and these may also limit the effectiveness of using a complex creep method. One simplification which has some effect on creep results is the problem of using uniaxial creep data to represent multiaxial creep behaviour. Creep strains from experimental and prediction equations are usually derived from uniaxial stress states, while concrete is usually subjected to multiaxial stresses. Jordaan and Illston (28) found that although there were strong similarities between uniaxial, biaxial, and triaxial creep, there were also significant differences. Since the results from uniaxial tests are usually used to represent the three dimensional case, it is inevitable that this factor will cause some error in the solution.

Another simplification affecting creep analysis to some degree is the assumption that creep in tension is the same as creep in compression. The range of tests on creep in tension is inadequate for any systematic quantitative information to be derived (37), but experimental results tend to indicate that there can be significant differences between tensile and compressive creep. It is difficult to assess the importance of the difference between creep in tension and compression because the tensile stresses in beams are not very high, but it is important to recognize this as a possible source of error.

Another source of inaccuracy present in all of the methods dealing with variable stresses is the assumption that stresses are constant through each time increment, and that when changes do occur they occur in discrete steps. This is not really true for the class of structures which were examined in this study because the stresses in

these members did not change in a stepwise fashion. A highly accurate solution would require the selection of very small time increments which would drastically increase the computational costs. If this was not done the accuracy could be reduced.

Summary

Research into concrete creep is usually related to constant stress states but since concrete structures are usually subjected to variable stresses it is important to consider this fact in a creep analysis. The four techniques described in this section for treating variable stresses ranged from simple and inaccurate formulations to complex and fairly accurate formulations. Unanimous agreement between researchers about which is the best method for handling variable stresses does not exist. It seems that Europeans tend to favour the Rate of Flow Method while North Americans seem to prefer some form of the Method of Superposition. This is reflected in the literature on the subject. In this study it was determined that the Rate of Creep Method was probably the most suitable method for inclusion in the finite element model presented later in this chapter. It was fairly simple to apply and its accuracy was expected to be acceptable. Neville (37) concluded that the Rate of Creep Method was adequate for most creep analyses where exact results were not required, and this suggestion weighed heavily in the choice. Basic inaccuracies not related to the methods themselves tended to reduce the advantages of the more complex and accurate methods, and thus their additional cost and effort were deemed unjustifiable.

3.1.5 Bond Stress And Bond Slip

Introduction

The exact nature of the bonding between concrete and reinforcement is both complex and largely unknown. This is unfortunate because a proper representation of reinforced concrete behaviour using the finite element method requires some understanding of the interaction between the concrete and the reinforcement. In an attempt to model the bond phenomenon, a few simple bond stress-slip relationships have been proposed. Unfortunately there is a limited amount of useful experimental data available, and current relationships are probably only preliminary attempts in an ongoing search for an accurate constitutive law. The difficulty in accurately measuring and interpreting experimental data on bond characteristics has seriously impeded a proper understanding of this subject, and this has led to problems in identifying and quantifying the elements in a constitutive law. Despite the deficiencies in current bond stress-slip relationships, the following section will attempt to review the present status of this topic, and select the most appropriate technique for modelling the phenomenon in a finite element model.

Mechanisms

Bond stress can be characterized as the shearing stress which acts parallel to the reinforcement along the steel-concrete interface. It is thought that bond is created by three main mechanisms. These are

chemical adhesion, friction, and mechanical interlocking between concrete and steel (31). Chemical adhesion and friction are considered the primary reasons for the bond of plain reinforcing bars, while mechanical interlocking is thought to be the most prevalent for deformed bars (31).

Bond slip is present in reinforced concrete when reinforcing steel moves in relation to the surrounding concrete. Before cracking concrete beams exhibit very low bond stresses and little or no slip. The rate of change of stress in the steel along the length of the bars is relatively small at this point. It is only after cracking that bond stress and bond slip become significant. There is no real consensus on the reason for bond slip. Lutz and Gergely (31) attributed bond slip to the crushing of the concrete paste in front of the ribs of the deformed bars. This conclusion was disputed by Mirza and Houde (35) on the basis of their observations of pullout tests. They suggested that bond slip was caused by the internal cracking of the concrete layer closest to the bar, and the cracking of the small concrete teeth near the bar lugs.

Test Methods

Before discussing the prediction of bond stress and bond slip, it may be informative to examine the tests used to determine them. This will highlight the limitations and relative accuracy of any empirical formulas that were developed from them. The procedure which has been used most frequently to evaluate bond properties is the pullout test.

In this test, an embedded reinforcing bar is pulled out of a concrete cylinder or prism. Depending on the type of test, the maximum axial stress in the concrete can be compression or tension, and the reinforcing bar can be pulled out from one or both ends.

Each variation possesses a number of fundamental weaknesses. Cracking has a profound effect on bond, but when the concrete is in triaxial compression there is no possibility for the formation of transverse tension cracking. This does not reflect the behaviour in beams. This problem can be partially corrected by placing the concrete in tension, but when the reinforcement is concentrically located, the horizontal shearing stresses in the specimen may not be representative of the stresses that actually exist in beams (42). Eccentrically reinforced pullout specimens have been used occasionally to correct this problem, but even this does not eliminate all of the problems. In light of the many difficulties which are associated with the pullout test, there is some question about the validity of using it at all to simulate local bond behaviour (49).

A limited number of beams have been used to measure bond properties but these results alone are insufficient for developing empirical prediction equations. Extensive testing of full size beams would probably produce more useful and realistic data than is possible from pullout specimens, but the cost has so far been prohibitive. Even if these tests were done the results would still be flawed. The determination of local bond stress and slip is extremely difficult and very sensitive to experimental error (35). This may account for the

disparity in the results which have been published on bond properties, and the subsequent differences in reported prediction methods.

Prediction Methods

An accurate finite element model requires a reliable representation of the interaction between steel and concrete. Bond in a finite element model is usually simulated with spring elements. The stiffnesses of these elements are defined by the bond stress-slip relationship. A few simple empirical equations have been developed to relate local bond stress to local bond slip, but in view of the limitations mentioned earlier it seems probable that these formulas really only approximate the correct behaviour.

Nilson 1968 (40)

Initially, a linear bond stress-slip law was proposed by Ngo and Scordelis (39), but Nilson (40) recognized that the actual response was nonlinear. At that time the available experimental data was insufficient for the derivation of a fundamental bond law, so Nilson devised an equation indirectly from the results of Bresler and Bertero. Bresler and Bertero studied the distribution of steel strain in concentrically reinforced tensile pullout specimens. From measurements of steel strain along the reinforcing bars, Nilson was able to calculate the average local bond stresses. Bond slip was found indirectly by estimating the concrete displacements on the basis of the measured slips at the faces of the test specimens. Although there was considerable scatter, a

definite trend was recognized. The following third degree polynomial was fitted to the data and an equation was obtained which related the local bond stress to the local bond slip.

$$u = 3606 \times 10^3 d - 5356 \times 10^6 d^2 + 1986 \times 10^9 d^3$$

where u = local bond stress

d = local bond slip

No claim was made about the accuracy or generality of this equation, and it was really only intended as an example of a possible bond stress-slip law. A slip limit of 449×10^{-6} inches, corresponding to a local bond stress of 719 psi, was used as the termination point of the relationship. Nilson assumed that when the slip limit was exceeded the local bond stress became zero in the immediate vicinity of a crack. When the slip limit was exceeded elsewhere, Nilson assumed that the local bond stress remained essentially constant. Even though this equation was not practical as a universal prediction formula, it was an important preliminary step in the development of a realistic bond-slip relationship.

Nilson 1972 (41)

Further research by Nilson in 1972 resulted in a more generally applicable bond stress-slip relationship. Nilson performed pullout tests on concentrically reinforced tension specimens. He measured steel strains with strain gauges mounted in the reinforcement, and concrete

strains with embedded strain gauges. The bond slip was found indirectly from the differences between the concrete and steel strains. Using curve fitting techniques, the following bond stress-slip law was proposed which was a function of the concrete strength and the distance from the loaded end.

$$u = 3100 (1.43c + 1.5)d f'c$$

where u = local bond stress (psi) $< (1.43c + 1.5) f'c$

c = distance from the loaded end (inches)

$f'c$ = compressive strength (psi)

d = local bond slip (inches)

The most unique feature of this relationship was the dependence of the bond stress on the distance from the loaded end. In a beam this represents the distance from a crack face. Unfortunately this conclusion has not been supported by subsequent research. Edwards and Yannopoulos (19) tested a large number of pullout specimens and concluded from their results that the distance from the loaded end had no effect on bond stress or slip. This was also the finding of Mirza and Houde (35).

Venkateswarlu and Gesund 1972 (52)

Venkateswarlu and Gesund (52) approached the formulation of a bond stress-slip relationship from an entirely different direction.

They used a slip modulus to relate bond stress to bond slip. This slip modulus was derived indirectly from a crack width prediction equation. The crack width formula was obtained from experimental beam crack width data reported by other researchers. The two authors found that their slip modulus depended on the steel stress, the modulus of rupture of the concrete, the tension steel ratio, and the modular ratio. The idea of using crack widths to calculate bond slip is an interesting one, and one that probably deserves further study.

Mirza and Houde 1979 (27) (35)

Mirza and Houde tested 62 tension specimens to determine the bond properties of reinforced concrete. From these test results they developed an empirical bond slip prediction equation. This equation related the bond slip to the steel stress and the ratio of concrete to steel areas. The authors recognized that their equation was only an approximation, but in view of the high experimental variability usually experienced in tension tests, this was not considered a serious problem. To develop the bond stress-slip relationship, tension specimens with internally instrumented bars were employed. Using this data to find the bond stress, and the slip prediction equation to calculate the bond slip, an empirical nonlinear bond law was proposed. This equation was normalized to a common concrete strength and cover as follows:

$$u = 1.95 \times 10^6 - 2.35 \times 10^9 d^2 + 1.35 \times 10^{12} d^3 - .33 \times 10^{15} d^4 \quad (3.4)$$

where u = local bond stress (psi)

d = local bond slip (inches)

The maximum local bond stress for all concrete strengths and covers was reached at a local slip of about .0012 inches. After this point the bond stress was assumed to depend upon the distance from a crack face. Mirza and Houde observed from their test data that the bond stress beyond a distance of 3 to 4 inches from a cracked surface remained relatively constant after the slip limit was exceeded. When the slip limit was exceeded within 3 to 4 inches from a crack face, the bond stress was found to decrease progressively to zero. This finding agreed with Nilson's earlier comments about bond behaviour past the slip limit.

The accuracy of Mirza and Houde's bond stress-slip equation is difficult to assess because bond slip was calculated by what was admittedly an approximate equation. When the variability of this slip equation is combined with the errors which usually accumulate in pullout test results, it seems reasonable to assume that this empirically derived stress-slip formula would not give an exact representation of the bond relationship. Realistically it may only provide a rough estimation of the correct behaviour. On the positive side, the fact that some of Mirza and Houde's findings were also supported by other researchers (19)(40), and none have been seriously refuted, tends to give credence to the validity of their results. One very attractive feature of this relationship is the ease with which it can be incorporated into a finite element model.

All of the bond relationships reported in this section were developed from short term results. The main purpose of this study's analytical model however was aimed at long term behaviour. It should be recognized that the bond relationships may not be strictly applicable for this application. However until research work is done in this area it is necessary to assume that the bond behaviour of reinforced concrete for long term loading is the same as for short term loading.

Summary

It is obvious from the preceeding review that there is still a great deal of confusion surrounding the subject of bond in reinforced concrete. There is no real consensus on the true relationship between bond stress and bond slip, and researchers are still attempting to identify the parameters that affect them. The uncertainty surrounding this subject is quite understandable because of the difficulty in measuring and interpreting experimental bond data. The development of usable bond stress-slip relationships is therefore still in a preliminary stage, and current equations are simple and relatively inaccurate. Despite the weaknesses in current prediction methods, some representation of bond was required for the finite element model that was developed in this study. The equation developed by Mirza and Houde was chosen for this. Their equation was readily adaptable to a computer program, and some of their findings have also been supported by other researchers. Their equation is therefore probably as accurate as any other. More research in this area would help in clearing up the uncertainties about bond behaviour, and might aid in the development of

a more accurate bond stress-slip relationship. Until this is done, modelling of bond will always be very approximate.

3.2 Finite Element Modelling

3.2.1. Literature Review

The finite element method is a very powerful analytical tool which has only recently gained wide acceptance in the analysis of reinforced concrete. With the advent of modern high speed computers, this tool has become a practical and cost effective way to simulate the behaviour of concrete members. However, a number of material and geometric problems make the application of this method to reinforced concrete very difficult. For instance, reinforced concrete is a highly variable three-dimensional material that is composed of both steel and concrete. These materials have very different properties and the interaction between them is not well understood. The stress and stress-strain relationships for concrete are nonlinear which makes their analysis very complicated. Another significant nonlinearity is caused by progressive cracking which not only changes the geometry, but also introduces the effects of dowel action, aggregate interlocking, and tension stiffening. Concrete is also influenced by the nonlinear time dependent effects of creep and shrinkage. Modelling all of these factors with the finite element method is a significant numerical problem, that is further complicated by the fact that many of the effects are not well understood.

To date, researchers using the finite element method for reinforced concrete have focused most of their attention on developing numerical techniques which can simulate the behaviour of some of the more important factors that influence reinforced concrete behaviour. The purpose of this section is to examine some of the developments that have been made in finite element modelling of reinforced concrete, and hopefully shed some light on the possibilities and limitations that currently exist with this approach.

Ngo and Scordelis 1967 (37)

Ngo and Scordelis were among the first in 1967 to use the finite element method for reinforced concrete. In their model, the steel and concrete were both represented with two-dimensional triangular elements of unit width. Transformed section concepts were used to formulate the properties of the elements at the level of the reinforcement. The steel and concrete were both considered as linearly elastic materials. This was a significant simplification because concrete is actually highly nonlinear. The interaction between the steel and the concrete was modelled with special linkage elements. Horizontal springs connecting the steel and concrete nodes were used to represent the bond behaviour, and vertical springs were used to represent the dowel action. There was insufficient data available for the derivation of stiffnesses for the vertical springs and they were not included in the analysis. However the horizontal springs were included.

One discovery made by Ngo and Scordelis was that the horizontal linkage elements were not very sensitive to errors, since substantial variations in the stiffness of the horizontal springs did not affect the results very much. Five beams with predefined crack patterns were analyzed to illustrate the proposed model. Cracking was simulated by separating the nodes at the crack locations. This model was one of the first attempts at modelling reinforced concrete with the finite element method and although Ngo and Scordelis' model was not very practical, it did demonstrate the potential of the finite element method as an analytical tool for studying reinforced concrete.

Nilson 1968 (38)

In 1968, Nilson extended the work of Ngo and Scordelis by including nonlinear effects and progressive cracking. Plane stress triangular elements were again used to model the steel and concrete, but Nilson added the effect of concrete's nonlinear stress-strain relationship. A nonlinear bond stress-slip law was used to define the horizontal stiffness of the spring linkage elements. Instead of using transformed section concepts to evaluate the elements at the level of the reinforcement, the two materials were considered separately. To facilitate the analysis, the round reinforcing bars were replaced by an equivalent square bar. The thickness of the concrete at the level of the reinforcement was also reduced to account for the concrete material that was displaced by the steel. An incremental loading procedure was used to incorporate nonlinear effects and progressive cracking. When the principal tensile stress in two adjacent elements exceeded the

tensile strength, a crack was simulated by separating the nodes along the common edge of the two elements. This restricted the crack orientation because cracks were forced to form along element boundaries. Unfortunately this could result in incorrect crack patterns. When a crack formed the element grid was modified, and the load on the structure was released completely. Then the load was reapplied incrementally until the next crack formed. This model was much more practical than Ngo and Scordelis' model, but there was still some need for improvement.

Will, Uzumeri, and Sinha 1972 (53)

Will, Uzumeri, and Sinha analyzed the behaviour of reinforced concrete joints using plane stress rectangular elements. Cracks were assumed to form when the maximum principal tensile stress exceeded the tensile strength, but in this analysis the proper orientation of cracks was considered. The orientation of cracks was assumed to form in a direction perpendicular to the principal tensile stress. Instead of separating the nodes along cracked element boundaries, cracks were simulated by modifying the properties of elements which had failed. This was done by eliminating the stiffness of an element in the direction normal to a crack. Essentially when a normally isotropic element cracked, it became an orthotropic element. This technique is often called the smeared crack concept and has subsequently been used by most researchers to simulate cracks in reinforced concrete structures.

Spokowski 1972 and Houde 1973 (47) (25)

At McGill University, Spokowski (47) and Houde (25) were also studying the application of the finite element method to reinforced concrete. They added stirrups to their models by representing them as four degree of freedom bar elements. They assumed that for stirrups there was no significant displacement between the steel and concrete, and therefore it was reasonable to ignore the slip between them. Both researchers used the Ngo and Scordelis spring linkages for steel-concrete interaction, but this time the dowel action was also considered. The stiffnesses of the vertical springs used to simulate dowel action were estimated from empirically derived prediction equations. Houde (25) also used spring linkage elements to model aggregate interlock along cracks. When this was done it was necessary to use a predefined crack pattern. An incremental loading procedure was used by both researchers and the maximum principal tensile stress was used to define the failure criteria. At the end of each load increment all of the elements were checked for failure, and the elements that had cracked during that increment were identified. The nodal forces of these elements were reapplied to adjacent elements and redistributed in the following load increment. Spokowski and Houde both assumed that cracked elements were incapable of carrying any stresses, and the stiffnesses of these elements were completely deleted from the system. This assumption is not really correct because cracked elements actually have some load carrying capacity. The smeared crack approach would probably have given a more exact answer.

Scanlon and Murray 1972 (46)

Scanlon and Murray used layered plate bending elements to simulate the behaviour of reinforced concrete slabs. Each layer of an element was permitted to have different properties and in this way it was possible to include the effects of reinforcement and progressive cracking. The stiffness of the layer at the level of the reinforcement was calculated by superimposing the individual stiffness of the steel and the concrete. Unfortunately, this technique made it impossible to consider bond slip because it was necessary to assume that there was perfect bond between the concrete and the steel. This requirement may have seriously affected the observed crack patterns because the progression of cracking is highly influenced by bond slip. The smeared crack concept was used to simulate cracks, and when the maximum principal tensile stress exceeded the tensile strength, the modulus of elasticity and the Poisson's ratio were reduced. In cracked elements the shear modulus was retained and although it was not stated explicitly, this may have been done to account for aggregate interlock. Tension stiffening was another feature included in Scanlon and Murray's model. Instead of immediately releasing the tensile stresses in cracked layers, Scanlon and Murray simulated tension stiffening by slowly reducing the tensile stresses. There was still some stiffness retained in cracked elements in the direction perpendicular to the cracks. Scanlon and Murray reported that this modification did not affect the prediction of the failure load, but did have an influence on the load-deflection curve.

Hand, Pecknold, and Schnobrick 1973 (23)

Hand, Pecknold, and Schnobrick used 20 degree of freedom shallow shell layered elements to investigate the load deflection history of reinforced concrete plates and shells. Cracked layers were represented by the smeared crack concept, and aggregate interlocking and dowel action were simulated by retaining a fraction of the shear modulus. This fraction was defined as a shear retention factor, and it was assumed that this factor was constant. The authors recognized that a variable shear retention factor that depended on the crack width would probably give a better representation of the correct behaviour, but they did not include this in their analysis.

Phillips and Zienkiewicz 1976 (41)

In 1976 Phillips and Zienkiewicz presented a model which used 12 node isoparametric elements to analyze reinforced concrete structures. Special axial elements lying inside the boundaries of the concrete isoparametric elements were used to simulate the reinforcement. It was necessary to assume that there was perfect bond between the steel and the concrete because the strains in the steel elements had to be the same as those in the surrounding concrete elements. Smeared cracks were assumed to form across part of an isoparametric element when the maximum principal tensile stress or strain at an integration point exceeded a limiting value. Crack closure was included in the model. Phillips and Zienkiewicz concluded that cracks would close when the direct strain across a cracked region became compressive, and when this occurred the

cracked elements took on the properties of uncracked elements. Since the authors recognized that a plane of weakness still existed along the crack, the shear resistance of a previously cracked region was assumed to be less than that for a region that had never been cracked.

Cedolin and Dei Poli 1977 (14)

Cedolin and Dei Poli analyzed shear critical reinforced concrete beams with plane strain triangular elements. A limiting tensile strain was used as the failure criterion, and the smeared crack approach was used to represent the cracked elements. The shear retention factor that was suggested by Hand et al (23) was used to simulate aggregate interlocking and dowel action. Instead of using a constant shear retention factor, Cedolin and Dei Poli introduced a variable factor which decreased linearly with increasing crack widths. As mentioned earlier this improvement would probably give a better representation of the actual behaviour of concrete because it is well known that aggregate interlocking is very dependent on crack widths (23).

Sallam 1978 (45)

Sallam investigated the behaviour of reinforced concrete joints with the finite element method. He used the four node Goodman joint (21) in place of the normal, Ngo and Scordelis linkages to model the interaction between the steel and the concrete. The stiffness of the joint elements were evaluated by averaging the displacements between the steel and concrete nodes. This meant that the stiffness of each joint

was constant all along its length, which is really only an approximation because the stiffness actually varies nonlinearly.

Bazant and Cedolin 1979 (5)

Bazant and Cedolin investigated the treatment of crack propagation in finite element analyses of reinforced concrete and suggested some improvements to them. They suggested that models which used a limiting tensile stress or strain as the failure criterion were not always accurate. This conclusion was based on the observation that crack propagation could be significantly influenced by the element grid. They suggested that fracture mechanics criteria should be used to determine crack initiation and propagation, and the failure in an element should be expressed in terms of the energy required for crack extension.

Conclusion

Although the preceding review is by no means complete, it does show that significant progress has been made in the area of reinforced concrete modelling by the finite element method. With varying degrees of success, numerical techniques have been developed to simulate the effects of aggregate interlocking, dowel action, tension stiffening, bond slip, and progressive cracking. Despite this progress there are still many areas requiring further study. Examples of these areas include concrete-steel interaction, failure criteria, three-dimensional action, and the effects of time dependent behaviour. Researchers who

wish to improve the finite element modelling of reinforced concrete must also deal with the fact that many of the factors which still need to be simulated are not very well understood to start with. This will continue to cause problems with accuracy. Another consideration that has not yet been mentioned is the cost of a finite element analysis. The improved accuracy which may be achieved through the use of complex numerical techniques, must be balanced against the cost. Finite element modelling of reinforced concrete has made considerable progress in the time since it was first introduced, but there are still many areas where significant advancements can still be made.

3.2.2 Concrete Elements

The concrete in the finite element model was represented with constant stress triangular elements. An option for the inclusion of geometric nonlinearity was incorporated into the analysis even though this was not really necessary. Service loaded beams rarely have large-deflection effects and small deflection theory is usually applicable. However this option was included for possible later applications. The elements in this analysis were assumed to be in a state of plane stress, and an iterative, incremental solution scheme was used to deal with the many nonlinearities. In this section the derivation and solution of the finite element equations which were used to model the concrete will be explained.

Stiffness Matrix and Load Vector

The derivation of the stiffness matrix and load vector for constant stress triangular elements with geometric nonlinearities is available in many finite element textbooks (34)(55), but is briefly presented here for completeness. The 3 node, 6 degree of freedom element is shown in Figure 3.1. The principle of virtual work was used to formulate the problem and define the element properties.

The displacement functions u and v in the x and y directions for the triangular element were given by:

$$u = L_1 u_1 + L_2 u_2 + L_3 u_3 \quad (3.5)$$

$$v = L_1 v_1 + L_2 v_2 + L_3 v_3$$

These equations gave a linear approximation for u and v within the element.

The principle of virtual work was used to derive a function which represented the sum of internal and external generalized forces.

$$\int_v B_n^T \sigma_n dV - R_n = 0 \quad (3.6)$$

Where R_n is the nodal load vector, and B_n is the kinematic large displacement matrix which relates incremental displacements to incremental strains. The definition for B_n is characterized as:

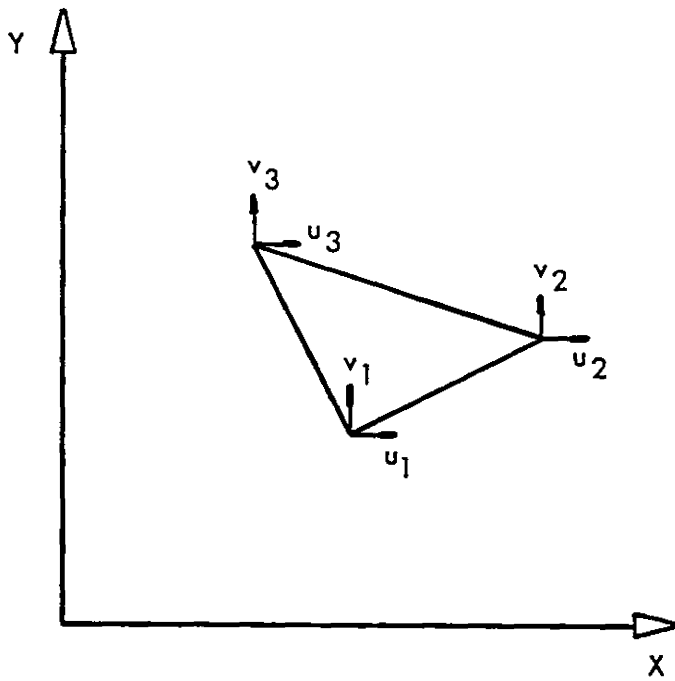


FIGURE 3.1. 3 NODE CONCRETE ELEMENT

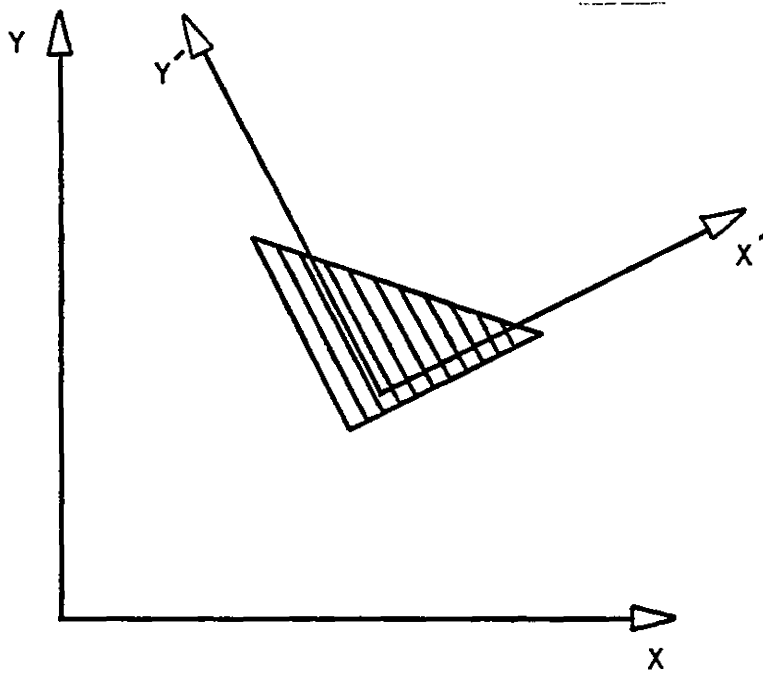


FIGURE 3.2 CRACKED CONCRETE ELEMENT

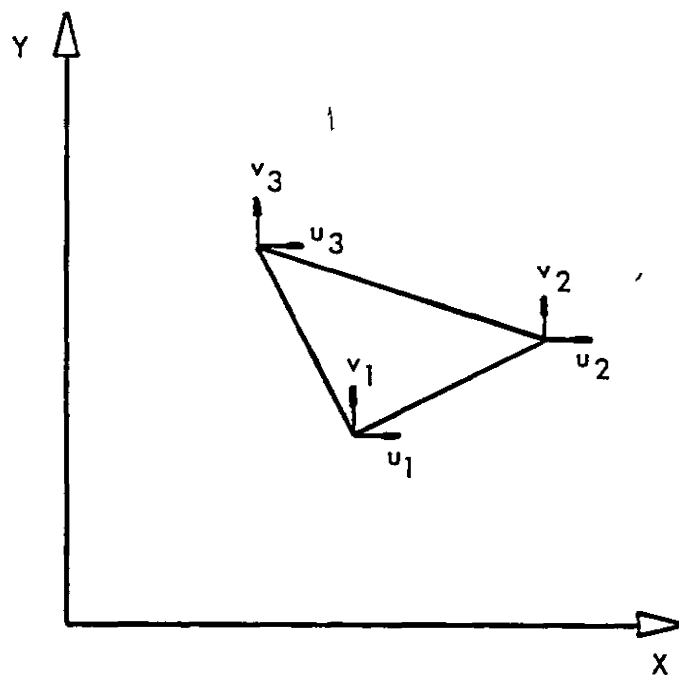


FIGURE 3.1 3 NODE CONCRETE ELEMENT

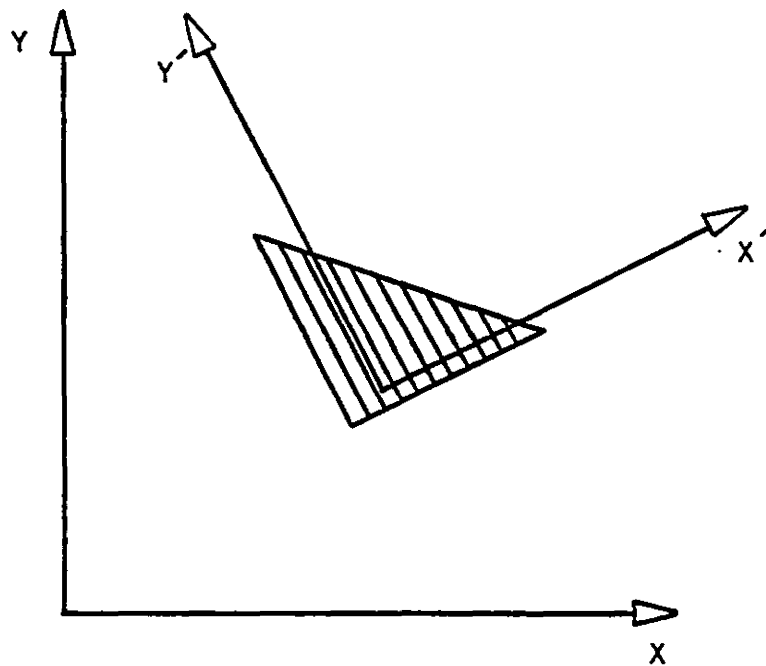


FIGURE 3.2 CRACKED CONCRETE ELEMENT

$$\Delta \epsilon_n = B_n \Delta u_n \quad (3.7)$$

where u_n = nodel displacements.

For small strains, the stresses were written as a function of the elasticity matrix D , the initial strains, ϵ_0 , and the initial stresses, σ_0 , so that:

$$\sigma = D(\epsilon - \epsilon_0) + \sigma_0 \quad (3.8)$$

The solution of Equation (3.6) required an iterative solution procedure for which the Newton Raphson method was used. To do this it was necessary to find a relationship between Equation (3.6) and Δu_n . This was accomplished by first writing Equation (3.6) in an incremental form.

$$\int_v B_n^T \Delta \sigma_n dV + \int_v \Delta B_n^T \sigma_n dV - \Delta R_n = 0 \quad (3.9)$$

where $\Delta R_n = 0$ if there is no change in the external loads

Then Equations (3.7) and (3.8) were combined to give:

$$\Delta \sigma_n = D B_n \Delta u_n \quad (3.10)$$

The stiffness matrices were then defined by using Equation (3.10) and writing Equation (3.9) as:

$$K \sigma_n \Delta u_n + K_n \Delta u_n = 0 \quad (3.11)$$

$$\text{where } K \sigma_n \Delta u_n = \int_v \Delta B_n^T \sigma_n dV$$

$$\text{and } K_n = \int_v B_n^T D B_n dV$$

When cracking occurs during loading, Equation (3.6) may not be completely satisfied in one iteration. If this is the case, it may be necessary to correct the error through an iterative process. Iteration continues until the error is reduced to a value small enough not to affect the results.

Summary

The nonlinear analysis presented in this section was used to define the properties of the concrete in the finite element model and an iterative incremental solution procedure was employed to solve the required equations. It was assumed that the two-dimensional triangular element gave an acceptable representation of the states of stress and strain in the concrete. Although it may be possible to increase the accuracy of the analysis by using more complex elements, it was decided that the increased cost, the extra memory requirements, and the complexity were not justified.

3.2.3 Cracked Concrete Elements

When the maximum principal tensile stress in a concrete element exceeded the tensile strength, that element was assumed to crack. Cracking is very difficult to simulate in a finite element model because of problems with computer storage limitations, confusion about concrete's proper failure criterion, and uncertainty about the true material response. Various techniques have been suggested to deal with concrete cracking but there are inherent weaknesses in all of them. This section contains a review of the methods which have been suggested for treating cracking in a finite element analysis, and the modifications which were made to the concrete elements to simulate this effect.

Probably the best way to model cracking is to redefine the element mesh by introducing new nodes along crack boundaries. Unfortunately this creates irregularly shaped elements and substantially increases the required memory storage. A related alternative is to separate the nodes along the closest element boundary to a crack. Unfortunately this modification usually creates incorrect crack patterns, and may also substantially increase the computational effort and required memory storage. A simpler modelling technique is to completely delete the stiffness of elements which exceed the cracking criteria. This means that cracking does not change the element grid and causes no increases in memory requirements. Realistically however, cracked elements actually retain much of their stiffness after cracking, and completely eliminating their stiffness may introduce a considerable

loss of accuracy. However this idea of cracked regions rather than discrete cracks leads to a more accurate technique called the smeared crack approach. Cracks are simulated in this method by reducing the stiffness of cracked elements according to a technique reported by Zienkiewicz (55) for anisotropic materials. Bazant and Cedolin (5) reported that the smeared crack assumption of cracked regions may actually be closer to reality than the assumption of discrete cracks because of material inhomogeneity and the stabilizing effect of the reinforcement.

In this study the smeared crack approach was used to simulate cracks in the finite element model. According to this technique, an infinite number of finely spaced cracks form in an element when the failure criteria for that element is exceeded. For this model, failure took place when the maximum principal tensile stress exceeded the tensile strength. Cracks were assumed to form normal to the direction of the maximum principal tensile stress. Some disagreement exists among researchers about whether cracking should be controlled by the maximum stresses, the maximum strains, or some other failure criteria, but since tests for tensile capacity are usually related to stress, the maximum stresses were used in this study.

The following assumptions were made concerning cracked elements:

- 1) No stiffness was retained in the direction normal to a crack
- 2) Poisson's effect was neglected
- 3) Shear stiffness was omitted

These assumptions meant that no provision was made for the effects of aggregate interlocking and tension stiffening.

Cracked elements were analyzed by rotating their x and y axes to coincide with the crack direction. The idealization and orientation of cracked concrete elements is shown in Figure 3.2. To comply with the assumptions about cracking, the elasticity matrix, [D], in the global coordinate system was changed for cracked elements to [D'] in the local coordinate system x', y'.

$$[D'] = E \begin{bmatrix} 0 & 0 & 0 \\ 0 & 1 & 0 \\ 0 & 0 & 0 \end{bmatrix} \quad (3.12)$$

The local stiffness matrix and load vector of the cracked elements in the local coordinate system were derived from virtual work in the same way as for uncracked elements. To form the global stiffness matrix and load vector in the x, y system, appropriate transformations were necessary. Displacements in the x, y system were converted to the x', y' system with the following transformations.

$$\begin{aligned} u' &= u \cos \beta + v \sin \beta \\ v' &= -u \sin \beta + v \cos \beta \end{aligned} \quad (3.13)$$

where the prime denotes the local coordinate system. Nodal displacements in local coordinates were related to nodal displacements in global coordinates with the following transformation matrix.

$$\{\delta'\} = [T] \{\delta\}$$

$$\text{where } [T] = \begin{bmatrix} \cos\beta & \sin\beta & 0 & 0 & 0 & 0 \\ -\sin\beta & \cos\beta & 0 & 0 & 0 & 0 \\ 0 & 0 & \cos\beta & \sin\beta & 0 & 0 \\ 0 & 0 & -\sin\beta & \cos\beta & 0 & 0 \\ 0 & 0 & 0 & 0 & \cos\beta & \sin\beta \\ 0 & 0 & 0 & 0 & -\sin\beta & \cos\beta \end{bmatrix} \quad (3.14)$$

This leads to the transformation of the stiffness matrix and load vector to the global system.

From the potential energy theorem.

$$U = \frac{1}{2} \{\delta'\}^T [K'] \{\delta'\} \quad (3.15)$$

$$W = \{P'\}^T \{\delta'\} \quad (3.16)$$

Where K' is the cracked element stiffness matrix in the local coordinate system, U is the strain energy, P is the local load vector, and W is the potential energy of loading.

By combining Equations (3.15) and (3.16) with Equation (3.14), the strain energy and potential energy for the element in the global system were defined as:

$$U = \frac{1}{2} \{\delta\}^T [T] [K'] [T] \{\delta\} \quad (3.17)$$

$$W = \{P'\}^T [T] \{\delta\} \quad (3.18)$$

The stiffness matrix can be extracted from Equation (3.17) and defined as:

$$K = [T]^T [K'] [T] \quad (3.19)$$

The load vector comes from Equation (3.18) and is written as:

$$P = \{P'\}^T [T] \quad (3.20)$$

This formulation was expected to provide a relatively simple and accurate way to simulate cracks in concrete. Even though such factors as aggregate interlocking and tension stiffening were omitted, the results should realistically reflect the initiation and progression of cracks.

3.2.4 Steel Elements

The steel in the finite element model was represented with four degree of freedom bar elements. It was assumed that the transverse stiffness of the reinforcement was negligible compared to the concrete. Therefore only the axial stiffness of the steel was included. This assumption seemed to be reasonable and it substantially reduced the size and cost of the analysis. Geometric nonlinearity was not incorporated

into the analysis of the reinforcement because large deflections were not expected to be present in the beams studied. However provision was made so that this refinement could be added later if necessary.

Stiffness Matrix

The stiffness matrix of the bar element is available in any finite element textbook (34)(55), but a brief derivation is provided here for completeness. The bar element used in the analysis is shown in Figure 3.3. Since geometric nonlinearities were not considered in the derivation, the displacements in the transverse direction were omitted. The linear displacement function of the bar element was thus given by:

$$u = \left(1 - \frac{x}{l}\right) u_1 + \frac{x}{l} u_2 \quad (3.22)$$

The stiffness matrix was developed from the strain energy expression for an axial element where:

$$U = \frac{EA}{2} \int_0^l (u')^2 dx \quad (3.23)$$

and:

$$K = \frac{EA}{l} \begin{bmatrix} 1 & 0 & -1 & 0 \\ 0 & 0 & 0 & 0 \\ -1 & 0 & 1 & 0 \\ 0 & 0 & 0 & 0 \end{bmatrix}$$

Transformation matrices can be used if the direction of the steel is not parallel to the x-axis. The solution procedure outlined in the section

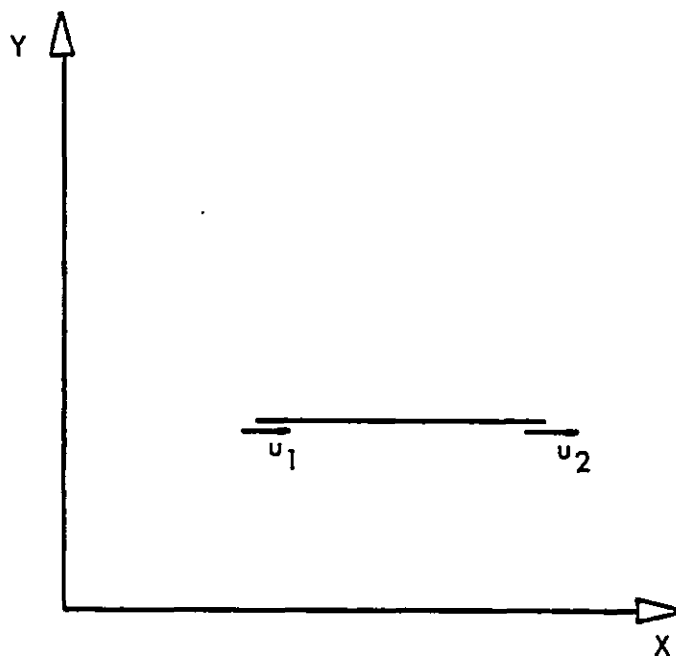


FIGURE 3.3 2 NODE BAR ELEMENT

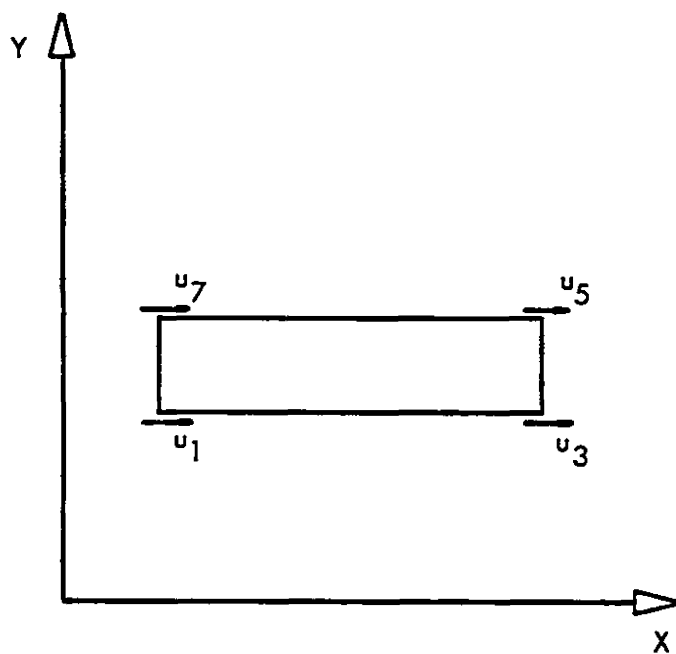


FIGURE 3.4 4 NODE GOODMAN JOINT ELEMENT

on the concrete elements was also followed for the steel elements. Even though there were no nonlinearities in the behaviour of the steel elements, it was necessary to follow an incremental solution procedure because of nonlinearities elsewhere in the analysis. It was felt that the bar element gave a good approximation of the stress and strain states in the reinforcement and that this simple element gave the best combination of accuracy and computational efficiency.

3.2.5 Bond Elements

The interaction between steel and concrete is very important to the overall response of concrete members. It is therefore essential to model this phenomenon as accurately as possible in a finite element model even though there is still a great deal of uncertainty surrounding it. Ngo and Scordelis (37) suggested using special spring linkage elements to represent the bond characteristics. However, since these elements only satisfy compatibility at the nodes they may not be very accurate when a nonlinear bond relationship is used. A different kind of element was proposed by Goodman, Taylor, and Brekke (21) to study jointed rock masses. This element can be made to ensure compatibility along the interface between constant stress elements and is therefore more suited for concrete bond representations. For this reason the Goodman joint element was chosen to represent the bond behaviour in the finite element model of this study. The derivation presented by Goodman et al, with a few modifications is presented in this section.

The Goodman joint, shown in Figure 3.4, is a 4 node element which has a finite length but no width. Initially, the adjacent nodal pairs (1,4) and (2,3) seen in Figure 3.4 have the same coordinates, but when forces are applied to the joint, these pairs separate. The properties of the element are dependent on the relative movement between the top and bottom faces, and are defined with empirical relationships. Dowel action was neglected in this study, so the relative displacements in the vertical direction were restrained. Only horizontal displacements were allowed. The following paragraphs contain details on the derivation of the stiffness matrix and load vector for the joint element.

Stiffness Matrix

The displacement at the top and bottom of the joint element were defined in terms of a nondimensional coordinate α , where:

$$u_T = \left(\frac{1-\alpha}{2}\right) u_7 + \frac{1+\alpha}{2} u_5 \quad (3.24)$$

$$u_B = \left(\frac{1-\alpha}{2}\right) u_1 + \frac{1+\alpha}{2} u_3$$

where u_T = displacement of top of element

u_B = displacement of bottom of element

u_1, u_3, u_5, u_7 = nodal displacements

The relative displacement between the top and bottom of the element were then defined at any point along the length by:

$$u_T - u_B = - \left(\frac{1-\alpha}{2}\right) u_1 - \left(\frac{1+\alpha}{2}\right) u_3 + \left(\frac{1+\alpha}{2}\right) u_5 + \left(\frac{1-\alpha}{2}\right) u_7 \quad (3.25)$$

The stiffness of the element was found by making use of the Potential Energy Theorem, the relative displacements, and Mirza and Houde's nonlinear bond relationships (25)(33) as:

$$k_{ij} = \frac{L}{2} \int_{-1}^1 \{N_i\} k_s \{N_j\} d\alpha \quad (3.26)$$

$$\text{where } \{N\} = \begin{pmatrix} - \left(\frac{1-\alpha}{2}\right) \\ - \left(\frac{1+\alpha}{2}\right) \\ \left(\frac{1+\alpha}{2}\right) \\ \left(\frac{1-\alpha}{2}\right) \end{pmatrix}$$

The stiffness, k_s , comes from the local bond stress-slip equation developed by Mirza and Houde. It was expressed by the following polynomial:

$$u_{bs} = 1.95 \times 10^6 d - 2.35 \times 10^9 d^2 + 1.39 \times 10^{12} d^3 - .33 \times 10^{15} d^4 \quad (3.27)$$

where u_{bs} = local bond stress (psi)

d = local bond slip (in)

Differentiation of Equation (3.27) with respect to slip gave the bond stiffness per unit length as:

$$k_s = \frac{du_{bs}}{dd} \pi D N \quad (3.28)$$

where D = diameter of reinforcing bar

N = number of bars in the cross-section

The variation of displacements along the boundaries of the constant stress triangular elements and the axial bar elements was linear. However, since the bond stress-slip law was nonlinear, the variation in stiffness along the interface was also nonlinear. Therefore the stiffness at the nodes was defined using three point Gauss Quadrature Numerical Integration. In this way the nonlinear nature of the bond behaviour could be represented. This modification seemed to represent a significant improvement over previous methods which have assumed that the bond stiffness between nodes is linear.

Load Vector

Like the stiffness matrix, the load vector, shown below, was also defined in terms of the relative displacement, the nondimensional coordinate, α , and the bond relationship.

$$F_i = \frac{L}{2} \int_{-1}^1 \{N_i\} T_s d\alpha \quad (3.29)$$

The shape factor, $\{N\}$, is the same as that given in Equation (3.26), and the bond stress, T_s , came from the local bond stress-slip law of Equation (3.27). The bond stress given by Mirza and Houde's equation leads to the bond stress per unit length as shown in Equation (3.30) below:

$$T_s = u_{bs} \pi D N \quad (3.30)$$

The terms in this equation are the same as those in Equation (3.28). Since the bond stress equation was a nonlinear function, three point Gauss Quadrature Numerical Integration was used to solve Equation (3.30).

This formulation appears to be a significant improvement over the Ngo and Scordelis spring linkages because compatibility can be provided all along the steel-concrete interface. Unfortunately the accuracy of the solution generated with this approach is also dependent on the accuracy of the bond relationship. Improvements in the modelling of bond are therefore very dependent on improvements in the accuracy of this relationship.

3.2.6 Creep and Shrinkage Formulation

The technique adopted for treating the effect of time dependent strains on the finite element model was first proposed by Kanchi, Zienkiewicz, and Owen (27). They developed an implicit visco-plastic model which incorporated material and geometric nonlinearities. This model was used in the finite element model of this study to treat creep and shrinkage strains. In the analysis, an incremental solution procedure was used to determine the cumulative effects of the changing inelastic strains. The basic formulation of this procedure can be found in the paper by Kanci et al, but since concrete does not exactly follow

this formulation the equations were redefined to reflect the differences.

Creep Strain Increments

The explicit form of the concrete creep strain rate is dependent on the applied stresses and the time under load. It can be written as:

$$\dot{\epsilon}^c = f(\sigma, t) \quad (3.31)$$

A creep strain increment $\Delta \epsilon_n^c$, was defined for a time interval $\Delta t = t_{n+1} - t_n$, by using the following formulation.

$$\Delta \epsilon_n^c = \Delta t [(1-\phi) \dot{\epsilon}_n^c + \phi \dot{\epsilon}_{n+1}^c] \quad (3.32)$$

In this case $\phi = 0$, is the Euler scheme or "fully explicit"

$\phi = 1$, is "fully implicit"

$\phi = \frac{1}{2}$, is the implicit trapezoidal scheme, or Crank-

Nicolson rule, which is used for linear equations

A truncated Taylor series expansion was used to define $\dot{\epsilon}_{n+1}^c$.

$$\dot{\epsilon}_{n+1}^c = \dot{\epsilon}_n^c + H_n \Delta \sigma_n \quad (3.33)$$

$$\text{where } H_n = \left(\frac{\partial \dot{\epsilon}^c}{\partial \sigma} \right) = H_n(\sigma_n) \quad (3.34)$$

The matrix H_n depends on the stress level at the nth creep increment.

This formulation is very good for linear creep laws, but since concrete has a nonlinear creep law, Equation (3.33) is not always very accurate. This has an adverse effect on the convergence rate. To ensure proper convergence either an iterative scheme or a residual load vector may be used. In both cases an accurate prediction of $\dot{\epsilon}_{n+1}^c$ is preferable. To accelerate the rate of convergence and to improve the accuracy of $\dot{\epsilon}_{n+1}^c$, the Taylor series was modified. With the addition of an extra term, Equation (3.33) can now be written as:

$$\dot{\epsilon}_{n+1}^c = \dot{\epsilon}_n^c + \ddot{\epsilon}_n^c \frac{\Delta t}{2} + H_n \Delta \sigma_n \quad (3.35)$$

Equation (3.35) is no longer a proper Taylor series, but, for the given creep curve, the additional term provided a much better prediction of $\dot{\epsilon}_{n+1}^c$. The creep strain increment could now be redefined as:

$$\Delta \epsilon_n^c = \dot{\epsilon}_n^c \Delta t + \phi \ddot{\epsilon}_n^c \frac{\Delta t^2}{2} + \phi H_n \Delta \sigma_n \Delta t \quad (3.36)$$

Shrinkage Strain Increments

The explicit form of the shrinkage strain rate can be written as:

$$\dot{\epsilon}^{sh} = f(t) \quad (3.37)$$

The shrinkage strain increment $\Delta \epsilon_n^{sh}$, for time increment $\Delta t = t_{n+1} - t_n$, was defined as:

$$\Delta \epsilon_n^{sh} = \epsilon_{n+1}^{sh} - \epsilon_n^{sh} \quad (3.38)$$

A limited Taylor series expansion was used to define ϵ_{n+1}^{sh} implicitly.

$$\epsilon_{n+1}^{sh} = \epsilon_n^{sh} + \dot{\epsilon}_n^{sh} \Delta t + \frac{\ddot{\epsilon}_n^{sh}}{2} \frac{\Delta t^2}{2} \quad (3.39)$$

The shrinkage strain increment was then written as:

$$\Delta \epsilon_n^{sh} = \dot{\epsilon}_n^{sh} \Delta t + \frac{\ddot{\epsilon}_n^{sh}}{2} \frac{\Delta t^2}{2} \quad (3.40)$$

Stress Increments

The stress increments were obtained from the elasticity matrix, the total strain increment, and the inelastic strains as:

$$\begin{aligned} \Delta \sigma_n &= D (\Delta \epsilon_n - \Delta \epsilon_n^c - \Delta \epsilon_n^{sh}) \\ &= D (B_n \Delta u_n - \Delta \epsilon_n^c - \Delta \epsilon_n^{sh}) \end{aligned} \quad (3.41)$$

In this case, Δu_n is the incremental nodal displacement vector, and B_n is the kinematic large displacement matrix which relates displacement increments to strain increments. The B_n matrix is composed of two parts, corresponding to the linear and nonlinear terms used in the Lagrangian formulation for geometric nonlinearities.

Substituting $\Delta \epsilon_n^c$ and $\Delta \epsilon_n^{sh}$ from Equations (3.36) and (3.40), into Equation (3.41), gave the stress increment implicitly as:

$$\Delta \sigma_n = F_n^{-1} D [B_n \Delta u_n - (\epsilon_n^c \Delta t + \phi \epsilon_n^c \frac{\Delta t^2}{2}) - (\epsilon_n^{sh} \Delta t + \epsilon_n^{sh} \frac{\Delta t^2}{2})] \quad (3.42)$$

$$\text{where } F_n = [I + \phi \Delta t D H_n] \quad (3.43)$$

and I = the identity matrix.

Equations of Equilibrium

The equilibrium equation which must be satisfied for any time was:

$$\int_v B_n^T \sigma_n dV - R_n = 0 \quad (3.44)$$

The R_n term is the equivalent nodal load vector due to the external loading.

The incremental form of this equation was written as:

$$\int_v B_n^T \Delta \sigma_n dV + K_{\sigma n} \Delta u_n - \Delta R_n = 0 \quad (3.45)$$

where $K_{\sigma n}$ is the initial stress matrix which is dependent on the stress level, and ΔR_n is the change in the external loads during the time increment. The matrix ΔR_n is equal to zero if the external load remains constant throughout the time increment, or is applied in discrete steps.

The incremental nodal displacements were determined by combining Equations (3.42) and (3.43) with Equation (3.45). The total displacements, stresses, and strains were then found.

The incremental stresses obtained from Equation (3.45) may not satisfy the total equilibrium condition of Equation (3.44). This is due to the fact that the strain rates calculated by Equations (3.35) and (3.39) are not exactly the same as those given by the creep and shrinkage laws. An iterative solution procedure is often used to reduce the error to an acceptable level. Another suggestion, which was adopted in this model, is to correct the error in the next time increment with the residual load vector:

$$R_{n+1}^* = R_{n+1} - \int B_{n+1}^T \sigma_{n+1} dV \quad (3.46)$$

where R_{n+1}^* is the residual load vector which is calculated from the total load vector, R_{n+1} , the updated kinematic large displacement matrix, B_{n+1} , and the updated stress vector, σ_{n+1} .

3.3 Sensitivity

No discussion about the proposed finite element model would be complete without providing some analysis of its sensitivity. This is especially important for an investigation involving reinforced concrete because of concrete's complex nature and inherent variability. It is unrealistic to expect a theoretical tool like the finite element method to precisely model the behaviour of a reinforced concrete beam, but as

long as there is a proper appreciation of the limitations and relative accuracy of the model, it can be used successfully with some confidence.

The performance of the model is affected to varying degrees by numerical and material factors. Its overall accuracy can only be assessed after a complete examination of each individual contributing factor. Some insights into some of the factors which influence the model were presented in previous sections dealing with modelling and material properties. These included discussions about the accuracy of the creep, shrinkage, and bond equations, and the expected accuracy of finite element models in general. However at that time there was no attempt to quantify their effects on results from the analytical model. The objective of the following section is to provide this information and to give some indication of the probable accuracy that might be expected from the proposed finite element model.

In a sensitivity study, it is only possible to examine factors which can be varied within the program or changed through input variables. Any source of inaccuracy which cannot be quantified within the program cannot be tested for sensitivity. For this reason the effects of dowel action, tension stiffening, aggregate interlocking, crack modelling, two-dimensional plane stress modelling, material nonhomogeneity, and other similar factors were not studied. No alternatives to the way the model simulated reinforced concrete were compared. Instead, the investigation was limited to those influences which were supplied as independent variables such as the modulus of elasticity, tensile

strength, bond stiffness, creep, shrinkage, and the finite element mesh size.

The standard beam used in the sensitivity study was Corley and Sozen's Beam C1 (17), details of which can be found in Section 3.42. By varying some of the parameters of this beam and comparing the results with those obtained from the standard beam, it was hoped that some indication of the sensitivity of the model would become apparent. It should be recognized that this sensitivity study is only concerned with the response of a representative beam, and changes in geometry or boundary conditions may also have an effect on the results.

The sensitivity study was divided into two main sections. The first one contained an examination of a beam stressed well beyond its cracking load. The second was concerned with a beam stressed to approximately its cracking load. It was felt that the behaviour of the two extremes would give a more complete picture of the behaviour of all load levels. These two main sections were each divided into two subsections so that short term and long term deflections could be investigated separately. In each case only one variable was varied at a time and all other variables were kept constant. The results of the sensitivity study are shown in Figures 3.5 through 3.22.

3.3.1 Higher Stress Case

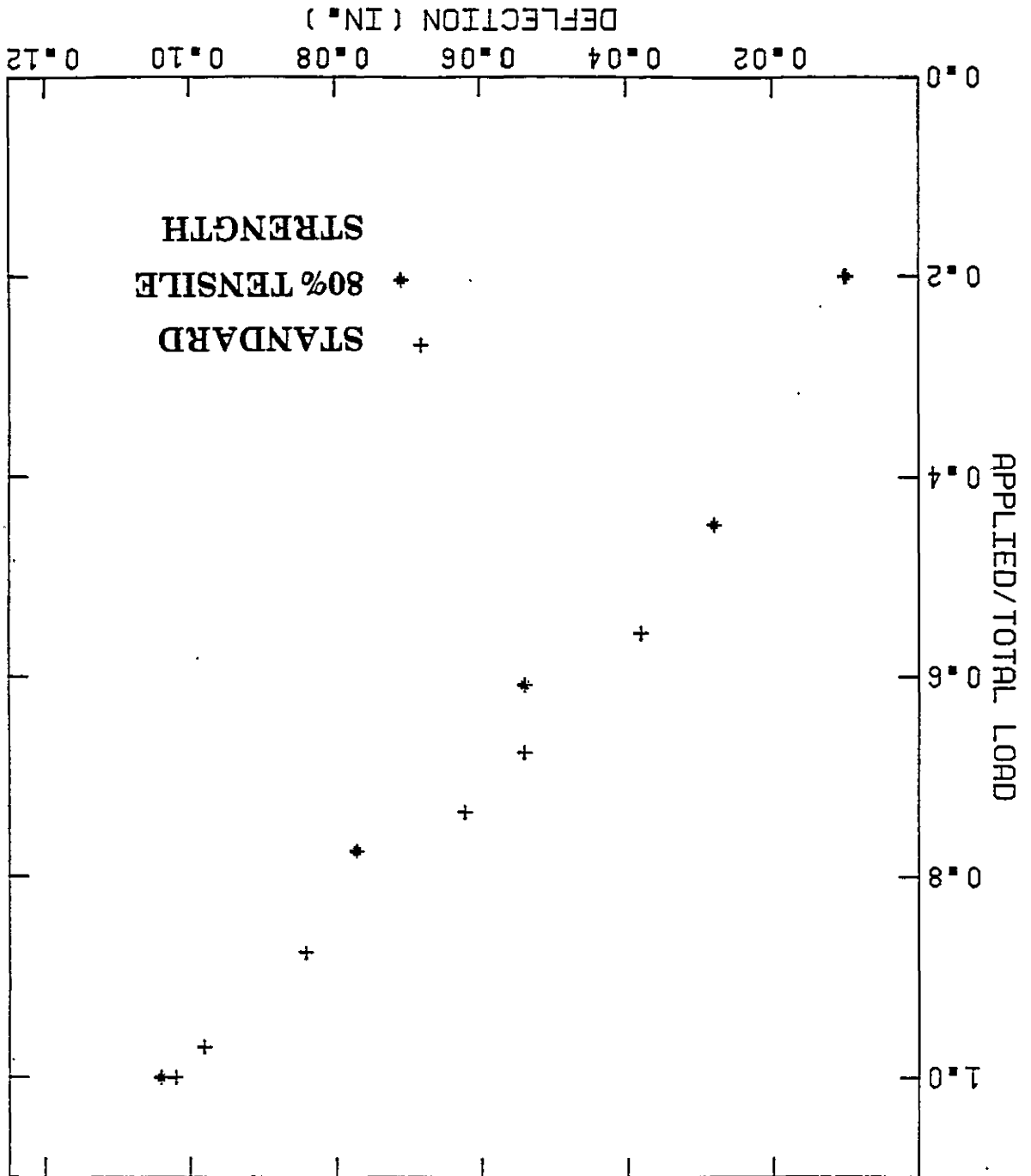
The immediate and long term deflections of the sample beam under relatively high stresses (47% of ultimate using $f_y = 40$ ksi) are shown

in Figure 3.5 to Figure 3.12. Each material variable was varied by 20%, and the number of elements along the length was doubled. In this section very little discussion will be centered on the beam's behaviour at low load levels since this will be examined later in more detail. A general examination of the deflections seems to indicate that no single variable had an undue effect on the final beam deflections. Under short term loading, the maximum difference between the standard case and the varied cases was only about 8%. For the long term loading the largest discrepancy at the end of the loading period was about 9%. It should be noted that the discrepancies at the end of the loading period included both short term and long term effects.

Tensile Strength

The effect of decreasing the tensile strength by 20% from the standard value is shown in Figure 3.5 and Figure 3.6. The main influence on the short term load-deflection curve (Figure 3.5) of changing this parameter was observed in the early stages of loading near the cracking load. In this range, the load level of crack initiation has a significant effect on the deflections. The curve for the lower tensile strength deflections began to diverge from the standard curve at about 40% of the total load. This was due to earlier cracking. When the load was increased further however, the curves began to converge again as the degree of cracking in the two cases became more similar. In fact, the difference between the two curves at the end of the loading period was only 2%, which certainly indicated that the tensile strength was not as

FIGURE 3.5 INFLUENCE OF TENSILE STRENGTH ON SHORT TERM DEFLECTIONS AT HIGH LOADS



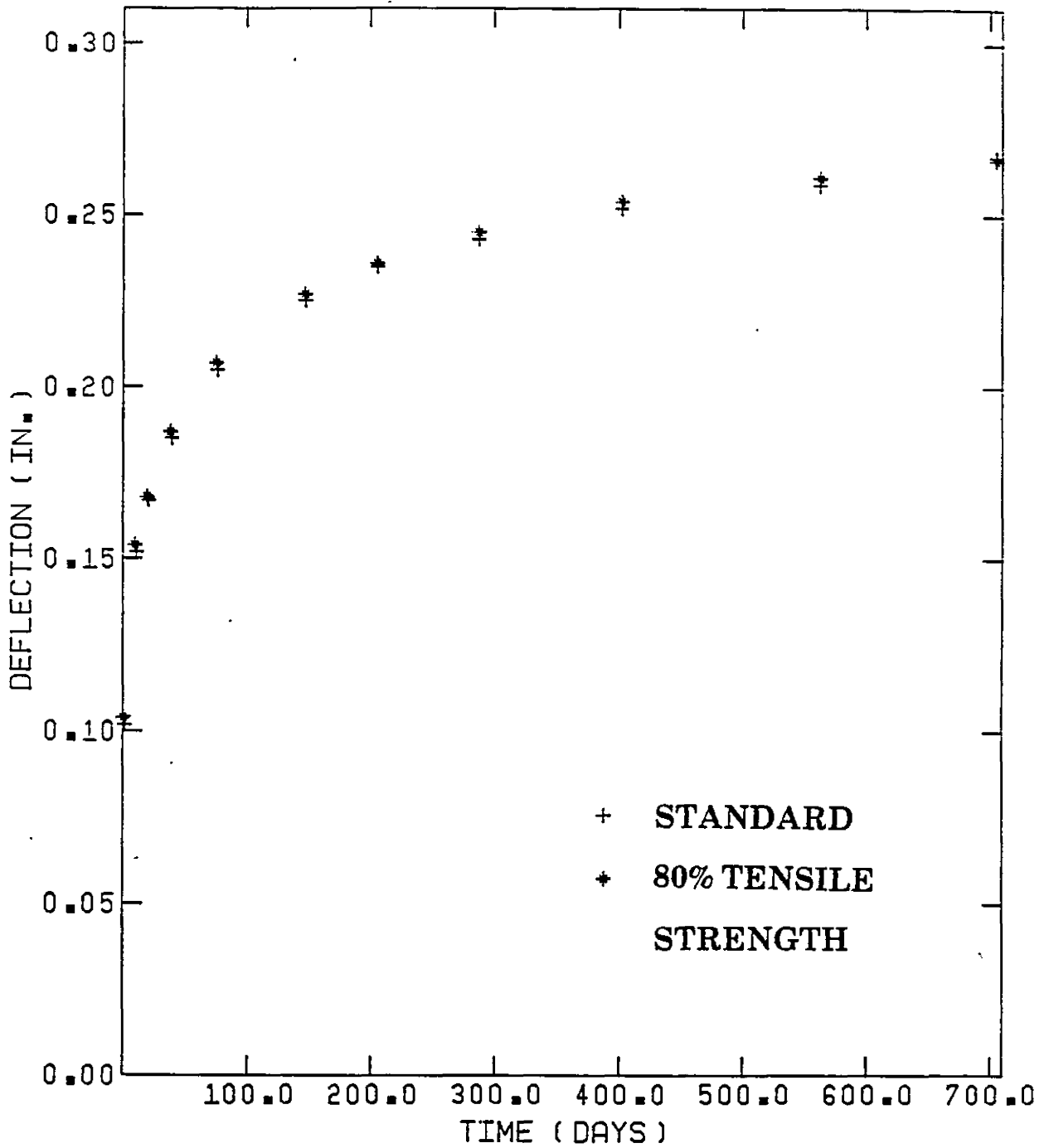


FIGURE 3.6 INFLUENCE OF TENSILE STRENGTH ON LONG TERM DEFLECTIONS AT HIGH LOADS

significant a factor when the loads were much higher than the cracking load.

This conclusion also seemed valid for long term deflections. It can be seen in Figure 3.6 that for the two cases there was very little difference between the variations in deflection at the beginning and end of the loading period. This behaviour was not totally unexpected because the main effect of cracking had already been felt. After cracking the tensile strength is no longer as important a parameter.

Modulus of Elasticity

The modulus of elasticity of the concrete was also decreased by 20% and the results are shown in Figures 3.7 and 3.8. All other properties of the concrete remained unchanged. The results from Figure 3.7, the short term data, were similar to the varied tensile strength results in that the influence of the modulus of elasticity was more pronounced at the lower end of the load deflection curve. The final deflection was about 8% greater than the corresponding deflection in the standard beam. This was considerably better than the 20% difference that one might expect for a normal elastic solid. The improvement may be attributed directly to the effect of cracking. Factors which influence the stiffness of a beam, such as cracking and bond deterioration, probably overshadowed the effect of the modulus of elasticity in the highly cracked beam.

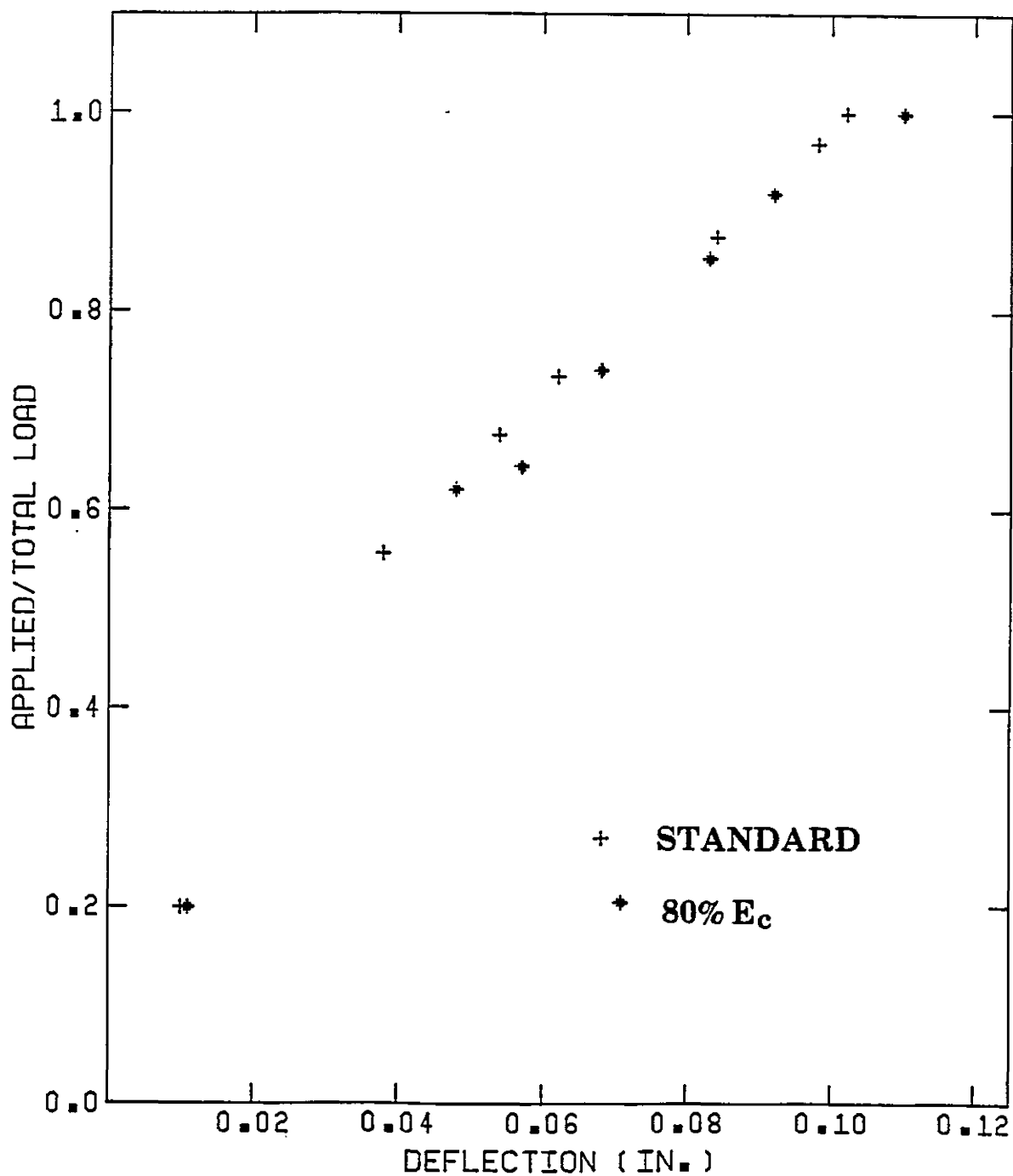


FIGURE 3.7 INFLUENCE OF E_c ON SHORT TERM DEFLECTIONS AT HIGH LOADS

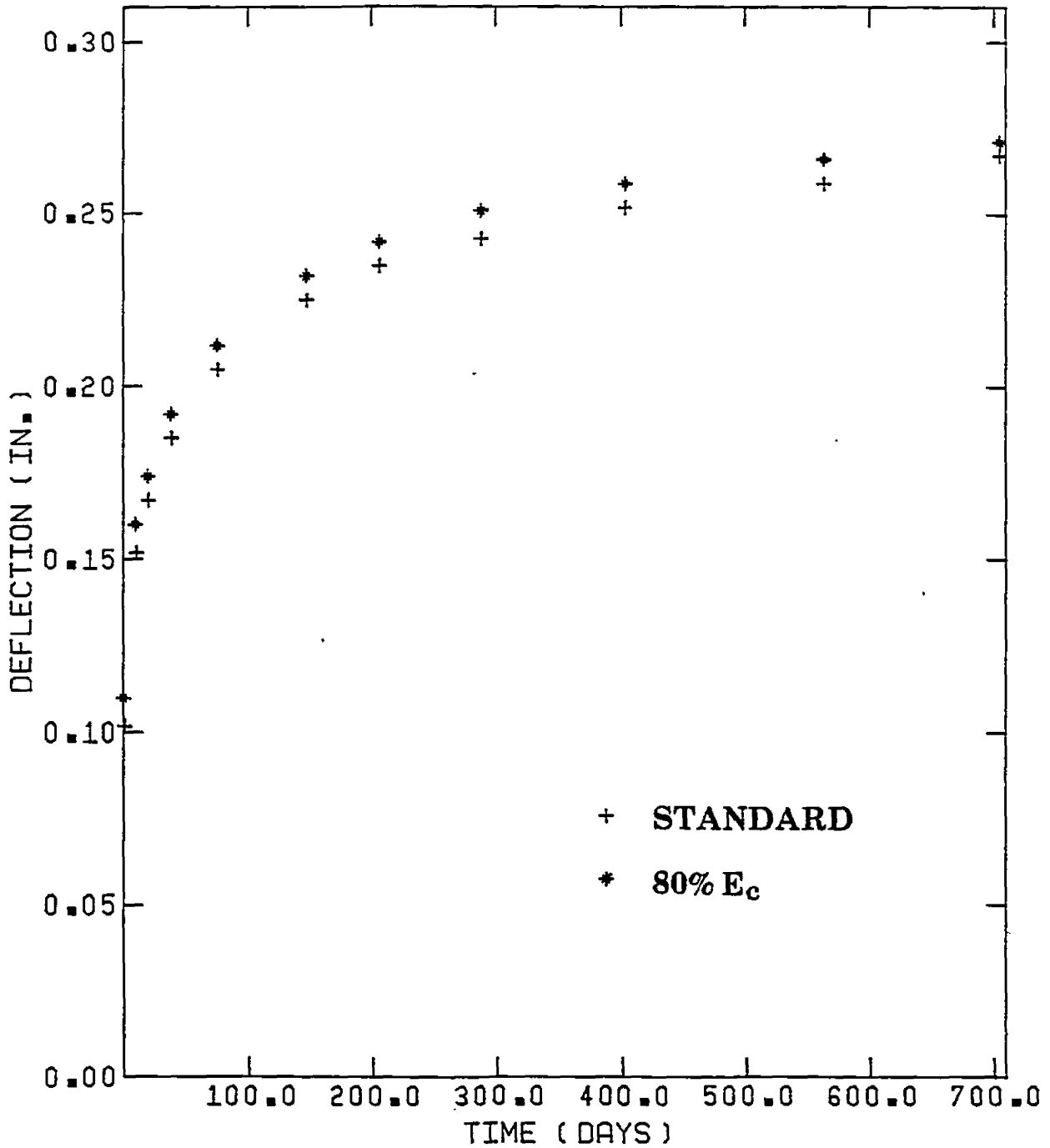


FIGURE 3.8 INFLUENCE OF E_c ON LONG TERM DEFLECTIONS AT HIGH LOADS

The influence of the modulus of elasticity on the long term deflections is shown in Figure 3.8. The modulus of elasticity had no apparent effect on the long term behaviour of this beam. The difference in deflections between the standard beam and the reduced modulus beam was the same at the end of 705 days as it was at the beginning of the loading period. This result was not really surprising because the modulus of elasticity has little effect on the factors relating to the prediction of long term deflections.

Bond Stiffness

Very little needs to be said about the effect of increasing the bond stiffness by 20% because this change seemed to have no real effect on any of the deflections. The deflections for this case represented a highly cracked beam where the effect of bond properties should have been most visible, and yet the standard deflections were almost the same as for the varied bond stiffness. Since significant variations were not apparent, it seems safe to say that the results were not very sensitive to changes in bond stiffness. These results support the conclusions of Ngo and Scordelis (39) who also contended that the actual value of the bond stiffness was not critical for a finite element analysis.

Shrinkage

The effect of increasing the shrinkage strains by 20% is shown in Figure 3.9. The influence of this change was observed almost immediately, but the deflections never varied from the standard deflections

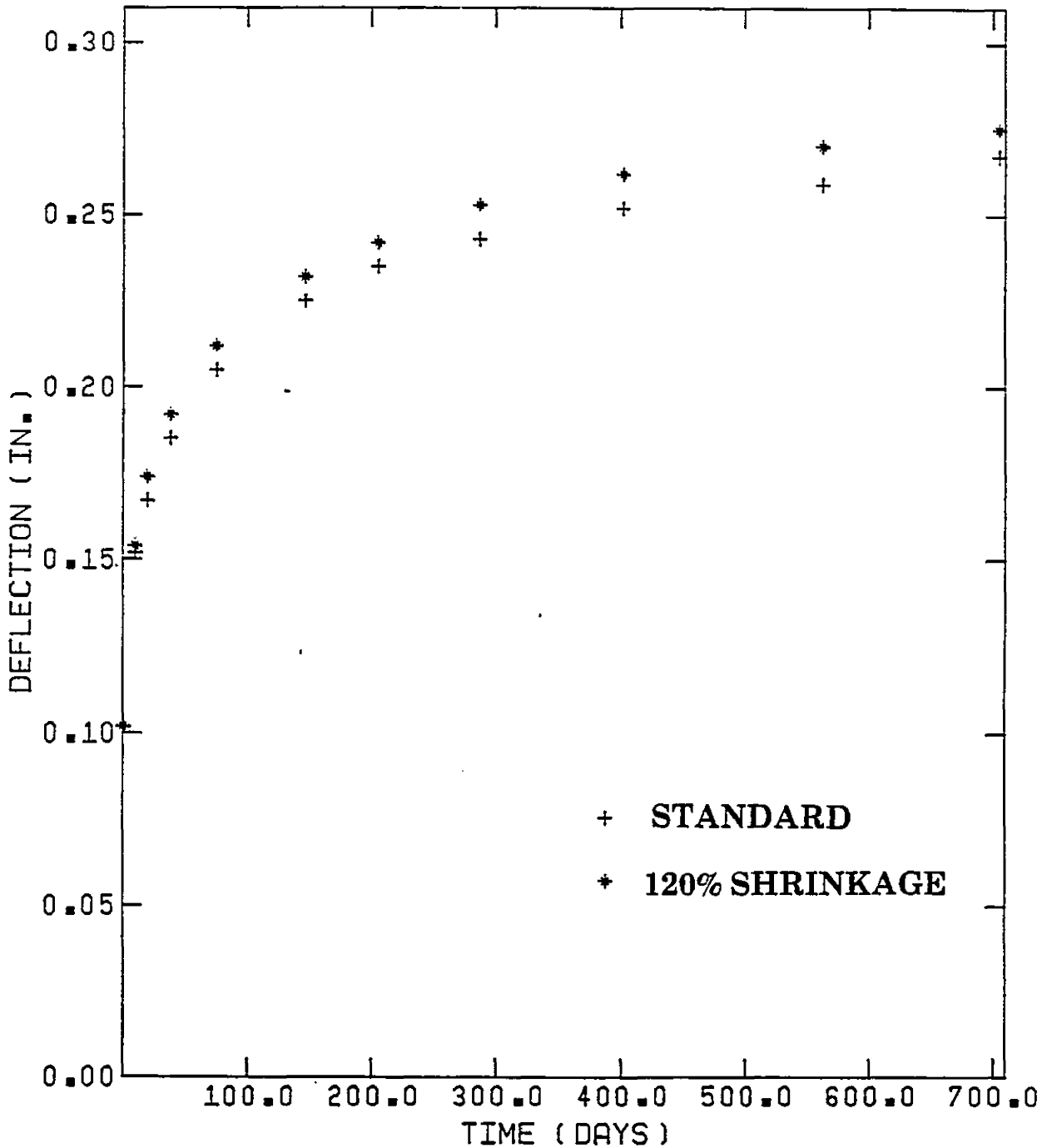


FIGURE 3.9 INFLUENCE OF SHRINKAGE ON LONG TERM DEFLECTIONS AT HIGH LOADS

by more than a reasonably constant 5%. This indicated that for this particular beam, significant changes in shrinkage strains had a lesser effect on deflections. This is a reasonable conclusion because shrinkage is only one factor in time dependent deflections. In a highly stressed beam like the one represented here, the creep effect would be more likely to dominate.

Creep

The effect on long term deflections of increasing the creep by 20% is shown in Figure 3.10, and, as just predicted, the effect was more pronounced than for shrinkage. Creep is a load dependent phenomenon. Therefore, when the concrete stresses are high, it plays a significant role in determining the long term deflection. By increasing the creep by 20%, the total deflection at the end of the loading period increased by about 8%. Unlike the shrinkage results, this percentage difference was not constant throughout the loading period but increased with time at a decreasing rate.

Element Mesh Size

The accuracy of a finite element solution can be significantly affected by the finite element mesh. To get some idea of the influence of this factor the number of elements along the length of the beam was doubled. The results are shown in Figure 3.11 and Figure 3.12. From the nature of the finite element method, it would be expected that increasing the number of elements would increase the deflection and this

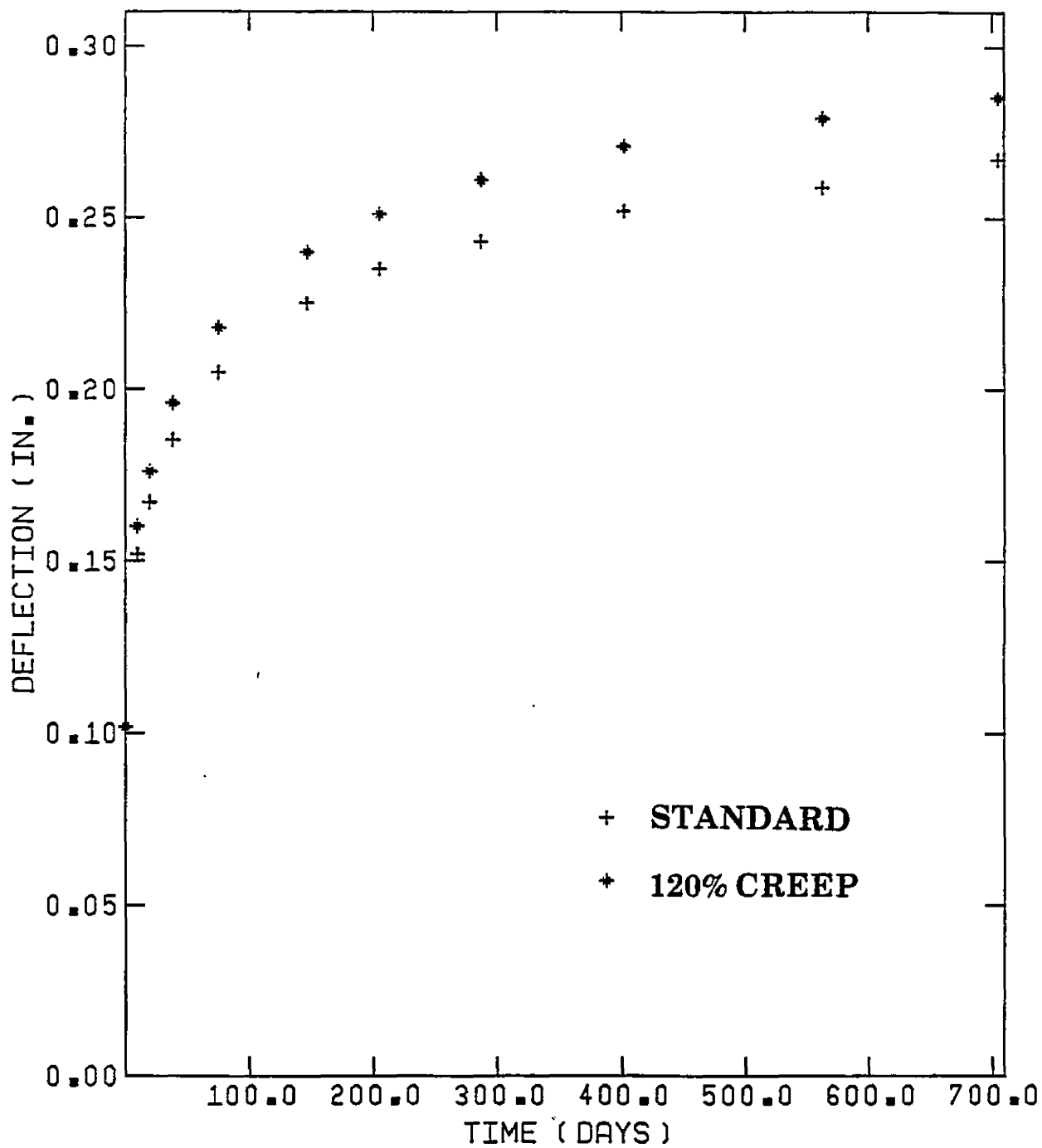


FIGURE 3.10 INFLUENCE OF CREEP ON LONG TERM DEFLECTIONS AT HIGH LOADS

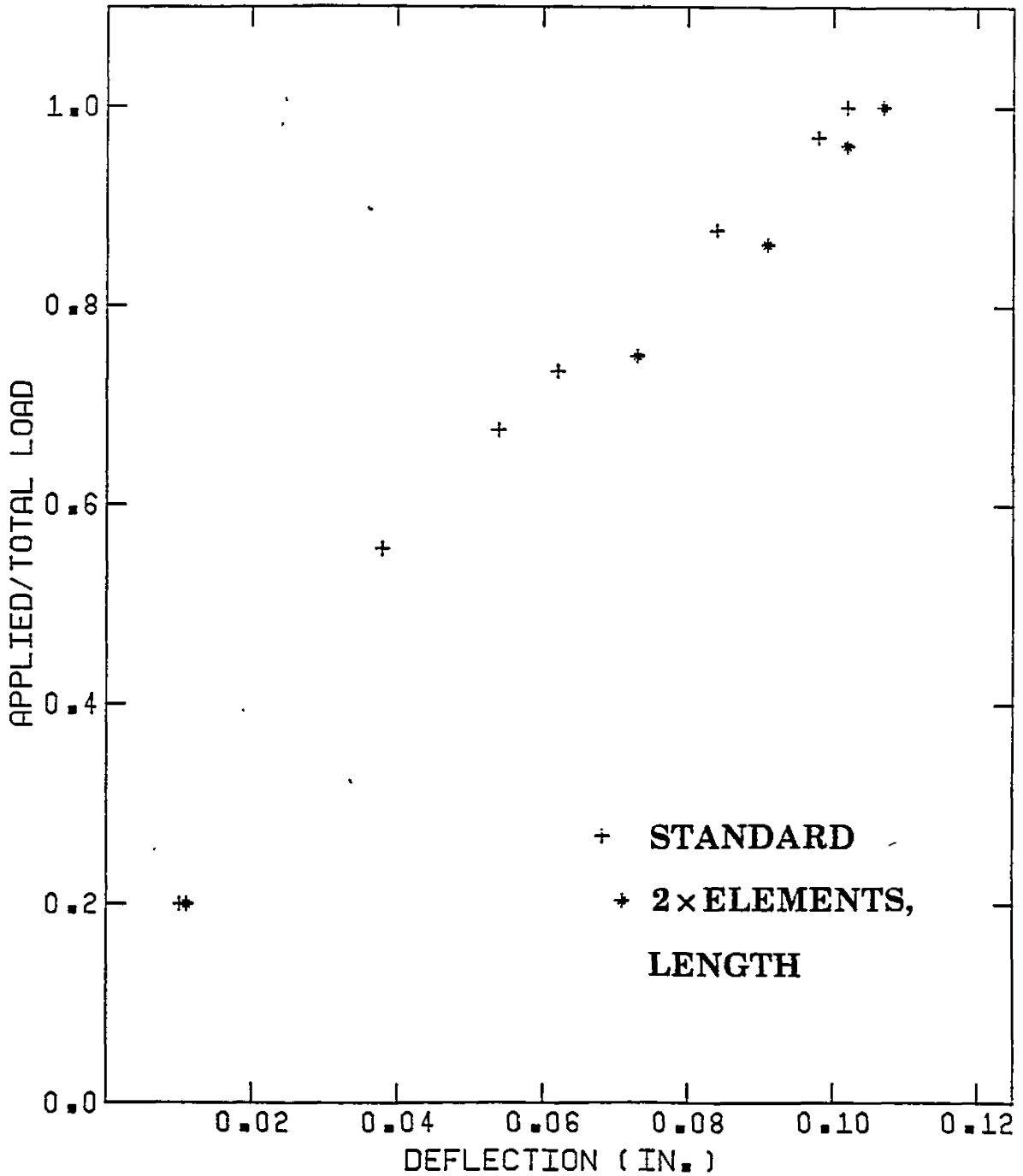


FIGURE 3.11 INFLUENCE OF DOUBLE THE NUMBER OF ELEMENTS ALONG THE LENGTH ON SHORT TERM DEFLECTIONS AT HIGH LOADS

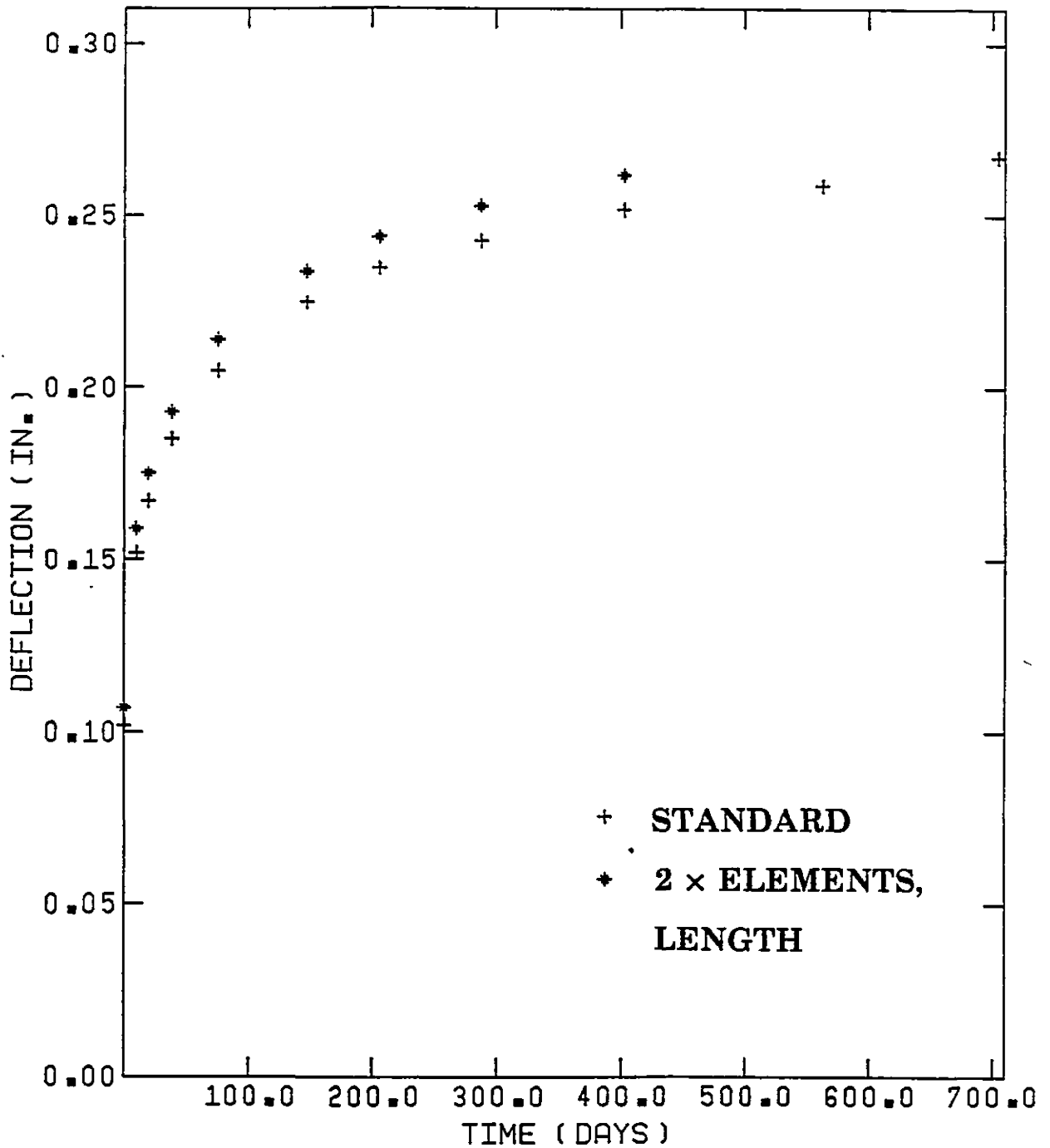


FIGURE 3.12 INFLUENCE OF DOUBLE THE NUMBER OF ELEMENTS ALONG THE LENGTH ON LONG TERM DEFLECTIONS AT HIGH LOADS

is indeed what happened. Doubling the number of elements increased the deflection by 5% for the short term case, and slightly less for the long term case. Since the convergence of a finite element solution is not linear, further doubling of the number of elements would probably have a lesser effect on the deflections. This means that the results shown in Figures 3.11 and 3.12 really only illustrate the relative influence on the meshes used in these examples.

3.3.2 Lower Stress Case

In Figure 3.13 to Figure 3.22, the sensitivity results for a reinforced concrete beam loaded to very close to the cracking load (24% of ultimate using $f_y = 40$ ksi) are shown. As was the case for the higher stressed examples, each material variable was varied by 20%. The finite element mesh size was tested by doubling the number of elements along the length of the beam and by doubling the number of elements along the height of the beam. An inspection of the short term results indicated that the model did not perform as well for this level of loading as it did for the previous one. This was primarily due to the fact that some variable changes caused the beam to crack while others did not. The difference in deflections between a cracked beam and an uncracked beam can be substantial. Under the given loading, cracking was not observed in the finite element analysis of the standard beam. However, a simple stress check of this beam indicated that the beam should have cracked. The fact that it did not, emphasises the fact that a finite element solution underestimates the exact solution. An inspection of the long term deflection results showed that the short

term variations decreased considerably with time. This occurred because those beams which did not crack under short term loads, did so when the load was sustained. The largest difference in the results for the short term case was approximately 82%, while the largest final difference in the long term results was only about 7%. The following paragraphs will discuss these results in more detail.

Tensile Strength

Tensile strength has a significant effect on the lower end of the load-deflection curve, and Figure 3.13 confirms this. Lowering the tensile strength of this beam by 20% caused a crack to form, whereas this was not the case for the standard beam. Obviously a beam with a single crack in it has a much lower stiffness than an uncracked beam. In this case the increase in deflection was 63%. When the long term deflection was included in the analysis, Figure 3.14, the difference in deflections dropped dramatically. This occurred because the standard beam cracked with time, and the final stiffnesses of the two beams became very similar. At the end of the loading period the difference between the two curves was less than 2%. Therefore, in this case a lowering of the tensile strength accelerated the initiation of cracking. It also had a significant effect on the individual magnitudes of the short and long term deflections, but had little effect on the total deflection.

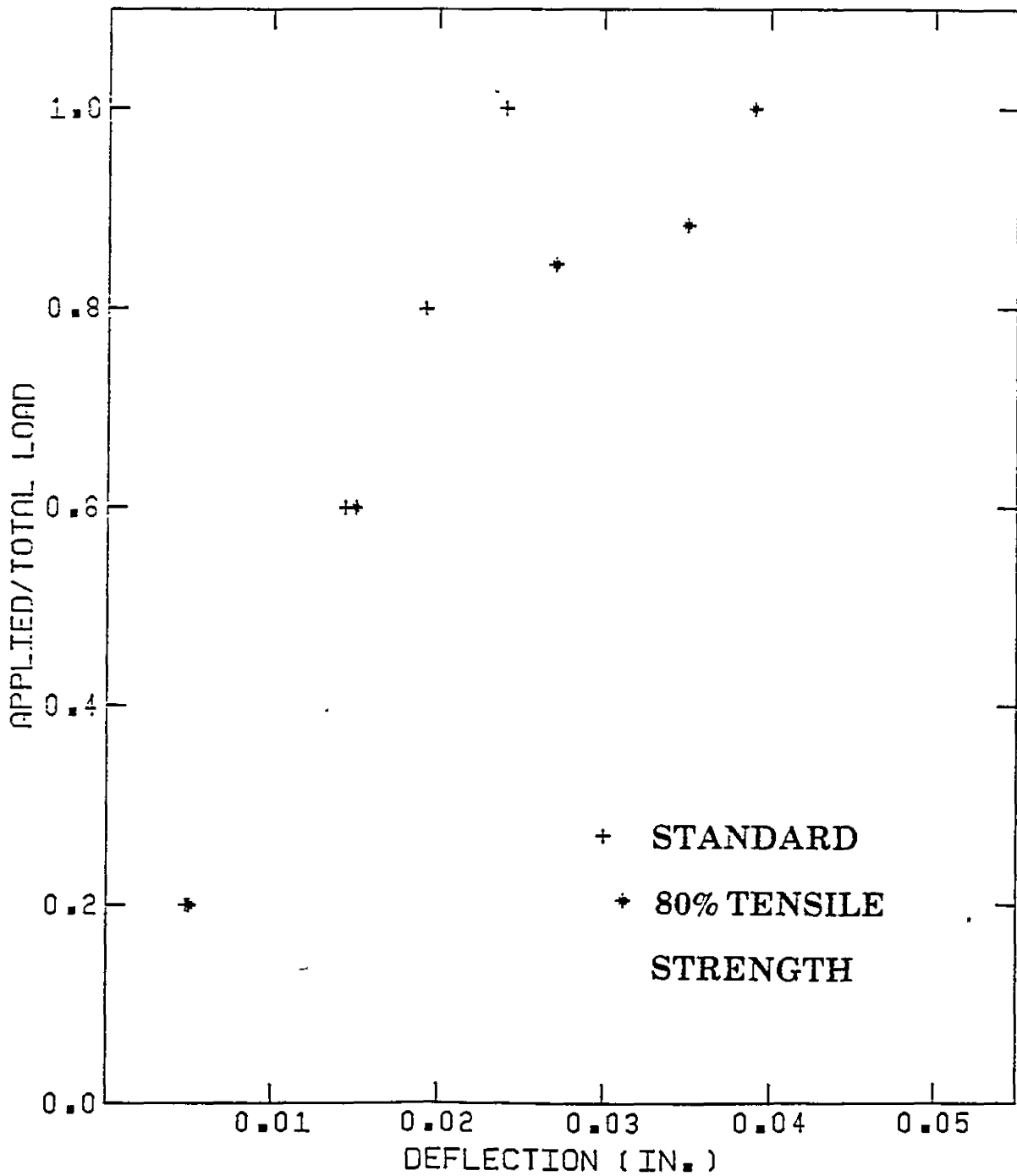


FIGURE 3.13 INFLUENCE OF TENSILE STRENGTH ON SHORT TERM DEFLECTIONS AT LOADS NEAR CRACKING

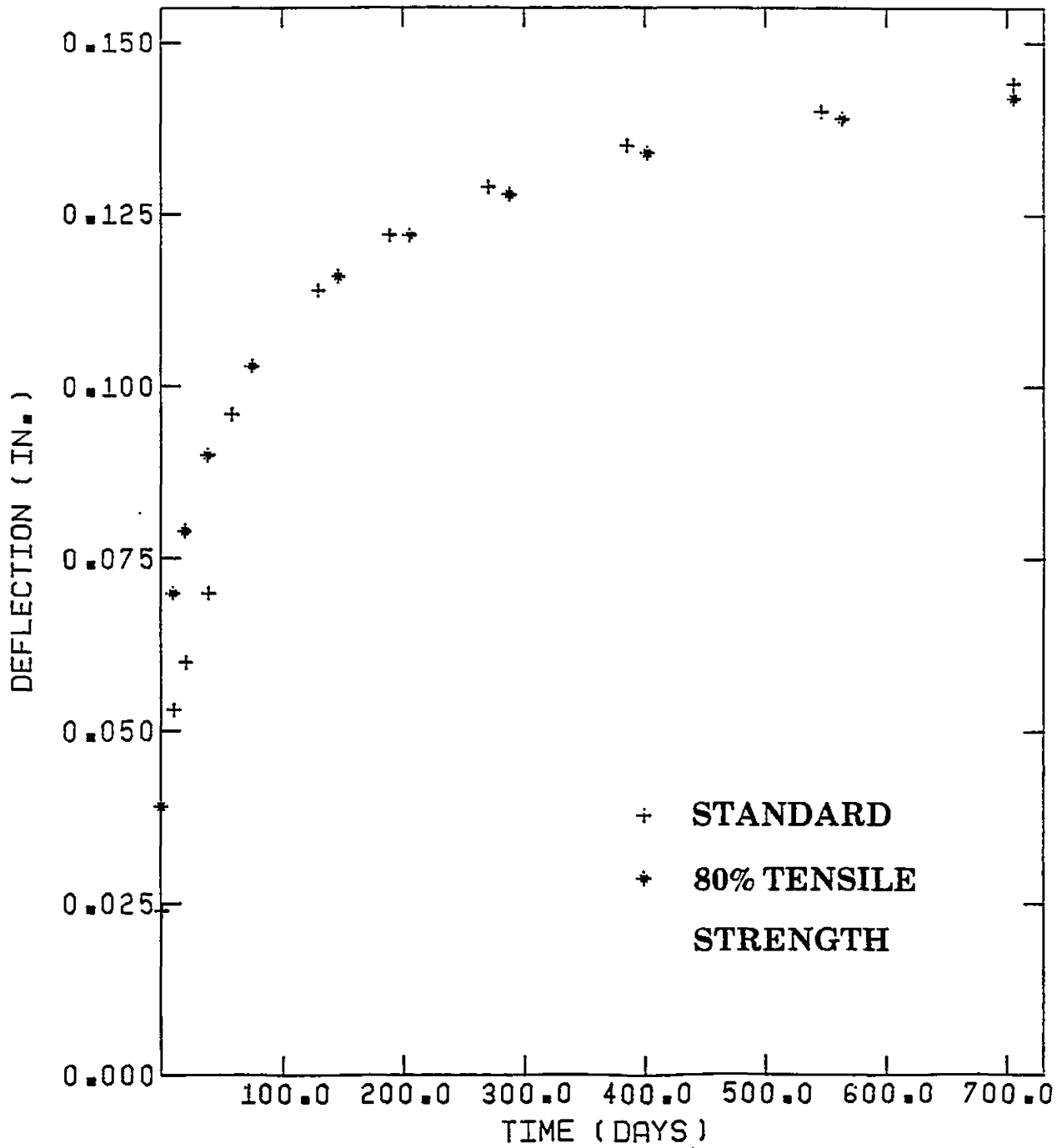


FIGURE 3.14 INFLUENCE OF TENSILE STRENGTH ON LONG TERM DEFLECTIONS AT LOADS NEAR CRACKING

Modulus of Elasticity

The modulus of elasticity is another variable which has a significant influence on the stiffness of a beam loaded to around its cracking load. In an uncracked beam, the modulus of elasticity is the major material property affecting the stiffness of the beam. Decreasing the modulus of elasticity by 20% affected the entire load-deflection curve, as shown in Figure 3.15. At the end of the short term loading period the standard deflection was 20% less than the deflection for the low modulus of elasticity. The inclusion of time dependent effects reduced this discrepancy significantly. The difference between the two curves at the end of the sustained loading period, shown in Figure 3.16, was only about 2%. The modulus of elasticity had little effect on creep and shrinkage, and after the beam cracked, its influence was not very strong. As was the case for the tensile strength results, the short term and long term deflections from this comparison were different, but the total deflections were almost the same.

Bond Stiffness

The bond stiffness was decreased by 20% to test the sensitivity of this variable. The results of this comparison were not plotted because there was no appreciable difference between this case and the standard one. This fact was not really surprising because bond stiffness is not much of a factor in a lowly stressed, lightly cracked beam. Until cracking, the steel stresses are low and there is no slip between the steel and the concrete.

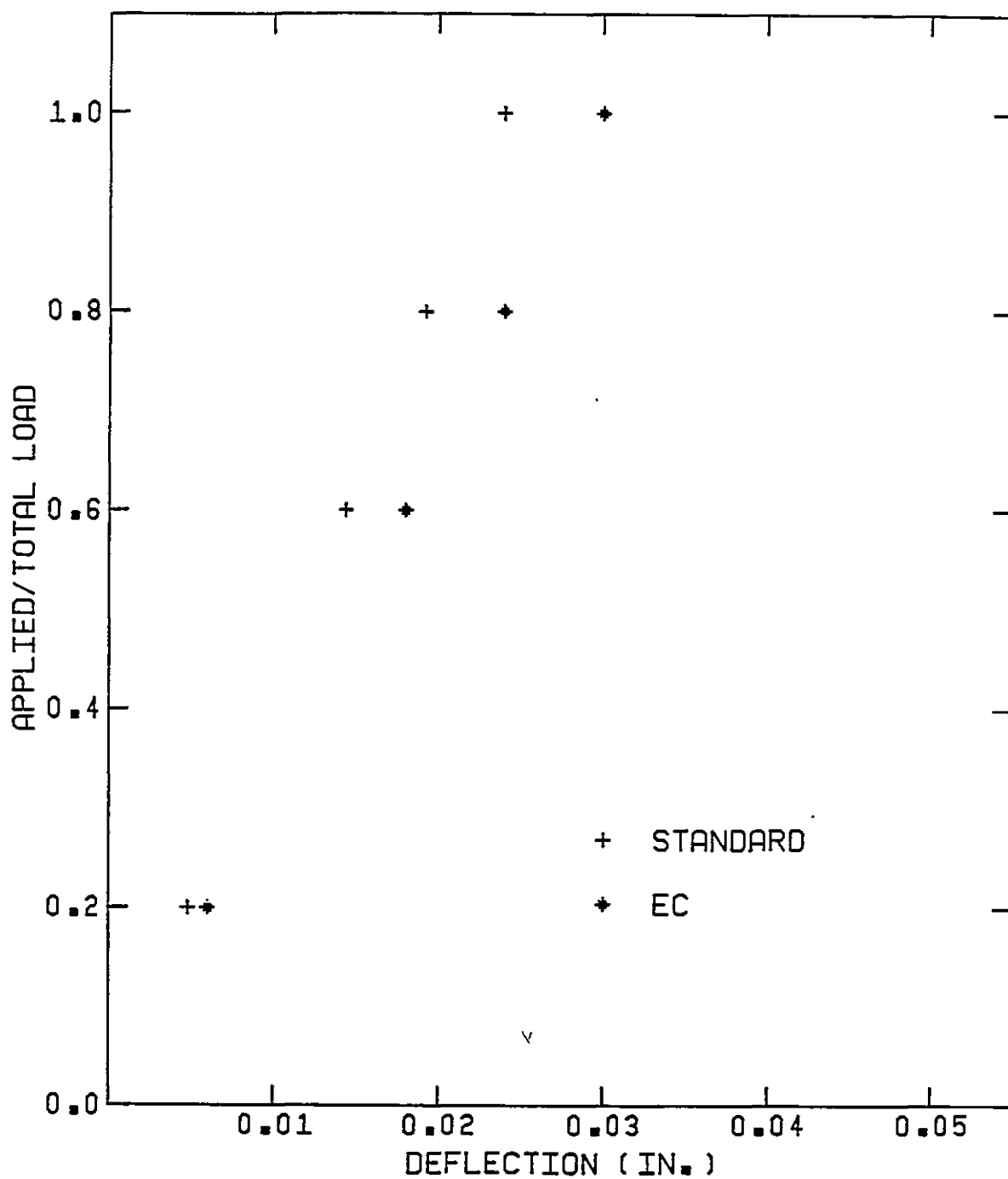


FIGURE 3.15 INFLUENCE OF E_C ON SHORT TERM DEFLECTIONS AT LOADS NEAR CRACKING

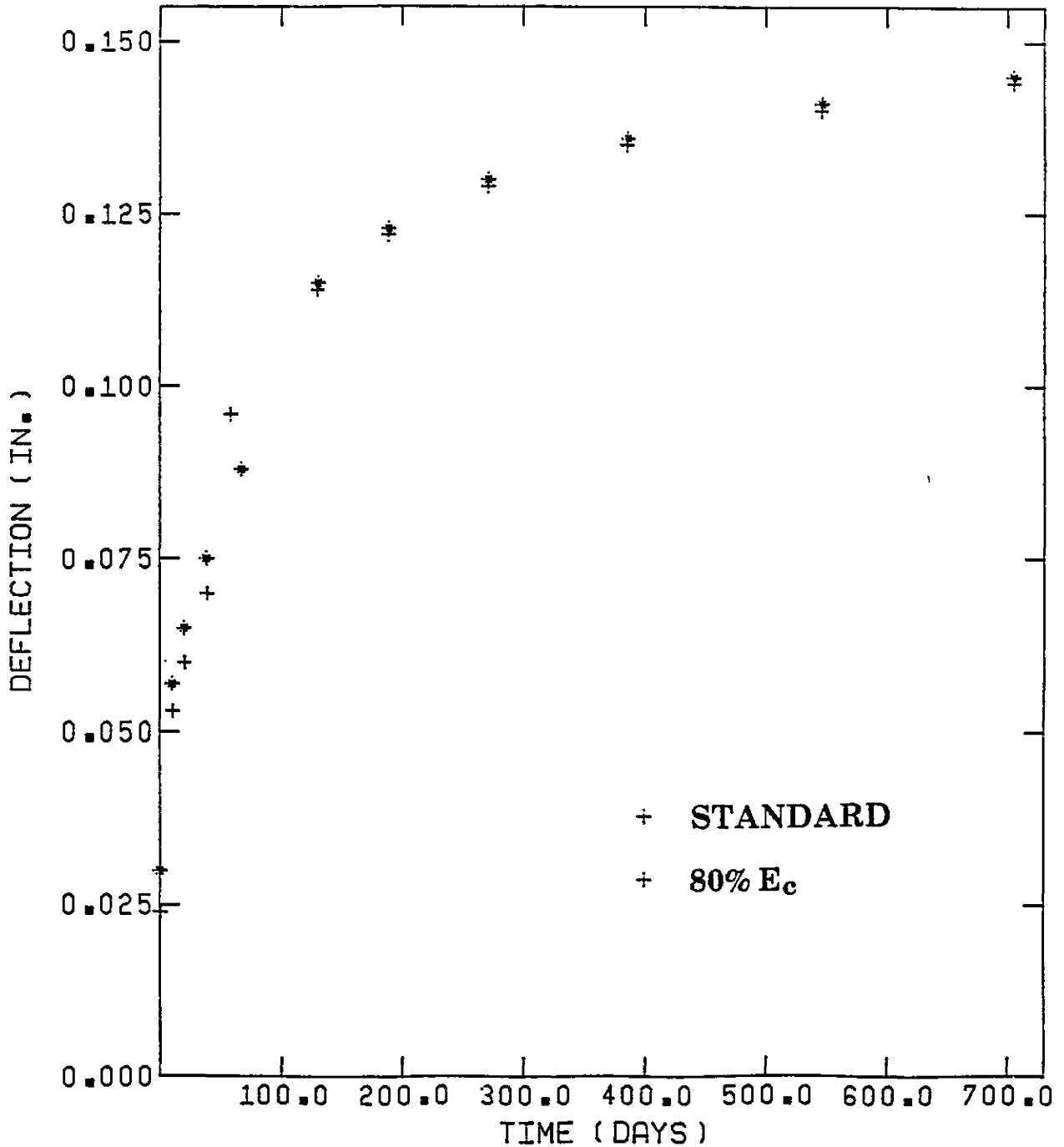


FIGURE 3.16 INFLUENCE OF E_c ON LONG TERM DEFLECTIONS AT LOADS NEAR CRACKING

Shrinkage

The effect of increasing the shrinkage strains by 20% is shown in Figure 3.17. At the end of the loading period an increase of 7% was observed in the deflections. The magnitude of the deflection difference between this case and the standard one is almost the same as for the highly stressed beam. This is not very surprising because shrinkage is not a load-dependent property.

Creep

Increasing the creep strains by 20% did not have as significant an effect on the lower stressed beam as it did on the higher stressed beam. Unlike shrinkage, creep is a load dependent property. When stresses are low, variations in creep strains have less effect on the deflections. As shown in Figure 3.18, the final difference between the standard beam and the beam with the higher creep strains was about 4%. The notable aspect of this variation was the fact that the beam with the higher creep strains had a lower deflection. This may seem contradictory at first, but creep in a simply supported beam relieves some of the stresses in the tensile zone. This means that cracks initiate later and do not progress as far into the beam as when creep is less. Creep also tends to close up existing cracks. Figure 3.18 supports these conclusions because it shows that the first crack initiated later than the crack in the standard beam. Also, the crack did not progress as far into the beam.

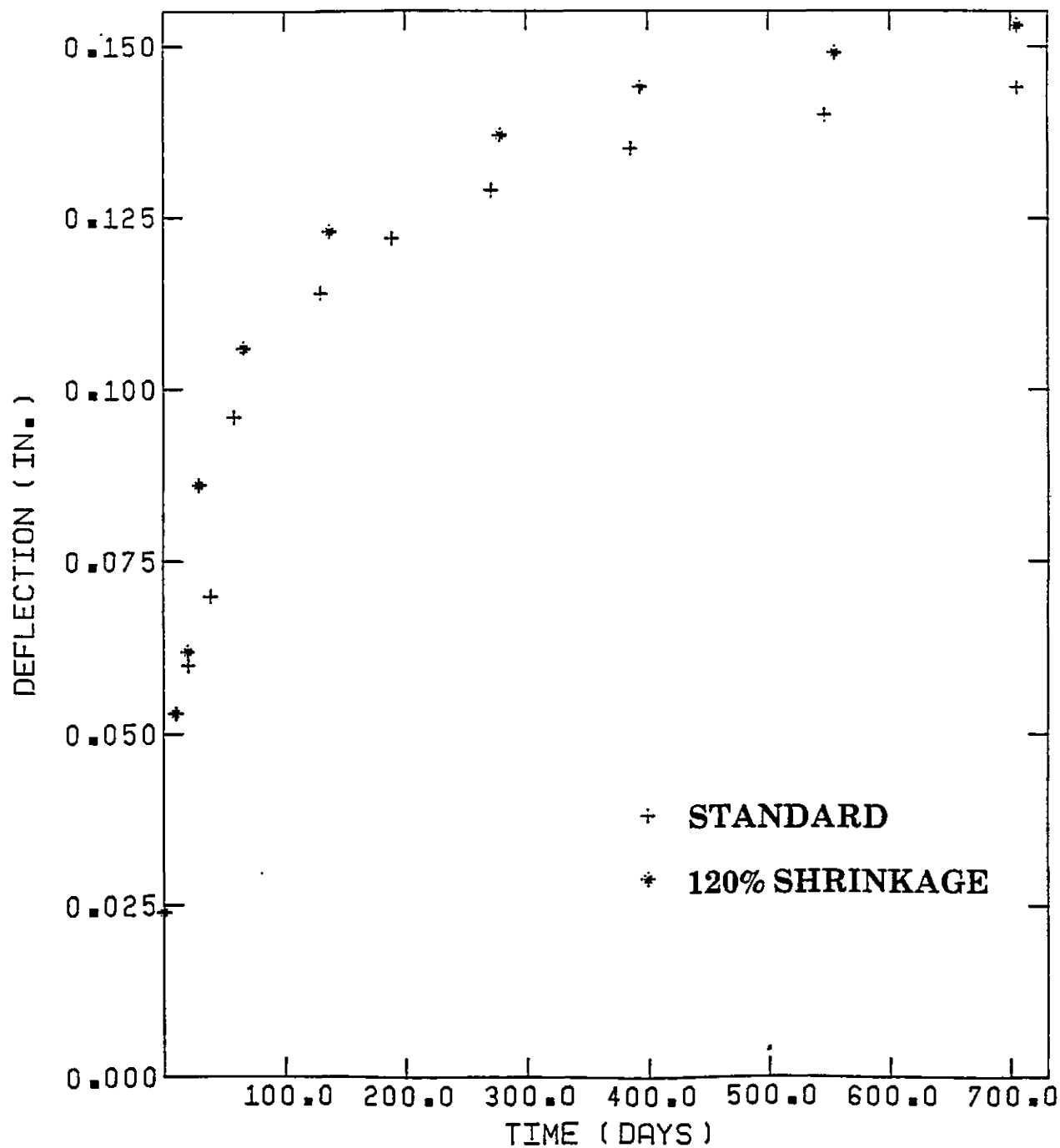


FIGURE 3.17 INFLUENCE OF SHRINKAGE ON LONG TERM DEFLECTIONS AT LOADS NEAR CRACKING

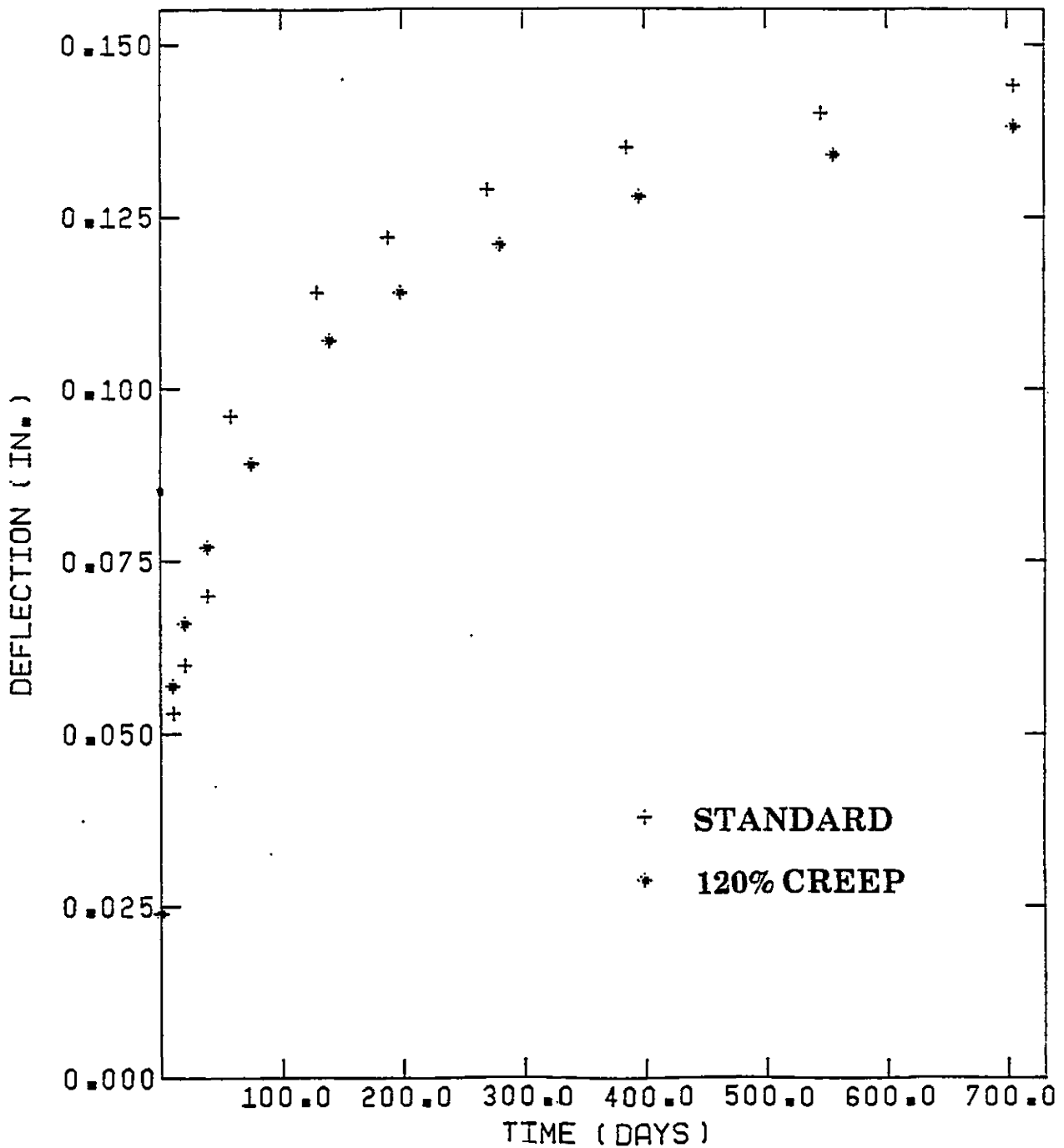


FIGURE 3.18 INFLUENCE OF CREEP ON LONG TERM DEFLECTIONS AT LOADS NEAR CRACKING

Finite Element Mesh Size

The effect of doubling the number of elements along the length of the lower stressed beam had a significant effect on the instantaneous results. Unlike the standard beam, this beam cracked during the application of the load. For this reason the deflection shown in Figure 3.19 was 50% higher than the standard case. Earlier it was stated that increasing the number of elements increases the displacements. This causes an increase in stresses, which speeds up the cracking process. With time, the standard beam also cracked and this brought the standard beam deflection more in line with the variable beam deflection, shown in Figure 3.20. At the end of 705 days, the difference in deflections was only about 2%. The effect of cracking on the beam stiffness was obviously more important than the effect of increasing the number of elements. In a beam that does not crack however, the number of elements can make a significant difference. To eliminate the effect of this variable the number of elements should be as high as is economically feasible.

For the lower stressed beam, the number of elements through the height of the beam was also doubled. This particular variation had the greatest effect on the instantaneous results. The deflections are shown in Figure 3.21. The standard beam had a deflection which was 45% less than the deflection of the larger mesh beam. The main reason for the difference was the fact that this beam cracked, whereas the standard beam did not. The deflection of this beam was also higher than the deflections of the other cracked beams, probably because the first crack

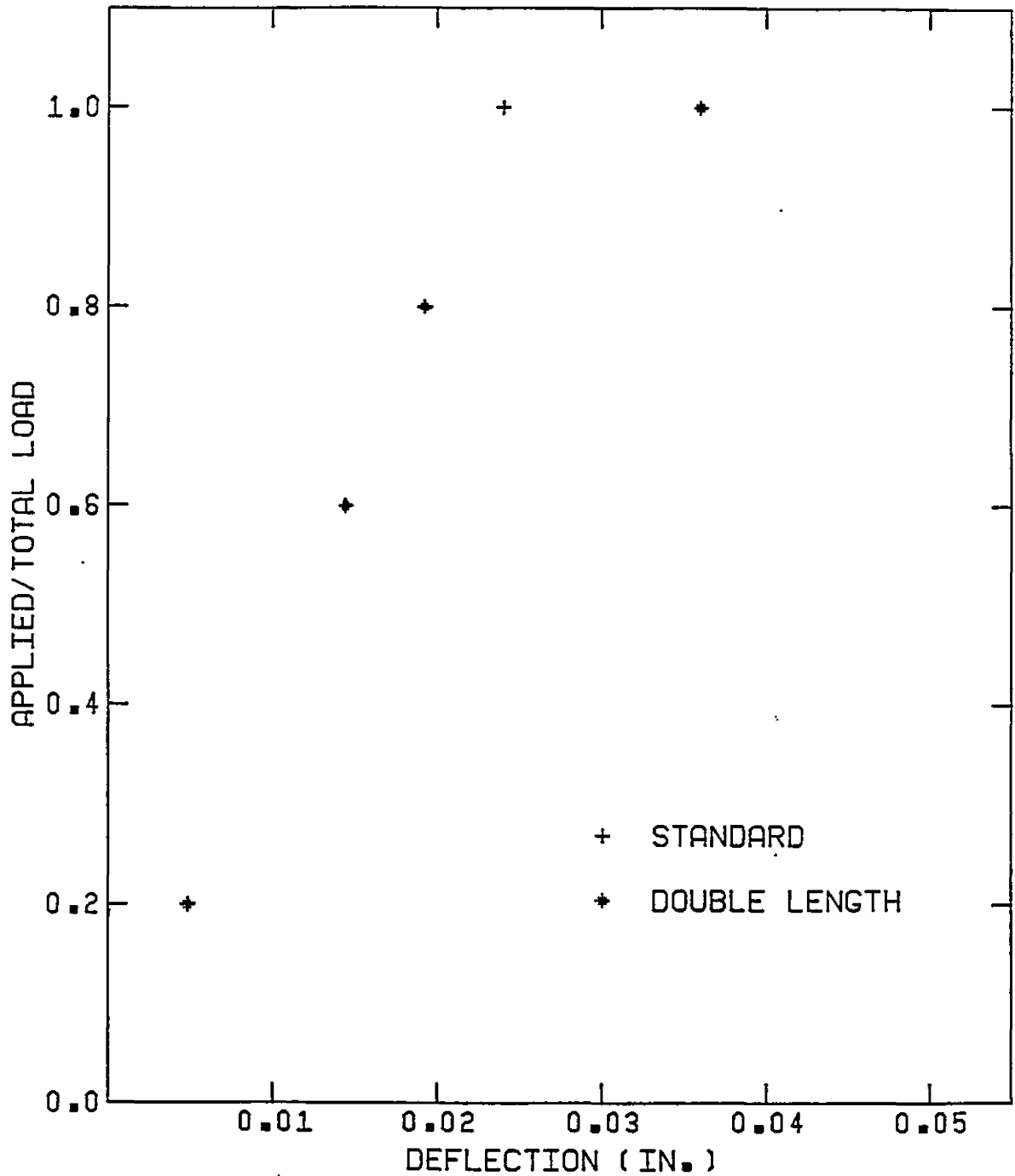


FIGURE 3.19 INFLUENCE OF DOUBLE THE NUMBER OF ELEMENTS ALONG THE LENGTH ON SHORT TERM DEFLECTIONS AT LOADS NEAR CRACKING

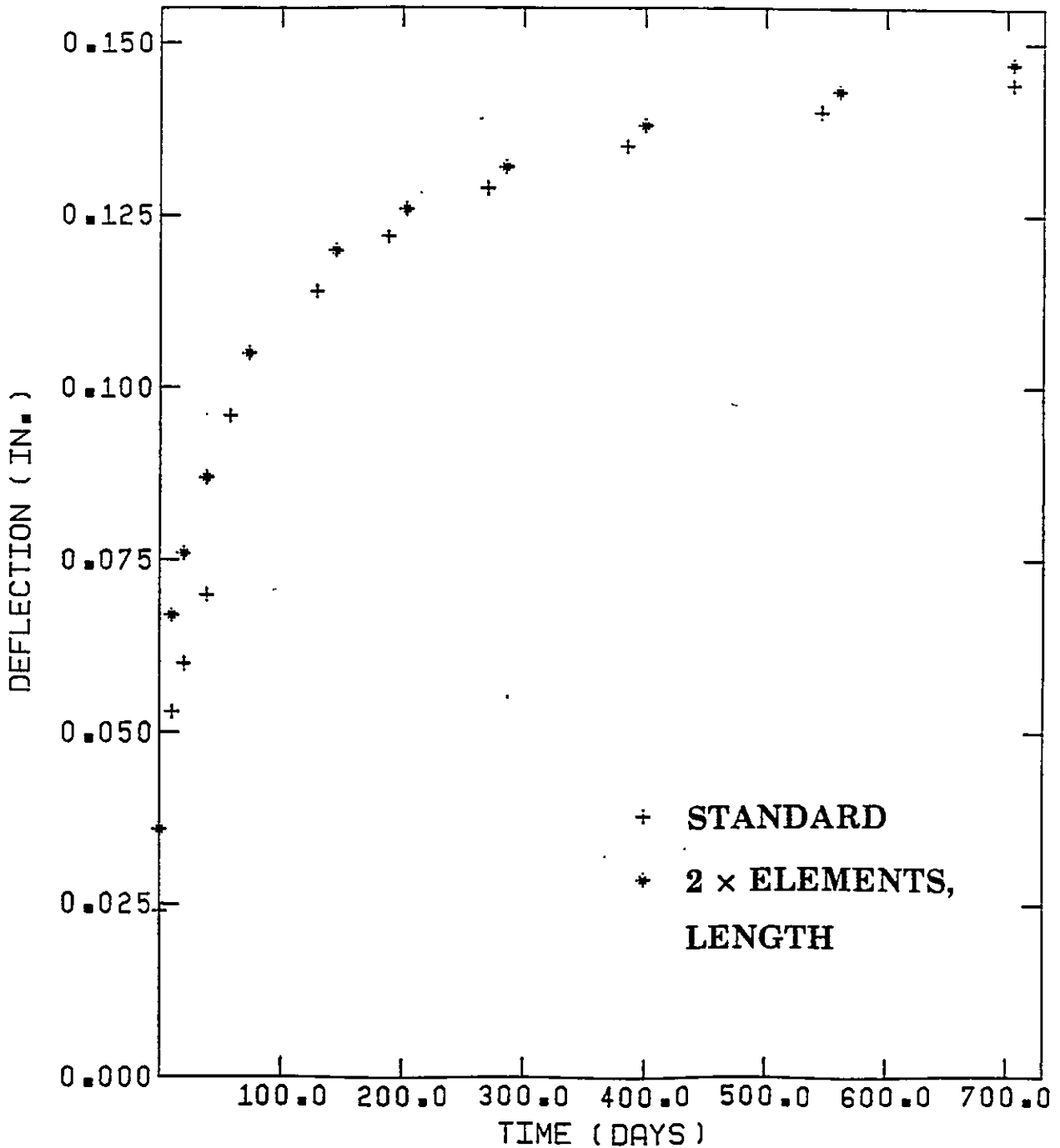


FIGURE 3.20 INFLUENCE OF DOUBLE THE NUMBER OF ELEMENTS ALONG THE LENGTH ON LONG TERM DEFLECTIONS AT LOADS NEAR CRACKING

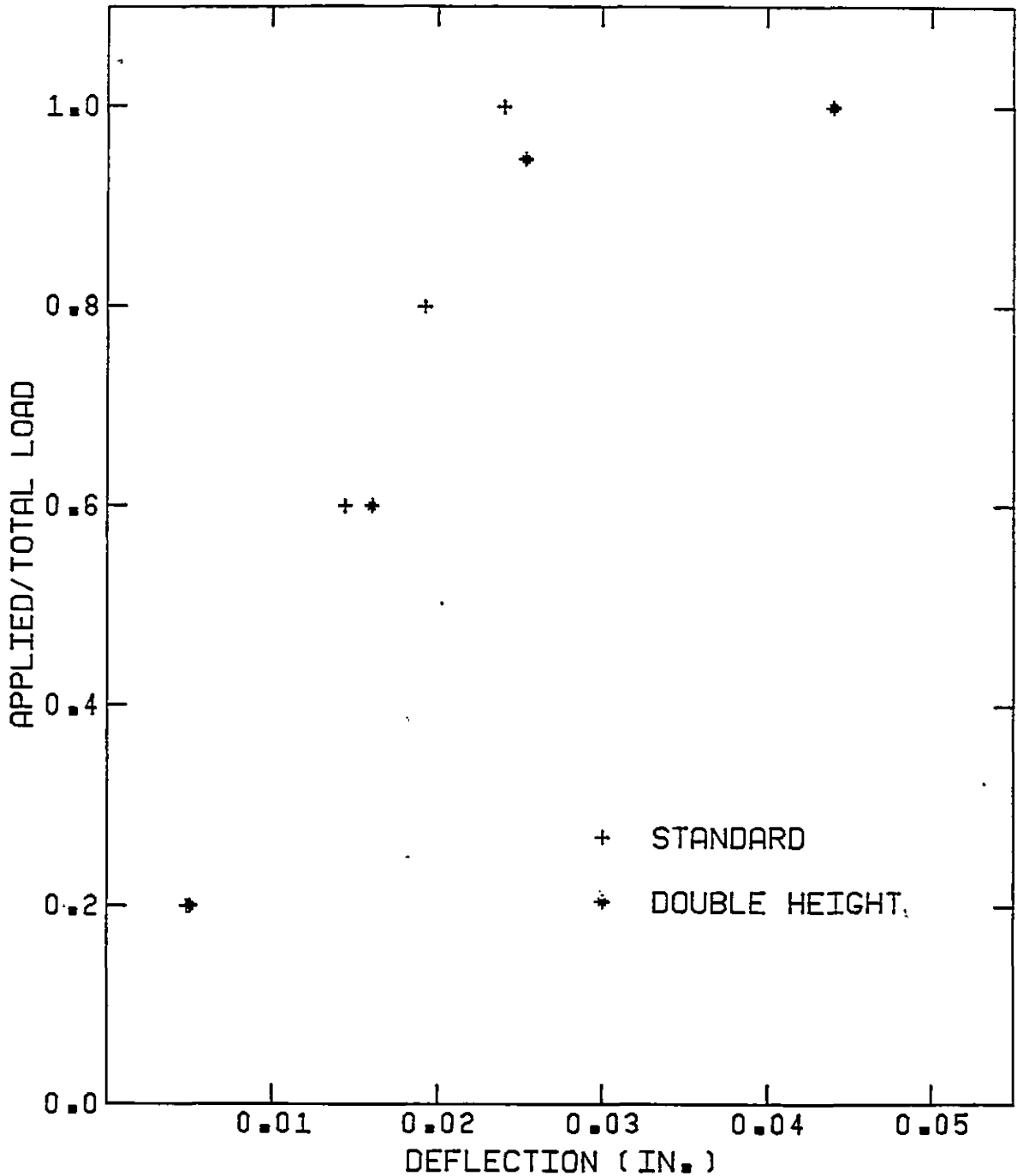


FIGURE 3.21 INFLUENCE OF DOUBLE THE NUMBER OF ELEMENTS ALONG THE DEPTH ON SHORT TERM DEFLECTIONS AT LOADS NEAR CRACKING

progressed further into this beam. Until cracking took place, the deflections of the standard and variable beams were similar. It seems likely that the variable beam cracked first because the centroids of the lowest elements in this beam were closer to the extreme tension fibre than the corresponding elements in the standard beam. Since the stresses in an element were calculated at the centroid, the variable mesh beam reached its cracking load first. It is also possible that the crack progressed further into this beam because the centroids of the elements above the crack were also closer to the crack tip. Stresses around a crack tip are high and this may have influenced the growth of the crack.

The long term deflections of this example are shown in Figure 3.22. The standard beam cracked with time and at the end of the loading period the variable beam deflection was about 5% higher than the deflection of the standard beam. Once again the effect of cracking overshadowed other effects. Since the crack in the standard beam never progressed as deep as for the finer mesh beam, the relative deflections for this case were not as close as for some of the other examples.

Summary

In this sensitivity study the effects of changing many of the finite element model input variables were examined. It is important to understand the effects of these changes because concrete itself is a highly variable material. The main conclusion which may be drawn from this study was that cracking had the greatest influence on the stiffness

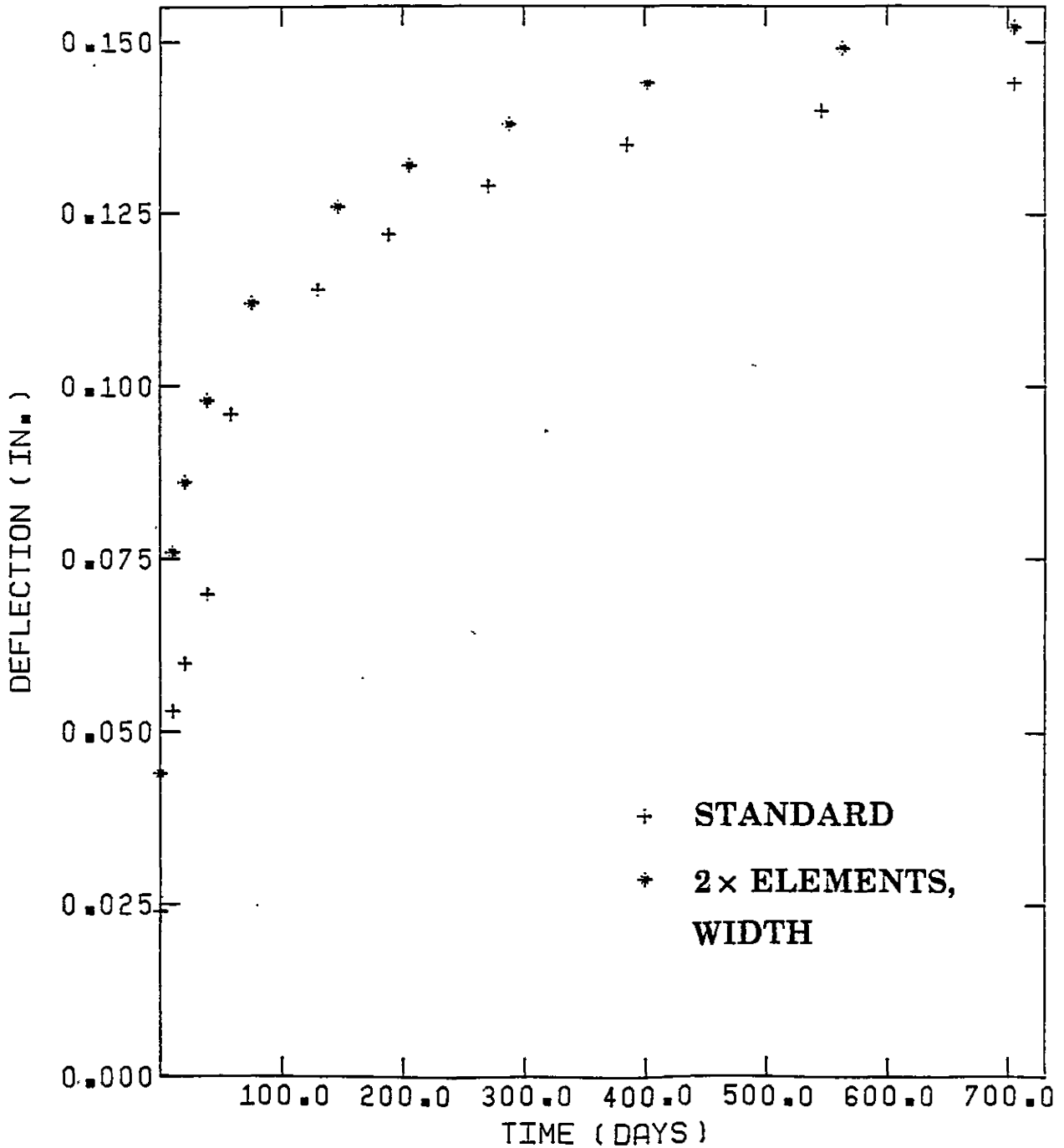


FIGURE 3.22 INFLUENCE OF DOUBLE THE NUMBER OF ELEMENTS ALONG THE DEPTH ON LONG TERM DEFLECTIONS AT LOADS NEAR CRACKING

of the reinforced concrete beam. It tended to overshadow the effects of all other influences. Since the accuracy of the crack modelling technique could not be tested directly, its effect on the results is unknown.

For the beam stressed well beyond its cracking load there was no single variable that had more than an 8% effect on the instantaneous deflections for a 20% difference. When long term effects were varied by 20%, only creep and shrinkage strains had differences as large as 8%. In all cases the influence on deflection was not nearly as great as the variation of the parameter.

The beam loaded to around its cracking load was influenced mostly by variables which hastened or delayed the onset of cracking. When the beam was uncracked, the material and mesh size parameters had a much larger influence than for a cracked beam. When even a single crack was formed there was no other single parameter which changed the deflections by more than a few percent. The ratio of long term to short term deflections in the lower stressed beam was greatly affected by whether major cracking took place during loading or with time. Obviously the model is much more sensitive to variations when the stresses in the concrete are near failure.

One factor that has not been addressed yet is the fact that even when one parameter does not affect the results very much on its own, the combined effects of a few parameters can influence the results substantially. Obviously the proposed finite element model will not duplicate

experimental results exactly. There are far too many possible variations in the input parameters, and the prediction methods that were used can only approximate the correct results. However the preceding sensitivity study showed that small variations in the parameters did not usually have a significant effect on deflections. Therefore the model can be used with some confidence in this regard.

3.4 Evaluation of Model for Short Term Loads

The short term behaviour predicted by the proposed finite element model was evaluated by comparing its results with experimental data obtained from a number of different sources. It was important for the model to accurately predict the immediate deflection of concrete beams so that the emphasis of this study could be focussed on the long term effects. Not all of the information required for a complete finite element analysis was provided in the literature, and it was usually necessary to estimate some of the material properties. Experimentally observed crack patterns, concrete strains, and mid-span deflections from the literature were used to check all aspects of the accuracy of the finite element model. It should be noted that concrete is a highly variable material and an exact duplication between the finite element model and experimental data is never possible. In general however, the following examples will show that the model performed very well in most cases, and, considering the number of assumptions that were made, was able to simulate the short term behaviour of reinforced concrete beams.

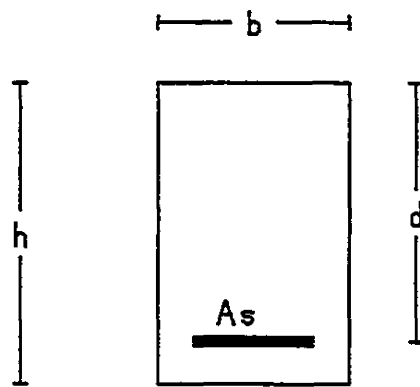
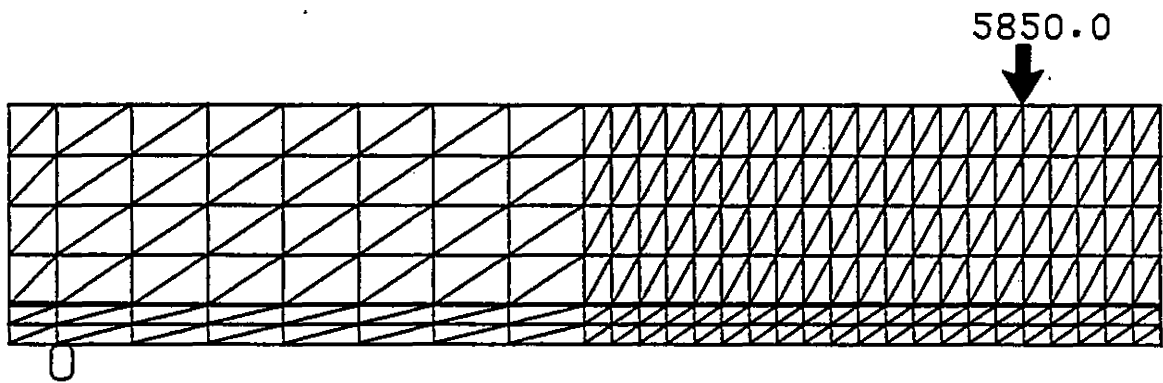
The short term test deflections reported in the literature did not include self-weight deflections. Since self weight influences cracking behaviour, the deflections from the finite element model were determined by subtracting self weight deflections from the total deflections. The results and conclusions from the Sensitivity section should be kept in mind when reviewing this chapter.

Beam 7/1

The first beam used to verify the accuracy of the analytical model was tested by Leonhardt and Walther (30) in 1962. They studied the moment-shear relationship of reinforced concrete beams. Since not all of the required information was available, it was necessary to estimate those values using the empirical relationships reported in section 3.11. The compressive strength of the concrete in this test was specified as a cube strength. To convert this quantity to a comparable cylinder strength, an equation developed by L'Hermite and reported by Neville (38) was used.

The properties of Leonhardt and Walthers Beam 7/1 as well as the finite element discretization used is shown in Figure 3.23. The tensile strength of the concrete was estimated using Equation (3.2), and the concrete modulus of elasticity was estimated using Equation (3.1). The ultimate load of this beam was 13.5 kips, so the ratio of applied load to ultimate load was .433.

BEAM 7/1



$$f'_c = 4300 \text{ psi}$$

$$b = 7.48 \text{ in}$$

$$L = 12 \text{ in.}$$

$$f_t = 490 \text{ psi}$$

$$d = 10.6 \text{ in}$$

$$A_s = 1.65 \text{ sq. in.}$$

$$E_c = 3727 \text{ ksi}$$

$$E_s = 28450 \text{ ksi}$$

$$h = 12.6 \text{ in}$$

FIGURE 3.23 DETAILS FOR BEAM 7/1

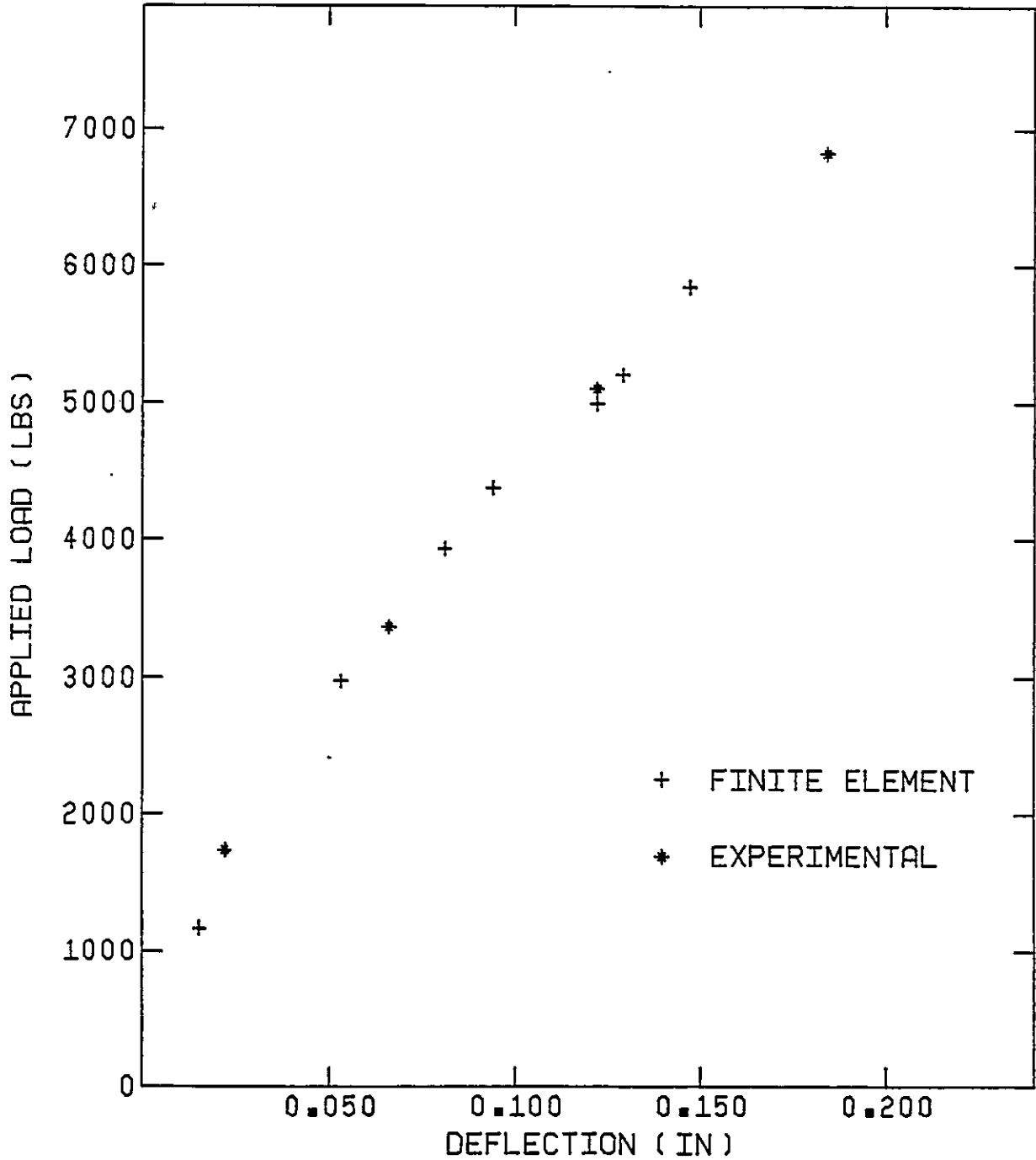


FIGURE 3.24 EXPERIMENTAL AND FINITE ELEMENT DEFLECTIONS FOR BEAM 7/1

The experimental load-deflection curve for Beam 7/1 is compared in Figure 3.24 with the finite element predictions. The correlation between the experimental and finite element results is almost unbelievable considering the number of approximations which were made. At no time was there a variation of more than a few percent between the two curves. It was probably coincidence that the results were this good since experimental variability and the sensitivity of the model would be expected to create greater differences. However the excellent agreement between the experimental and finite element deflections indicates that the model accurately simulated each stage of the loading and cracking process.

Beam OA-2

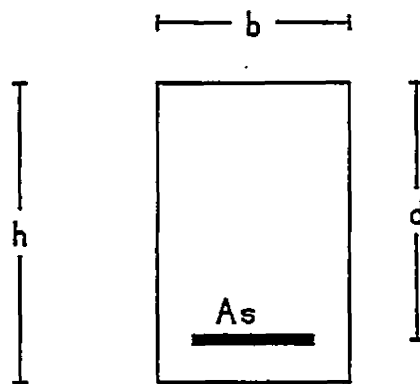
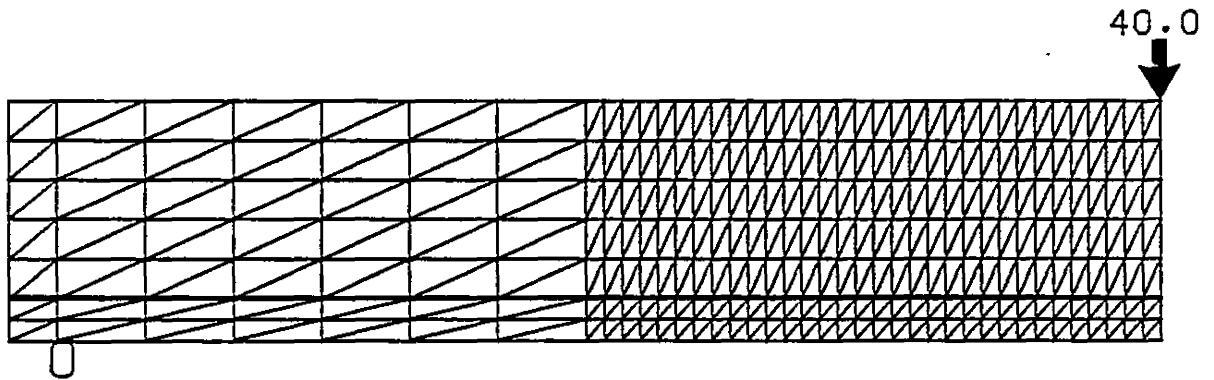
Testing the accuracy of a finite element model with one set of experimental data does not in itself prove the validity of the model. A model must demonstrate consistency in simulating correct behaviour. To achieve this goal the results from a beam tested by Bresler and Scordelis (10) were compared with the results from the finite element model. Bresler and Scordelis tested a number of different beams to determine their shear strength properties. The beam they designated as OA-2 was chosen for the verification. The authors reported crack patterns as well as midspan deflections for this beam, so a more detailed comparison between experimental and finite element results was possible.

Pertinent information about the test beam and the finite element discretization are presented in Figure 3.25. The modulus of elasticity of the concrete was estimated using Equation (3.1). The ultimate load of this beam was 80 kips, and the ratio of applied to ultimate load was 0.45.

The experimental and finite element generated deflections are presented in Figure 3.26. Loading for this beam was high enough to cause significant cracking. The correlation between the two deflection curves was again excellent. The difference between the finite element predictions and experimental results at 45% of the ultimate load was only about 8%. The behaviour of the finite element curve was almost identical to the behaviour of the experimental curve. This indicated that the loss of stiffness in the two beams took place at almost the same rate.

Since cracking is the most significant factor contributing to the instantaneous deflection of a reinforced concrete beam, it was vital that the finite element model simulate it correctly. Bresler and Scordelis supplied the crack pattern for Beam OA-2 and this is compared in Figure 3.27 with the finite element solution. It is important to remember that since cracking is influenced by many different factors, it is unrealistic to expect the model to duplicate the experimental results exactly. Rather, it is the general behaviour which is important. Although the crack patterns in Figure 3.27 were not identical, there were many similarities. A common feature of both beams was the tendency for some of the cracks to form at the level of the reinforcement rather

BEAM OA-2



$f'_c = 3440$ psi	$b = 12.0$ in	$A_s = 5.0$ sq. in.
$f_t = 629$ psi	$d = 18.0$ in	
$E_c = 3465$ ksi		
$E_s = 31600$ ksi	$h = 21.75$ in	

FIGURE 3.25 DETAILS FOR BEAM OA-2

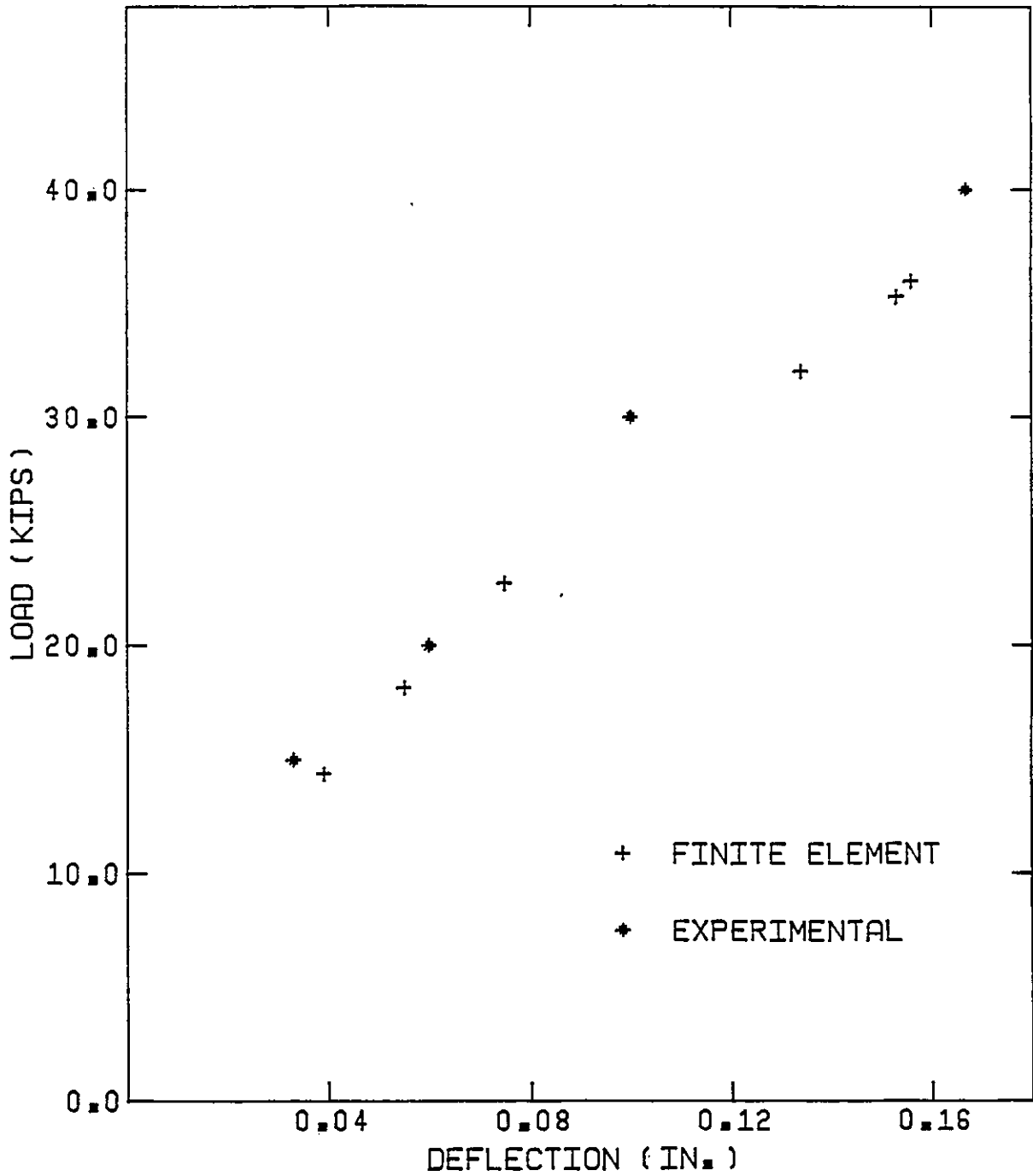
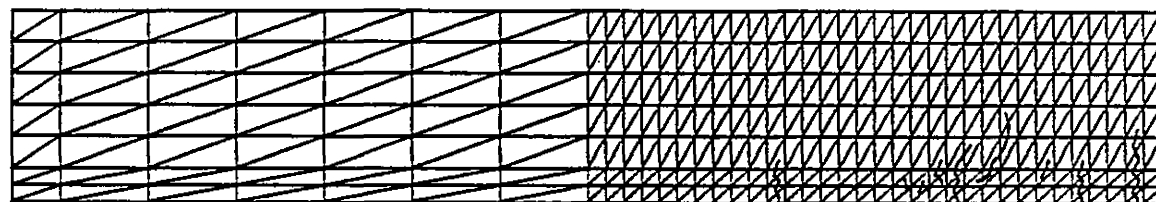
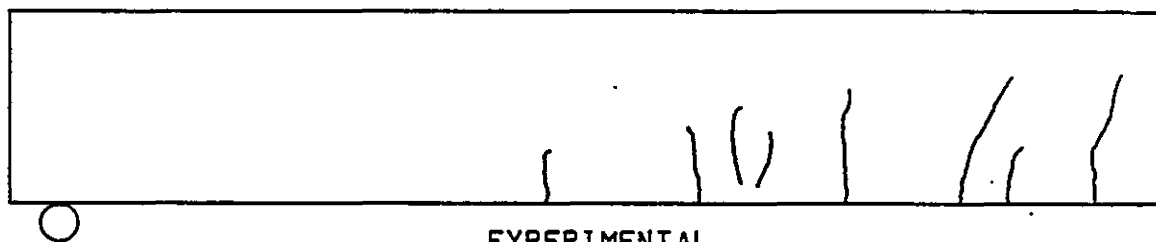


FIGURE 3.26 EXPERIMENTAL AND FINITE ELEMENT DEFLECTIONS FOR BEAM OA-2

BEAM OA-2



FINITE ELEMENT



EXPERIMENTAL

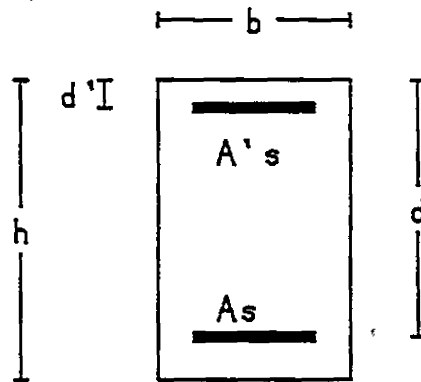
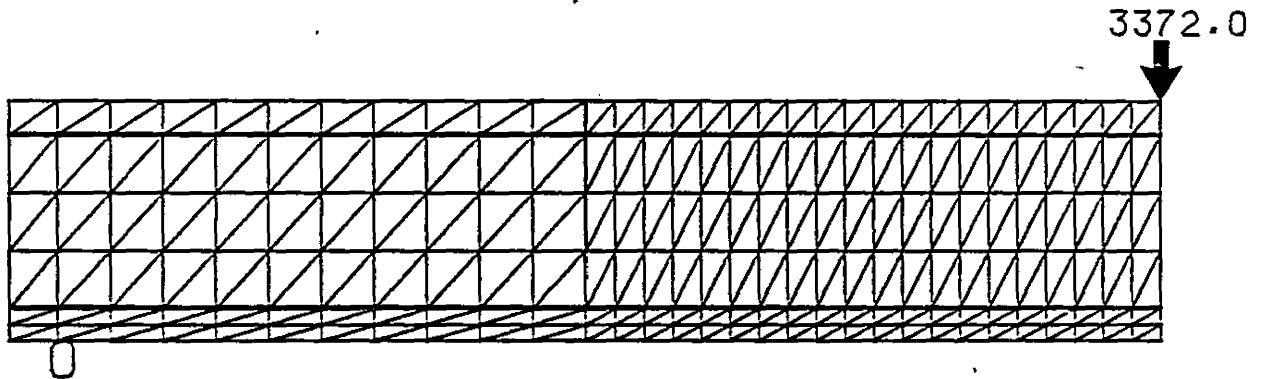
**FIGURE 3.27 EXPERIMENTAL AND FINITE ELEMENT
CRACK PATTERNS FOR BEAM OA-2**

than at the extreme tension fibre. This common feature gave a good indication that the steel-concrete interaction was realistically simulated by the finite element model. The crack spacings were also similar. The major difference between the beams was the fact that more cracks were observed in the experimental beam than were predicted by the model. They were also initiated at lower loads and progressed further into the beam. This may have been due to the size of the elements, a lower tensile strength, or a slightly different stress distribution. The difference in cracking was reflected to some degree in the deflections, since the experimental deflections were always slightly greater than the finite element ones. However the effect was not very large and it decreased as the load increased.

Beam DR10

In the course of an investigation into steel fibre concrete, Swamy and Al-Ta'an (51) reported on the deflection characteristics of a simply supported beam with tension and compression steel. Beam DR10 was selected for the comparison with the finite element model. This beam was made from normal concrete without steel fibres and most of its material properties were reported. The details for this test are presented in Figure 3.28. The ratio of applied load to ultimate load was about 0.47 in this comparison. Since the cube test was used to define the concrete compressive strength, L'Hermite's equation was used to find a comparable cylinder strength.

BEAM DR10



$$f'_c = 4371 \text{ psi}$$

$$b = 5.12 \text{ in}$$

$$L = 98.42 \text{ in.}$$

$$f_t = 505 \text{ psi}$$

$$d = 6.93 \text{ in}$$

$$A_s = .351 \text{ sq. in.}$$

$$E_c = 4079 \text{ ksi}$$

$$d' = 1.14 \text{ in}$$

$$A's = .243 \text{ sq. in.}$$

$$E_s = 29000 \text{ ksi}$$

$$h = 8.0 \text{ in}$$

FIGURE 3.28 DETAILS FOR BEAM DR10

The load-deflection curves comparing the experimental results with the analytical results are shown in Figure 3.29. The correlation between the two curves is reasonable, but not as good as for the previous examples. This was the case even though more material properties were given. The apparent anomaly is not remarkable in itself because the standard tests which were used to determine the material properties do not exactly represent the conditions that actually exist in beams. In addition, the significant effect of normal experimental variability must also be recognized. It is evident from Figure 3.29 that the model predicted a stiffer beam than was actually observed. The largest difference between the two curves occurred towards the lower end of the load-deflection diagram where the modulus of elasticity and the tensile strength are important parameters. After about 40% of the load had been applied, the slopes of the two curves became very similar. The percentage variation between the finite element and experimental curves decreased considerably after the cracking load was exceeded. This is the same behaviour observed during the Sensitivity Study. The final difference between the finite element generated curve and the experimental curve was about 25%.

Experimental variability seems to be the most likely reason for the finite element model predicting a stiffer beam than was observed experimentally. The evidence for this conclusion comes from further data in Swamy and Al-Ta'an's test (51). They tested another beam which was almost identical in every way to Beam DR10 except for the strength of the tension steel. In the lower region of the load-deflection curve this other beam should have had nearly the same deflections as Beam

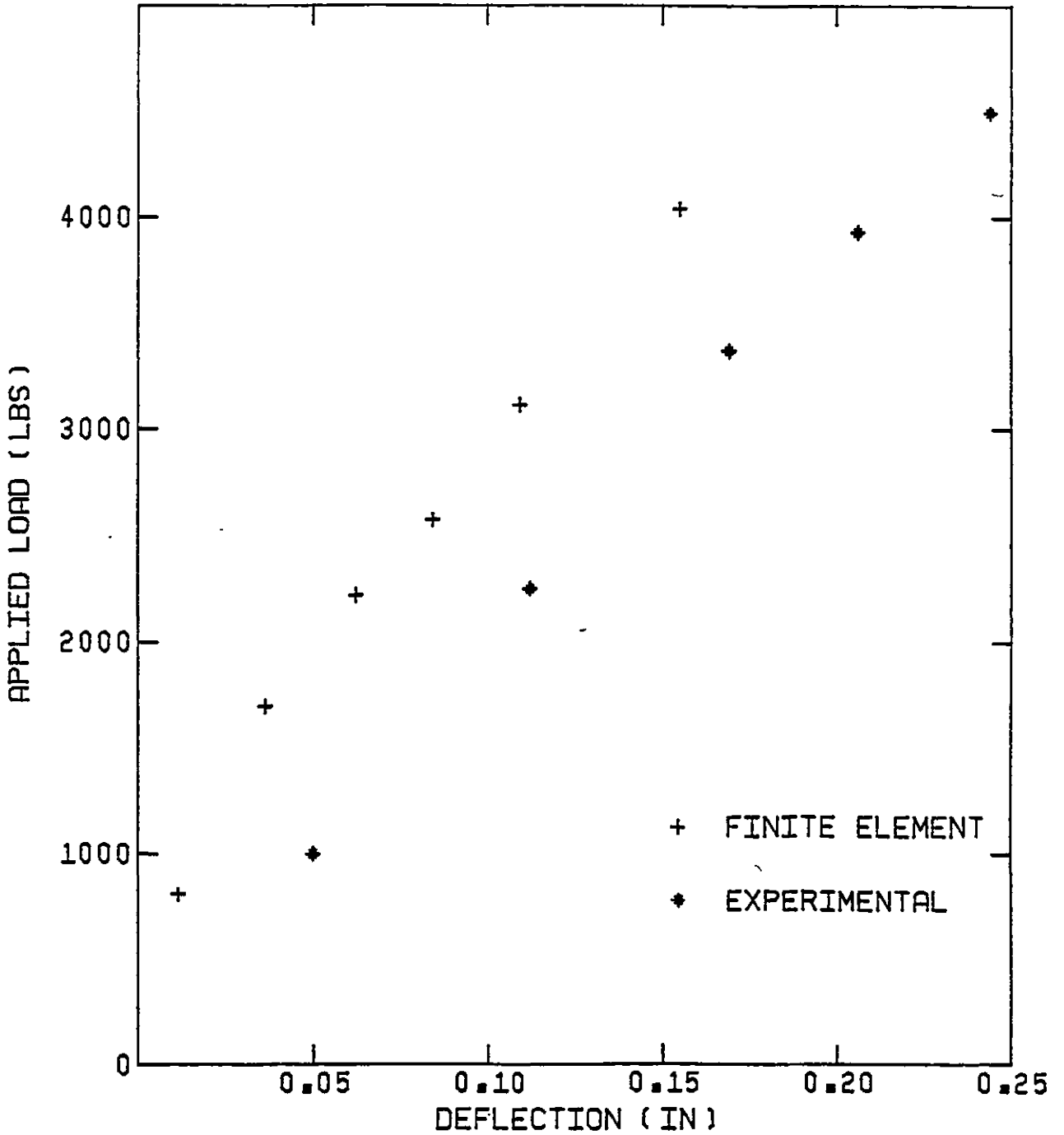


FIGURE 3.29 EXPERIMENTAL AND FINITE ELEMENT DEFLECTIONS FOR BEAM DR10

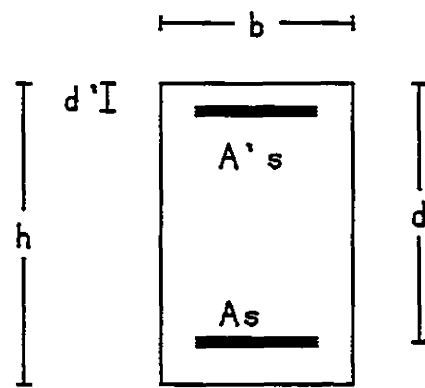
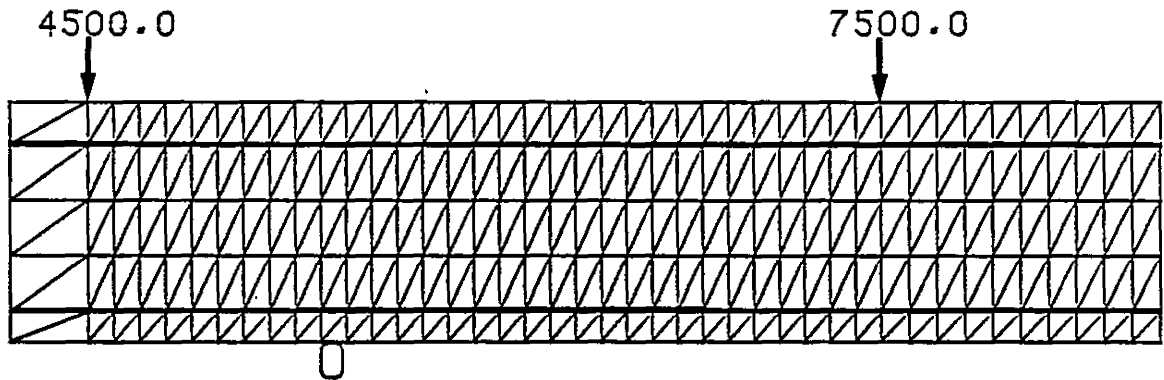
DR10. Any differences would be mainly caused by experimental variability. In fact, this beam had deflections which were almost identical to the finite element model predictions. This strongly suggests that the variation between the finite element predictions and the experimental results from Beam DR10 fell within the bounds of experimental variability. No model can do better than this.

Beam E3A1

Rodriguez, Bianchini, Viest, and Kesler (44) tested fifty two two-span continuous beams to determine various shear strength properties. One of their test beams, Beam E3A1, was chosen for the comparison. This was the first beam that tested the accuracy of the finite element model in simulating the behaviour of a reinforced concrete beam with positive and negative moments. All material properties except for the concrete modulus of elasticity were provided by the authors. Equation (3.1) was used to determine this value. The information that was used in this analysis is presented in Figure 3.30. An applied load to ultimate load ratio of 0.4 was employed in this example to represent the service load condition.

The deflection results from the comparison between the experimental data and the finite element solution is presented in Figure 3.31. For most of the diagram these results were almost as good as for the Leonhardt and Walther beam. The only appreciable difference between the two curves was observed during the latter loading stages. Normally the

BEAM E3A1



$$f'_c = 3500 \text{ psi}$$

$$b = 6.0 \text{ in}$$

$$L = 88.95 \text{ in.}$$

$$f_t = 503 \text{ psi}$$

$$d = 12.25 \text{ in}$$

$$A_s = 1.2 \text{ sq. in.}$$

$$E_c = 3230 \text{ ksi}$$

$$d' = 2.5 \text{ in}$$

$$A'_s = 1.2 \text{ sq. in.}$$

$$E_s = 29500 \text{ ksi}$$

$$h = 14.0 \text{ in}$$

FIGURE 3.30 DETAILS FOR BEAM E3A1

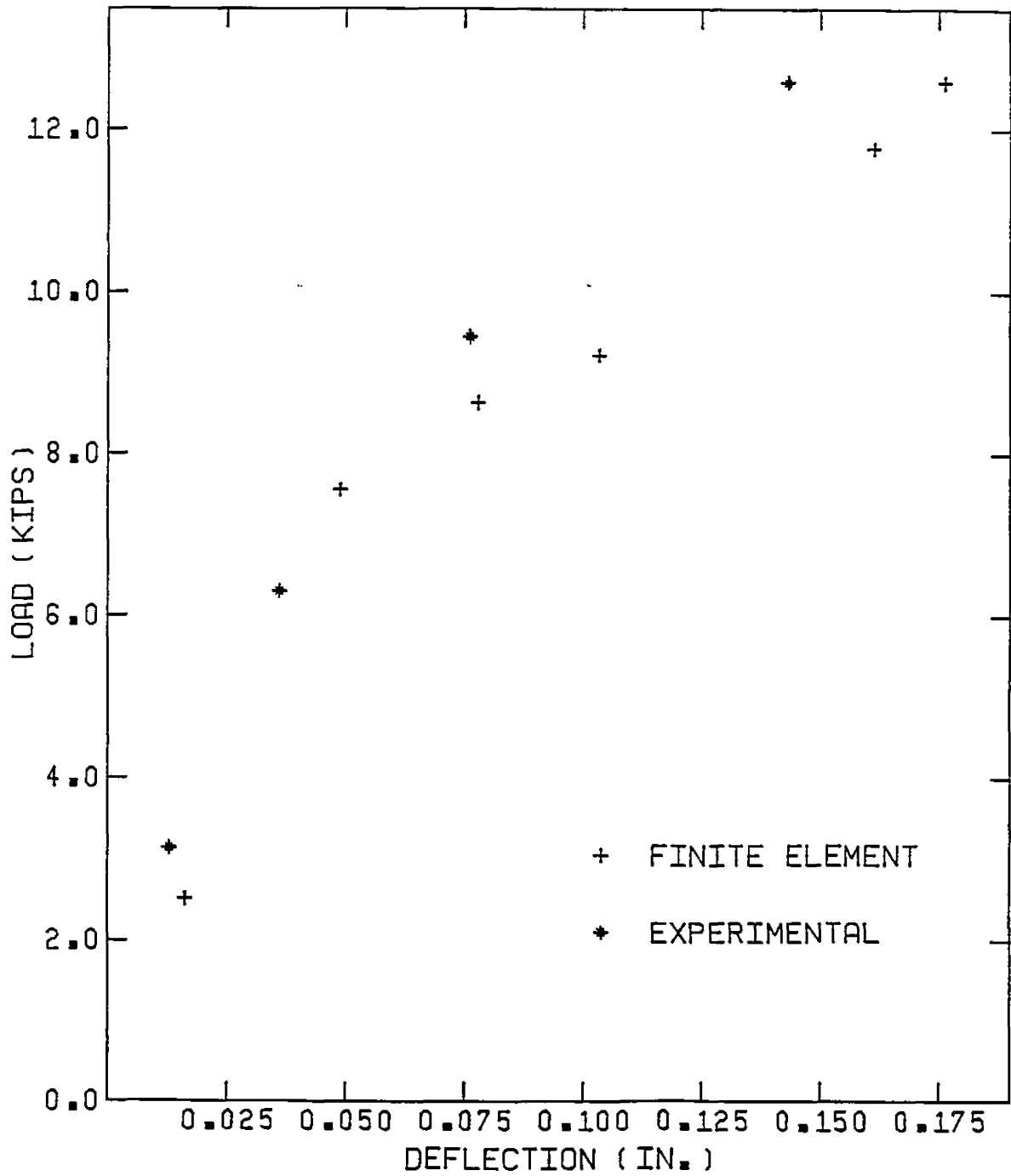


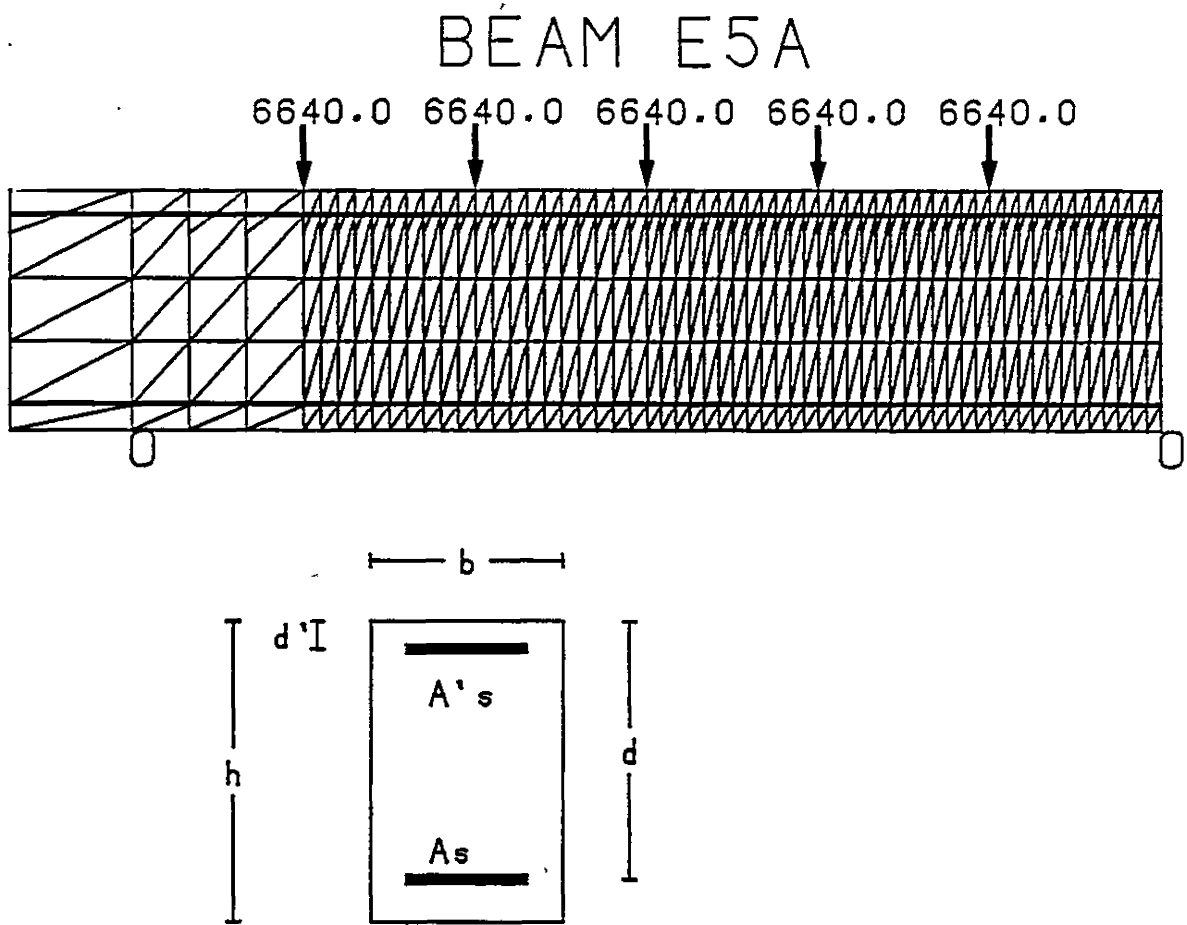
FIGURE 3.31 EXPERIMENTAL AND FINITE ELEMENT DEFLECTIONS FOR BEAM E3A1

experimental and finite element curves converged when the load was increased, but for Beam E3A1 the opposite was true. The final difference between the finite element deflections and the experimental deflections were about 24%. This value was not representative of the entire curve however. Extensive cracking took place in both the top and the bottom of the beam and the good results indicate that the model was very successful in handling the effects of the changing moment directions.

Beam E5A

The second continuous beam compared with the finite element model was tested by Bryant, Bianchini, Rodriguez, and Kesler (11). They were interested in the shear strength of two-span continuous beams with multiple point loading. Beam E5A had five equal point loads in each span. The beam and material properties reported for this beam are presented in Figure 3.32. The applied load to ultimate load ratio used in the analysis was 0.38.

The finite element and experimental load-deflection profiles for Beam E5A are shown in Figure 3.33. The correlation between the two curves was reasonably good, and at the end of loading the difference between them was about 17%. At low load levels the model predicted a stiffer beam than was observed experimentally, but as cracking took place the two curves began to converge. As mentioned in the Sensitivity Section this behaviour may take place when the modulus of elasticity or the tensile strength are overestimated.



$$f'_c = 3720 \text{ psi}$$

$$f_t = 457 \text{ psi}$$

$$E_c = 3707 \text{ ksi}$$

$$E_s = 28500 \text{ ksi}$$

$$b = 6.0 \text{ in}$$

$$d = 13.0 \text{ in}$$

$$d' = 1.5 \text{ in}$$

$$h = 14.5 \text{ in}$$

$$L = 114 \text{ in.}$$

$$A_s = 1.2 \text{ sq. in.}$$

$$A's = 2.0 \text{ sq. in.}$$

FIGURE 3.32 DETAILS FOR BEAM E5A

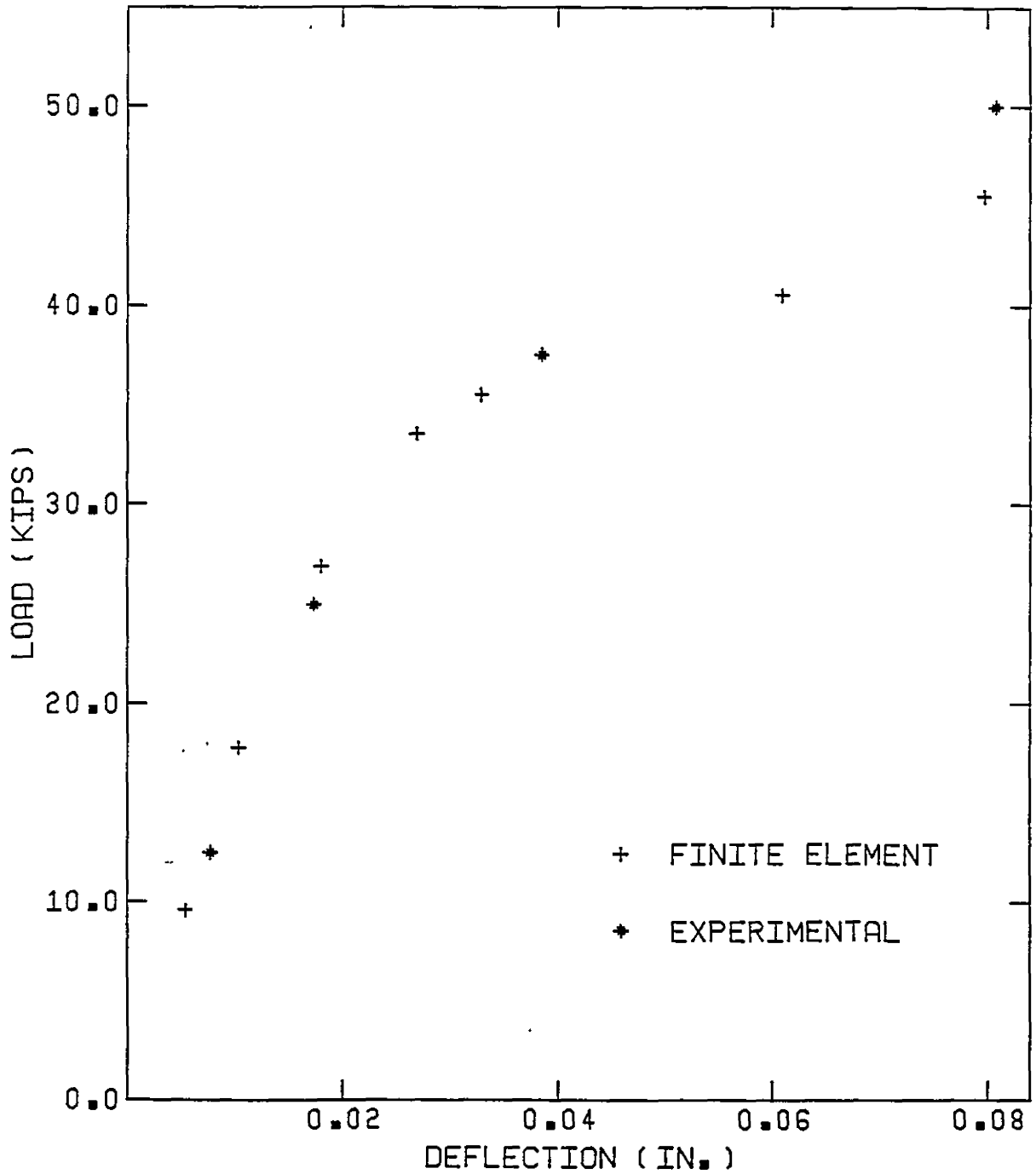
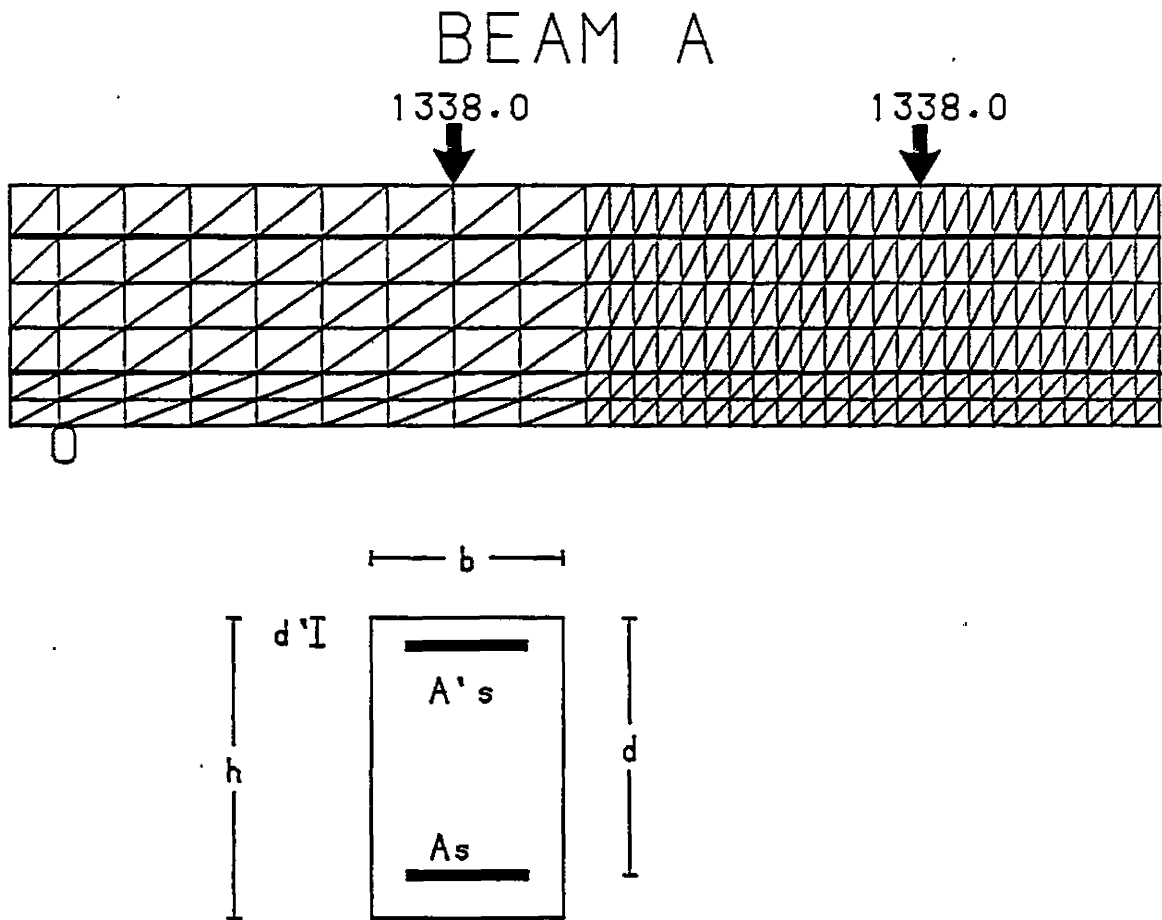


FIGURE 3.33 EXPERIMENTAL AND FINITE ELEMENT DEFLECTIONS FOR BEAM E5A

Beam A,B,C,D

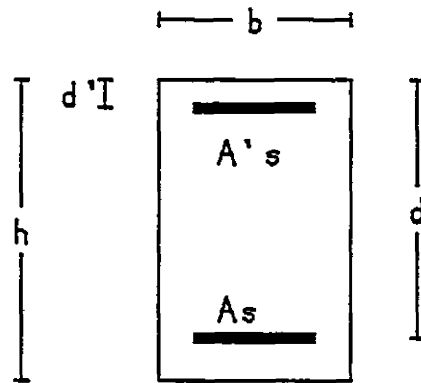
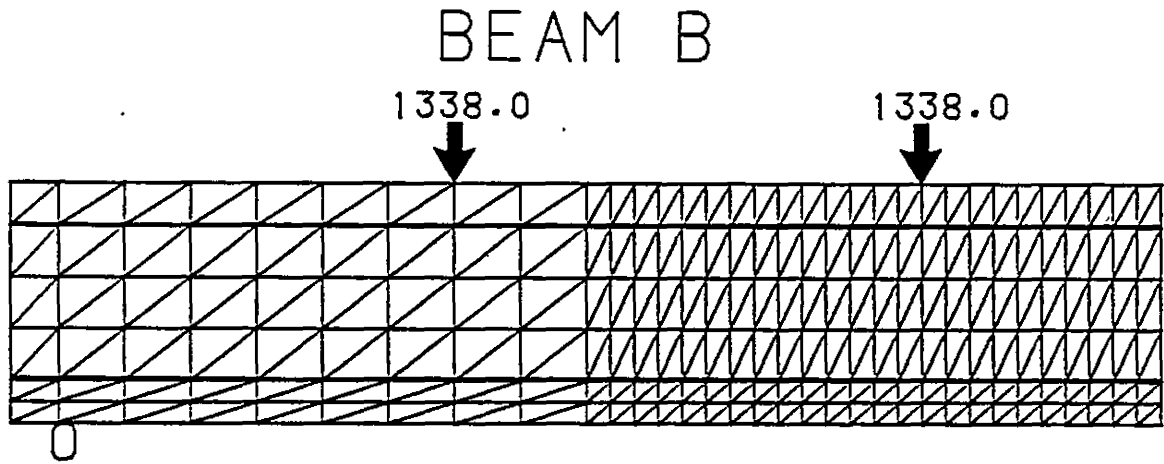
The deflection results from the experimental beams presented in Chapter 2 were also used to validate the finite element model. The first beams that were compared with the instantaneous results from the model were Beams A,B,C and D. Beam A and Beam B were full size, simply supported members which had both tension and compression steel. Beams C and D were full size, simply supported continuous members. Complete details about these beams were presented earlier and will not be repeated here. Relevant information needed for the finite element simulations are shown in Figures 3.34 through 3.37. The tensile strength and the modulus of elasticity of the steel were determined from the relationships in Section 3.11. For Beam A and Beam B the modulus of elasticity of the concrete was also calculated as in Section 3.11.

The load-deflection results comparing the finite element model deflections with the experimental deflections are shown in Table 3.1. A short explanation is provided here about why the full curves were not presented. The load-deflection curves for Beam A and Beam B were not used because both beams were loaded twice. When the beams were first loaded there was a problem with the equipment and the load had to be released. On reloading, the resulting load-deflection curves represented an already partially cracked beam and were not really comparable with the curves generated by the model. When loading Beam C and Beam D the load was applied in stages so that the final loads at the ends of the beams were reached before the final loads in the interior span. The load application in the finite element simulation was arranged so that



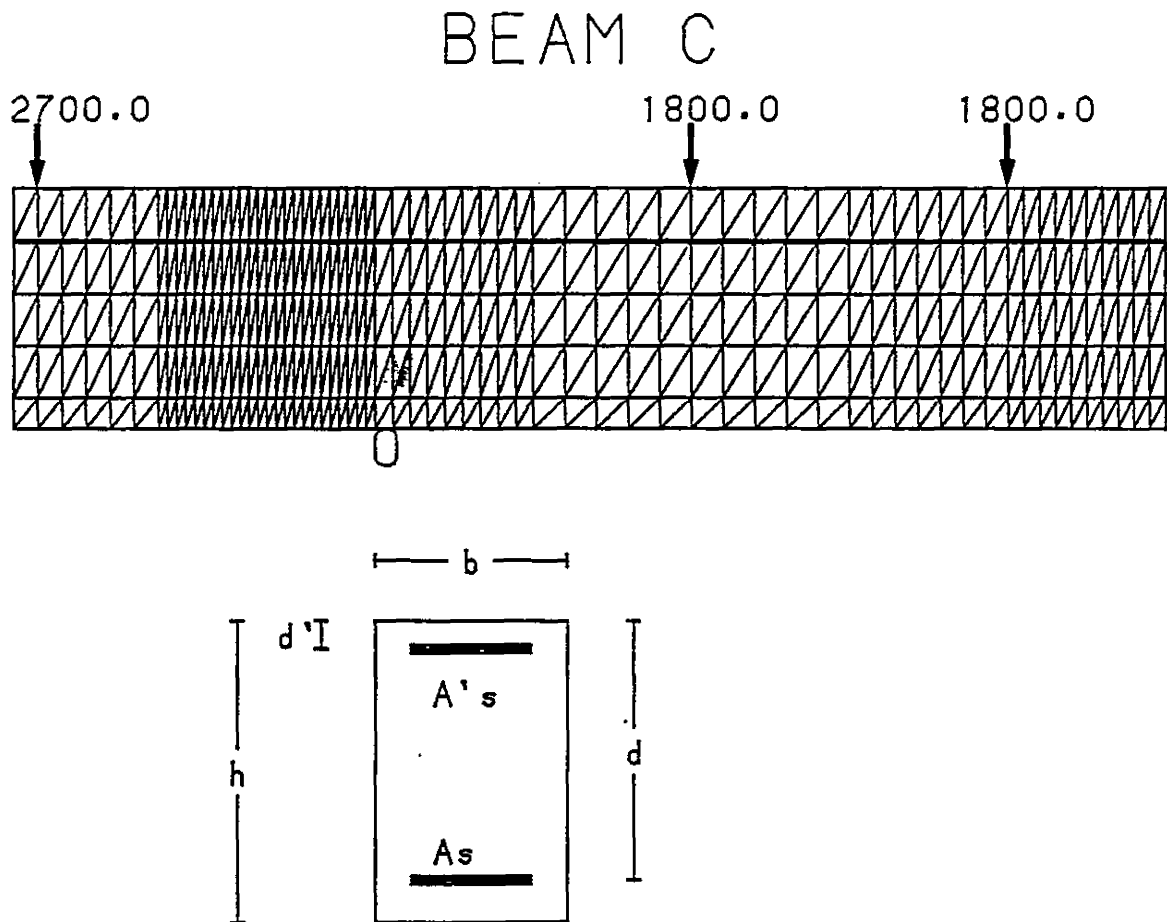
$f'_c = 3650$ psi	$b = 6.0$ in	$A_s = 1.2$ sq. in.
$f_t = 330$ psi	$d = 9.0$ in	$A's = .10$ sq. in.
$E_c = 3355$ ksi	$d' = 2.5$ in	
$E_s = 29000$ ksi	$h = 11.5$ in	
MIX 1.0:3.33:2.17	$w/c = .65$	R.H. = .50

FIGURE 3.34 DETAILS FOR BEAM A



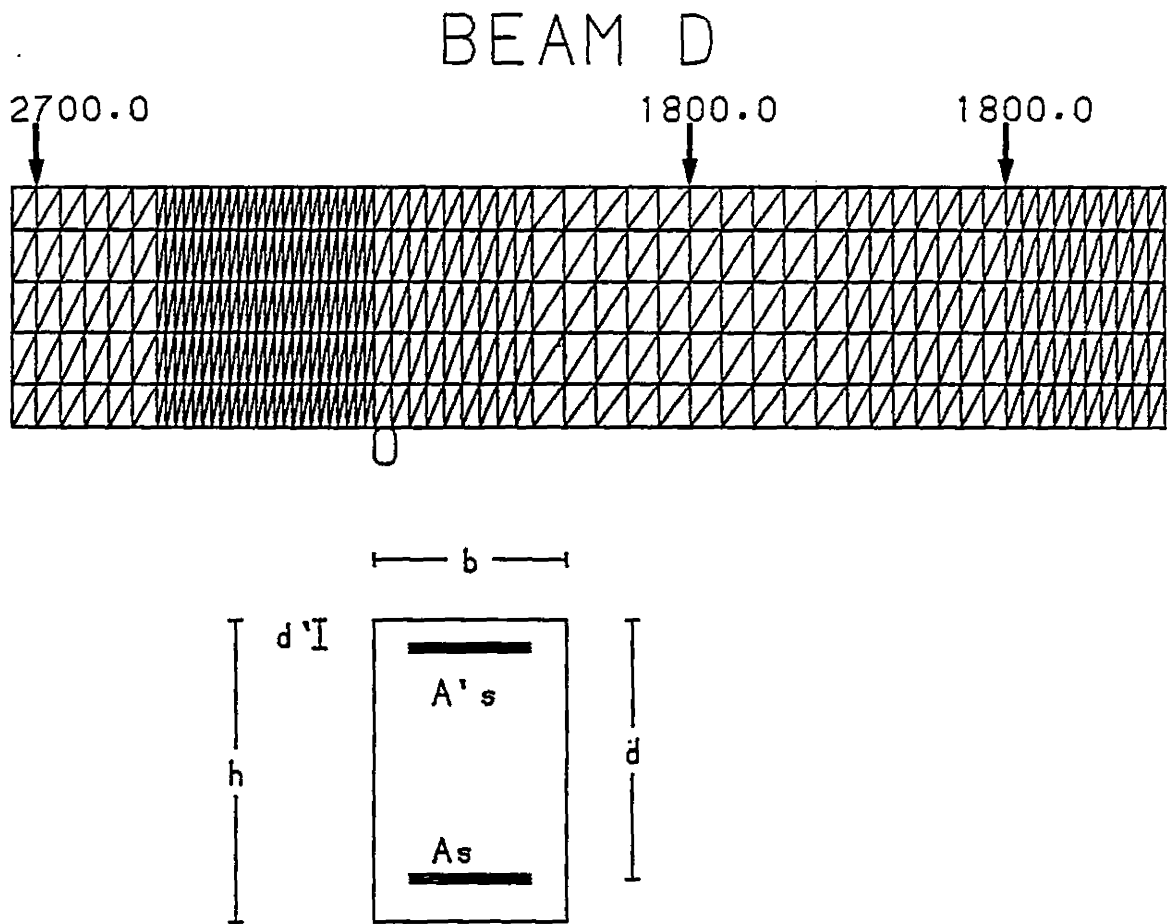
$f'_c = 3650$ psi	$b = 6.0$ in	$A_s = .62$ sq. in.
$f_t = 330$ psi	$d = 11.5$ in	$A'_s = .10$ sq. in.
$E_c = 3355$ ksi	$d' = 2.5$ in	
$E_s = 29000$ ksi	$h = 14.0$ in	
MIX 1.0:3.33:2.17	$w/c = .65$	R.H. = .50

FIGURE 3.35 DETAILS FOR BEAM B



$f'_c = 3336 \text{ psi}$	$b = 6.0 \text{ in}$	$L = 144 \text{ in.}$
$f_t = 433 \text{ psi}$	$d = 9.0 \text{ in}$	$A_s = .88 \text{ sq. in.}$
$E_c = 3607 \text{ ksi}$	$d' = 2.5 \text{ in}$	$A's = 1.2 \text{ sq. in.}$
$E_s = 29000 \text{ ksi}$	$h = 11.5 \text{ in}$	
MIX 1.0:3.33:2.17	$w/c = .65$	$R.H. = .50$

FIGURE 3.36 DETAILS FOR BEAM C



$f'_c=3336$ psi	$b=6.0$ in	$L=144$ in.
$f_t=433$ psi	$d=11.5$ in	$A_s=.40$ sq.in.
$E_c=3607$ ksi	$d'=2.5$ in	$A's=.62$ sq.in.
$E_s=29000$ ksi	$h=14.0$ in	
MIX 1.0:3.33:2.17	$w/c=.65$	$R.H.=.50$

FIGURE 3.37 DETAILS FOR BEAM D

the final loads were reached simultaneously. Thus only the final conditions were comparable.

Generally the results presented in Table 3.1 were very good and the only appreciable difference between the experimental and analytical results was observed for Beam A. The variation from the experimental deflections was 58% for Beam A, 15% for Beam B, 15% for Beam C, and 12% for Beam D. It was mentioned in Chapter 2 that there were some problems with the loading for Beams A and B so the significance of the variation in the Beam A results is difficult to assess.

The deflection results of Beam D also need further explanation. No cracks were predicted by the model, yet cracks were observed experimentally. When a stress analysis was performed it became obvious that the model should have predicted cracking. The reason cracks were not predicted by the model was explained in the Sensitivity Study of Section 3.3, and had to do with the natural underestimation which is inherent with finite element models. The finite element deflections were still reasonably close to the experimental ones because cracking had only begun experimentally. The good results that were obtained for Beam B and Beam D were encouraging because they showed that the model was capable of accurately simulating the behaviour of lightly cracked beams. Most of the other beams in this verification section were highly cracked.

BEAM	EXPERIMENT DEFLECTION (in.)	FINITE ELEMENT DEFLECTION (in.)
A	.220	.349
B	.166	.141
C	.199	.229
D	.067	.059

TABLE 3.1 Short Term Deflection Results for Series 1 and Series 2
Beams From Experimental Program

Beam E

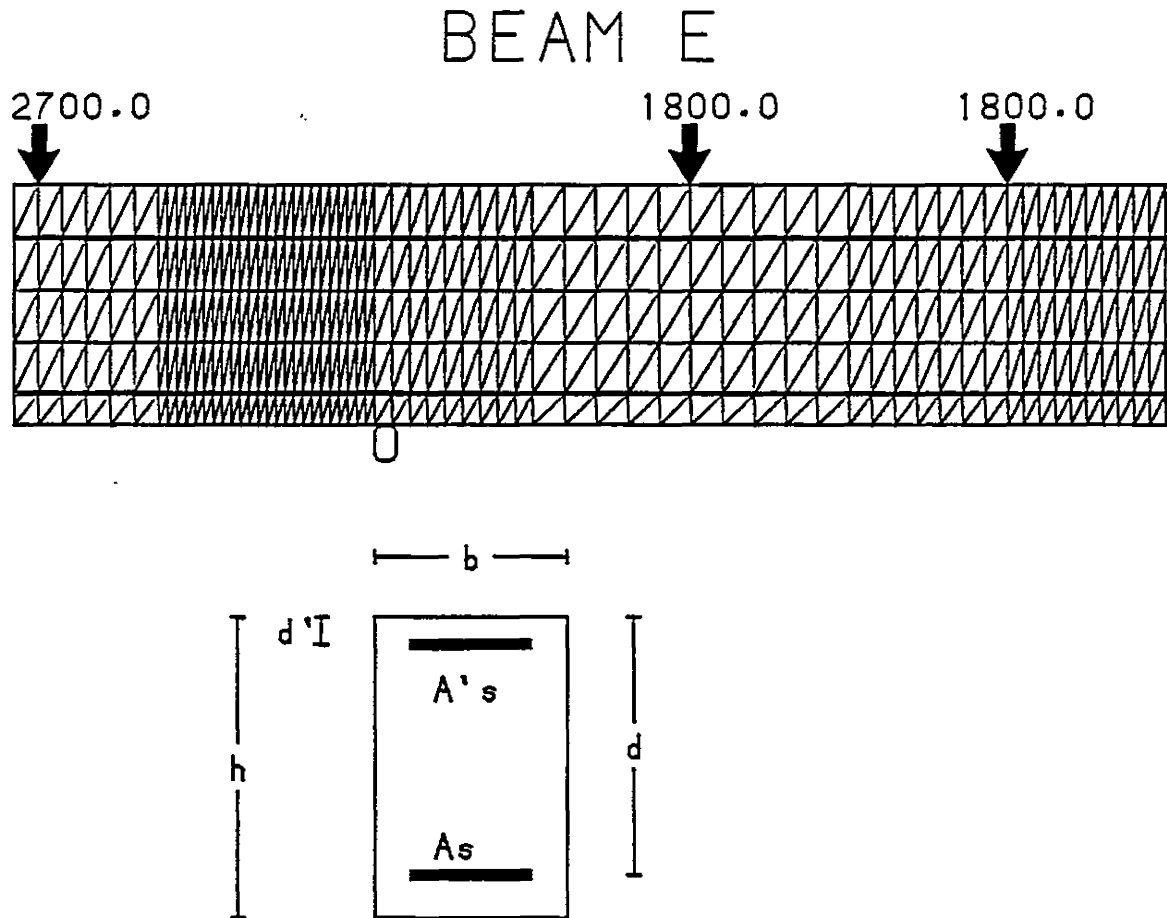
Beam E was one of the continuous beams reported in Chapter 2, and the results from this beam were used to validate the model. Beam E was identical in every way to Beam C except for the age at which it was loaded. The information which was used to generate the finite element results is presented in Figure 3.38.

The deflection results from the experiment and the finite element model are shown in Figure 3.39. The finite element curve followed the experimental curve very closely until about 70% of the total load. After this point the curves diverged slightly.

Beam F

The last beam from the experimental section, Beam F, was the final beam used in the short term verification. This beam was identical to Beam D except for the age of loading. Pertinent information needed for running the finite element program is provided in Figure 3.40.

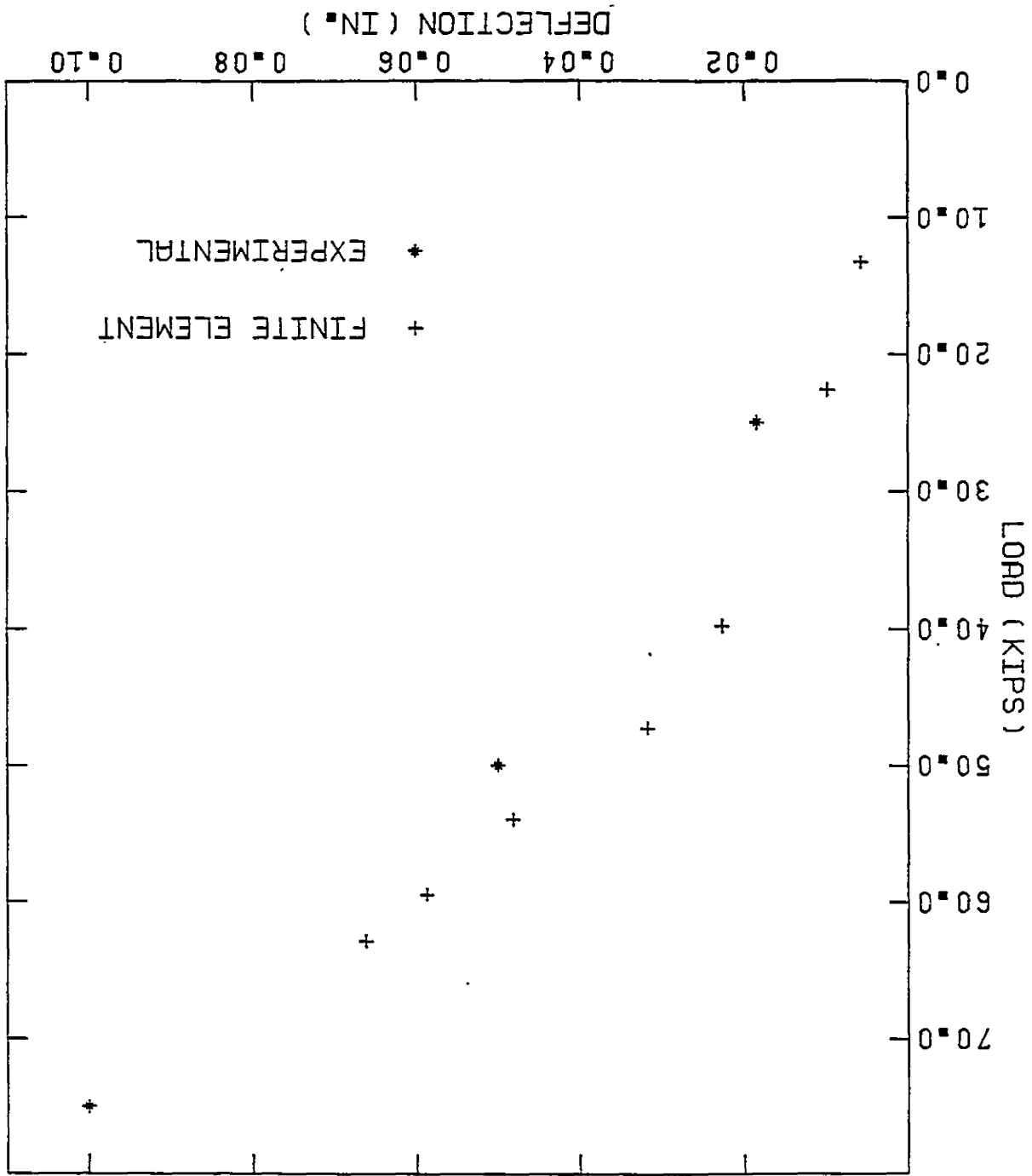
The behaviour of Beam F was very similar to Beam D except that the results were not quite as good. The finite element model again did not predict cracking even though cracking was observed experimentally. In the uncracked region of the load-deflection curve, the finite element and experimental curves were very nearly the same. When cracking started experimentally, the curves began to diverge. The difference

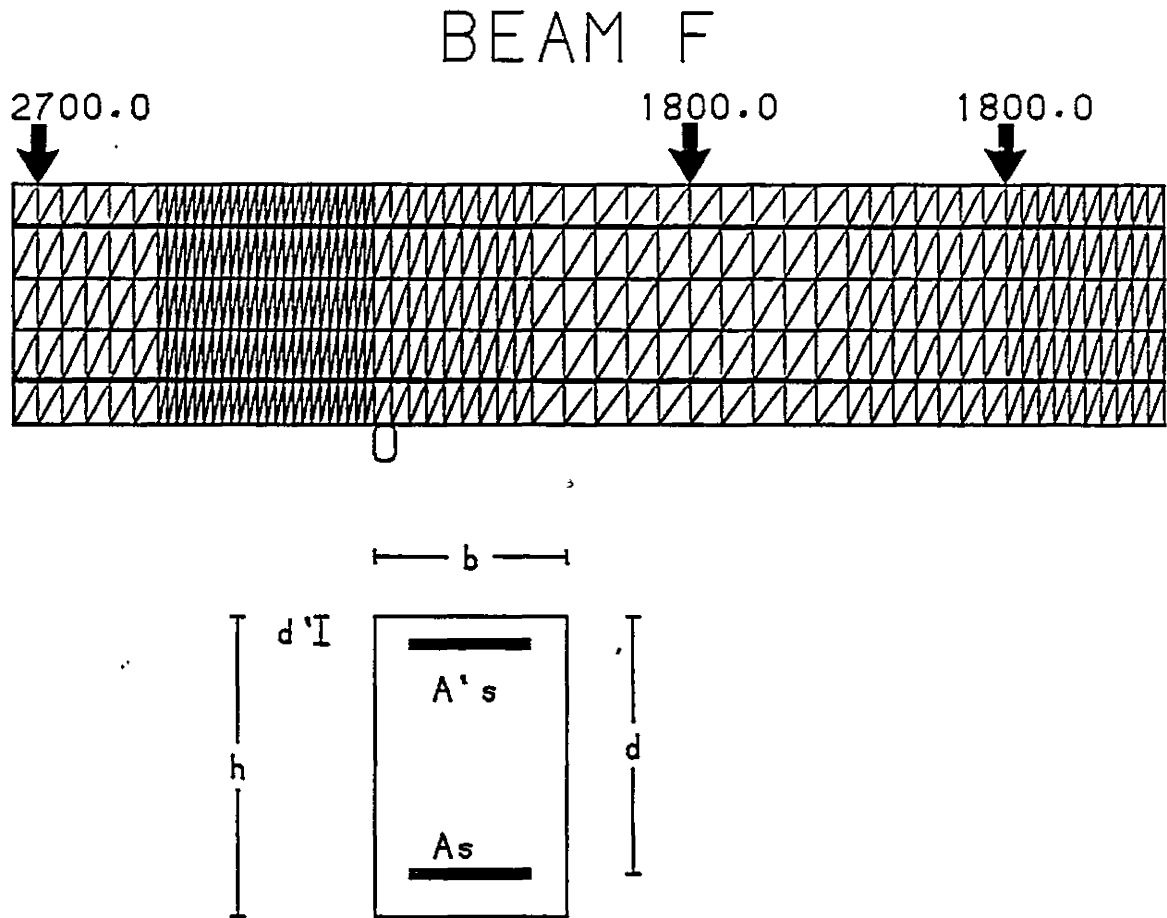


$f'_c=4272$ psi	$b=6.0$ in	$L=144$ in.
$f_t=490$ psi	$d=9.0$ in	$A_s=.88$ sq.in.
$E_c=3957$ ksi	$d'=2.5$ in	$A's=1.2$ sq.in.
$E_s=29000$ ksi	$h=11.5$ in	
MIX 1.0:3.33:2.17	$w/c=.65$	$R.H.=.50$

FIGURE 3.38 DETAILS FOR BEAM E

FIGURE 3.39 EXPERIMENTAL AND FINITE ELEMENT DEFLECTIONS FOR BEAM E





$f'_c = 4272$ psi	$b = 6.0$ in	$L = 144$ in.
$f_t = 490$ psi	$d = 11.5$ in	$A_s = .40$ sq. in.
$E_c = 3957$ ksi	$d' = 2.5$ in	$A's = .62$ sq. in.
$E_s = 29000$ ksi	$h = 14.0$ in	
MIX 1.0:3.33:2.17	$w/c = .65$	$R.H. = .50$

FIGURE 3.40 DETAILS FOR BEAM F

between the experimental and finite element deflections at the end of the loading was about 28%.

To get some idea about what accuracy could have been achieved if the effect of the finite element mesh size was removed, the tensile strength for Beam F was reduced by 50%. This change was implemented to ensure that extensive cracking would be produced in the finite element beam. Reducing the tensile strength by 50% should have had a much larger counterbalancing effect on the deflections than were initially caused by the mesh size considerations. The two finite element curves should have provided an upper and lower bound on the experimental curve. The results in Figure 3.41 show that this was precisely what happened. Therefore, if the mesh size had been reduced enough to allow for crack initiation, the variation between experimental and analytical deflections would have been much less. The results also showed that reducing the tensile strength may be a practical way to reduce the number of elements in the analysis while retaining realistic crack initiations.

Summary

The short term behaviour of 11 reinforced concrete beams were compared in this section with results generated by the finite element model. The finite element deflections for five of the beams were within 15% of the experimental ones, and nine were within 25%. Considering the fact that normal experimental variability often varies within this range, it seems safe to say that the model simulated the instantaneous behaviour of simply supported and continuous beams very well. The beams

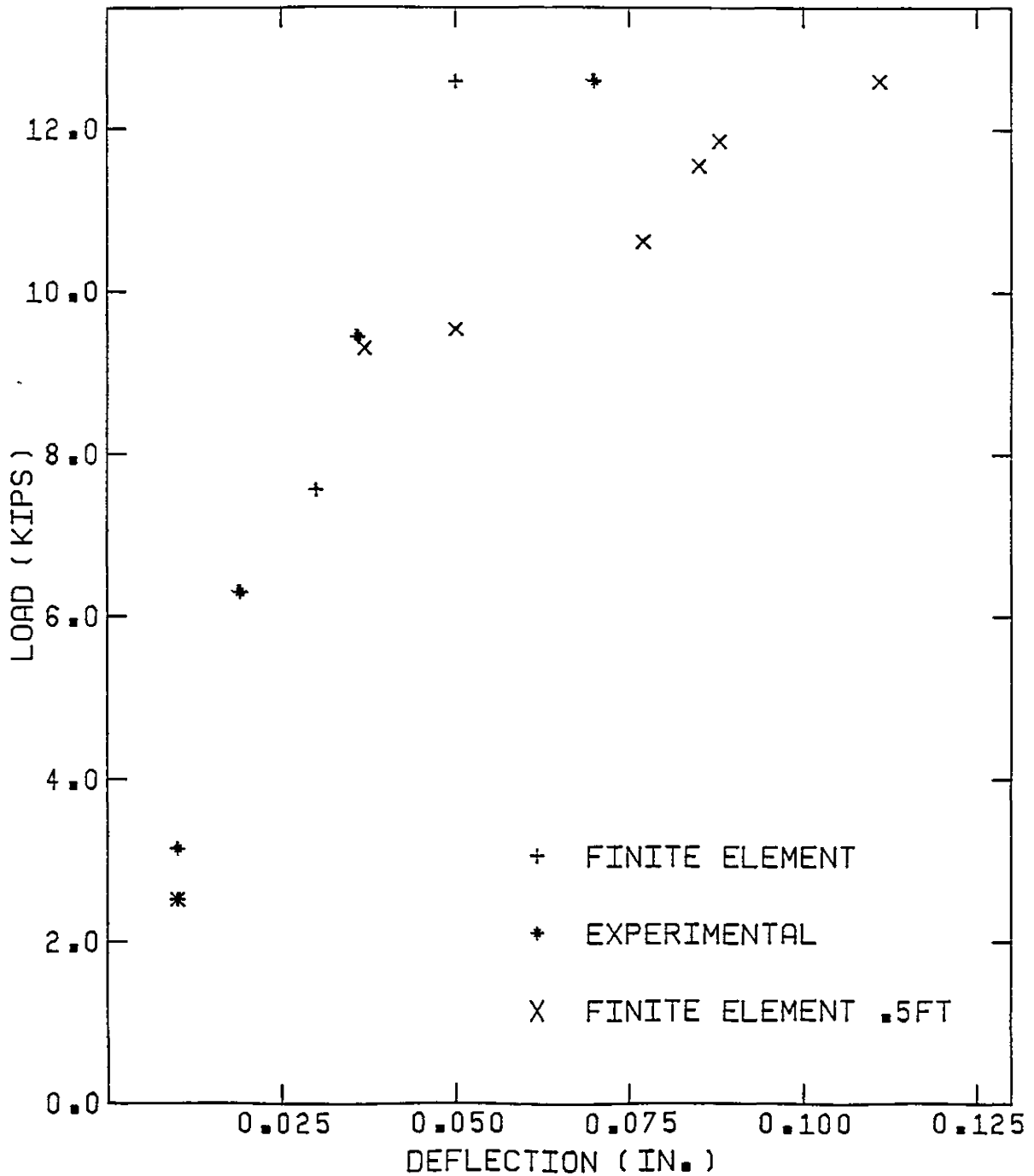


FIGURE 3.41 EXPERIMENTAL, STANDARD FINITE ELEMENT, AND 50% REDUCED TENSILE STRENGTH FINITE ELEMENT DEFLECTIONS

that were used in the comparison represented many different conditions and the model was reasonably successful in modelling all of them. The effect of cracking was successfully represented, as evidenced by the good agreement observed between the experimental and finite element load-deflection curves. The model was not exact in its predictions but exact predictions were never expected. Experimental variability in reinforced concrete and the complex interaction between its constituent parts precluded the possibility of an exact duplication between experimental and finite element results.

The question of experimental variability in reinforced concrete beam deflections is an important one. It is impossible to assess the accuracy of a finite element model without knowing something about the natural variability of the material. A brief examination of pertinent literature (6) showed that there can be significant variations in the tested deflections of identical beams. Of twenty six pairs of comparable beam deflections from this literature, about 50% of the pairs had variations in deflections less than 10%, and 90% of the pairs had variations less than 20%. This would indicate that 20% variability in laboratory tested beam deflections would not be uncommon. However variations much larger than this are still quite possible. This range of variability was also reported by Branson (8). Since most of the results in this section were very close to the 20% range, it seems safe to say that the proposed model was successful in simulating short term deflections.

3.5 Evaluation of Model for Long Term Loads

It was with particular interest that the proposed finite element model was evaluated for long term behaviour because this was the whole point of its development. Experimental results from a number of different sources were collected to test the accuracy of the finite element model. Although several references with experimental data were available, most did not provide information on the concrete creep and shrinkage characteristics. Fortunately there were a few references which gave either the creep and shrinkage strains, or sufficient concrete mix details for the use of prediction equations.

The results in this section generally combined the short term behaviour with the long term behaviour, but the long term behaviour alone was also examined. Since there seems to be more factors at work in the behaviour and testing of reinforced concrete beams over the long term, it seems reasonable that there should be a higher relative experimental variability associated with these deflections than there would be with short term deflections. The performance of the model must be judged accordingly. In this section the deflections, strain profiles, and crack patterns, from the reported experiments are compared with the results generated by the finite element model.

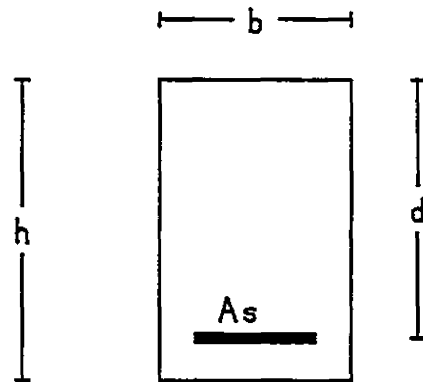
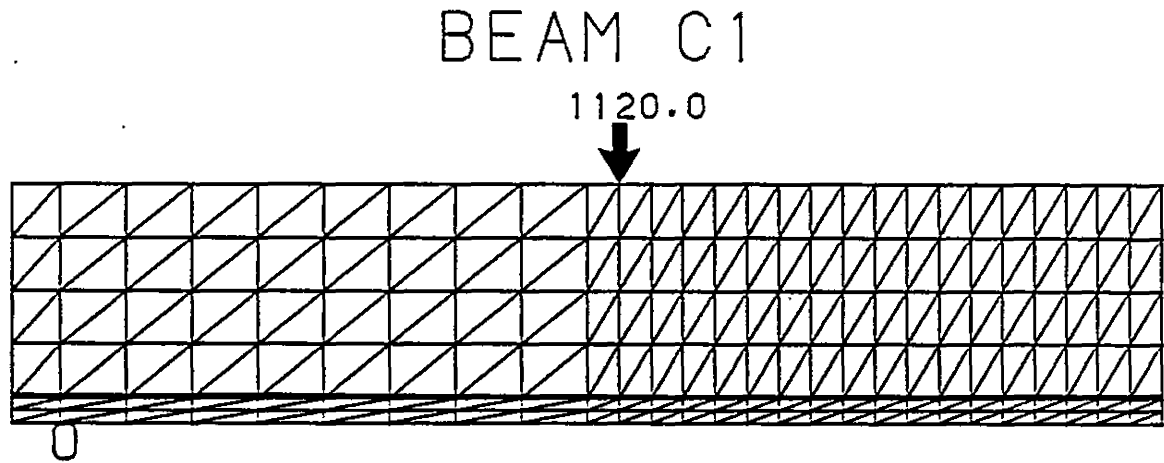
Beam C1

In 1966 Corley and Sozen (17) reported on the results of a two year study into the deflections of three reinforced concrete beams.

These beams were smaller than beams in service usually are, and it is possible that this may have influenced the results to some degree. However it was hoped that these small scale effects would be minimal. Beam C1 was the first of these beams which was compared with the results from the finite element model. Since the midspan deflections, crack patterns, and strain profiles were provided by the authors, an extensive comparison between the experimental and finite element results was possible. The relevant information used to generate the finite element results is presented in Figure 3.42. The tensile strength, concrete modulus of elasticity, and steel modulus of elasticity were estimated using the relationships presented in Section 3.11. Time dependent strains due to creep and shrinkage were calculated using Bazant and Panula's prediction method. Two values needed for this method, namely the concrete density and the cement content, were not reported by the authors. The density was estimated using an average value for concrete with a 3/8" maximum aggregate size. The cement content was approximated by proportioning the density according to the mix proportions.

The load-deflection profiles observed both experimentally and from the finite element model are shown in Figure 3.43. The correlation between these two curves was reasonable for total as well as long term deflections. The total difference between the deflections at the end of the 705 day loading period was about 23%. For the long term deflections alone, the difference was around 20%.

The crack pattern in the flexure span of Beam C1 was provided by Corley and Sozen and this was compared in Figure 3.44 with the finite



$f'_c = 3500$ psi	$b = 3.0$ in	$A_s = .22$ sq. in.
$f_t = 445$ psi	$d = 5.375$ in	
$E_c = 3414$ ksi		
$E_s = 29000$ ksi	$h = 6.0$ in	
MIX 1.0:4.2:4.5	$w/c = .85$	$R.H. = .50$

FIGURE 3.42 DETAILS FOR BEAM C1

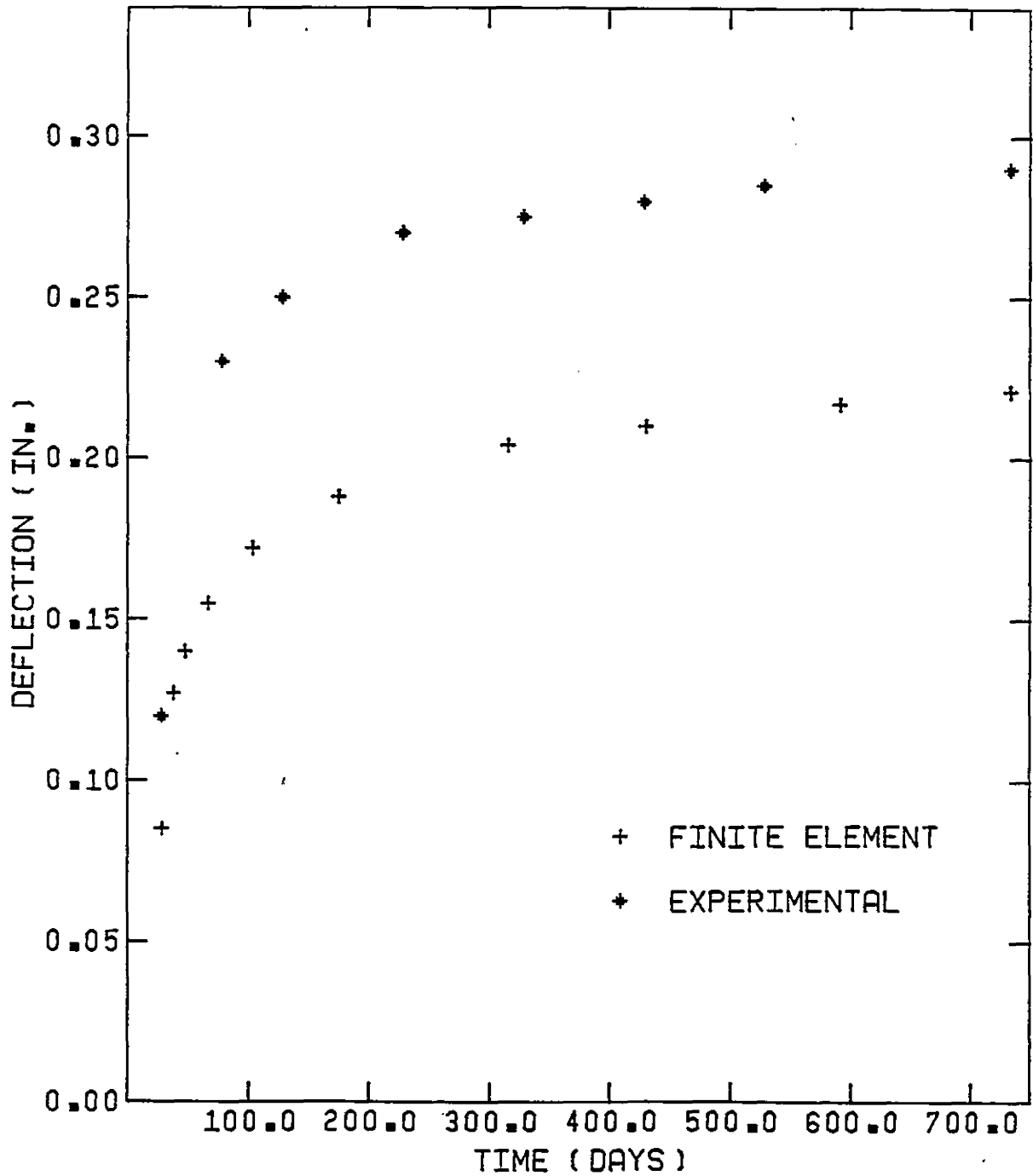
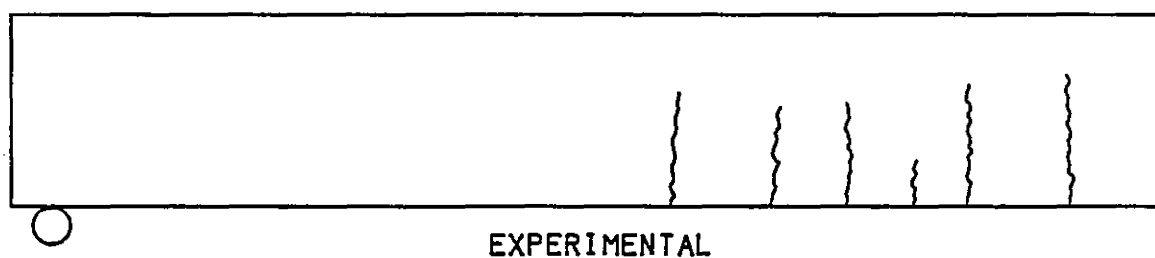
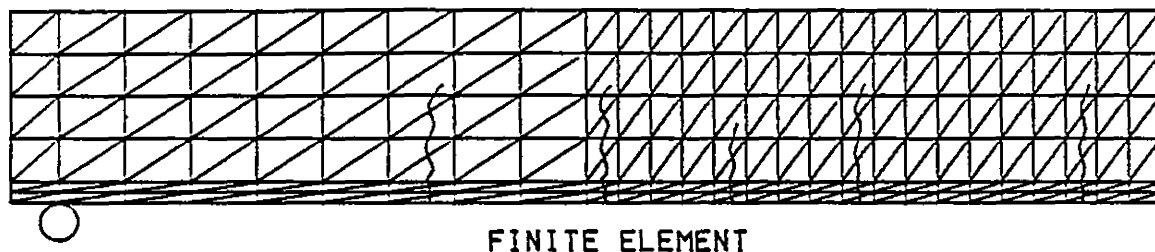
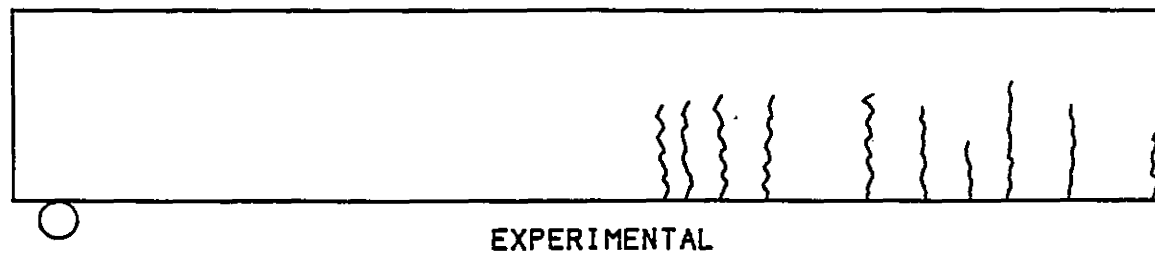
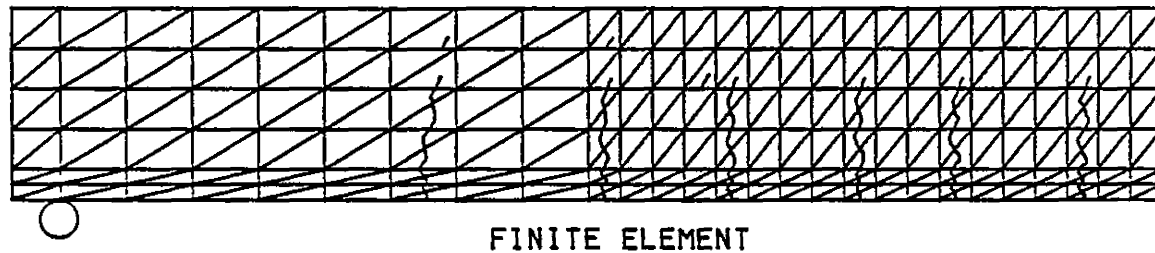


FIGURE 3.43 EXPERIMENTAL AND FINITE ELEMENT DEFLECTIONS FOR BEAM C1

BEAM C1



BEAM C3



**FIGURE 3.44 EXPERIMENTAL AND FINITE ELEMENT
CRACK PATTERNS FOR BEAM C1 AND
BEAM C3**

element solution. Since cracking is such a highly variable phenomenon the importance of this comparison was not in exactly reproducing the experimental crack pattern, but rather in properly reflecting the general cracking behaviour. An examination of this figure showed that the experimental crack spacing was a little smaller than that predicted by the model. This difference may have arisen because the model predicted no additional cracking after the load was applied, whereas one or two additional cracks were observed experimentally.

Small scale effects may also have been responsible for the smaller crack spacing in the experimental beam. The constitutive bond law used in the model was based on results obtained with # 8 bars, while Beam C1 contained # 3 bars. When testing the bond properties of # 4 bars, Mirza and Houde (35) determined that such small bars exhibited lower bond slip than did the larger bars. This would reduce the amount of bond deterioration and allow cracks to form closer together. Since the model did not include this characteristic it was not surprising that the crack spacings were somewhat different. Aside from the difference in spacings, the model predicted the height and orientation of the cracks quite well.

The experimental strain profile for this beam was also supplied by Corley and Sozen, and a comparison between these results and the finite element predictions is shown in Figure 3.45. The values plotted for the finite element strains are shown at the centroids of the elements. It is apparent from this figure that the correlation between the analytical and experimental short term strains was very good. Both strain profiles were linear and the curvatures were almost exactly the

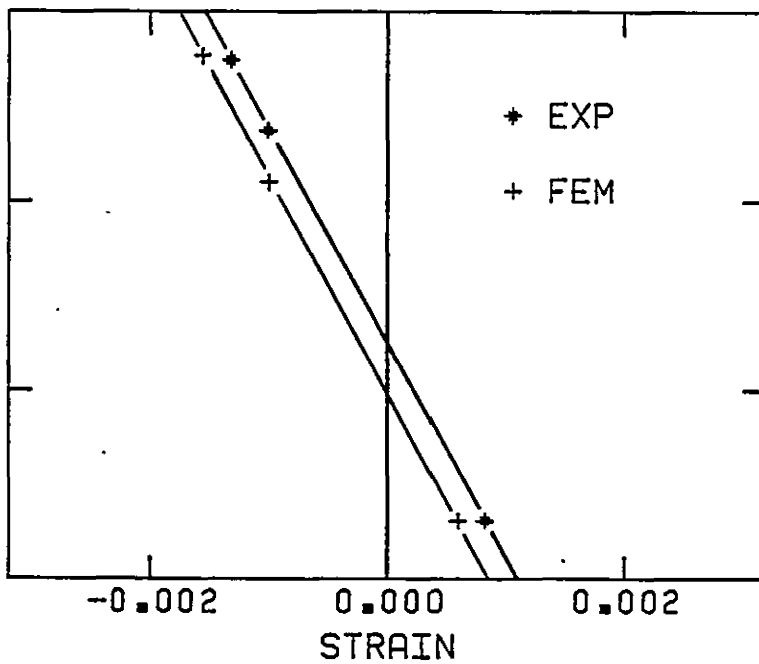
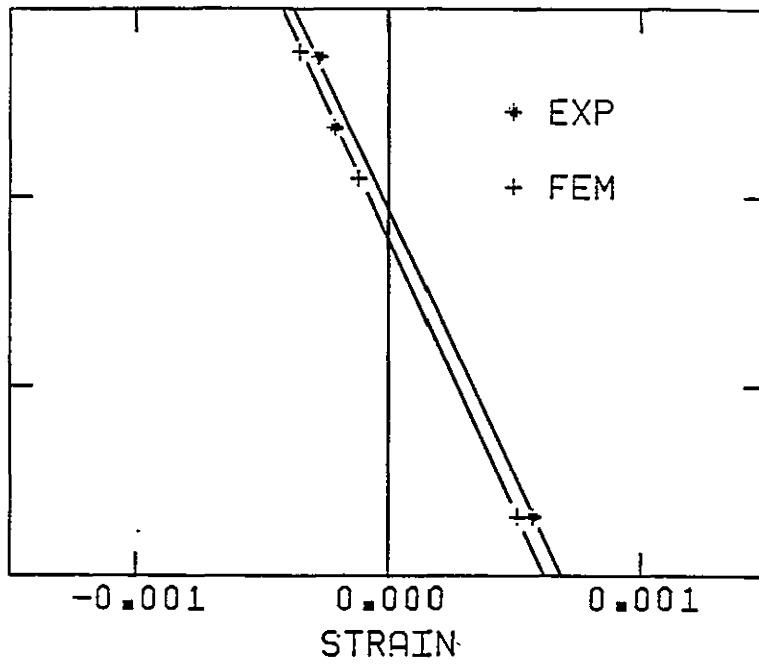


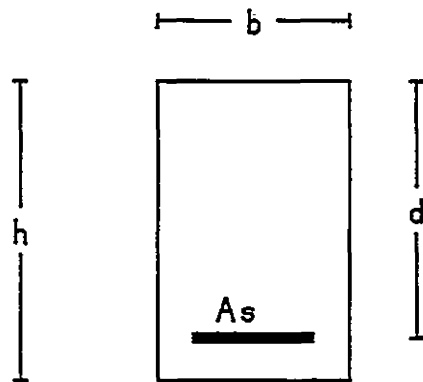
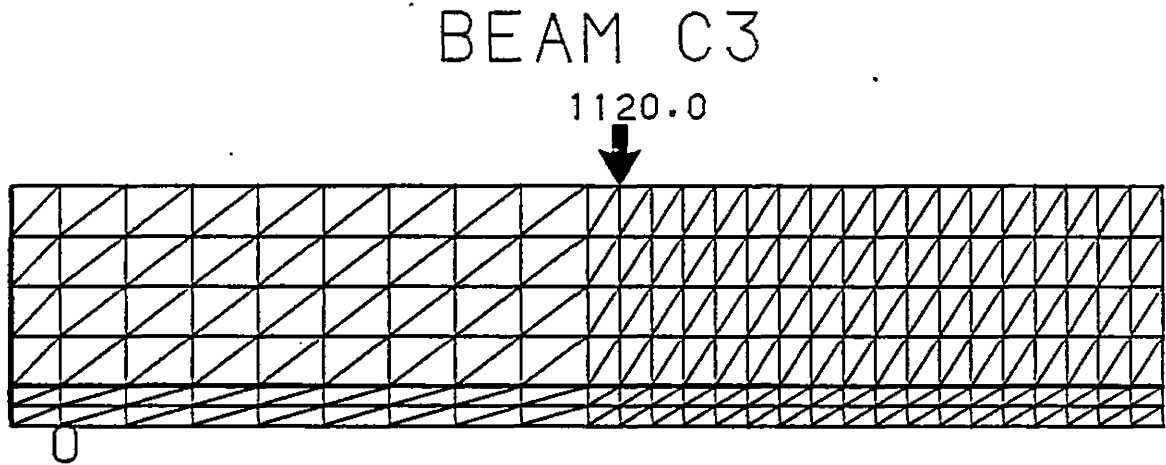
FIGURE 3.45 SHORT TERM AND LONG TERM STRAIN PROFILES FOR BEAM C1

same. The correlation for the long term strains was also very good. The long term strains were slightly overestimated, but the slope of the strain profiles, and thus the curvatures, were almost identical.

A note may be necessary here to explain why the deflection predictions were not as accurate as the strain predictions. With plane stress elements the strain is constant throughout each element. Therefore the strain changes at discrete intervals through the depth of the modelled beam. This is not the way strain is distributed in a real beam. In a real beam the strain changes continuously through the depth. The correspondence between strain distribution or curvature, and deflections, is therefore not as strong in the modelled beam as might be expected. This however does not take away from the importance of the model accurately predicting strains.

Beam C3

A second beam tested by Corley and Sozen, Beam C3, was used to check the consistency of the finite element model. Beam C3 was tested at the same time and under the same conditions as Beam C1. The only difference between them was their cross-sectional dimensions. The stresses in Beam C3 were much higher than the corresponding stresses in Beam C1, but it was assumed in the analysis that linear behaviour was still predominant. The conditions and properties reported for this beam are shown in Figure 3.46.



$f'_c = 3500$ psi	$b = 3.0$ in	$A_s = .22$ sq. in.
$f_t = 445$ psi	$d = 3.625$ in	
$E_c = 3414$ ksi		
$E_s = 29000$ ksi	$h = 4.3125$ in	
MIX 1.0:4.2:4.5	$w/c = .85$	R.H. = .50

FIGURE 3.46 DETAILS FOR BEAM C3

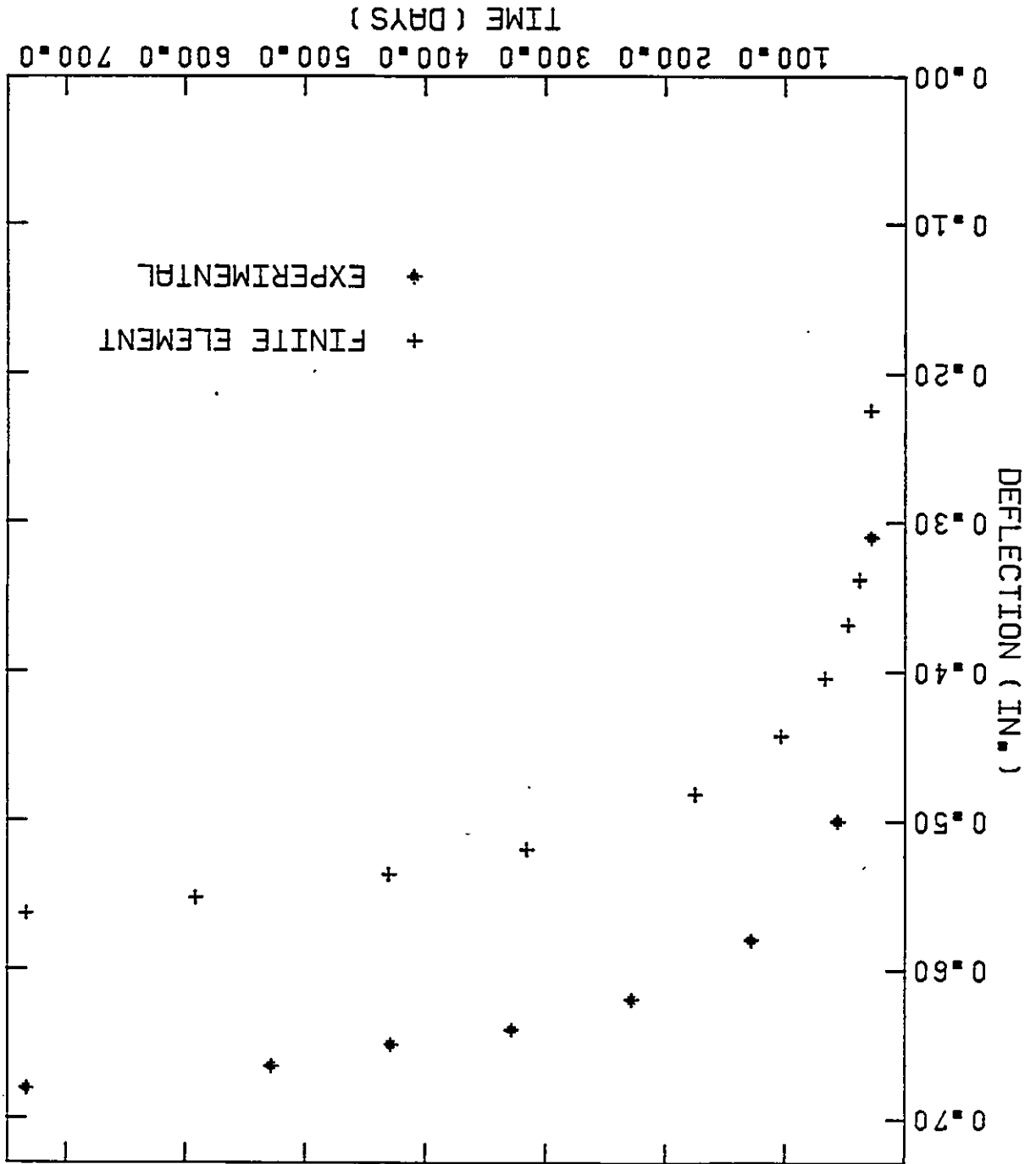
The experimental and finite element model deflections for Beam C3 are presented in Figure 3.47. These results were much better than the results for Beam C1. The variation in the deflection profiles for Beam C3 was about 17% for the total deflections, and less than 9% for the long term deflections. Reasons for the difference between the experimental and analytical results were discussed for Beam C1. Experimental variability is the most likely explanation for the improvement between the results for Beam C3 and the results from Beam C1. Another possibility for the improvement is the inelastic behaviour that was not predicted by the model. The effect of inelastic behaviour is an increase in short term strains and deflections, and a decrease in stresses. Inclusion of this behaviour would improve the short term and total deflection predictions, but since the creep law is stress dependent, it might slightly worsen the predictions of the long term deflections. In either case the results would still be excellent.

The crack patterns observed experimentally and from the finite element model are shown in Figure 3.44. The crack spacings obtained from the model were again somewhat larger than the experimental crack spacings. The most likely reasons for these differences are the same as for Beam C1.

The strain diagram comparing the results from the finite element model with the results from the experiment is shown in Figure 3.48. The short term strains in the flexure span predicted by the model were very close to the experimental values. In fact the strain predictions at centre span were much better than the deflection predictions. The

DEFLECTIONS FOR BEAM C3

FIGURE 3.47 EXPERIMENTAL AND FINITE ELEMENT



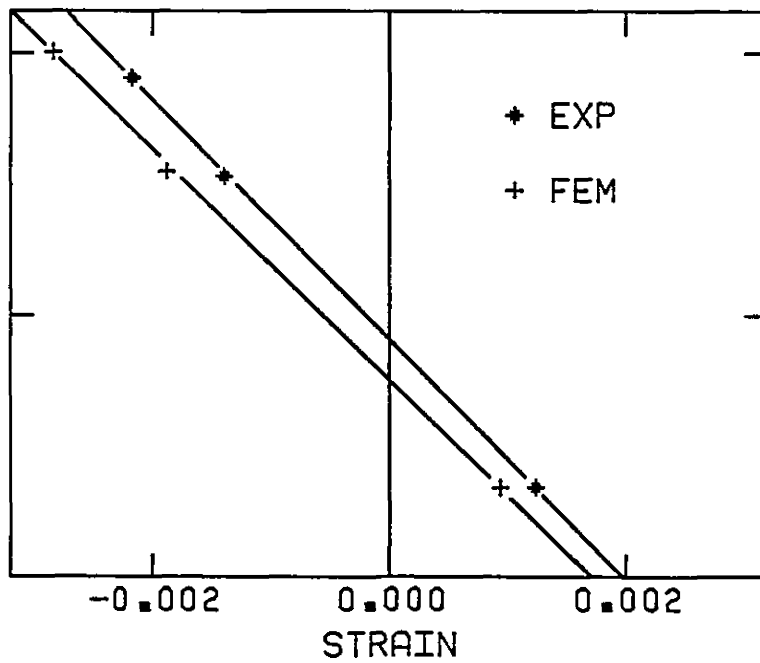
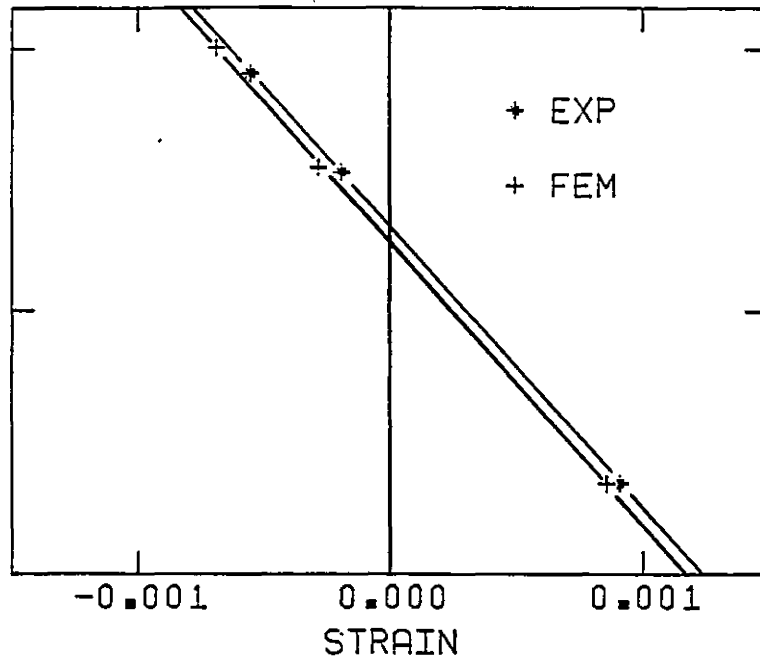


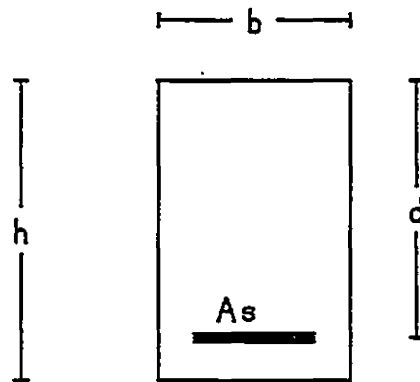
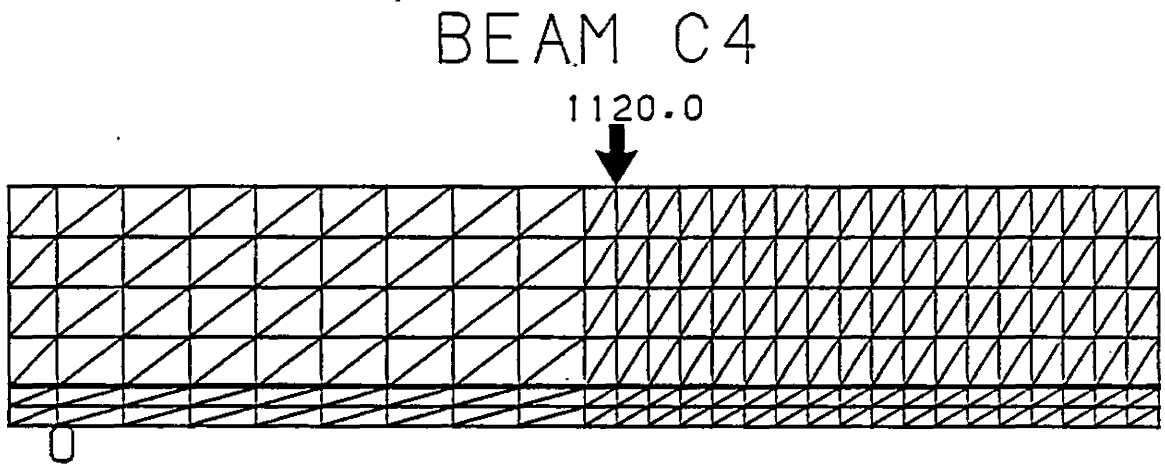
FIGURE 3.48 SHORT TERM AND LONG TERM STRAIN PROFILES FOR BEAM C3

predicted long term strain profile was not quite as close to the experimental values as the short term results were but they were still reasonably similar. There are a few possible reasons for this difference. One reason may be the effect of the inelastic behaviour described earlier. Since the model used a linear approximation for the stress-strain diagram, it would tend to overestimate the stresses. It would also underestimate short term strains, and because of the higher stresses, overestimate creep strains. This is precisely the behaviour which appears in the long term strain profile, but not exactly what was seen in the short term strain profile. Experimental variability may have disguised the short term effect. Another possibility is that normal experimental variability alone may have been the major contributing factor in the difference between the long term experimental and analytical strains.

Beam C4

Corley and Sozen also supplied the results for a third beam. This beam, designated C4, was identical to Beam C3 except for the amount of tension steel it contained. Figure 3.49 provides the necessary information for the finite element model.

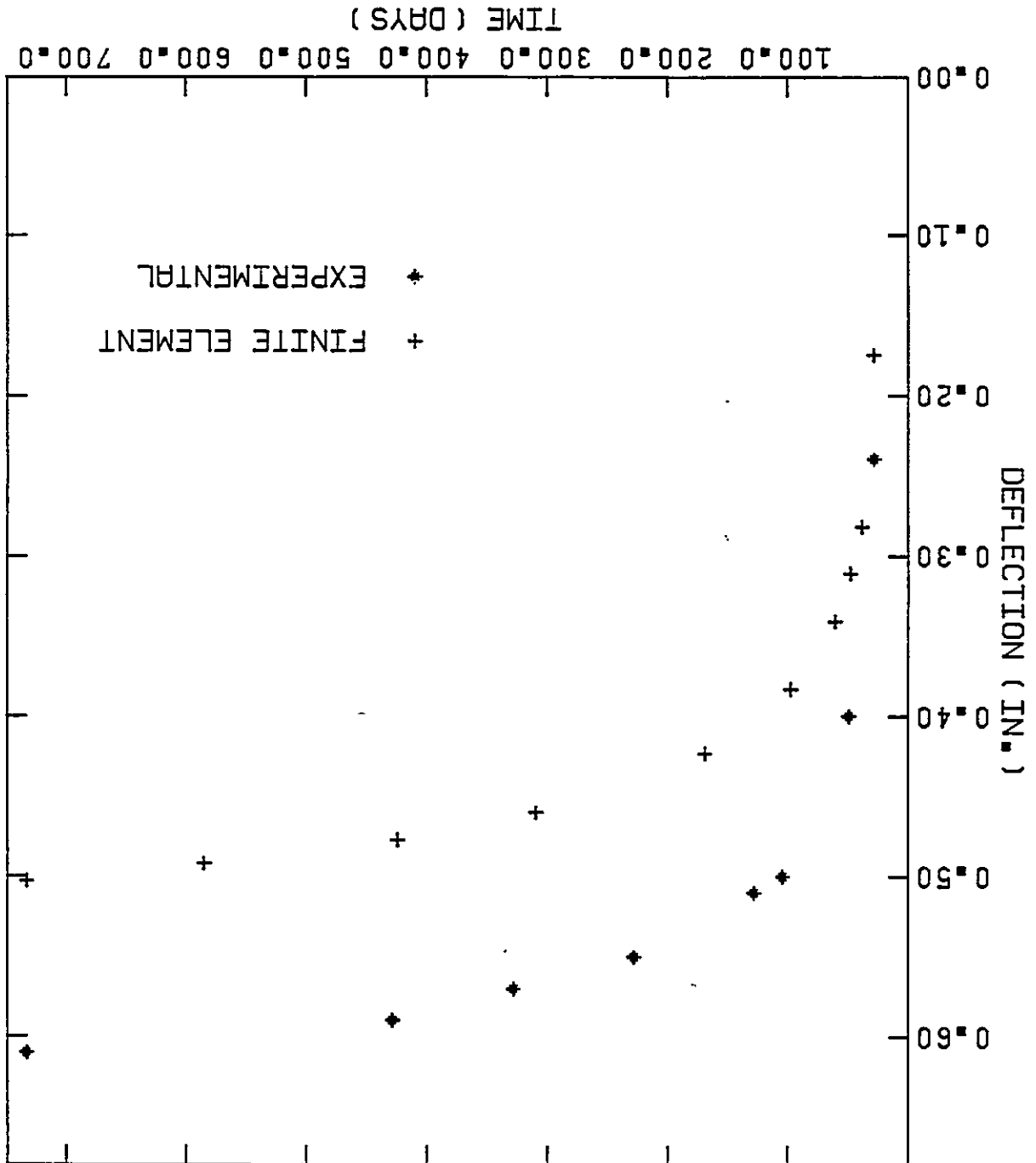
The predicted and observed deflection curves for Beam C4 are shown in Figure 3.50. Like Beam C3, the concrete stresses in Beam C4 were outside the service load range, and this undoubtedly had some effect on the results. The total and long term correlation between the



$f'_c=3500$ psi	$b=3.0$ in	$A_s=.33$ sq. in.
$f_t=445$ psi	$d=3.625$ in	
$E_c=3414$ ksi		
$E_s=29000$ ksi	$h=4.3125$ in	
MIX 1.0:4.2:4.5	$w/c=.85$	R.H.=.50

FIGURE 3.49 DETAILS FOR BEAM C4

DEFLECTIONS FOR BEAM C4
 FIGURE 3.50 EXPERIMENTAL AND FINITE ELEMENT



experimental and analytical curves was again reasonably good, and well within the normal variability limits associated with deflections in reinforced concrete beams. The total variation between the curves at the end of the 705 day loading period was about 17%, while the difference in the long term deflection alone was about 12%.

The experimental and finite element model crack patterns, shown in Figure 3.51, displayed the same general behaviour as observed for Beam C3. The model again predicted fewer cracks in the flexure span than were detected experimentally, but this was probably caused by the small scale effects mentioned earlier. The finite element mesh size was also not fine enough to allow cracks to form as close together as was observed experimentally. The heights of the cracks predicted by the model were somewhat higher than those observed in the experiment. A contributing factor in this discrepancy may have been the fact that the state of stress in the finite element beam was not exactly the same as in the experimental beam because the service load range was exceeded, and the model used constant stress elements. Another possibility is the accuracy with which Equation (3.2) estimated the tensile strength. Despite the differences the predicted crack pattern was still realistic.

The short and long term strain diagrams for Beam C4 are presented in Figure 3.52. The model predicted short term strains that were almost identical to the experimental values. The long term strains were also very similar, and in both cases the curvatures were almost

BEAM C4

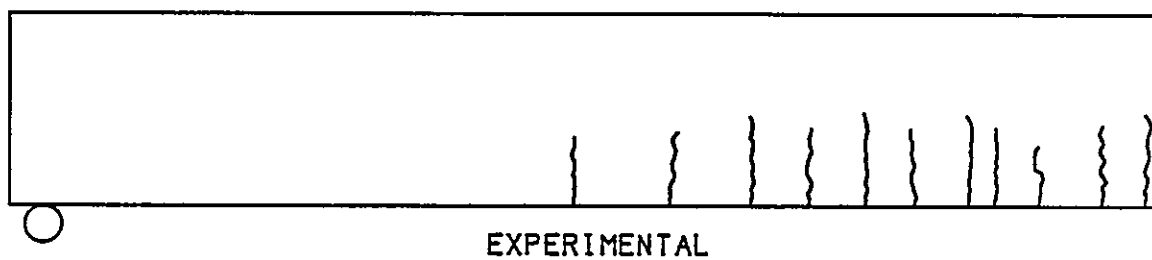
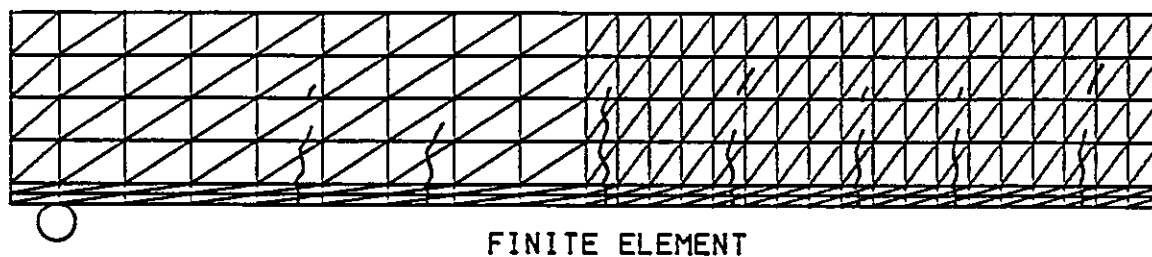


**FIGURE 3.51 EXPERIMENTAL AND FINITE ELEMENT
CRACK PATTERN FOR BEAM C4**

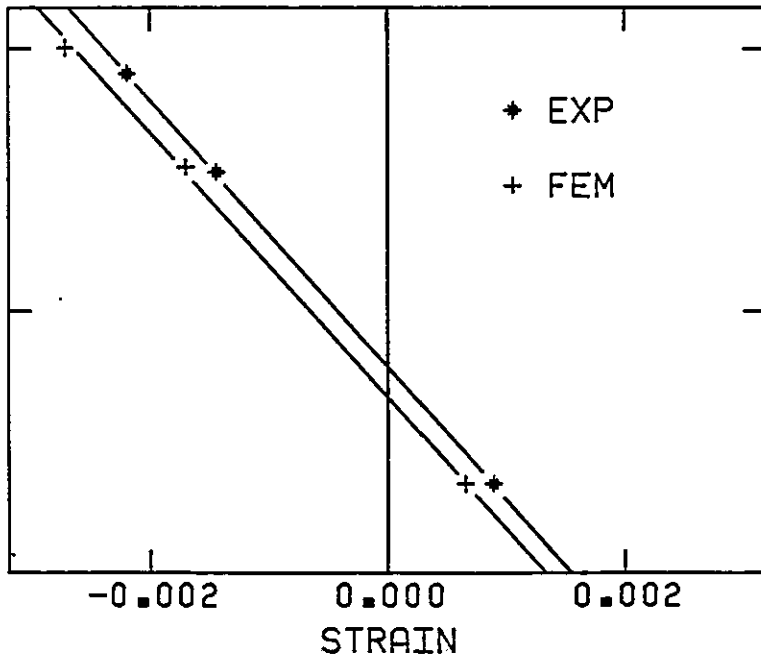
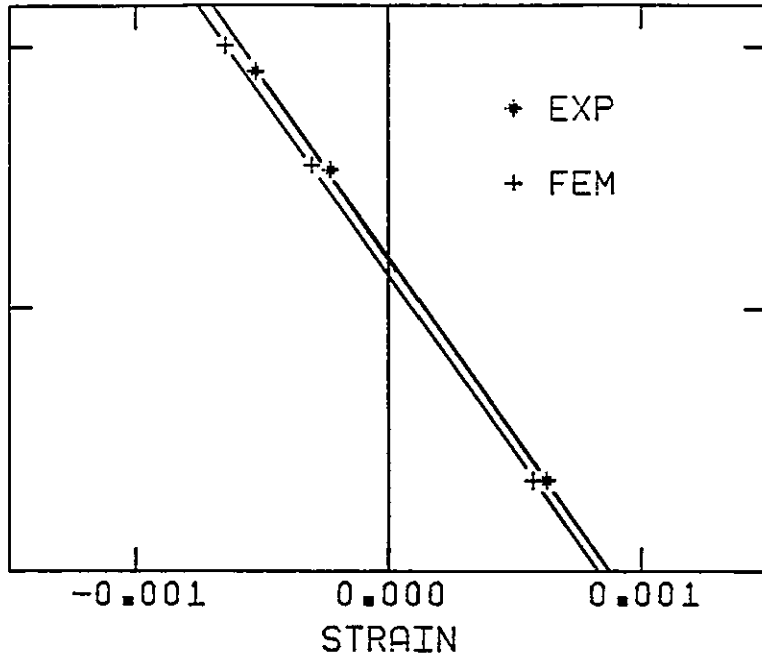


FIGURE 3.52 SHORT TERM AND LONG TERM STRAIN PROFILES FOR BEAM C4

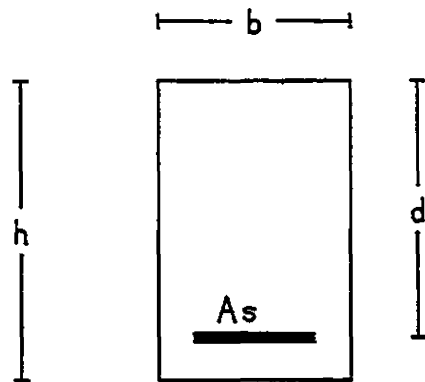
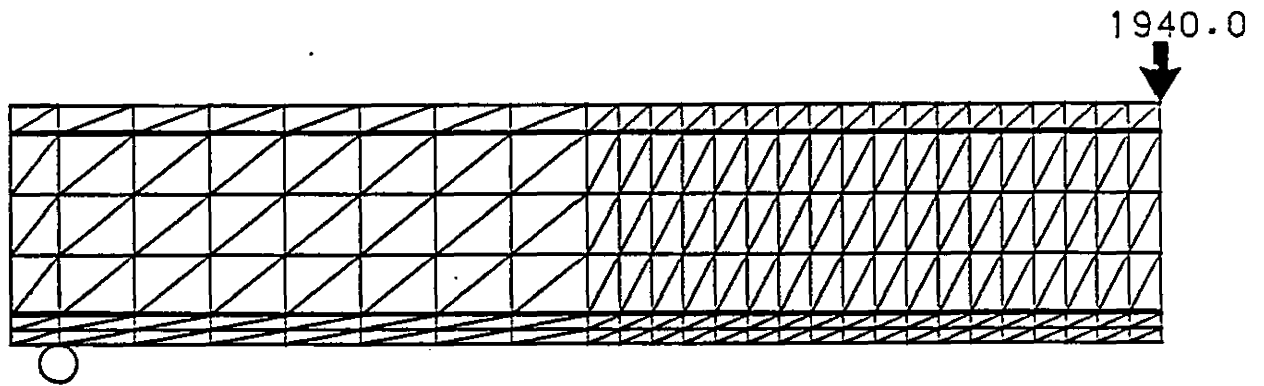
identical. Considering the approximations that were made the results were excellent.

The deflection results for all three Corley and Sozen beams were remarkably consistent. The short term deflections were all underestimated by the model, but the strain profiles and long term deflections were predicted very accurately. The fact that the short term deflections were not predicted as accurately as the short term strains was surprising, but this may have been due to the discrete strain changes from element to element that occurred in the model. Cracking away from midspan may also have been a factor.

Beam Ghali et al.

Ghali, Dilger, and Neville (21) measured the long term deflection of a reinforced concrete beam during an investigation into the time dependent settlement of beam supports. Although this beam was loaded for less than a year, it was still useful in providing a check on the accuracy of the model. The compression and tension steel contents of this beam were identical, and this significantly limited the effect of shrinkage. The information provided by the authors and estimated from empirical relationships are presented in Figure 3.53. The tensile strength, concrete modulus of elasticity, and steel modulus of elasticity were all calculated using the recommendations of Section 3.11. The relative humidity during the course of the test varied between 50% and 65%, so an average value of 58% was used in the analysis. The

DILGER



$f'_c = 4270 \text{ psi}$	$b = 4.0 \text{ in}$	$A_s = .39 \text{ sq. in.}$
$f_t = 490 \text{ psi}$	$d = 7.25 \text{ in}$	$A'_s = .39 \text{ sq. in.}$
$E_c = 3796 \text{ ksi}$	$d' = 1.0 \text{ in}$	
$E_s = 29000 \text{ ksi}$	$h = 8.25 \text{ in}$	
MIX 1.0:2.61:3.89	$w/c = .62$	$R.H. = .58$

FIGURE 3.53 DETAILS FOR DILGER ET AL. BEAM

density of the concrete and the cement content were estimated in the same way as for Beam C1.

The deflections reported for this beam were plotted in Figure 3.54 with the finite element predictions. The model accurately predicted the instantaneous deflection but underestimated the long term deflection. At the end of the 240 day loading period the variation between the experimental and finite element deflections was only about 12%. The long term variation alone was about 28%. The discrepancy in the long term deflections for this beam were larger than the previous examples and this fact may raise some questions about either the experiment or the model. Either the load on the beam actually increased with time, or the long term strains were significantly underestimated. This case highlights the difficulty in determining whether differences between the model and test data were caused by experimental error, experimental variability, inexact material properties, or problems with the model. Since good results were obtained for many of the other comparisons the problem was probably not with the model.

Beam A

Information about Beams A, B, E and F were provided earlier in Chapter 2 and Section 3.41, and most will not be repeated in this section. Briefly, Beam A was a full size, simply supported beam, with tension steel and nominal compression steel. The finite element discretization and the material properties from Beam A were presented in Figure 3.34. Since experimental creep and shrinkage strains were

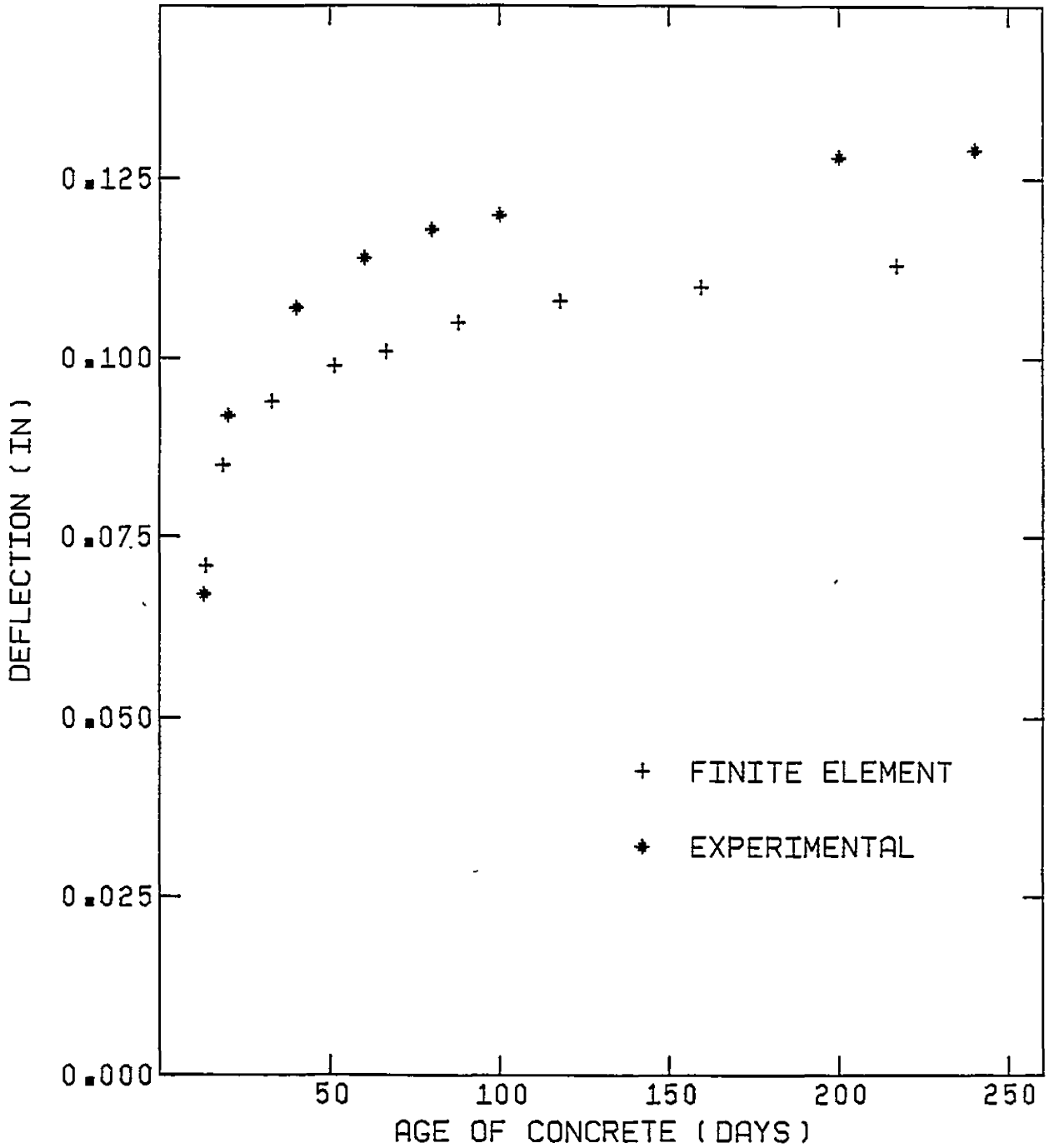


FIGURE 3.54 EXPERIMENTAL AND FINITE ELEMENT DEFLECTIONS FOR DILGER ET AL. BEAM

available it was not necessary to use Bazant and Panula's prediction equations. The experimental creep and shrinkage curves reported in Chapter 2 were reduced to usable mathematical equations by assuming that they followed a hyperbolic function similar to that of Meyers et al. (33).

At the end of the loading period, the applied load on Beam A had evidently dropped by about 22%. This decrease was approximated in the finite element representation with a simple logarithmic function where the load dropped with the log of time. Since the applied load varied with time the long term deflections were actually a combination of instantaneous and time dependent effects.

The long term deflection results for Beam A are shown in Figure 3.55. It is apparent from this figure that although the experimental and finite element short term deflections were not very close to each other, the total deflections were. The difference between the curves at the end of the loading period was less than 2% whereas the difference at the beginning was about 58%. The two curves converged in the first few days of loading, so delayed cracking in the experimental beam may have been the cause of the initial difference. If it was, it points out a weakness in using the ratio of long term to short term deflections as a prediction criterion. Even though the difference in initial deflections was significant, the actual difference in the long term deflections of the experimental and finite element beams was only about 17%.

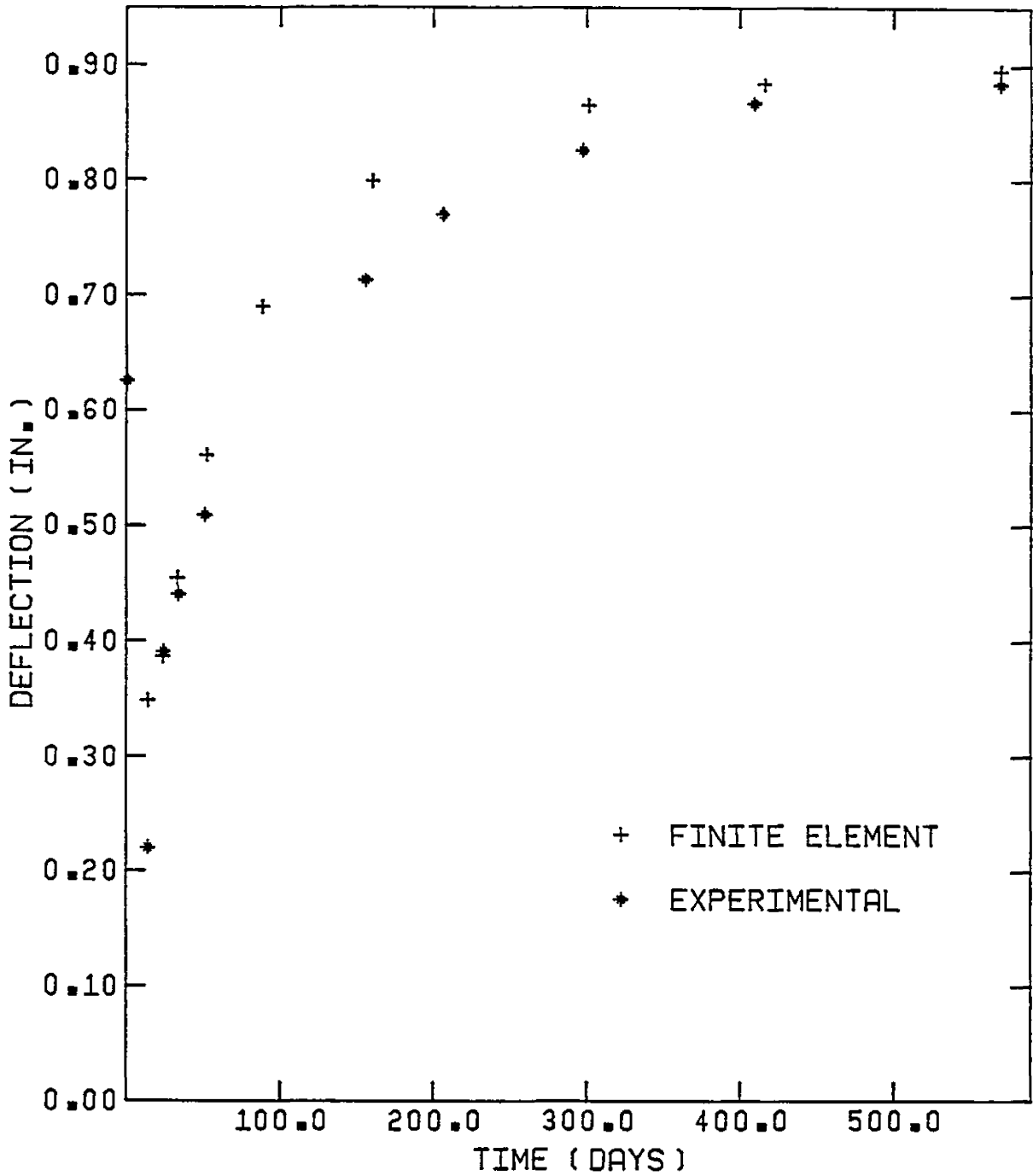


FIGURE 3.55 EXPERIMENTAL AND FINITE ELEMENT DEFLECTIONS FOR BEAM A

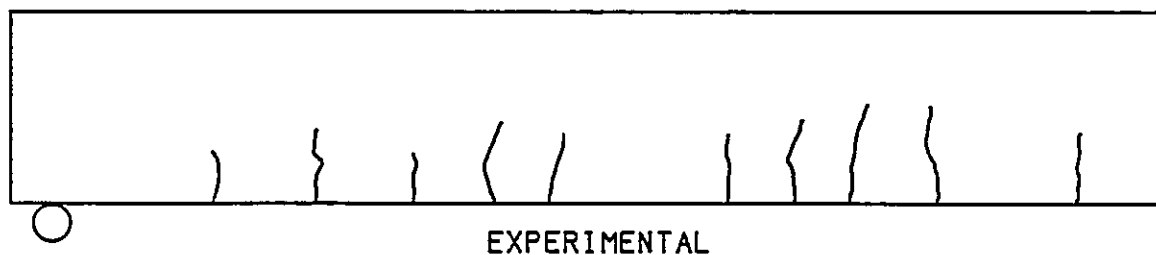
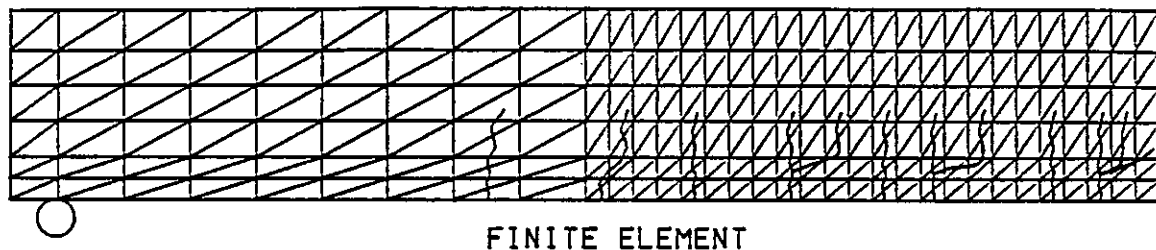
The Beam A crack patterns from the experiment and the finite element model are shown in Figure 3.56. It can be seen that the heights of the cracks for both beams were practically the same, and the average crack spacings were very similar. However, the model prediction of crack branching near the reinforcement was not observed experimentally, and the experimental cracking near the support was not seen in the model. Some similarities and some differences in crack patterns must be expected, but the degree of cracking in the tension zones were reasonably similar.

Beam B

Beam B was a simply supported beam with tension reinforcement and nominal compression reinforcement. It was subjected to the same external loads as was Beam A. The tension steel ratio of Beam B was lower than Beam A and the section depth was greater, but all other details were the same. The material properties, load reductions, and finite element discretization were also the same for Beam B as they were for Beam A. Further details about this beam can be found in Chapter 2, Section 3.41, and Figure 3.35.

The time-deflection curves for Beam B comparing experimental and finite element results can be found in Figure 3.57. From this figure it can be seen that the model underestimated the short term and long term deflections. The model underestimated the total deflections by about 32% and the long term deflections by about 41%. The probable reason for the underestimation of deflections may be answered by looking at the

BEAM A



BEAM B

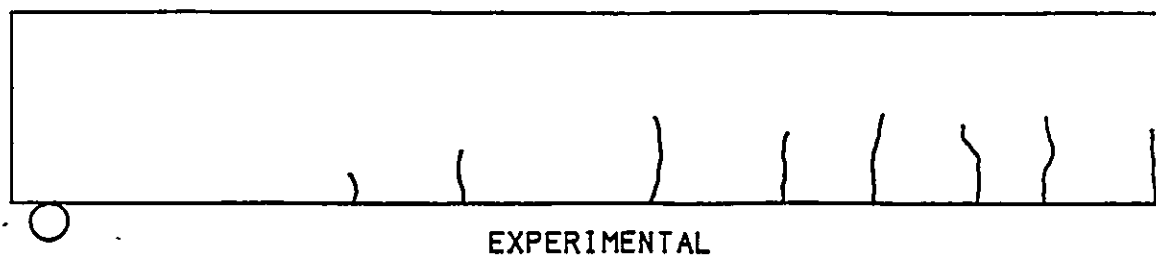
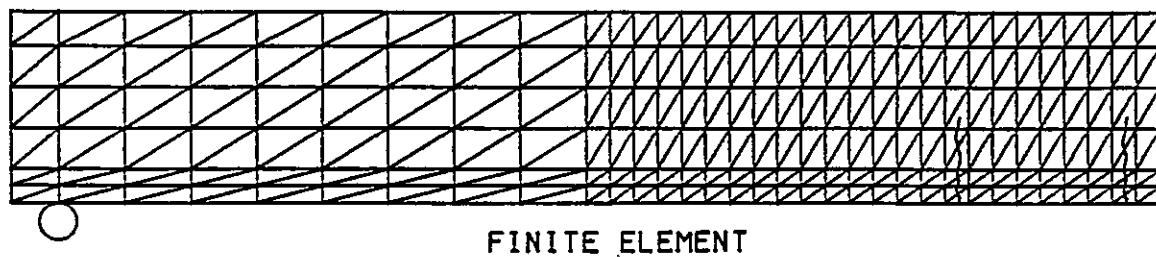


FIGURE 3.56 EXPERIMENTAL AND FINITE ELEMENT CRACK PATTERNS FOR BEAM A AND BEAM B

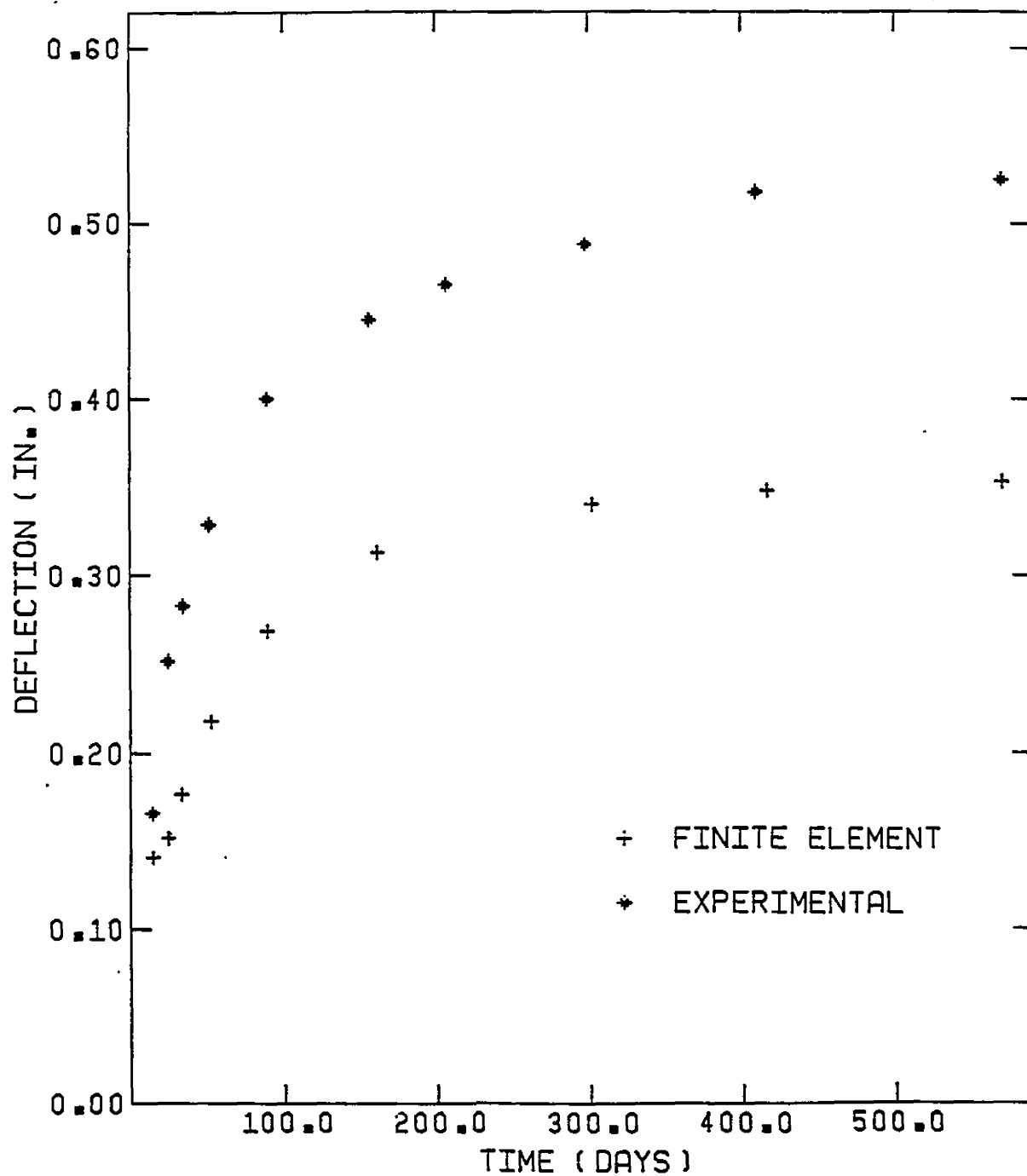


FIGURE 3.57 EXPERIMENTAL AND FINITE ELEMENT DEFLECTIONS FOR BEAM B

crack patterns contained in Figure 3.56. Although the crack heights were predicted well by the model, the degree of cracking was not. Eight cracks were observed experimentally and only two were predicted by the model. It was shown in the Sensitivity Section, and will be shown again in the Beam F comparison, that the amount of cracking may have a significant effect on both short and long term deflections. This is especially true when cracking is not very extensive. The root of the problem may have been the fact that finite element models underestimate displacements, stresses, and strains. When the stresses in the uncracked region of the finite element beam were examined it was observed that in many places they were almost as large as the tensile strength. In a more accurate formulation these elements would have cracked and the resulting deflections generated by the model may have been much closer to the experimental ones. Increasing the number of elements may have improved the results. This problem was discussed in the section on sensitivity.

Beam E

The results for Beam E, a 24 foot continuous beam, were reported in Chapter 2, and these results were used to verify the accuracy of the model. Information on the loading, material properties, dimensions, and finite element discretization were given in Chapter 2, Section 3.41, and Figure 3.38, and will not be repeated here. Loads on the beam were nearly constant throughout the loading period and no modifications to them were deemed necessary.

The experimental and finite element generated midspan long term deflection curves for Beam E are shown in Figure 3.58. For this beam there was excellent agreement between the total deflections from the finite element model and the test beam. At the end of the test the variation between them was only 3%. The variation in the long term deflections alone was also very good and was less than 16%. Cracking in this beam was extensive and if the deflection results are taken as an indicator, the model seemed capable of accurately simulating both cracking and the effect of changing moment directions.

The crack patterns from the experimental beam and the finite element beam are shown in Figure 3.59. It is shown in this figure that more cracks were observed in the test beam than were predicted by the model, especially in the negative moment region over the support. The model predicted one crack in this area while nine cracks were detected experimentally. In the middle of the beam the model predicted three cracks instead of the six observed in the test beam. Despite having fewer cracks, the model predicted a larger deflection, which might seem to be contradictory. However the number of cracks in a beam do not always relate to its stiffness. Crack heights, orientations, locations, as well as other factors, also have a bearing on the stiffness and thus the deflection of a beam. There were many similarities between the experimental and analytical crack patterns. The height of the first midspan crack nearest the support was almost the same in both beams, and in both cases this was the largest crack. The other cracks near the midspans were also very similar in heights and orientations. Therefore the predicted loss of stiffness due to cracking in the midspan of the

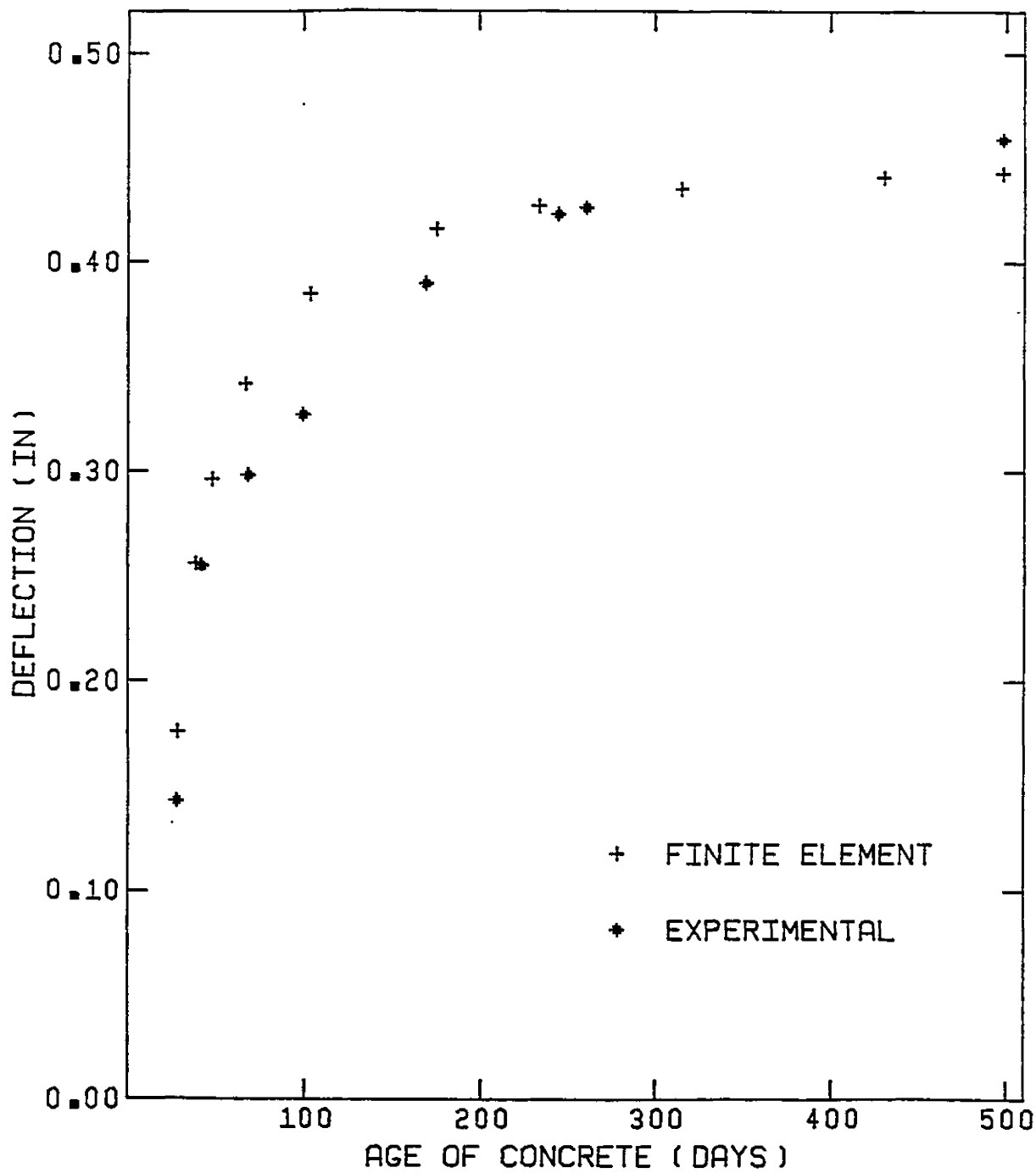
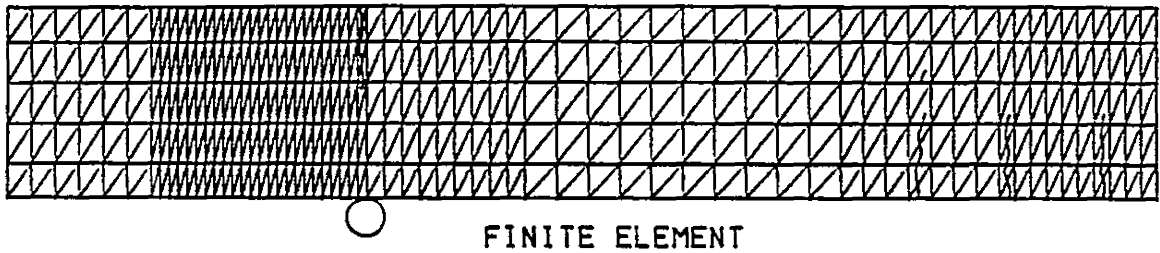
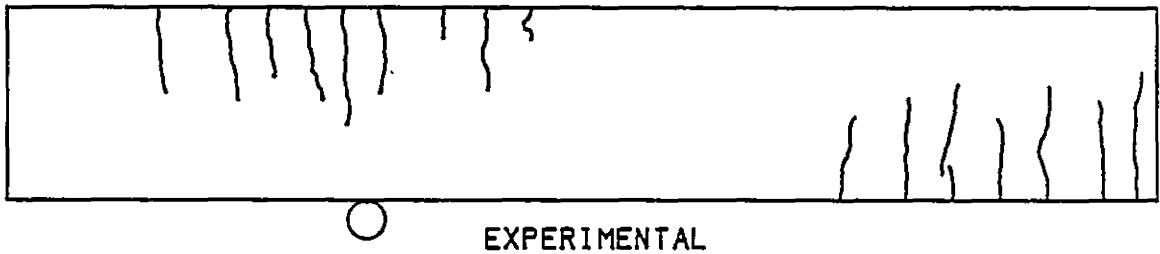


FIGURE 3.58 EXPERIMENTAL AND FINITE ELEMENT DEFLECTIONS FOR BEAM E

BEAM E

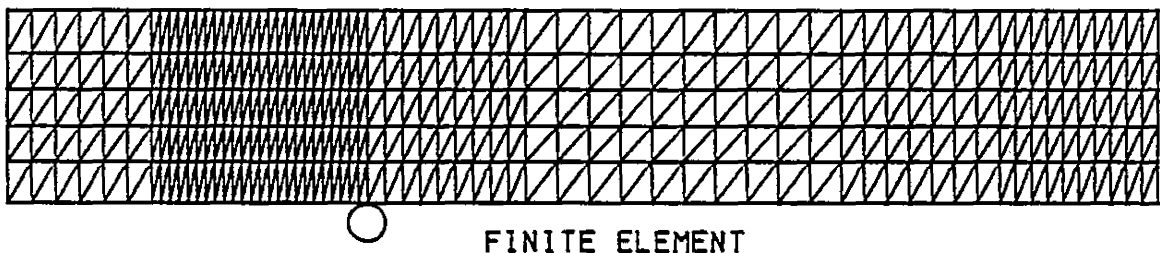


FINITE ELEMENT

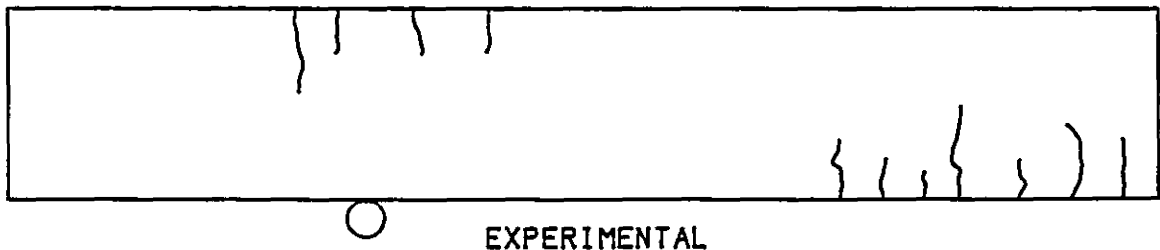


EXPERIMENTAL

BEAM F



FINITE ELEMENT



EXPERIMENTAL

FIGURE 3.59 EXPERIMENTAL AND FINITE ELEMENT CRACK PATTERNS FOR BEAM E AND BEAM F

finite element beam may have been very similar to the test beam, even though there were fewer cracks.

Beam F

Beam F was tested in the same apparatus as Beam E, and had the same external loads and material properties. The details needed for the finite element analysis were reported earlier in Section 3.41 and Figure 3.39. The midspan deflections for Beam F are presented in Figure 3.60. It is obvious from this figure that the finite element model significantly underestimated the long term deflections. As mentioned in Section 3.41, the model did not predict any cracks in this beam even though theoretically it should have. It didn't predict cracking because of the underestimation that is inherent in the finite element method. To test the effect that cracking would have had on the long term deflection of this beam the tensile strength in the model was reduced by 50%. Loading was stopped after a period of about a hundred days because of the cost of the analysis. The resulting deflections are also shown in Figure 3.60. This time the finite element model overestimated the deflections. Since the true conditions were really somewhere between the two cases it seems apparent that the model prediction would have been much better had the accuracy of the solution been improved by increasing the number of elements.

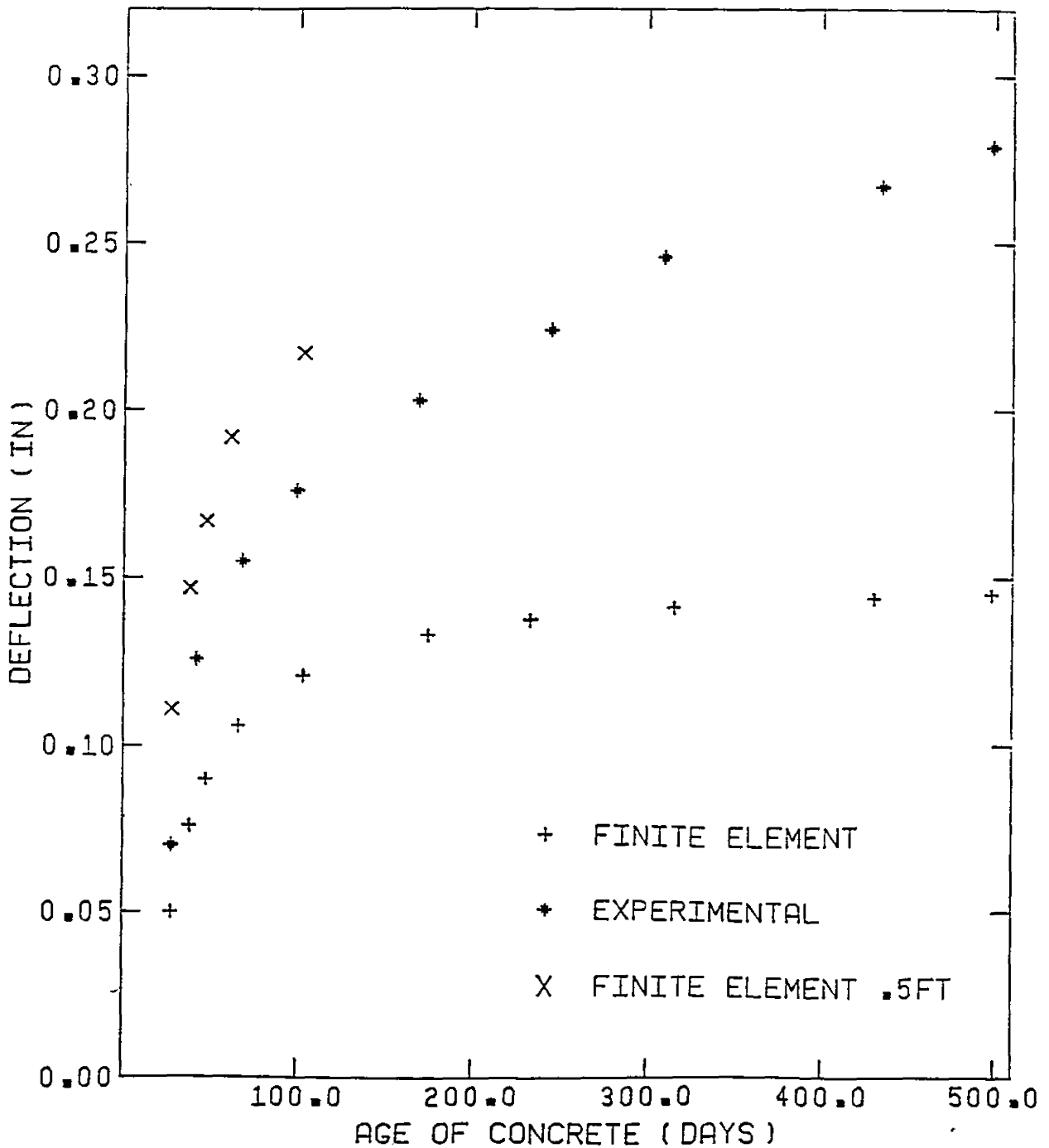


FIGURE 3.60 EXPERIMENTAL, STANDARD FINITE ELEMENT, AND 50% REDUCED TENSILE STRENGTH FINITE ELEMENT DEFLECTIONS

Summary

In this section the experimental results from eight reinforced concrete beams were compared with results generated by the finite element model. Of the eight, five beams had experimental long term deflections that were within 20% of the finite element model predictions. This was also the case for the total deflections, where five of the eight finite element simulations were within 20% of the experimental deflections.

Branson (8) reported that the coefficient of variation for long term deflections was 15 to 20 percent or even higher. The model must therefore be considered successful in modelling long term behaviour because this is the approximate range of the finite element results. Beyond natural variability however, the model is also subject to the sensitivity of the material and mesh parameters. Also, the model was based on a number of simplifications that were necessary to convert concrete behaviour to a mathematical model. These factors would obviously have some effect on the results, but the relatively good agreement observed indicates that their importance was not usually very significant.

Where differences did occur between the test data and the finite element results, the model generally underestimated the deflections. This fact is not really surprising because the finite element method theoretically provides a lower bound solution anyway. Judging by the deflections and strain profiles, the creep and shrinkage prediction

methods that were used with four of the beams also performed adequately. Cracking also seemed to have been simulated well. Experimental crack patterns were supplied for most of the beams and when these were compared with the finite element model solutions, the same general behaviour was usually observed. Usually the model did not predict as many cracks as were observed experimentally, but the loss of stiffness due to cracking seemed well represented. The model predicted strain profiles and curvatures even more accurately than it did deflections, so it can be said that the model was correctly simulating most aspects of beam behaviour. Both simply supported and continuous beams were examined in this comparison, and except for Beam F, the results were all reasonably consistent. Based on the results from this section, the finite element model which was described earlier in Chapter 3 has proven to be a reasonable method of simulating long term deflections in reinforced concrete beams.

CHAPTER 4

PARAMETRIC STUDY

4.1 Introduction

The major reason for the development of the finite element model presented in Chapter 3 was to use it to investigate the effect of various parameters on long term deflections, and to suggest possible improvements to current Building Code prediction methods. The Factorial Design Method was used to set up and analyze a parametric study designed to accomplish this goal. The deflection data needed for the parametric study was generated with the finite element model. A full parametric study using real life concrete beams would obviously have been preferable to one using the analytical model, but since this was not possible the analytical model provided the best alternative. The Factorial Design Method that was used in the parametric study is a well known, statistical, systematic, step-by-step approach, which identifies the influence and interaction of various independent variables on a dependent variable. In this case, the dependent variable was the long term-to-short term deflection ratio. If it is assumed that the finite element model gave good results, and the major parameters were properly identified, the relationship derived in this chapter with the Factorial Design Method should be realistic and accurate.

The major drawback of using an analytical model to derive an empirical relationship is that it cannot provide any measure of experimental variability. In reinforced concrete this is an important consideration. The range of $\pm 20\%$ on experimental deflections reported by Branson (8), and the sensitivity results from Section 3.3, must be kept in mind while reviewing the results from this chapter.

From the beginning it must be stated that it was never the object of this study to provide an in depth statistical analysis of all aspects of the design of a deflection experiment nor was it intended to use all of the capabilities of Factorial Designs. Instead, this study was centered on the development of a simple yet realistic approximation of the effect of long term loading on deflections using some statistical techniques. For this reason the number of variables was kept to a minimum, and no real "screening" was done with the variables. A description of the theory and application of Factorial Design will not be included here, but an excellent treatment of this subject can be found in the text by Box and Hunter (7).

4.2 Design of Experiment

The first stage in the parametric study was the identification of the influencing variables. These variables had to meet one main requirement. All of the variables had to be readily available to designers. A design equation containing variables which are not generally available to designers would not be useful. This requirement considerably limited the number of usable parameters.

In the Canadian Code (12), long term deflections were considered to be a function of the tension and compression steel areas and are now only a function of compression steel. However in this study, five parameters were chosen for study because it was felt that one or two parameters were not sufficient for a truly accurate relationship. The five parameters chosen for study included the tension steel ratio, the compression steel ratio, the span-to-depth ratio, the applied moment to ultimate moment ratio, and the concrete compressive strength. All of these values except for the concrete compressive strength have been identified in earlier studies (8)(9)(23)(54) as being important factors for long term deflections. The compressive strength was included in the parametric study because it was felt that this value might reflect the influence of the concrete mix parameters. Designers do not usually know much about the concrete mix, and the compressive strength is an available material value which might show its effect.

The ranges over which the identified parameters were assumed to act were fixed at the beginning of the parametric study. In a detailed experimental program this simplification would normally not be recommended because it might limit the flexibility of the analysis. However, since the variables for reinforced concrete beams have very definite ranges it was felt that this simplification would not adversely affect the analysis.

At the beginning of the design there was no real indication whether the effects of the parameters would be linear or nonlinear. This factor usually determines whether a two level Factorial Design is

used or whether a three level design is necessary. The two level design is used when the effect of the parameters is known to be linear, and the three level design is used whenever nonlinearities are present. Since the two level design is more economical to perform than the three level design, it is preferable to use it whenever possible. There is also a third alternative called a Star Design. This approach combines the economy of the two level design with the capabilities of the three level design. The Star Design is especially suited for studies where it is not clear at the beginning whether nonlinearities exist or not. When this alternative is used a normal two level design is performed, and the resulting relationship is checked for any nonlinearities. If nonlinearities are detected the nonlinear effects can be quantified by performing additional experiments on values outside the two level design limits. This means that care must be taken when choosing the ranges of the parameters during the initial two level design, since the expanded limits of the Star Design also need to represent realistic values.

It is possible to further increase the economy of a Factorial Design by using "Fractional Factorials". In this application a major variable is deliberately "confounded" or confused with one or more of the interaction effects. If they are confounded, the effect of an interaction term and the effect of a major variable will be indistinguishable from each other. However if the interaction effect is known to be very small, the effect of the major variable may be easily observed. For its economic benefits, Fractional Factorials were used in this parametric study and the compressive strength was confounded with the four factor interaction term. Four factor interaction terms are rarely

important so the results should not be adversely affected by this action.

The high and low levels of the five major variables examined in the initial two level design are listed below.

Variable	Range
ρ :	.72 - 1.78
ρ' :	.29 - 1.71
Mapp/Mult:	.24 - .46
l/d :	17 - 28
$f'c$ (psi):	3235 - 4560

Where ρ = tension steel ratio
 ρ' = compression steel ratio
Mapp = applied moment
Mult = ultimate moment
 l = length of beam
 d = depth of beam
 $f'c$ = compressive strength

(The ultimate moment should be calculated using 60 ksi reinforcing steel).

The confounding pattern used in the parametric study is shown below.

Resolution IV Design 2^{5-1}

$$I = \pm 12345$$

1 + 2345	12 + 345	24 + 135
2 + 1345	13 + 245	25 + 134
3 + 1245	14 + 235	34 + 125
4 + 1235	15 + 123	35 + 124
5 + 1234	23 + 145	45 + 123

It can be seen from this table that the major variables and the two factor interactions were all confounded with three factor interactions and higher. The possibility that these higher order interactions were important was very remote and the Fractional Factorial Design detailed here should be as accurate as a Full Factorial Design.

The Design Matrix used in the parametric study is shown in Table 4.1. The minus signs in this table represent the low levels of each variable, and the plus signs represent the high levels. Each row represents an experiment, or in this case a computer run of an individual reinforced concrete beam under long term loads.

4.3 Test Conditions

Once the levels of each variable were chosen they were included in the properties of a realistic reinforced concrete beam. The depth, thickness, concrete cover, relative humidity, yield stress of steel, age

RUN	I	1	2	3	4	5	12	13	14	15	23	24	25	34	35	45	$\frac{\Delta t}{\Delta i_{fem}}$	$\frac{\Delta t}{\Delta i_{calc}}$
1	+1	-1	-1	-1	-1	+1	+1	+1	+1	-1	+1	+1	-1	+1	-1	-1	3.59	2.79
2	+1	+1	-1	-1	-1	-1	-1	-1	-1	-1	+1	+1	+1	+1	+1	+1	1.38	1.07
3	+1	-1	+1	-1	-1	-1	-1	+1	+1	+1	-1	-1	-1	+1	+1	+1	1.18	.80
4	+1	+1	+1	-1	-1	+1	+1	-1	-1	+1	-1	-1	+1	+1	-1	-1	1.01	.73
5	+1	-1	-1	+1	-1	-1	+1	-1	+1	+1	-1	+1	+1	-1	-1	+1	.85	.79
6	+1	+1	-1	+1	-1	+1	-1	+1	-1	+1	-1	+1	-1	-1	+1	-1	1.40	1.25
7	+1	-1	+1	+1	-1	+1	-1	-1	+1	-1	+1	-1	+1	-1	+1	-1	.61	.54
8	+1	+1	+1	+1	-1	-1	+1	+1	-1	-1	+1	-1	-1	-1	-1	+1	.45	.43
9	+1	-1	-1	-1	+1	-1	+1	+1	-1	+1	+1	-1	+1	-1	+1	-1	2.54	1.95
10	+1	+1	-1	-1	+1	+1	-1	-1	+1	+1	+1	-1	-1	-1	-1	+1	2.91	1.82
11	+1	-1	+1	-1	+1	+1	-1	+1	-1	-1	-1	+1	+1	-1	-1	+1	.58	.37
12	+1	+1	+1	-1	+1	-1	+1	-1	+1	-1	-1	+1	-1	-1	+1	-1	.70	.51
13	+1	-1	-1	+1	+1	+1	+1	-1	-1	-1	-1	-1	-1	+1	+1	+1	1.78	1.27
14	+1	+1	-1	+1	+1	-1	-1	+1	+1	-1	-1	-1	+1	+1	-1	-1	.97	.87
15	+1	-1	+1	+1	+1	-1	-1	-1	-1	+1	+1	+1	-1	+1	-1	-1	.39	.34
16	+1	+1	+1	+1	+1	+1	+1	+1	+1	+1	+1	+1	+1	+1	+1	+1	.62	.57
17	+1	0	0	0	0	.15	0	0	0	0	0	0	0	0	0	0	.68	.54

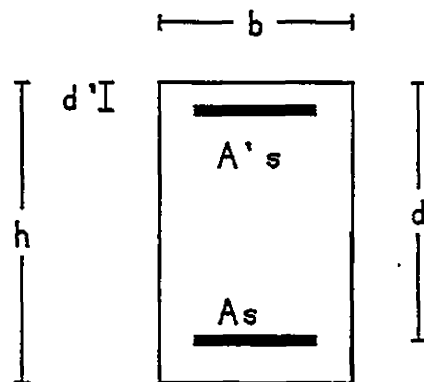
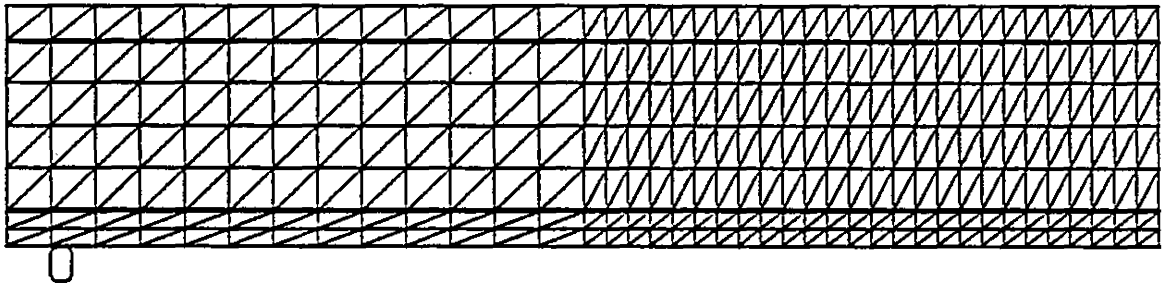
TABLE 4.1 Design Matrix and Deflection Ratios
for First 17 Computer Runs

of loading (7 days), and age when drying started (7 days), were all fixed at reasonable values as shown in Figure 4.1. Although the depth was part of the span-to-depth ratio, it was fixed so that the span length could be varied independently. Figure 4.1 shows the finite element discretization, dimensions, and properties of the beam which was used. The finite element discretization was chosen for its balance between accuracy and economy. Enough elements were provided to allow for realistic crack spacings and for a reasonable minimization of the potential energy.

The creep and shrinkage prediction methods developed by Bazant and Panula (3)(4) were used to calculate the long term strains. The mix details for the 3235 psi and 4560 psi concretes are shown in Table 4.2. These concrete mixes were taken from the literature (16)(25) and represent realistic values. The tensile strength, modulus of elasticity of concrete, and modulus of elasticity of steel were all estimated using the equations specified in Section 3.1.

It should be noted that the concrete tensile strengths used in the parametric study were not the same as those calculated by Equation (3.2). The tensile strengths were reduced from the calculated values to account for the underestimation of displacements and stresses which occurs in beams modelled with plane stress elements. It was observed in the sensitivity and verification sections that the level of crack initiation can have a profound effect on the deflections of beams loaded to around their cracking loads. Since the underestimation of stresses artificially raises the cracking load, the resulting deflections may not be realistic. Therefore the tensile strengths of the beams in the

BEAM



f'_c =VARIABLE

$b=8.0$ in

L =VARIABLE

E_c =VARIABLE

$d=12.0$ in

A_s =VARIABLE

$E_s=29000$ ksi

$d'=2.0$ in

$A's$ =VARIABLE

$h=14.0$ in

MIX-VARIABLE

w/c =VARIABLE R.H.=.5

FIGURE 4.1 DETAILS FOR BEAM USED IN PARAMETRIC STUDY

MIX #	f'c	MIX PROPORTIONS	w/c
1	3235	1.0:3.91:2.50	.699
2	4560	1.0:3.26:3.69	.656
3	4000	1.0:3.33:2.17	.65
4	2990	1.0:3.64:4.44	.700
5	4820	1.0:3.24:3.67	.596

TABLE 4.2 Details of Concrete Mixes Used in
Parametric Study

study were reduced by the amount of this underestimation. An elastic beam with the finite element grid of Figure 4.1 was loaded under uniform loads and the immediate deflection was compared with that calculated from elastic beam theory. The tensile strengths for the parametric study were then reduced by the same percentage difference as the underestimation. This difference was less than 10%.

In this study the dependent variable used for predicting long term deflections was the ratio of long term deflection to short term deflection. Two different long term-to-short term deflection ratios were investigated. In the first case, the ratio was defined using both the short term and long term deflections generated by the finite element program. In the second case the long term deflections were generated by the program, but the short term deflections were calculated using the Code (2)(12) equation. The main reason for looking at this second ratio was the recognition that in real life the long term deflection of a reinforced concrete beam would be predicted by multiplying the Code short term deflection by the long term-to-short term deflection ratio. The actual short term deflection would not be known at the design stage. It seems logical therefore to use the Code short term deflection to develop the deflection ratio. In this way it may be possible to reduce the effect of any errors in the Code short term deflection prediction. When the Code short term deflection is multiplied by the long term-to-Code short term deflection ratio, the Code short term deflection may be cancelled.

4.4 Results

The sixteen computer runs which made up the parametric study were completed according to the scheme detailed in Table 4.1, and the ratios of long term deflection-to-short term deflection for both cases were also recorded in this table. These values give a measure of the average effect of each variable over all conditions of the other variables. Combining these terms in a linear equation gives a relationship which relates all major and interaction variables with the deflection ratio. The notation in the design matrix of Table 4.1 assigns a level of +1 or -1 to each variable numbered 1 to 5. These nondimensional variables can be related to the actual variables through the ratios listed below.

$$\text{Variable 1} = \alpha_1 = \left(\frac{\rho - 1.25}{.53} \right)$$

$$\text{Variable 2} = \alpha_2 = \left(\frac{p' - 1.0}{.71} \right)$$

$$\text{Variable 3} = \alpha_3 = \left(\frac{\frac{\text{Mapp}}{\text{Multi.}} - 35}{.11} \right)$$

$$\text{Variable 4} = \alpha_4 = \left(\frac{\frac{l}{d} - 22.5}{5.5} \right)$$

$$\text{Variable 5} = \alpha_5 = \left(\frac{f'c - 3897.5}{662.5} \right)$$

Using the main and interaction effects from Table 4.1, and the variable ratio α_1 , an equation relating the long term-to-short deflection ratio to the variables can be written. For the first equation the short term deflections generated by the finite element analysis were used to provide the denominator of the ratio. The full equation can be written as follows:

$$\begin{aligned} \frac{\Delta t}{\Delta i} \text{ FEM} &= 1.310 - .130 \alpha_1 - .618 \alpha_2 - .426 \alpha_3 + .001 \alpha_4 + .252 \alpha_5 \\ &+ .133 \alpha_1 \alpha_2 + .106 \alpha_1 \alpha_3 + .119 \alpha_1 \alpha_4 + .053 \alpha_1 \alpha_5 \\ &+ .251 \alpha_2 \alpha_3 - .121 \alpha_2 \alpha_4 - .240 \alpha_2 \alpha_5 + .055 \alpha_3 \alpha_4 \\ &- .033 \alpha_3 \alpha_5 - .091 \alpha_4 \alpha_5 \end{aligned} \quad (4.1)$$

In the second case, where the short term deflection was calculated using the design code, the relationship can be written:

$$\begin{aligned} \frac{\Delta t}{\Delta i} \text{ CALC} &= .893 - .100 \alpha_1 - .470 \alpha_2 - .249 \alpha_3 - .044 \alpha_4 + .161 \alpha_5 \\ &+ .124 \alpha_1 \alpha_2 + .123 \alpha_1 \alpha_3 + .080 \alpha_1 \alpha_4 + 0.25 \alpha_1 \alpha_5 \\ &+ .183 \alpha_2 \alpha_3 - .045 \alpha_2 \alpha_4 - .145 \alpha_2 \alpha_5 + .049 \alpha_3 \alpha_4 \\ &- .011 \alpha_3 \alpha_5 - .116 \alpha_4 \alpha_5 \end{aligned} \quad (4.2)$$

Obviously these equations are very cumbersome, and some of the terms have very little effect on the deflection ratio. The main variable, l/d , obviously has little influence on either relationship, and some of the interaction effects are also not very significant. Eliminating the less significant terms by dropping those with values less than 0.100, results in the more simplified equations shown below.

$$\begin{aligned}
\frac{\Delta t}{\Delta i} \text{ FEM} &= 1.310 - .130 \alpha_1 - .618 \alpha_2 - .426 \alpha_3 + .252 \alpha_5 + .133 \alpha_1 \alpha_2 \\
&+ .106 \alpha_1 \alpha_3 + .119 \alpha_1 \alpha_4 + .251 \alpha_2 \alpha_3 - .121 \alpha_2 \alpha_4 \\
&- .240 \alpha_2 \alpha_5 \qquad (4.3)
\end{aligned}$$

$$\begin{aligned}
\frac{\Delta t}{\Delta i} \text{ CALC} &= .893 - .100 \alpha_1 - .470 \alpha_2 - .249 \alpha_3 + .161 \alpha_5 + .124 \alpha_1 \alpha_2 \\
&+ .123 \alpha_1 \alpha_3 + .183 \alpha_2 \alpha_3 - .145 \alpha_2 \alpha_5 - .116 \alpha_4 \alpha_5 \qquad (4.4)
\end{aligned}$$

These equations are still reasonably long, but all of the terms are important. The high degree of interaction present in the two deflection equations is interesting and unexpected. This high interaction may explain past difficulty in developing an accurate prediction equation.

The relationships in Equation (4.3) and Equation (4.4) are based on the assumption that the parameters vary linearly within their ranges. This is not necessarily true. The assumption must be verified before it can be accepted. Checking for nonlinearity involves performing an additional experiment with the variables set at the midpoint of their ranges. If the relationship is truly linear the deflection ratios for this run should correspond to the constants in Equation (4.3) or Equation (4.4). The results from this extra run are shown in Table 4.1 as Run 17. The compressive strength used in the additional run was not exactly at the midpoint of its range, but was close enough for comparison purposes. The concrete mix for this compressive strength is shown in Table 4.2.

For Equation (4.3) to be considered a linear relationship, the deflection ratio from the additional run should have been close to 1.31. The actual value was only 0.68, which is 48% less than expected. The expected value from Equation (4.4) was 0.89, but the actual value turned out to be 0.54. The error in this equation was 65%. Obviously high nonlinearity was present in both relationships. It was less evident for the long term-to-calculated short term deflection ratio equation, but neither relationship could be considered linear. The Star Design option was required to quantify the nonlinearities.

Choosing which of the variables contained nonlinear effects was not very straightforward and involved some guesswork. It seems likely that the variables which were most important to the linear relationship, were the one whose nonlinearities were most likely to be significant in the nonlinear relationship. However this assumption was not necessarily the case. Through some "screening" of the variables, the compression steel ratio, the applied moment to ultimate moment ratio, and the concrete compressive strength, were selected as having the most important nonlinear effects. The expanded high and low levels defining the new ranges for these parameters are shown below.

Variable	Range
ρ' :	0 - 2.00
Mapp/Multi:	.19 - .51
f'c (psi):	2990 - 4820

The concrete mix designs for these compressive strengths are shown in Table 4.2.

The twenty three computer runs which made up the total Star Design were completed according to the scheme detailed in Table 4.3. The notation used in this table was the same as in Table 4.1. The relationship between the nondimensional variables α_1 , and the actual variables were also the same as mentioned earlier.

The short term deflections from the finite element program, the long term deflections from the finite element program, the calculated short term deflections, and the deflection ratios from the twenty three computer runs are shown in Table 4.4. All deflections in Table 4.4 are in inches. The equation from the Star Design for the long term-to-short term deflection ratio is written below where all main and interaction effects with coefficients less than 0.100 have been eliminated.

$$\begin{aligned} \frac{\Delta t}{\Delta l} \text{ FEM} &= .519 - .130 \alpha_1 - .549 \alpha_2 - .425 \alpha_3 + .212 \alpha_5 + .133 \alpha_1 \alpha_2 \\ &+ .106 \alpha_1 \alpha_3 + .119 \alpha_1 \alpha_4 + .251 \alpha_2 \alpha_3 - .121 \alpha_2 \alpha_4 \\ &- .240 \alpha_2 \alpha_5 + .151 \alpha_2^2 + .310 \alpha_3^2 + .319 \alpha_5^2 \end{aligned} \quad (4.5)$$

For the long term-to-calculated short term deflection ratio the equation is:

$$\begin{aligned} \frac{\Delta t}{\Delta l} \text{ CALC} &= .366 - .100 \alpha_1 - .424 \alpha_2 - .231 \alpha_3 + .134 \alpha_5 + .124 \alpha_1 \alpha_2 \\ &+ .123 \alpha_1 \alpha_3 + .183 \alpha_2 \alpha_3 - .145 \alpha_2 \alpha_5 - .116 \alpha_4 \alpha_5 \\ &+ .161 \alpha_2^2 + .167 \alpha_3^2 + .297 \alpha_5^2 \end{aligned} \quad (4.6)$$

RUN	I	1	2	3	4	5	12	13	14	15	23	24	25	34	35	45	22	33	55	$\frac{\Delta t}{\Delta i}_{fem}$	$\frac{\Delta t}{\Delta i}_{calc}$	
1	+1	-1	-1	-1	-1	+1	+1	+1	+1	-1	+1	+1	-1	+1	-1	-1	+1	+1	+1	3.59	2.79	
2	+1	+1	-1	-1	-1	-1	-1	-1	-1	-1	+1	+1	+1	+1	+1	+1	+1	+1	+1	1.38	1.07	
3	+1	-1	+1	-1	-1	-1	-1	+1	+1	+1	-1	-1	-1	+1	+1	+1	+1	+1	+1	1.18	.80	
4	+1	+1	+1	-1	-1	+1	+1	-1	-1	+1	-1	-1	+1	+1	-1	-1	+1	+1	+1	1.01	.73	
5	+1	-1	-1	+1	-1	-1	+1	-1	+1	+1	-1	+1	+1	-1	-1	+1	+1	+1	+1	.85	.79	
6	+1	+1	-1	+1	-1	+1	-1	+1	-1	+1	-1	+1	-1	-1	+1	-1	+1	+1	+1	1.40	1.25	
7	+1	-1	+1	+1	-1	+1	-1	-1	+1	-1	+1	-1	+1	-1	+1	-1	+1	+1	+1	.61	.54	
8	+1	+1	+1	+1	-1	-1	+1	+1	-1	-1	+1	-1	-1	-1	-1	+1	+1	+1	+1	.45	.43	
9	+1	-1	-1	-1	+1	-1	+1	+1	-1	+1	+1	-1	+1	-1	+1	-1	+1	+1	+1	2.54	1.95	
10	+1	+1	-1	-1	+1	+1	-1	-1	+1	+1	+1	-1	-1	-1	-1	+1	+1	+1	+1	2.91	1.82	
11	+1	-1	+1	-1	+1	+1	-1	+1	-1	-1	-1	+1	+1	-1	-1	+1	+1	+1	+1	.58	.37	
12	+1	+1	+1	-1	+1	-1	+1	-1	+1	-1	-1	+1	-1	-1	+1	-1	+1	+1	+1	.70	.51	
13	+1	-1	-1	+1	+1	+1	+1	-1	-1	-1	-1	-1	-1	+1	+1	+1	+1	+1	+1	1.78	1.27	
14	+1	+1	-1	+1	+1	-1	-1	+1	+1	-1	-1	-1	+1	+1	-1	-1	+1	+1	+1	.97	.87	
15	+1	-1	+1	+1	+1	-1	-1	-1	-1	+1	+1	+1	-1	+1	-1	-1	+1	+1	+1	.39	.34	
16	+1	+1	+1	+1	+1	+1	+1	+1	+1	+1	+1	+1	+1	+1	+1	+1	+1	+1	+1	.62	.57	
7	+1	0	0	0	0	.15	0	0	0	0	0	0	0	0	0	0	0	0	0	.02	.68	.54
8	+1	0	-1/2	0	0	.15	0	0	0	0	0	0	0	0	0	0	0	2	0	.02	1.22	1.00
9	+1	0	+1/2	0	0	.15	0	0	0	0	0	0	0	0	0	0	0	2	0	.02	.44	.33
10	+1	0	0	+1/2	0	.15	0	0	0	0	0	0	0	0	0	0	0	0	2	.02	.55	.45
11	+1	0	0	-1/2	0	.15	0	0	0	0	0	0	0	0	0	0	0	0	2	.02	1.74	.90
12	+1	0	0	0	0	1.26	0	0	0	0	0	0	0	0	0	0	0	0	0	1.58	.98	.76
13	+1	0	0	0	0	-1.37	0	0	0	0	0	0	0	0	0	0	0	0	0	1.88	1.02	.84

TABLE 4.3 Design Matrix and Deflection Ratios For All 23 Computer Runs

RUN	Δi_{calc} (in)	Δi_{fem} (in)	Δi_{tot} (in)	Δ_{t} (in)	$\frac{\Delta \epsilon}{\Delta i_{\text{fem}}}$	$\frac{\Delta \epsilon}{\Delta i_{\text{calc}}}$
1	.0746	.0579	.2657	.2078	3.59	2.79
2	.2853	.2212	.5273	.3061	1.38	1.07
3	.0850	.0547	.1254	.0680	1.18	.80
4	.2697	.1951	.3921	.1970	1.01	.73
5	.3812	.3529	.6524	.2995	.85	.79
6	.5793	.5187	1.2438	.7251	1.40	1.25
7	.3071	.2727	.4387	.1660	.61	.54
8	.5532	.5290	.7662	.2372	.45	.43
9	.2222	.1705	.6028	.4323	2.54	1.95
10	.7523	.4708	1.8395	1.3687	2.91	1.82
11	.2020	.1267	.2004	.0737	.58	.37
12	.7622	.5554	.9418	.3864	.70	.51
13	.8642	.6135	1.7073	1.0938	1.78	1.27
14	1.5246	1.3805	2.7141	1.3336	.97	.87
15	.9975	.8836	1.2268	.3432	.39	.34
16	1.4834	1.3588	2.2024	.8436	.62	.57
17	.6666	.5325	.8923	.3598	.68	.54
18	.6691	.5479	1.2151	.6672	1.22	1.00
19	.6893	.5055	.7298	.2243	.44	.33
20	1.0515	.8758	1.3534	.4776	.55	.45
21	.2455	.1270	.3483	.2213	1.74	.90
22	.6170	.4799	.9511	.4712	.98	.76
23	.6898	.5716	1.1531	.5815	1.02	.84

TABLE 4.4 Deflections and Deflection Ratios From Computer Runs

It can be seen in both equations that the midpoint value was predicted better with these equations than the linear ones. For Equation (4.5) the error was 23%, and for Equation (4.6) the error was 31%. These errors seem high and may indicate that higher order non-linearity exists, or more likely, that there are more influences present in the deflection relationship than can be quantified with the five major variables. When the deflection relationship is limited to variables which are available to designers, it must be expected that the resulting relationship will not be exact. In the remainder of this chapter, Equation (4.5) will usually be referred to as the model short term equation, and Equation (4.6) will usually be referred to as the Code based short term equation. Hopefully this will prevent confusion.

The coefficients in the deflection relationships represent a best fit between the given equations and the computer generated deflection ratios. Despite the reliability of the Factorial Design Method, these relationships are only as accurate as the chosen major variables and equation form allow them to be. The only way to check the accuracy with which Equation (4.5) and Equation (4.6) represent the deflection ratios was to compare results with the original twenty-three deflection ratios. The comparisons between the results from the model short term equation and the twenty-three original deflection ratios are shown in Table 4.5, and the comparison for the Code based short term equation is shown in Table 4.6.

As shown in Table 4.5 the average error in the deflection ratios calculated with the model short term equation was 0.16. The standard

RUN	$\frac{\Delta t}{\Delta_{fem}}$ (Equation 4.5)	$\frac{\Delta t}{\Delta_{fem}}$ (Actual)	ERROR
1	3.35	3.59	.24
2	1.46	1.38	.08
3	1.30	1.18	.12
4	.80	1.01	.21
5	.88	.85	.03
6	1.23	1.40	.17
7	.68	.61	.07
8	.72	.45	.27
9	2.45	2.54	.09
10	2.85	2.91	.06
11	.76	.58	.18
12	.85	.70	.15
13	1.79	1.78	.01
14	.80	.97	.17
15	.26	.39	.13
16	.66	.62	.04
17	.56	.68	.12
18	1.69	1.22	.47
19	.03	.44	.41
20	.58	.55	.03
21	1.78	1.74	.04
22	1.29	.98	.31
23	.83	1.02	.19

average error = .16

$$S = \frac{\sum(x-\bar{x})}{n-1} = .12$$

TABLE 4.5 Deflection Ratios From Computer Results
and Equation 4.5 Predictions

RUN	$\frac{\Delta t}{\Delta_{fem}}$ (Equation 4.6)	$\frac{\Delta t}{\Delta_{fem}}$ (Actual)	ERROR
1	2.57	2.79	.22
2	1.09	1.07	.02
3	.61	.80	.19
4	.62	.73	.11
5	.71	.79	.08
6	1.30	1.25	.05
7	.48	.54	.06
8	.56	.43	.13
9	2.01	1.95	.06
10	1.65	1.82	.17
11	.59	.37	.22
12	.64	.51	.13
13	1.27	1.27	0
14	.74	.87	.13
15	.50	.34	.16
16	.54	.57	.03
17	.39	.54	.15
18	1.35	1.00	.35
19	.08	.33	.25
20	.40	.45	.05
21	1.05	.90	.15
22	1.01	.76	.25
23	.74	.84	.10

average error .13

$$s = \frac{\Sigma(x-\bar{x})}{n-1} .09$$

TABLE 4.6 Deflection Ratios From Computer Results and Equation 4.6 Predictions

deviation in this error was 0.12. The results for the Code based short term equation, shown in Table 4.6, were even better than this. The average error in the deflection ratio was 0.13, and the standard deviation was 0.09. Therefore it may be concluded that the relationships developed here accurately reflect the computer data.

The deflection relationships calculated with the two equations matched the finite element generated data quite well. However, since these equations were intended as prediction equations, they would only be useful if they could predict real life deflections. Comparing the results from the equations with the data that was used to derive them did not necessarily show how well they could predict other deflections. The only way to truly evaluate the equations was to compare them with independent experimental data.

Washa and Fluck's (54) long term deflection data was used to verify the accuracy of the two deflection relationships. Only the members of Series A and Series B were selected for comparison. These were the members that most resembled real beams. Washa and Fluck paired their Series B beams and only provided average deflections for each pair. The difference between each beam in a pair was the compressive strength. The l/d ratio for the Series B beams exceeded the range for which either of the deflection equations applied, but the effect should have been minimal.

The results from the comparison are shown in Table 4.7. In this comparison the long term deflections for the model short term equation

Beams	Equation 4.5 (in)	Equation 4.6 (in)	Experimental (in)
B1,B4	.42	.52	1.18
B2,B5	1.13	.75	1.58
B3,B6	2.25	1.30	2.36
A4	.21	.13	.40
A5	.74	.41	.65
A6	1.39	.86	1.09

TABLE 4.7 Deflections From Equation 4.5,
Equation 4.6, and Experiment

were calculated by multiplying the experimental short term deflections by the deflection ratio. For the Code based short term equation, the Code calculated short term deflections were multiplied by the deflection ratios.

It seems from the results of Table 4.7 that the model short term equation performed better than the Code based short term equation. The average error for the model short term equation was 0.31", ranging from a low of 0.09" to a high of 0.76". The average error for the Code based short term equation was 0.55" with a range of 0.23" to 1.06". The recent Canadian Concrete Code (12) had an imposed lower limit of 0.6 on the long term-to short term deflection ratio. If this limit was also imposed on Equation (4.5) and Equation (4.6), the deflection results would have been better. In this case the average error would have been 0.27" for the model short term equation and 0.49" for the Code based short term equation.

Equation (4.5) and Equation (4.6) were both intended as possible replacements for the ACI (2) and CSA (12) prediction equations. This recommendation could only be made if the equations proved to be more accurate than the current approaches. Therefore a comparison between the equations derived in this chapter and the CAN3-A23.3 (12) equations was required. The comparison showed how well the Code equations predicted the twenty-three deflection results from the parametric study. The results from this comparison are shown in Table 4.8. The long term deflections in this table were calculated by multiplying the model generated short term deflections by the deflection ratios for each case.

RUN	Δ Actual (in)	Δ Code (1977) (in)	Δ Code (1984) (in)	Δ Equation 4.5 (in)
1	.2078	.0874	.1001	.1940
2	.3061	.4004	.3849	.3230
3	.0680	.0344	.0619	.0746
4	.1970	.1658	.2107	.1561
5	.2995	.5329	.6100	.3106
6	.7251	.9388	.9025	.6380
7	.1660	.1636	.2945	.1854
8	.2372	.4497	.5714	.3809
9	.4323	.2575	.2948	.4177
10	1.3687	.8521	.8191	1.3418
11	.0737	.0760	.1368	.0963
12	.3864	.4721	.5998	.4721
13	1.0938	.9264	1.0605	1.0982
14	1.3336	2.4987	2.4021	1.1044
15	.3432	.5302	.9544	.2297
16	.8436	1.1550	1.4675	.8968
17	.3598	.5538	.7083	.2982
18	.6672	1.0958	1.0958	.9260
19	.2243	.3033	.5055	.0152
20	.4776	.9108	1.0772	.5080
21	.2213	.1321	.1562	.2261
22	.4712	.4991	.5903	.6191
23	.5815	.5945	.7031	.4744
	average error	.2182	.2792	.0743

TABLE 4.8 Deflection Predictions Using Equation 4.5
and the Code Equations

It is obvious from the results in Table 4.8 that the model short term equation performed far better than the Code equations. The average errors for the 1977 and 1984 Code equations was 0.218" and .279" respectively, while the average error for the model short term equation was only 0.074".

A comparison between the Code based short term equation and the CAN3-A23.3 (12) equations for the twenty-three computer generated deflections is presented in Table 4.9. In this example the long term deflections were calculated by multiplying the predicted Code short term deflections by the deflection ratios. Since the calculated short term deflections were used, this example is probably a more realistic evaluation of the prediction accuracy of the Code equations. The average error of the 1977 and 1984 Code equations in predicting the twenty-three deflections was 0.264" and .373" respectively. The average error for the Code based short term equation was only 0.075".

Probably the most significant observation that can be made from the results in Tables 4.8 and 4.9 was the lack of accuracy in the Code prediction equations. The good results from Equations (4.5) and (4.6) were not unexpected since this is the same data which was used to derive them. Conversely, if the Code equations were compared with Equations (4.5) and (4.6) using data which had been used to derive the Code equation, it might be expected that the Code equations would appear to be relatively more accurate. What is really important in the comparisons with the computer generated data, is first the accuracy of the Code equations themselves, and second, the order of the difference

RUN	Δ Actual (in)	Δ Code (1977) (in)	Δ Code (1984) (in)	Δ Equation 4.6 (in)
1	.2078	.1126	.1289	.1917
2	.3061	.5164	.4964	.3110
3	.0680	.0510	.0918	.0519
4	.1970	.2292	.2912	.1672
5	.2995	.5756	.6589	.2707
6	.7251	1.0485	1.0080	.7531
7	.1660	.1843	.3317	.1474
8	.2372	.4702	.5974	.3098
9	.4323	.3355	.3841	.4466
10	1.3687	1.3617	1.3090	1.2413
11	.0737	.1212	.2182	.1192
12	.3864	.6479	.8232	.4878
13	1.0938	1.3049	1.4938	1.0975
14	1.3336	2.7595	2.6528	1.1282
15	.3432	.5985	1.0773	.4988
16	.8436	1.2609	1.6021	.8010
17	.3598	.6933	.8866	.2600
18	.6672	1.3382	1.3382	.9033
19	.2243	.4136	.6893	.0551
20	.4776	1.0936	1.2934	.4206
21	.2213	.2553	.3019	.2578
22	.4712	.6417	.7589	.6232
23	.5815	.7174	.8485	.5104
	average error	.2643	.3726	.0747

TABLE 4.9 Deflection Predictions Using Equation 4.6
and the Code Equations

between the accuracy of the Code equations and the equations developed in this chapter.

A comparison between Washa and Fluck's experimental data and the predictions from the equations presented in this chapter was shown in Table 4.7. A natural extension of this comparison is to contrast those results with predictions using the Code equations. Before presenting the results from this comparison, it is necessary to point out that Washa and Fluck's data was used to derive the Code equations. As was mentioned earlier it is not always very informative to judge a prediction equation by comparing it with the data that was used to derive it. Therefore it might be expected that the Code equations should predict Washa and Fluck's data very well. What may be interesting is to see how closely the predictions using Equation (4.5) and Equation (4.6) compare with the predictions of the Code equations.

In the first comparison, shown in Table 4.10, the deflections predicted by the model short term equation and the Code equations were compared with Washa and Fluck's experimental data. The long term deflections in this table were calculated by multiplying the experimental short term deflections by the deflection ratios. The average error for the 1977 and 1984 Code equations were 0.24" and .22". This compared with an average error of 0.31" for the model short term equation, or 0.27" if the minimum deflection ratios were limited to 0.6. The Code equations therefore performed better than the model short term equation, but the difference was not very significant. Considering the

Beams	Equation 4.5 (in)	Code (1977) (in)	Code (1984) (in)	Experimental (in)
B1,B4	.42	.74	1.03	1.18
B2,B5	1.13	1.37	1.40	1.58
B3,B6	2.25	2.08	2.08	2.36
A4	.21	.42	.59	.40
A5	.74	.87	.89	.65
A6	1.39	1.34	1.34	1.09

TABLE 4.10 Deflection Predictions Using Equation 4.5
and the Code Equations

Beams	Equation 4.6 (in)	Code (1977) (in)	Code (1984) (in)	Experimental (in)
B1,B4	.52	.66	.92	1.18
B2,B5	.75	1.20	1.23	1.58
B3,B6	1.30	1.76	1.76	2.36
A4	.13	.42	.59	.40
A5	.41	.76	.78	.65
A6	.86	1.12	1.12	1.09

TABLE 4.11 Deflection Predictions Using Equation 4.6
and the Code Equations

fact that Washa and Fluck's data was used to derive the Code equations, the results seem encouraging for the model short term equation.

A comparison between Washa and Fluck's experimental data, predictions from the Code based short term equation, and predictions from the Code equations, are shown in Table 4.11. This time the long term deflections were calculated by multiplying the Code predicted short term deflections by the deflection ratios. The average errors for the 1977 and 1984 Code predictions was 0.28" and .26". The average error for the Code based short term equation, Equation (3.6), was 0.55" with no lower limit, and 0.49" with an imposed minimum deflection ratio of 0.6. In this case the performance of the Code based short term equation was not very good which may mean that this equation is not an appropriate prediction equation. However an interesting observation that may be made from the results in Tables 4.10 and 4.11 is that the Code equations do not even very accurately predict the data from which they were derived.

The results from the comparisons with Washa and Fluck's data indicates that neither Equation (4.5) nor Equation (4.6) were highly accurate for these examples. On the other hand the equations did give reasonable estimates of the long term deflections. The inaccuracy that did exist may have been caused by a number of different factors. One reason which was mentioned earlier was the supposition that there are other parameters not included in the equations which also influence long term deflections. Another possibility is the effect of the compressive strength. Different mixes with the same compressive strengths may have

different creep and shrinkage characteristics. A third possibility is experimental variability.

A fourth possibility, and one which may require further thought, is whether the long term-to-short term deflection ratio is really the best value to use in predicting long term deflections. If it is difficult to get highly accurate results using this ratio, it may be advisable to use some other criteria for dealing with these deflections.

It may be informative to examine some of the factors which will affect any prediction equation using a long term-to-short term deflection ratio. Delayed cracking is one of these factors. It is possible for significant cracking to occur in a beam at the end of its loading, however it is equally likely for an identical beam to experience this cracking in the first few days after loading. These two identical beams could have very different time dependent deflections, and quite different deflection ratios. Another factor is the accuracy of the short term deflection prediction. It was observed that Equation (4.5), Equation (4.6), and the results from these equations were quite different, even though the only real difference between them was whether the Code short term deflection was used or the finite element short term deflection was used. Perhaps in future it may be advisable to develop a prediction method that calculates the actual long term deflection and not a deflection ratio.

From the results in this chapter it seems more and more apparent that any equation predicting the actual long term deflection alone may never be highly accurate under every circumstance. If this is the case it should either be recognized that a prediction equation only gives an approximate value, or some other criteria must be suggested. Perhaps this could take the form of general guidelines about when, and under what conditions, long term deflections may be a problem. Another possibility is to calculate the total deflections rather than long term deflections. This would also reinforce the idea that it is sometimes difficult to separate long term deflections from short term deflections.

4.5 Summary

In this chapter a parametric study was conducted to develop an equation for predicting long term deflections of reinforced concrete beams. Two equations were presented since there may be some question about whether a deflection ratio should be derived using actual short term deflections or calculated deflections. The first equation was developed using short term deflections generated by the finite element model. The second used Code calculated short term deflections. Of the two equations presented, the one that was derived using the finite element generated short term deflections seemed superior to the one derived from calculated deflections. Comparisons with more independent experimental evidence may be necessary to finalize this conclusion. The CAN3-A23.3-M77 suggestion of a lower limit of 0.6 on the deflection ratio seems advisable for the equations developed in this chapter. In

comparisons with twenty-three deflection results generated with the finite element model, the equations developed in this chapter proved to be far superior to the Code predictions. When compared with the experimental data of Washa and Fluck, one of the equations was almost as accurate as the Code equations. When more experimental data becomes available it should be possible to further verify these results. It should be strongly stated at this point that the equations presented in this chapter are only applicable for the ranges that were set during their derivation. Values lying outside these boundaries may produce inaccurate results and should be used with discretion.

In the future it may be advisable to study alternatives to predicting long term deflections with a long term-to-short term deflection ratio. General guidelines about when long term deflections may be a problem, a prediction equation calculating actual long term deflections, or the prediction of total deflections, may be preferable to the deflection ratio approach. However at this stage it seems apparent that the past and current Code prediction equations are not very accurate and the equation developed in this chapter should be seriously considered as a replacement.

CHAPTER 5

CONCLUSIONS

5.1 General

Long term deflections in reinforced concrete beams have become increasingly important in the last few years, and this investigation was launched to further the understanding of this subject. The three main objectives of this study were to provide experimental data on long term deflections of reinforced concrete beams, to develop an accurate finite element model to simulate reinforced concrete beam behaviour, and to develop an empirical long term deflection prediction equation using the finite element model. The results from this work provided interesting insights into the time dependent behaviour of reinforced concrete and the modelling of this complex material.

5.2 Experimental Work

In the experimental program, six reinforced concrete beams, of which four were continuous, were subjected to sustained load for a period of 1 1/2 years. The resulting deflections were reported in Chapter 2. These results were used to evaluate the CAN3-A23.3 (12) Code prediction equation and later to evaluate the finite element model.

The most striking fact observed from the long term deflection results was the evident inaccuracy of the CAN3-A23.3 (12) Code long term deflection prediction equation. In every case, the prediction equation significantly underestimated the experimental deflections, even for those beams which had decreasing loads. In a deflection sensitive structure this lack of conservatism could have serious consequences.

Another detail that only became apparent at the end of the test program was the long term sensitivity of the instrumentation. The readings from the load cells drifted with time even though the cells tested perfectly at the beginning of the test. The durability of the equipment in a long term test is at least as important as its initial accuracy, and this fact must be kept in mind by future researchers.

The results from the continuous beams indicated that their deflection behaviour may not be the same as that for simple beams. Even though these beams had more compression steel than tension steel in their positive moment regions, their long term to short term deflection ratios were comparable to the deflection ratios of a simple beam with no compression steel. This may indicate that the effects of high moments in one region of a reinforced concrete beam may significantly affect the long term deflections in another. If this is true an accurate long term deflection prediction equation must include this factor. Not much experimental long term deflection data for beams with changing moment directions exists, and more data is needed before the deflections of these beams can be predicted confidently.

5.3 Finite Element Model

A great deal of time and effort went into the development of a finite element model that would accurately simulate the long term behaviour of reinforced concrete beams. Since complete material property data is rarely available, a number of empirical prediction methods were investigated to determine which ones should be used when the true values were not available. Judging by the deflection results, the chosen methods were reasonably good for predicting the required values. The finite element model itself was a combination of plane stress triangular elements for concrete, bar elements for steel, and Goodman Joint Elements for bond. An implicit visco-plastic model was used for the creep formulation.

From the results presented in Chapter 3 it is possible to say that the model performed reasonably well for both short term and long term loadings, and was generally successful in simulating the behaviour of reinforced concrete beams. Probably the most important factor affecting the finite element results was cracking. For beams stressed near the cracking load, the finite element model was sensitive to any factor which might accelerate or delay the onset of cracking. Although the model was sometimes sensitive to variations in the material properties and the finite element mesh, especially at low loads, it usually generated deflections which were very close to experimental data. When differences did occur, the model almost always underestimated the correct deflections. This was not unexpected because underestimation is an inherent characteristic of the finite element method. Since the

model was usually very successful in simulating reinforced concrete beam deflections it was used confidently in the parametric study.

5.4 Parametric Study

The goal of the parametric study was to produce an accurate long term deflection design equation using the finite element program from Chapter 3, and the Factorial Design Method. A Fractional Factorial Design using Star Design capabilities was initiated to study the effect of the tension steel ratio, compression steel ratio, applied moment to ultimate moment ratio, span-to-depth ratio, and compressive strength, on the long term-to-short term deflection ratio. Two equations were ultimately developed. In the first equation the deflection ratio was derived from computer generated short term and long term deflections. In the second equation the deflection ratio represented long term deflections from the program, and short term deflections calculated using the Code equation. Of the two equations the one that appeared most successful was the one derived from computer generated short term and long term deflections. This equation proved to be very accurate in predicting the long term deflections generated with the finite element model, and was reasonably successful in predicting experimental long term deflections.

A number of observations were made during the work in the parametric study. One such observation was that designers probably do not have access to enough parameters for a highly accurate prediction equation. It seems that reasonable estimates may be the best that can

be hoped for. It also seems that the deflection ratio approach for predicting long term deflections may have some weaknesses. Delayed cracking and other influences may adversely affect predictions using the deflection ratio approach for both long term deflections and total deflections. In addition, the accuracy of deflection predictions using this approach is very dependent on predictions of short term deflections.

In light of these observations it may be advisable in future to investigate other approaches besides the deflection ratio concept for dealing with long term deflections. A few suggestions were discussed in Chapter 4. However unless some other approach proves to be superior, it appears that the prediction equation presented in Chapter 4, may provide an excellent replacement for current prediction equations.

5.5 Recommendations for Future Research

The objectives laid out at the beginning of this thesis led to an interesting study of many different aspects of long term deflections in reinforced concrete beams. It is hoped that the work presented here will be useful for future researchers. Throughout this thesis many areas which require future research attention have been identified. A general overview is provided here.

1) The acquisition of more experimental long term deflection data, particularly for continuous or restrained beams, is required. The data in this study indicated that there may be significant differences between the long term deflection behaviour of continuous beams and simple beams. This possibility should be investigated further.

2) More research into material properties and their modelling in a finite element model is necessary. The modelling of cracking, tension stiffening, bond, aggregate interlocking, failure criteria, and other properties, still needs work. In part, improvements in these subjects may depend on researchers learning more about their physical behaviour.

3) Designers and researchers must decide whether deflection prediction equations should be concentrated on long term deflections or total deflections. The best approach may be different depending on which is required.

4) An enquiry into alternative methods for treating long term deflections may be warranted. As an example it may now be preferable to use a simple computer program for deflections instead of prediction equations.

REFERENCES

1. ACI Committee 209, 'Designing for Effects of Creep, Shrinkage, and Temperature in Concrete Structures', Designing for Effects of Creep, Shrinkage, and Temperature in Concrete Structures, Publication SP-27, American Concrete Institute, Detroit, 1971, pp. 51-93.
2. ACI Committee 318, 'Building Code Requirements for Reinforced Concrete', ACI 318-77, American Concrete Institute, Detroit, 1977. (Also ACI 318-83).
3. Bazant, Z.P., Panula, L., 'Practical Prediction of Time-Dependent Deformations of Concrete', Materials and Structures, Parts I and II, No. 65, 1978, pp. 307-328, Part III, No. 66, 1978, pp. 414-424.
4. Bazant, Z.P., Panula, L., 'Creep and Shrinkage Characterization For Analyzing Prestressed Concrete Structures', PCI Journal, Vol. 25, No. 3, May-June 1980, pp. 86-122.
5. Bazant, Z.P., Cedolin, L., 'Blunt Crack Band Propagation in Finite Element Analysis', Journal of the Engineering Mechanics Division, ASCE, Vol. 105, No. EM2, Apr. 1979, pp. 297-315.
6. Beeby, A.W., 'Short Term Deformations of Reinforced Concrete Members', Cement and Concrete Association, Technical Report TRA 408, London, Mar. 1968.
7. Box, G.E.P., Hunter, W.G., 'Statistics for Experimenters: An Introduction to Design, Data, Analysis, and Model Building', Wiley, New York, 1978.
8. Branson, D.E., 'Deformation of Concrete Structures', McGraw-Hill, New York, 1977.
9. Branson, D.E., 'Compression Steel Effect on Long-Time Deflections', ACI Journal, Proceedings Vol. 68, No. 8, Aug. 1971, pp. 555-559.
10. Bresler, B., Scordelis, A.C., 'Shear Strength of Reinforced Concrete Beams', ACI Journal, Proceedings Vol. 60, No. 1, Jan. 1963, pp. 51-72.
11. Bryant, R.H., Bianchini, A.C., Rodriguez, J.J., Kesler, C.E., 'Shear Strength of Two-Span Continuous Reinforced Concrete Beams with Multiple Point Loading', ACI Journal, Proceedings Vol. 59, No. 44, Sept. 1962, pp. 1143-1176.

12. Canadian Standards Association, 'Code for the Design of Concrete Structures for Buildings', CSA Standard CAN3-A23.3-M77, CSA, Rexdale, Ontario, 1977. (also CAN3-A23.3-M84).
13. CEB-FIP Model Code for Concrete Structures, Comité Eurointernationale du Béton-Fédération Internationale de la Précontrainte, CEB Bulletin No. 124/125-E, Paris, 1978.
14. Cedolin, L., Dei Poli, S., 'Finite Element Studies of Shear-Critical R/C Beams', Journal of the Engineering Mechanics Division, ASCE Vol. 103, No. EM3, June 1977, pp. 395-410.
15. Chan, D.H.K., 'Creep and Fracture Simulation of Ice Using the Finite Element Method', M. Eng. Thesis, McMaster University, June 1981.
16. Cordon, W.A., Gillespie, H.A., 'Variables in Concrete Aggregates and Portland Cement Paste which Influence the Strength of Concrete', ACI Journal, Proceedings Vol. 60, No. 8, Aug. 1963, pp. 1029.
17. Corley, W.G., Sozen, M.A., 'Time Dependent Deflections of Reinforced Concrete Beams', ACI Journal, Proceedings Vol. 63, No. 3, Mar. 1966, pp. 373-386.
18. Dilger, W.H., 'Methods of Structural Creep Analysis', Creep and Shrinkage in Concrete Structures, John Wiley and Sons, 1982.
19. Edwards, A.D., Yannopoulos, P.J., 'Local Bond Stress to Slip Relationships for Hot Rolled Deformed Bars and Mild Steel Plain Bars', ACI Journal, Proceedings, Vol. 76, No. 3, Mar. 1979, pp. 405-420.
20. Gesund, H., 'Shrinkage and Creep Influence on Deflections and Moments of Reinforced Concrete Beams', ACI Journal, Proceedings Vol. 59, No. 5, May 1962, pp. 687-703.
21. Ghali, A., Dilger, W., Neville, A.M., 'Time-Dependent Forces Induced by Settlement of Supports in Continuous Reinforced Concrete Beams', ACI Journal, Proceedings Vol. 66, No. 11, Nov. 1969, pp. 907-915.
22. Goodman, R.E., Taylor, R.L., Brekke, T.L., 'A Model for the Mechanics of Jointed Rocks', Journal of the Soil Mechanics and Foundations Division, ASCE, Vol. 94, No. SM3, May 1968, pp. 637-659.
23. Hajnal-Kónyi, K., 'Tests on Beams with Sustained Loading', Magazine of Concrete Research (London), Vol. 15, No. 43, Mar. 1963, pp. 3-14.
24. Hand, F.R., Pecknold, D.A., Schnobrich, W.C., 'Nonlinear Layered Analysis of RC Plates and Shells', Journal of the Structural Division, ASCE, Vol. 99, No. ST7, July 1973, pp. 1491-1505.

25. Hanson, J.A., 'Effects of Curing and Drying Environments on Splitting Tensile Strength of Concrete', ACI Journal, Proceedings Vol. 65, No. 7, July 1968, pp. 535-543.
26. Hobbs, D.W., 'Shrinkage and Load Induced Curvature of Reinforced Concrete Beams', 'Fundamental Research on Creep and Shrinkage of Concrete', Martinus Nijhoff Publishers, The Hague, 1982, pp. 439-449.
27. Houde, J., 'Study of Force-Displacement Relationships for the Finite Element Analysis of Reinforced Concrete', Ph.D. Thesis, McGill University, Dec. 1973.
28. Jordaan, I.J., Illston, J.M., 'Time Dependent Strains in Sealed Concrete Under Systems of Variable Multiaxial Stress', Magazine of Concrete Research, Vol. 23, No. 75-76, June-Sept. 1971, pp. 79-87.
29. Kanchi, M.B., Zienkiewicz, O.C., Owen, D.R.J., 'The Visco-Plastic Approach to Problems of Plasticity and Creep Involving Geometric Non-Linear Effects', International Journal for Numerical Methods in Engineering, Vol. 12, No. 1, 1978, pp. 169-181.
30. Leonhardt, F., Walther, R., 'Contribution to the Treatment of Shear in Reinforced Concrete', Technical Translation 1172, National Research Council of Canada, Translated by J.P. Ver Schuren, J.G. MacGregor, Ottawa, 1965.
31. Lutz, L.A., Gergley, P., 'Mechanics of Bond and Slip of Deformed Bars in Concrete', ACI Journal, Proceedings Vol. 64, No. 11, Nov. 1967, pp. 711-721.
32. Lutz, L.A., Sharma, N.K., Gergley, P., 'Increase in Crack Width in Reinforced Concrete Beams Under Sustained Loading', ACI Journal, Proceedings Vol. 64, No. 45, Sept. 1967, pp. 538-546.
33. Meyers, B.L., Branson, D.E., Schumann, C.G., Christiason, M.L., 'The Prediction of Creep and Shrinkage Properties of Concrete', Final Report of Project HR-136, Iowa Highway Commission, Report 70-5, Aug. 1970.
34. Miller, A.L., 'Warping of Reinforced Concrete Due to Shrinkage', ACI Journal, Proceedings Vol. 54, No. 11, May 1958, pp. 939-950.
35. Mirza, S.M., Houde, J., 'Study of Bond Stress-Slip Relationships in Reinforced Concrete', ACI Journal, Proceedings Vol. 76, No. 1, Jan. 1979, pp. 19-46.
36. Mirza, F.A., 'Course Notes for CE 713', McMaster University, 1982.
37. Neville, A.M. Dilger, W., 'Creep of Concrete: Plain, Reinforced and Prestressed', North Holland Publishing Company, Amsterdam, 1970.

38. Neville, A.M., 'Properties of Concrete', Pitman Publishing, Bath, 1972.
39. Ngo, Scordelis, A.C., 'Finite Element Analysis of Reinforced Concrete Beams', ACI Journal, Proceedings Vol. 64, No. 3, Mar. 1967, pp. 152-163.
40. Nilson, A.H., 'Non-Linear Analysis of Reinforced Concrete by the Finite Element Method', ACI Journal, Proceedings Vol. 65, No. 9, Sept. 1968, pp. 757-766.
41. Nilson, A.H., 'Internal Measurements of Bond-Slip', ACI Journal, Proceedings Vol. 69, No. 7, July 1972, pp. 439-441.
42. Perry, E.S., Thompson, J.N., 'Bond Stress Distribution on Reinforcing Steel in Beams and Pullout Specimens', ACI Journal, Proceedings Vol. 63, No. 8, Aug. 1966, pp. 865-874.
43. Phillips, D.V., Zienkiewicz, O.C., 'Finite Element Nonlinear Analysis of Concrete Structures', Proc. Instn. Civ. Engrs., Vol. 61, Mar. 1976, pp. 59-88.
44. Rodriguez, J.J., Bianchini, A.C., Viest, I.M., Kesler, C.E., 'Shear Strength of Two-Span Continuous Reinforced Concrete Beams', ACI Journal, Proceedings Vol. 55, No. 66, Apr. 1959, pp. 1089-1130.
45. Ross, A.D., 'Creep of Concrete Under Variable Stress', ACI Journal, Proceedings Vol. 54, No. 9, Mar. 1958, pp. 739-757.
46. Rüsçh, H., Jungwirth, D., Hilsdorf, U.K., 'Creep and Shrinkage', Springer-Verlag Inc., New York, 1983.
47. Sallam, S.E.A., 'Behaviour of Reinforced Concrete Joints', Ph.D. Thesis, McMaster University, Apr. 1978.
48. Scanlon, A., Murray, D.W., 'An Analysis to Determine the Effects of Cracking in Reinforced Concrete Slabs', Finite Element Method in Civil Engineering, Engineering Institute of Canada, Montreal, 1972.
49. Spokowski, R.W., 'Finite Element Analysis of Reinforced Concrete Members', M. Eng. Thesis, McGill University, May 1972.
50. Stevens, R.F., 'Deflexions of Reinforced Concrete Beams', Proc. Instn. Civ. Engrs., Part 2: Research and Theory, Vol. 53, Sept. 1972, pp. 207-224.
51. Swamy, R.N., Al-Ta'an, S.A., 'Deformation and Ultimate Strength in Flexure of Reinforced Concrete Beams Made with Steel Fiber Concrete', ACI Journal, Proceedings Vol. 78, No. 5, Sept.-Oct. 1981, pp. 395-405.
52. Venkateswarlu, B., Gesund, H., 'Cracking and Bond Slip in Concrete Beams', Journal of Structural Division, ASCE, Vol. 98, No. ST11, Dec. 1972, pp. 2663-2685.

53. Washa, G.W., Fluck, P.G., 'Effect of Compressive Reinforcement on the Plastic Flow of Reinforced Concrete Beams', ACI Journal, Proceedings Vol. 49, No. 2, Oct. 1952, pp. 89-108.
54. Washa, G.W., Fluck, P.G., 'Plastic Flow (Creep) of Reinforced Concrete Continuous Beams', ACI Journal, Proceedings Vol. 52, No. 5, Jan. 1956, pp. 549-562.
55. Will, F.T., Uzumeri, S.M., Sinha, S.K., 'Application of the Finite Element Method to the Analysis of Reinforced Concrete Beam-Column Joints', Finite Element Method in Civil Engineering, Engineering Institute of Canada, Montreal, 1972.
56. Yu, Wei-Wen, Winter, G., 'Instantaneous and Long-Time Deflections of Reinforced Concrete Beams Under Working Load', ACI Journal, Proceedings Vol. 57, No. 1, July 1960, pp. 29-50.
57. Zienkiewicz, O.C., 'Finite Element Method', McGraw-Hill, London, 1977.
58. 'Building Code Requirements for Reinforced Concrete', ACI 318-83, American Concrete Institute, Detroit, 1983.

APPENDIX A

COMPUTER PROGRAM LISTING

The finite element computer program listing for the program used in this thesis is presented here. This program is an extended version of an existing program developed by F.A. Mirza at McMaster University. The program listed here is most efficient for continuous beams, where bond slip may be present in both top and bottom steel. For simple beams where the top steel is entirely in compression, it is most efficient to consider the top steel as being fixed to the concrete which enables the use of common nodes. This reduces the number of degrees of freedom.

The input variables needed for running the finite element program are listed below.

Input Variables

NPROB	Problem number
IGR	= 0 For no self weight = 1 For self weight inclusion
ILIN	= 1
IT	= Maximum Number of Newton-Raphson iterations allowed

JGR = 0 For manual element data input
 = 1 For automatic element data generation

ILO Number of load increments (sets the size of the load
 increments)

ITYPE = 0 For simply supported at ends
 = 1 For continuous beams

THICK Thickness of beam

GR Self weight of beam

CHECK Tolerance for Newton-Raphson iterations (percentage)

KV = 0 For elastic solution
 = 1 For creep solution

IDM Printout required after IDM creep increments

TIF Multiplier on each successive creep increment

TL Total time of loading

NEL Number of concrete elements

NNOD Total number of nodes

NVAR Number of variables per node (=2)

NNODEL Number of nodes per concrete element (=3)

NBSE Number of bottom steel elements

NTSE Number of top steel elements

NNSP Number of nodes per Goodman Joint Element (=4)

NNSEL Number of nodes per steel element (=2)

NBAR Number of reinforcement bars in tension zone

BDIA	Diameter of bottom reinforcing bars
TDIA	Diameter of top reinforcing bars
ABOT	Cross-sectional area of bottom steel
ATOP	Cross-sectional area of top steel
X	X-Coordinate of nodes
Y	Y-Coordinate of nodes
XW	Height of beam
D	Depth of reinforcement
ICO	Element node numbers
E	Modulus of elasticity for concrete
ANU	Poisson's ratio for concrete
ES	Modulus of elasticity for steel
FT	Tensile strength of concrete
FC	Compressive strength of concrete
NCON	Number of boundary constraints
ICON	Identification of constrained degrees of freedom
CON	Constrained boundary conditions

```

* PROGRAM TST IS A FINITE ELEMENT PROGRAM FOR THE
** ANALYSIS OF REINFORCED CONCRETE. THIS PROGRAM
** USES PLANE STRESS TRIANGULAR ELEMENTS FOR CONCRETE,
** AXIAL BAR ELEMENTS FOR REINFORCEMENT, AND GOODMAN
** JOINT ELEMENTS FOR BOND. PROGRAM TST IS CAPABLE OF
** HANDLING PROGRESSIVE CRACKING, BOND SLIP, SHRINKAGE
** AND CREEP.
PROGRAM TST(INPUT, OUTPUT, TAPE5=INPUT, TAPE6=OUTPUT, TAPE1, TAPE2,
*TAPE3, TAPE4, TAPE7)
  DIMENSION LJ(8), X(3), Y(3), S(8,8), FL(8), AT(3), BT(3), U(8), V(8),
  1A(1700), B(1100), BB(1100), CC(1100), DD(1100), XX(1100), YY(1100),
  2IX(1100), JX(1100), CON(50), ICON(50), Z(3,6), BL(3,6), CS(3), DU(1100),
  3ICD(6), AREA(800), SIG(800,3), EPS(800,3), STR(800,3), AIN(800,3)
  4, ICR(800), ANG(800), XLEN(200), IBF(2,200)
  WRITE(6,40)
* INPUT OF PROGRAM VARIABLES
3 READ(5,41) NPROB, IGR, ILIN, IT, JGR, ILO, ITYP, THICK, GR, CHECK
  IF(EOF(5).EQ.1.0) GO TO 999
  READ(5,901) KV, NPT, IDM, TIF, TL
  IF(NPT.EQ.0) NPT=1
  IF(ILIN.EQ.0.AND.KV.EQ.0) WRITE(6,1500)
  IF(ILIN.EQ.0.AND.KV.GT.0) WRITE(6,1501)
  IF(ILIN.GT.0.AND.KV.EQ.0) WRITE(6,1502)
  IF(ILIN.GT.0.AND.KV.GT.0) WRITE(6,1503)
  IF(IPS.EQ.0) WRITE(6,1504)
  WRITE(6,1506)
  WRITE(6,135) ILIN, IT, IGR, IPS, ILO, THICK, GR, CHECK
  READ(5,47) NEL, NNOD, NVAR, NNODEL, NBSE, NTSE, NNSP, NNSSEL, NBAR
  READ(5,48) BDIA, TDIA, ABOT, ATOP
  NVEL=NVAR*NNODEL
  NVELS=NVAR*NNSSEL
  NVSEL=NVAR*NNSP
  NSP4=NBSE*4
  INEL=NEL+NBSE
  JNEL=INEL+NTSE
  KNEL=JNEL+NBSE
  LNEL=KNEL+ITYP*NTSE
  REWIND 1
  REWIND 2
  REWIND 4
* SUBROUTINE LAYOUT SETS THE GEOMETRY OF THE
* PROBLEM AND NUMBERS THE DEGREES OF FREEDOM
CALL LAYOUT(XX, YY, ICD, IX, JX, AREA, NEL, NNOD, NVAR, NMAT, NNET, NNODEL,
* NNSSEL, XLEN, NNSP, INEL, JNEL, KNEL, LNEL, JGR, COVER)
  REWIND 4
* SUBROUTINE BANDWH CALCULATES THE HALF BANDWIDTH
CALL BANDWH(ICD, JX, LJ, NEL, NVAR, LBAND, NNODEL)
  LBAND=LBAND+2
  NB3=LBAND+1
  NVA=NB3*NNET
  WRITE(6,42) NPROB, NNET, LBAND, NVA
* INITIALIZATION OF ARRAYS AND VARIABLES
CALL PRESET(BL, 3, 6)
CALL PRESET(Z, 3, 6)
CALL PRESET(SIG, 800, 4)
CALL PRESET(EPS, 800, 3)
CALL PRESET(STR, 800, 3)
CALL PRESET(AIN, 800, 3)
CALL PRESET(IBF, 2, 200)
CALL PSET(CS, 3)

```

```

CALL PSET(A, NVA)
CALL PSET(BB, NNET)
CALL PSET(DU, NNET)
CALL PSET(CC, NNET)
CALL PSET(DD, NNET)
CALL PSET(ICR, JNEL)
CALL PSET(ANG, JNEL)
IC=0
JJJ=0
IF(ILIN.EQ.0) JJJ=1
DDET=1. DO
CR1=0. DO
C1=0. DO
C2=0. DO
C3=0. DO
AL=0. DO
BE=0. DO
GA=0. DO
DE=0. DO
IIII=0
IM=1
KR=0
DELT=1. DO
TIME=0.1 DO
COR=0. DO
YYY=0. DO
SSS=0. DO
EQSIG=0. DO
* INPUT OF MATERIAL PROPERTIES
READ(5,43) E, ANU, ES, FT, FC
READ(5,47) NCON
WRITE(6,92) E, ANU, NCON
CF=SQRT(FC/5000.)*(0.04*2*COVER*THICK)**.3333
IF(KV.EQ.0) GO TO 381
* SUBROUTINE CONST CALCULATES THE CONSTANTS FOR
* USE WITH BAZANT AND PANULA'S CREEP AND SHRINKAGE
* PREDICTION METHOD
CALL CONST(BCOEF, DCOEF, POWER, AN, TSH, TCREEP, E, SHCOEF, TDRY,
*FC1, DENS)
* CALCULATION OF ELASTICITY MATRIX FOR CONCRETE
381 E1=E/(1.DO-(ANU**2))
EA=E1
E2=ANU
E3=(1.DO-ANU)/2. DO
CR1=E
382 IF(NCON.EQ.0) GO TO 350
READ(5,45) (ICDN(I), I=1, NCON)
WRITE(6,46) (ICDN(I), I=1, NCON)
READ(5,93) (CON(I), I=1, NCON)
WRITE(6,94)
WRITE(6,95) (CON(I), I=1, NCON)
350 IF(IC.EQ.0) GO TO 600
IF(IC.GT.1) GO TO 603
DELT=.05
ILO=1. DO
GO TO 603
600 JC=-1
IF(ILIN.EQ.0) JC=0
GO TO 661
* TIME INCREMENTING

```

```

603 TIME=TIME+DELT
    IF (TIME.LE.TL) GO TO 660
DELT=TL-TIME+DELT
TIME=TL
660 WRITE(6,1350) IC
    DT=TIME-DELT
    DELT1=DELT
    LOAD INCREMENTING
661 TTT=1. DO
    XXX=1. DO
    IF (ILO.GT.O) XXX=TTT/ILO
    IF (IC.EQ.O) GO TO 87
    FUNCTION ESHR CALCULATES THE SHRINKAGE STRAIN INCREMENTS
    DESH=ESHR(TIME,TCREEP,TDRY,DELT,SHCOEF,TSH)
    CALL PSET(B,NNET)
    RTIM=TIME+TCREEP
    FT=.5*FCI*(RT/(4+.85*RT))+RTIM/(4+.85*RTIM))
87 REWIND 1
    REWIND 2
    REWIND 3
    REWIND 4
    REWIND 7
    IF (IC.EQ.O OR KR.EQ.1) CALL PSET(B,NNET)
    CALL PSET(FL,B)
    CALL PRESET(S,B,B)
    LOOP FOR THE CALCULATION OF THE STIFFNESS MATRICES
    AND LOAD VECTORS OF THE TRIANGULAR CONCRETE
    ELEMENTS
    DO 91 IEL=1,NEL
    AR=AREA(IEL)
    IF (ILIN.GT.O AND JC.GT.O AND KR.NE.1) GO TO 721
    IF (ILIN.GT.O AND JC.GT.-1 AND KR.NE.1) GO TO 721
    ARR=2. DO*AR
    READ(4) (ICD(J),J=1,5)
    LOOP FOR THE TRANSFORMATION OF ELEMENT AXES FOR
    CRACKED CONCRETE ELEMENTS
    DO 70 I=1,NMODEL
    ICD0=ICD(I)
    COT=COS(ANG(IEL))
    SIT=SIN(ANG(TEL))
    X(I)=XX(ICD0)*COT+YY(ICD0)*SIT
    Y(I)=YY(ICD0)*COT-XX(ICD0)*SIT
70 CONTINUE
    IS=ICD(NMODEL+1)
    IB=ICD(NMODEL+2)
    CALCULATION OF AREA COORDINATES
    AT(1)=(X(3)-X(2))/ARR
    AT(3)=(X(1)-X(3))/ARR
    AT(2)=(X(2)-X(1))/ARR
    BT(1)=(Y(2)-Y(3))/ARR
    BT(3)=(Y(3)-Y(1))/ARR
    BT(2)=(Y(1)-Y(2))/ARR
    IF (JC.GT.O) GO TO 360
    IF (JC.JJ) 501,360,360
    SUBROUTINE BONDARY PLACES THE EXTERNAL LOADS IN THE
    ELEMENT LOAD VECTOR
    CALL BONDARY (X,Y,FL,AR,GR,THICK,IB,IGR,IS,NVEL)
**
**
501 CALL LJMAT(LJ,NMODEL,NVAR,ICD,JX,IEL)

```

```

WRITE(3) (LJ(I), I=1, 6)
360 WRITE(2) (AT(I), I=1, 3), (BT(I), I=1, 3)
   IF(ILIN.EQ.0) GO TO 725
   GO TO 722
721 READ(2) (AT(I), I=1, 3), (BT(I), I=1, 3)
   IF(ILIN.EQ.0) READ(2) ((BL(I, J), J=1, 6), I=1, 3)
722 IF((JC-JJJ).GE.0) READ(3) (LJ(I), I=1, 6)
   IF(ILIN.EQ.0) GO TO 602
* SUBROUTINE UMAT DEFINES THE NODAL DISPLACEMENTS
* FOR THE ELEMENT
   CALL UMAT(CC, LJ, U, NVEL)
   IF(ICR(IEL).EQ.0) GO TO 725
* LOOP TRANSFORMS ELEMENT DISPLACEMENTS FROM GLOBAL
* SYSTEM TO LOCAL SYSTEM
   DO 371 I=1, NVEL, 2
   U1=U(I)*COT+U(I+1)*SIT
   U2=U(I+1)*COT-U(I)*SIT
   U(I)=U1
371 U(I+1)=U2
* SUBROUTINE BLMAT SETS THE KINEMATIC LARGE DISPLACEMENT
* MATRIX
725 CALL BLMAT(BL, AT, BT, U, AL, BE, GA, DE, ILIN, JC)
   IF(ILIN.EQ.0.AND.IC.EQ.0) WRITE(2) ((BL(I, J), J=1, 6), I=1, 3)
   IF(ILIN.EQ.0.AND.KR.EQ.1.AND.IC.GT.0) WRITE(2) ((BL(I, J), J=1, 6)
*, I=1, 3)
602 IF(IC.EQ.0) GO TO 821
   CALL CREEP(SIG, CS, ANU, E, EA, E1, E2, E3, EGSIG, CSR, DELT, IEL, MM, BCOEF,
*DCOEF, POWER, AN, TSH, DT, NEL, ICR, ANG, CR1)
821 IF(JC.LT.JJJ.AND.IC.EQ.0) GO TO 822
   IF(ILIN.EQ.0.AND.IC.EQ.0) GO TO 822
   CALL DLOAD(BL, FL, CS, SIG, AR, THICK, E1, E2, E3, NEL, IEL, IC, ILIN,
*Z, DESH, ICR, ANG, CR1)
822 IF(JC.GT.-1.AND.ILIN.GT.0) IS=1
   IF(IC.GT.0.AND.ILIN.EQ.0) IS=1
   IF(ICR(IEL).EQ.0) GO TO 823
* SUBROUTINE NONLIN AND NONLIN CALCULATE THE ELEMENT
* AND UNCRACKED ELEMENTS RESPECTIVELY
   CALL NONLINC(S, SIG, AT, CR1, AR, THICK, IS, IEL, ILIN, BL, ANG, NEL)
   GO TO 713
* SUBROUTINE NONLIN CALCULATES THE ELEMENT STIFFNESS
* MATRIX FOR UNCRACKED CONCRETE ELEMENTS
823 CALL NONLIN(S, SIG, AT, BT, E1, E2, E3, AR, THICK, AL, BE, GA, DE, IS, NEL,
*IEL, ILIN)
* SUBROUTINE SETUP PLACES THE ELEMENT STIFFNESS MATRIX
* AND LOAD VECTOR INTO THE GLOBAL STIFFNESS MATRIX
* AND LOAD VECTOR
713 CALL SETUP(A, B, S, FL, NVEL, LJ, NVAR, LBAND)
   WRITE(1) (CS(I), I=1, 3), CSR, E1, E2, E3, EGSIG, CR1
   IF(ILIN.GT.0) WRITE(1) ((BL(I, J), J=1, 6), I=1, 3)
91 CONTINUE
   CALL PSET(FL, 8)
   KKK=NEL+1
* LOOP FOR THE CALCULATION OF THE STIFFNESS MATRICES
* AND LOAD VECTORS OF THE STEEL ELEMENTS AND THEIR
* INSERTION INTO THE GLOBAL MATRICES
   DO 191 IEL=KKK, JNEL
   ARST=ABOT
   IF(IEL.GT.INEL) ARST=ATOP
   IF(ILIN.EQ.0.AND.JC.GT.0) GO TO 181
   IF(ILIN.GT.0.AND.JC.GT.-1) GO TO 181

```

```

READ(4) (ICD(J), J=1, 4)
CALL LJMAT(LJ, NNSSEL, NVAR, ICD, JX, IEL)
WRITE(3) (LJ(I), I=1, 4)
ST=ES*ARST/XLEN(IEL-NEL)
*
* SUBROUTINE STIFF PLACES THE BAR ELEMENT STIFFNESS
* INTO THE STIFFNESS MATRIX FOR STEEL ELEMENTS
CALL STIFF(S, ST, 0, 0)
DO 180 I=1, 8
180 WRITE(7) (S(I, J), J=1, 8)
GO TO 182
181 READ(3) (LJ(I), I=1, 4)
DO 184 I=1, 8
184 READ(7) (S(I, J), J=1, 8)
182 IF(JC.LT.JJJ.AND.IC.EQ.0) GO TO 183
IF(ILIN.EQ.0) GO TO 183
FL(1)=-ARST*SIG(IEL, 1)
FL(3)=-FL(1)
183 CALL SETUP(A, B, S, FL, NVELS, LJ, NVAR, LBAND)
191 CONTINUE
KKK=JNEL+1
*
* LDOOP FOR THE CALCULATION OF THE STIFFNESS MATRICES
* AND LOAD VECTORS OF THE 4 NODE GOODMAN JOINT
* ELEMENT
DO 291 IEL=KKK, LNEL
CALL PSET(FL, 8)
IF(ILIN.EQ.0.AND.JC.GT.0) GO TO 281
IF(ILIN.GT.0.AND.JC.GT.-1) GO TO 281
READ(4) (ICD(J), J=1, 6)
CALL LJMAT(LJ, NNSP, NVAR, ICD, JX, IEL)
WRITE(3) (LJ(I), I=1, 8)
GO TO 282
281 READ(3) (LJ(J), J=1, 8)
282 CALL UMAT(CC, LJ, U, NVSEL)
MEL=IEL-NBSE-NTSE
IF(SIG(MEL, 1).GE.0) GO TO 285
CALL PRESET(S, 8, 8)
DO 201 I=1, 7, 2
S(I, I)=1E10
201 CONTINUE
S(1, 3)=-5E9
S(1, 5)=-5E9
S(1, 7)=-1E10
S(3, 5)=-1E10
S(3, 7)=-5E9
S(5, 7)=5E9
DO 202 I=1, 7, 2
DO 202 J=I, 7, 2
S(J, I)=S(I, J)
202 CONTINUE
GO TO 284
285 KEL=IEL-JNEL
IF(IEL.GT.KNEL) KEL=IEL-KNEL
SDIA=BDIA
IF(IEL.GT.JNEL) SDIA=TDIA
*
* SUBROUTINE BONDEL CALCULATES THE STIFFNESS MATRIX
* AND LOAD VECTOR FOR THE GOODMAN JOINT ELEMENT
CALL BONDEL(S, U, XLEN, SDIA, NBAR, KEL, FL, ILIN, JC, IBF, CF)
284 CALL SETUP(A, B, S, FL, NVSEL, LJ, NVAR, LBAND)
291 CONTINUE
IF(ILIN.EQ.0.AND.IC.GT.0) GO TO 132

```

```

* *      IF (ILIN.EG.O.AND.JC.GT.O) GO TO 102
* *      IF (ILIN.GT.O.AND.JC.GT.-1) GO TO 102
* *      SEPARATION OF THE INCREMENTAL LOAD VECTOR FROM THE
* *      TOTAL LOAD VECTOR
* *      DD 352 I=1, NNET
* *      BB(I)=BB(I)
* *      B(I)=XXX*BB(I)
* *      WRITE(3) (BB(I), I=1, NNET)
* *      GO TO 131
* *      READ(3) (BB(I), I=1, NNET)
* *      DD 353 I=1, NNET
* *      B(I)=(XXX-YYY)*BB(I)-B(I)
* *      DD(I)=B(I)
* *      GO TO 132
* *      WRITE(6, 10)
* *      IF (NCON.EG.O) GO TO 351
* *      SUBROUTINE PLACEZ TAKES CARE OF THE CONSTRAINED
* *      BOUNDARY CONDITIONS
* *      CALL PLACEZ(B,A,CON,ICON,NCON,NNET,LBAND)
* *      DET=1.E-8
* *      SUBROUTINE BAND SOLVES THE SIMULTANEOUS LINEAR
* *      EQUATIONS AND CALCULATES THE NODAL DISPLACEMENTS
* *      CALL BAND(A,B,NNET,NB3,1,DET)
* *      IF (DET.LE.(O.DO)) GO TO 85
* *      CALL PSET(A,NVA)
* *      DD 106 I=1, NNET
* *      CC(I)=CC(I)+B(I)
* *      CHECK ON CONVERGENCE OF ITERATION
* *      IF (ILIN.EG.O.AND.IC.EG.O) DDET=DET
* *      RATIO=100.DO*ABS(DDET-DET)/DDET
* *      IF (JC.LE.-1.AND.IC.EG.O) RATIO=100.DO
* *      WRITE(6, 101) JC, RATIO
* *      WRITE(6, 50) DET
* *      DECISION ON DESIRABILITY OF OUTPUT
* *      IPR=0
* *      IF (ILIN.EG.ILD.AND.IC.EG.O) IPR=1
* *      IF (ILIN.EG.O.AND.KV.EG.O) IPR=1
* *      IF (ILIN.GT.O.AND.RATIO.GT.CHECK) IPR=0
* *      IF (ILIN.EG.O.AND.RATIO.LT.CHECK.AND.IC.EG.O) IPR=1
* *      IF (IC.GT.IDM) IPR=1
* *      CONTINUE
* *      IF (RATIO.LT.CHECK.AND.IC.EG.O) IM=IM+1
* *      IF (MOD(IM,2).NE.O.AND.IC.EG.O) IPR=C
* *      IF (MOD(IC,2).EG.O.AND.IC.GT.O) IPR=0
* *      IF (XXX.LT.75.AND.RATIO.LT.CHECK.AND.IC.EG.O) IPR=1
* *      IF (IC.EG.O) IPR=0
* *      IF (XXX.GT.9999.AND.XXX.LT.1.0001.AND.IC.EG.O) IPR=1
* *      IF (IC.GT.20) IPR=1
* *      IF (IPR.EG.O) GO TO 604
* *      IF (ILIN.EG.O.AND.IC.LT.O) WRITE(6, 710)
* *      IF (ILIN.GT.O.AND.JC.LT.O) WRITE(6, 710)
* *      REWIND 1
* *      REWIND 3
* *      SUBROUTINE CEP SIG CALCULATES AND PRINTS THE STRESSES
* *      AND STRAINS DUE TO ELASTIC AND TIME DEPENDENT
* *      EFFECTS FOR ALL ELEMENTS. CONCRETE ELEMENTS ARE
* *      CHECKED FOR FAILURE
* *      CALL CEP SIG(BL,CS,SIG,EPS,B,V,Z,EGSIG,ANU,E,E1,E2,E3,CSR,

```

```

*NEL, LJ, AT, BT, ILIN, IC, IPR, DELT, DESH, COR, NVEL, ICR, ANG, CR1, KR, RATIO
*, CHECK, STR, AIN, JNEL, XLEN, ES, FT, CC, IBF, KNEL, LNEL)
IF(RATIO.GT.CHECK.AND.IC.EQ.0) GO TO 724
DO 20 IEL=1, JNEL
  JJ=3
  IF(IEL.GT.NEL) JJ=1
  IF(ICR(IEL).NE.1) GO TO 372
*
* TRANSLATION OF CRACKED ELEMENT COORDINATE AXES
  TO LOCAL AXES
  CD=COS(2*ANG(IEL))
  SI=SIN(2*ANG(IEL))
  SIG(IEL,1)=0.DO
  SIG(IEL,2)=.5DO*(SIG(IEL,1)+SIG(IEL,2))-SIG(IEL,3)*SI
  $-.5DO*(SIG(IEL,1)-SIG(IEL,2))*CO
  SIG(IEL,3)=0.DO
  EXP=.5DO*(EPS(IEL,1)+EPS(IEL,2))+.5DO*(EPS(IEL,1)-EPS(IEL,2))
  $*CO+.5DO*EPS(IEL,3)*SI
  EYP=.5DO*(EPS(IEL,1)+EPS(IEL,2))- .5DO*(EPS(IEL,1)-EPS(IEL,2))
  $*CD-.5DO*EPS(IEL,3)*SI
  EXYP=-(EPS(IEL,1)-EPS(IEL,2))*SI+EPS(IEL,3)*CO
  EPS(IEL,1)=EXP
  EPS(IEL,2)=EYP
  EPS(IEL,3)=EXYP
*
* ALL ELEMENT STRESSES AND STRAINS AT THE BEGINNING
  OF A LOAD OR TIME INCREMENT ARE STORED
372 DO 20 I=1, JJ
  STR(IEL,I)=SIG(IEL,I)
  AIN(IEL,I)=EPS(IEL,I)
  20 CONTINUE
  21 IF(KR.NE.1) GO TO 719
  DO 718 I=1, NNET
  CC(I)=DU(I)
718 CONTINUE
*
* IF(CRACKING OCCURS DURING A TIME INCREMENT THE TIME
  INCREMENT IS ADJUSTED
  TIME=TIME-COR*DELT
  DELT=DELT*(1.DO-COR)
  GO TO 719
918 TTT=TTT-COR*(TTT-SSS)
  XXX=TTT/ILO
719 IF(IC.GT.0) WRITE(6,1351) DELT, TIME
  IF(IC.EQ.0) WRITE(6,375) XXX
  DO 723 I=1, NNET
723 DU(I)=CC(I)
724 IF(IPR.EQ.0) GO TO 717
*
* SUBROUTINE EXPAND PRINTS THE NODAL DISPLACEMENTS
  CALL EXPAND(DD, NMAT, CC, JX, NNOD, NVAR)
717 CALL PSET(B, NNET)
  IF(KR.EQ.2) KR=0
  IF(XXX.GT.2.) GO TO 85
  IF(IC.GT.0) GO TO 606
  IF(RATIO.GT.CHECK) GO TO 88
  GO TO 86
88 IF(JC.GT.IT) WRITE(6,111) JC, IT
  IF(JC.GT.IT) GO TO 85
  DDET=DET
  JC=JC+1
  GO TO 87
86 JC=1

```

```

IF(KR.EQ.1) GO TO 87
IF(ABS(TTT-ILO).LT.1E-6) GO TO 606
SSS=TTT
TTT=TTT+1.D0
IF(TTT.GT.FLOAT(ILO)) TTT=ILO
IF(ILIN.EQ.0) YYY=XXX
IF(ILO.GT.0) XXX=TTT/ILO
GO TO 87
606 IF(KV.EQ.0) GO TO 85
IF(KR.EQ.1) GO TO 87
IC=IC+1
IF(IC.EQ.1) GO TO 350
DELT=TIF*DELT1
IF(ABS(TIME-TL).LT.1E-6) GO TO 85
GO TO 603
85 WRITE(6,112)
GO TO 3
999 STOP
*
OUTPUT FORMATS
40 FORMAT('1',10X,' ***** 2-DIMENSIONAL FINITE ELEMENT ANA
1 LYSIS ***** ',//)
41 FORMAT(7I5,3F10.0)
42 FORMAT(/,5X,'PROB. NO.',I5,3X,'TOTAL UNKNOWN',I5,3X,'BANDWIDTH',I
15,3X,'MATRIX SIZE',I8)
43 FORMAT(5F10.0)
44 FORMAT(25I3)
45 FORMAT(/,5X,'CONSTRAINTS ON',20I5)
46 FORMAT(/,5X,'DETERMINANT IS',E20.8)
47 FORMAT(11I5)
48 FORMAT(4F10.0)
49 FORMAT(/,5X,'MODULUS OF ELASTICITY =',F12.1,5X,'POISSONS RATIO =
1 /,F6.4,/,5X,'NUMBER OF CONSTRAINTS NCON =',I6)
93 FORMAT(8F10.0)
94 FORMAT(/,5X,'BOUNDARY CONSTRAINED VALUES ARE',/)
95 FORMAT(5X,8E15.7)
101 FORMAT(/,5X,'SOLUTION AFTER THE NO. OF ITERATIONS =',I5,5X,'AND
1 RATIO =',F10.5,//)
110 FORMAT(/,5X,'GLOBAL LOAD VECTOR IS',/)
111 FORMAT(/,5X,'TOTAL ITERATIONS=',I5,3X,'IS EQUAL TO THE TOTAL ALL
1 OWNED NO. OF ITERATIONS =',I5,//)
112 FORMAT(/,10X,'***** EN
1 D *****')
135 FORMAT(/,5X,'ILIN =',I2,5X,'IT =',I3,5X,'IGR =',I2,5X,'IPS =',
1 I2,/,5X,'ILD =',I3,5X,'THICK =',F7.3,5X,'GR = DENSITY OF MATERI
2 AL =',F10.4,5X,'CHECK =',F7.3,//)
375 FORMAT(/,5X,'SOLUTION FOR',F8.4,3X,'OF TOTAL LOAD',//)
710 FORMAT(/,5X,'**** LINEAR ELASTICITY SOLUTION ****',//)
716 FORMAT(/,5X,'**** RESIDUAL LOAD VECTOR IS ****',//)
901 FORMAT(3I5,2F10.0)
1350 FORMAT(/,5X,'**** SOLUTION AFTER CREEP INCREMENT',I5,' ****',//)
1351 FORMAT(/,5X,'TIME INCREMENT =',F9.3,5X,'TOTAL TIME ELAPSED=',F9.3)
1500 FORMAT(10X,'***** LINEAR ELASTIC *****',//)
1501 FORMAT(10X,'***** SMALL DEFLECTION CREEP *****
1 **',//)
1502 FORMAT(10X,'***** LARGE DEFLECTION ELASTIC *****
1 ****',//)
1503 FORMAT(10X,'***** LARGE DEFLECTION CREEP *****
1 *',//)
1504 FORMAT(10X,'***** PLANE STRESS ANALYSIS *****
1 *',//)

```

```

1506 FORMAT(///,15X,'***** GOOD LUCK *****')
1****',////)
END
* SUBROUTINE PRESET INITIALIZES A 2 DIMENSIONAL
* ARRAY
SUBROUTINE PRESET(A,M,N)
DIMENSION A(M,1)
DO 1 I=1,M
DO 2 J=1,N
2 A(I,J)=0.DO
1 CONTINUE
RETURN
END
* SUBROUTINE PSET INITIALIZES A 1 DIMENSIONAL ARRAY
SUBROUTINE PSET(A,M)
DIMENSION A(1)
DO 1 I=1,M
1 A(I)=0.DO
RETURN
END
SUBROUTINE LJMAT(LJ,NNODEL,NVAR,ICD,JX,IEL)
DIMENSION LJ(1),ICD(1),JX(1)
DO 72 J=1,NNODEL
J1=(J-1)*NVAR
J2=NVAR*(ICD(J)-1)
DO 72 I=1,NVAR
72 LJ(I+J1)=JX(J2+I)
RETURN
END
* SUBROUTINE UMAT DEFINES THE NODAL DISPLACEMENTS
* FOR THE ELEMENT
SUBROUTINE UMAT(CC,LJ,U,NVEL)
DIMENSION CC(1),LJ(1),U(1)
DO 30 I=1,NVEL
IKK=LJ(I)
IF(IKK) 20,10,20
10 U(I)=0.DO
GO TO 30
20 U(I)=CC(IKK)
30 CONTINUE
RETURN
END
* SUBROUTINE STIFF PLACES THE BAR ELEMENT STIFFNESS
* INTO THE STIFFNESS MATRIX FOR STEEL ELEMENTS
SUBROUTINE STIFF(S,ST,OR)
DIMENSION S(8,8)
CALL PRESET(S,8,8)
CO=COS(OR)*COS(OR)*ST
SI=SIN(OR)*SIN(OR)*ST
S(1,1)=CO
S(3,1)=-CO
S(1,2)=-CO
S(2,2)=SI
S(2,4)=-SI
S(4,2)=-SI
S(3,3)=CO
S(4,4)=SI
RETURN
END
SUBROUTINE XYGRID(X,Y,XL,XW,D,DP,NELW,NELL,IX,NVAR,NN,IS,IT,IB)

```

```

DIMENSION X(1),Y(1),IX(1)
CON=(D-DP)/(IB-IT)
NL=NELL+1
L=NELW+3
X1=0
DO 200 I=1,NL
M=(I-1)*L+1
N=M-1
DO 170 J=1,L
170 X(N+J)=X1
CONTINUE
X1=X1+XI
Y(M)=XW
Y(M+1)=XW-DP
Y(M+2)=Y(M+1)
N=M+3
K=NELW-3+N
IF(IT.EQ.0) N=N-1
DO 190 J=N,K
Y(J)=XW-DP-(J-N+1)*CON
IF(J.NE.K) GO TO 190
Y(J+1)=Y(J)
190 CONTINUE
Y(K+2)=Y(K)-(XW-D)
200 CONTINUE
DO 300 I=1,NN
I2=NVAR*I
I1=I2-NVAR+1
IX(I1)=1
IX(I2)=1
IF(I.GE.(NN-L+1)) IX(I1)=0
M2=I+NELW-IB
M3=I+NELW-IT+1
IF(MOD(M2,L).EQ.0) IX(I2)=0
IF(MOD(M3,L).EQ.0) IX(I2)=0
300 CONTINUE
I2=L*2*(IS+1)
IX(I2)=0
RETURN
END
SUBROUTINE ICOGR(NELL,NELW,IT,IB)
L=3
IB1=IB+1
IT1=IT+1
DO 100 I=1,NELL
DO 100 J=1,NELW
I1=I*(NELW+L)+J
IF(J.GT.IT1) I1=I1+1
IF(J.GT.IB1) I1=I1+1
I2=I1-NELW-L
I3=I2+1
IF(J.EQ.IT1) I3=I3+1
IF(J.EQ.IB1) I3=I3+1
JB=0
WRITE(1) I1, I2, I3, 1, JB
I2=I3
I3=I1+1
IF(J.EQ.IT1) I3=I3+1
IF(J.EQ.IB1) I3=I3+1
WRITE(1) I1, I2, I3, 1, 0

```

```

100 CONTINUE
N=2
I2=NELW+N
IF(IT.EQ.0) N=1
DO 200 J=1,N
DO 200 I=1,NELL
I1=I2
I2=I1+NELW+L
WRITE(1) I1, I2, 1, 0
I3=I2-1
I4=I1-1
WRITE(2) I1, I2, I3, I4, 1, 0
IF(I.EQ.NELL) I2=IT+2
200 CONTINUE
RETURN
END
SUBROUTINE SGEOM(M, N, ICD, NNS, XLEN, X, NE, JGR)
DIMENSION ICD(1), XLEN(1), X(1)
DO 14 II=M, N
JJ=II-NE
IF(JGR.EQ.0) READ(5, 45) (ICD(J), J=1, NNS)
IF(JGR.EQ.1) READ(1) (ICD(J), J=1, NNS)
WRITE(4) (ICD(J), J=1, NNS)
XLEN(JJ)=ABS(X(ICD(2))-X(ICD(1)))
14 CONTINUE
45 FORMAT(4I3, F20. 6)
RETURN
END
SUBROUTINE DLOAD(BL, FL, CS, SIG, AR, H, E1, E2, E3, NEL, IEL, IC, ILIN,
*Z, DESH, ICR, ANG, CR1)
DIMENSION BL(3, 1), FL(1), Z(3, 6), CS(1), SIG(800, 1), ICR(1), ANG(1)
IF(IC.EQ.0) GO TO 10
IF(ICR(IEL).EQ.0) GO TO 5
DO 4 II=1, 6
Z(1, II)=0. DO
Z(2, II)=CR1*BL(2, II)
4 Z(3, II)=0. DO
GO TO 10
5 XA=E1*E2
XB=E1*E3
DO 20 J=1, 6
Z(1, J)=E1*BL(1, J)+XA*BL(2, J)
Z(2, J)=E1*BL(2, J)+XA*BL(1, J)
20 Z(3, J)=XB*BL(3, J)
10 EE=AR*H
DO 1 I=1, 6
XX=0. DO
YY=0. DO
DO 2 J=1, 3
IF(ILIN.EQ.0) GO TO 30
YY=YY+BL(J, I)*SIG(IEL, J)
IF(IC.EQ.0) GO TO 2
30 XX=XX+Z(J, I)*CS(J)
2 CONTINUE
FL(I)=EE*(YY-XX)
IF(IC.EQ.0) GO TO 3
FL(I)=FL(I)+EE*DESH*(Z(1, I)+Z(2, I))
3 IF(ILIN.GT.0) GO TO 1
FL(I)=-FL(I)
1 CONTINUE

```

```

IF(ICR(IEL).EQ.0) GO TO 40
DO 50 J=1,5,2
A=FL(J)*COS(ANG(IEL))-FL(J+1)*SIN(ANG(IEL))
B=FL(J)*SIN(ANG(IEL))+FL(J+1)*COS(ANG(IEL))
FL(J)=A
50 FL(J+1)=B
40 RETURN
END
**
** SUBROUTINE CEPSIG CALCULATES AND PRINTS THE STRESSES
** AND STRAINS DUE TO ELASTIC AND TIME DEPENDENT
** EFFECTS FOR ALL ELEMENTS. CONCRETE ELEMENTS ARE
** CHECKED FOR FAILURE
*
* SUBROUTINE CEPSIG(BL,CS,SIG,EPS,DD,V,Z,EGSIG,ANU,E,E1,E2,
* E3,CSR,NEL,LJ,AT,BT,ILIN,IC,IPR,DELT,DESH,COR,NVEL,ICR,ANG,
* CR1,KR,RATIO,CHECK,STR,AIN,JNEL,XLEN,ES,FT,CC,IBF,KNEL,LNEL)
DIMENSION BL(3,1),CS(1),SIG(800,1),EPS(800,1),DD(1),
1 V(1),Z(3,1),DSIG(4),DEPS(3),DSIGC(4),LJ(1),AT(1),BT(1),
2 ANU,DE(800,3),DEPSH(3),ICR(1),ANG(1),STR(800,1),AIN(800,1),DS(800,3)
3 ,DE(800,3),XLEN(1),CC(1),IBF(2,1)
SIGMX=0. DO
URELM=0. DO
UREL1=0. DO
IF(KR.EQ.1.AND.RATIO.LT.CHECK) KR=2
IF(KR.EQ.1.AND.IC.GT.0) KR=2
COR=0. DO
DO 4 IEL=1,NEL
READ(1) (CS(I),I=1,3),CSR,E1,E2,E3,EGSIG,CR1
IF(ILIN.GT.0) READ(1) ((BL(I,J),J=1,6),I=1,3)
READ(2) (AT(I),I=1,3),(BT(I),I=1,3)
READ(3) (LJ(I),I=1,6)
IF(ILIN.EQ.0) READ(2) ((BL(I,J),J=1,6),I=1,3)
21 CALL UMAT(DD,LJ,V,NVEL)
IF(ICR(IEL).EQ.0) GO TO 50
DO 49 I=1,NVEL,2
V1=V(I)*COS(ANG(IEL))+V(I+1)*SIN(ANG(IEL))
V2=V(I+1)*COS(ANG(IEL))-V(I)*SIN(ANG(IEL))
V(I)=V1
49 V(I+1)=V2
DO 41 J=1,6
Z(1,J)=0. DO
Z(2,J)=CR1*BL(2,J)
41 Z(3,J)=0. DO
GO TO 51
50 XA=E1*E2
XB=E1*E3
DO 1 J=1,6
Z(1,J)=E1*BL(1,J)+XA*BL(2,J)
Z(2,J)=E1*BL(2,J)+XA*BL(1,J)
1 Z(3,J)=XB*BL(3,J)
51 DO 6 I=1,3
ZZ=0. DO
XX=0. DO
DO 7 J=1,6
ZZ=ZZ+BL(I,J)*V(J)
7 XX=XX+Z(I,J)*V(J)
DSIG(I)=XX
SIG(IEL,I)=SIG(IEL,I)+DSIG(I)
DEPS(I)=ZZ
6 EPS(IEL,I)=EPS(IEL,I)+DEPS(I)
IF(IC.EQ.0) GO TO 24

```

```

XA=E1*E2
DSIGC(1)=E1*CS(1)+XA*CS(2)
DSIGC(2)=E1*CS(2)+XA*CS(1)
DSIGC(3)=E1*CS(3)*E3
DSIGSH(1)=(E1+XA)*DESH
DSIGSH(2)=DSIGSH(1)
DSIGSH(3)=0.0
DO 26 J=1,3
DSIG(J)=DSIG(J)-DSIGC(J)+DSIGSH(J)
26 SIG(IEL,J)=SIG(IEL,J)-DSIGC(J)+DSIGSH(J)
24 IF(RATIO.GT.CHECK.AND.IC.EQ.0) GO TO 22
DO 42 I=1,3
DS(IEL,I)=SIG(IEL,I)-STR(IEL,I)
DE(IEL,I)=EPS(IEL,I)-AIN(IEL,I)
42 CONTINUE
IF(ICR(IEL).EQ.1) GO TO 32
SIGM=.5DO*(SIG(IEL,1)+SIG(IEL,2))+SQRT(.5*(SIG(IEL,1)
-SIG(IEL,2))**2+SIG(IEL,3)**2)
IF(SIGM.LT.SIGMX) GO TO 22
SIGMX=SIGM
IANG=IEL
GO TO 22
32 CO=COS(2*ANG(IEL))
SI=SIN(2*ANG(IEL))
SYY=SIG(IEL,2)
DSY=DS(IEL,2)
SIG(IEL,1)=.5DO*SYY-.5DO*SYY*CO
SIG(IEL,2)=.5DO*SYY+.5DO*SYY*CO
SIG(IEL,3)=-.5DO*SYY*SI
DS(IEL,1)=.5DO*DSY-.5DO*DSY*CO
DS(IEL,2)=.5DO*DSY+.5DO*DSY*CO
DS(IEL,3)=-.5DO*DSY*SI
EPX=EPS(IEL,1)
EPY=EPS(IEL,2)
EPXY=EPS(IEL,3)
EDX=DE(IEL,1)
EDY=DE(IEL,2)
EDXY=DE(IEL,3)
EPS(IEL,1)=.5DO*(EPX+EPY)+.5DO*(EPX-EPY)*CO-.5DO*EPXY*SI
EPS(IEL,2)=.5DO*(EPX+EPY)-.5DO*(EPX-EPY)*CO+.5DO*EPXY*SI
EPS(IEL,3)=(EPX-EPY)*SI+EPXY*CO
DE(IEL,1)=.5DO*(EDX+EDY)+.5DO*(EDX-EDY)*CO-.5DO*EDXY*SI
DE(IEL,2)=.5DO*(EDX+EDY)-.5DO*(EDX-EDY)*CO+.5DO*EDXY*SI
DE(IEL,3)=(EDX-EDY)*SI+EDXY*CO
22 IF(IPR.EQ.0) GO TO 4
IF(IEL.EQ.1) WRITE(6,12)
4 CONTINUE
KKK=NEL+1
DO 60 IEL=KKK,JNEL
READ(3) (LJ(J),J=1,4)
CALL UMAT(DD,LJ,V,4)
UREL=V(3)-V(1)
DEPS(1)=UREL/XLEN(IEL-NEL)
DSIG(1)=ES*DEPS(1)
SIG(IEL,1)=SIG(IEL,1)+DSIG(1)
EPS(IEL,1)=EPS(IEL,1)+DEPS(1)
DS(IEL,1)=SIG(IEL,1)-STR(IEL,1)
DE(IEL,1)=EPS(IEL,1)-AIN(IEL,1)
60 CONTINUE
IF(RATIO.GT.CHECK.AND.IC.EQ.0) GO TO 27

```

```

IF(SIGMX.LT.FT) GO TO 28
ICR(IANG)=1
ANG(IANG)=.5DO*ATAN(2*SIG(IANG,3)/(SIG(IANG,1)-SIG(IANG,2)))
AN=2*ANG(IANG)
SX=.5*(SIG(IANG,1)+SIG(IANG,2))+.5*(SIG(IANG,1)-SIG(IANG,2))
$*CDS(AN)+SIG(IANG,3)*SIN(AN)
IF(SIGMX.GT.(SX-.1).AND.SIGMX.LT.(SX+.1)) GO TO 70
ANG(IANG)=ANG(IANG)-ASIN(1.0)
70 AII=90.0*ANG(IANG)/ASIN(1.0)+90.0
WRITE(6,38) IANG,AII
DSIGM=.5DO*(DS(IANG,1)+DS(IANG,2))+SQRT(.5*(DS(IANG,1)-
$DS(IANG,2))**2+DS(IANG,3)**2)
COR=(SIGMX-FT)/DSIGM
IF(COR.GT.1.0) COR=1.0
IF(KR.EQ.2) COR=0.
KR=1
IPR=0
GO TO 27
28 KKK=JNEL+1
DO 33 IEL=KKK,LNEL
READ(3) (LJ(J),J=1,8)
CALL UMAT(CC,LJ,V,8)
IF(IEL.NE.KKK.AND.IEL.NE.(KNEL+1)) GO TO 29
IF(IBF(1,1).EQ.1) GO TO 29
UREL=ABS(V(7)-V(1))
IF(UREL.GT..0012) UREL1=UREL
29 IF(IBF(2,IEL-JNEL).EQ.1) GO TO 33
UREL=ABS(V(5)-V(3))
IF(UREL.LT.URELM) GO TO 33
URELM=UREL
MAX=IEL-JNEL
33 CONTINUE
IF(UREL1.LE.URELM) GO TO 34
IBF(1,1)=1
KR=1
IPR=0
GO TO 27
34 IF(URELM.LE..0012) GO TO 27
IBF(1,MAX+1)=1
IBF(2,MAX)=1
KR=1
IPR=0
PRINT*, ' FAILURE IN ELEMENT ', MAX
27 IF(RATIO.GT.CHECK.AND.IC.EQ.0) GO TO 25
DO 100 IEL=1,JNEL
MM=3
IF(IEL.GT.NEL) MM=1
IF(KR.NE.1) GO TO 201
DO 200 I=1,MM
SIG(IEL,I)=STR(IEL,I)
EPS(IEL,I)=AIN(IEL,I)
200 CONTINUE
201 IF(IPR.EQ.0) GO TO 100
WRITE(6,13) IEL,(SIG(IEL,J),J=1,MM)
WRITE(6,14) (EPS(IEL,J),J=1,MM)
100 CONTINUE
38 FORMAT(/, ' ELEMENT ', I4, ' IS CRACKED AT AN ANGLE ', F10.4)
12 FORMAT(/, 2X, 'ELEM. ', 7X, 'TXX', 9X, 'TYX', 9X, 'TXY', 9X, 'DTS', 9X, 'DXX',
19X, 'DYY', 9X, 'DXY', 9X, 'DES', 6X, 'EGSTRESS', 4X, 'EGSTRAIN', /, 14X, 'EXX',
2, 9X, 'EYY', 9X, 'EXY', 8X, 'CEXX', 8X, 'CEYY', 8X, 'CEXY', 7X, 'DCEXX', 7X, 'DC

```

```

3EYV',7X,'DCEXY',//)
13 FORMAT(2X,I5,10E12.3)
14 FORMAT(7X,9E12.3)
25 RETURN
END
*
SUBROUTINE LAYOUT SETS OUT THE GEOMETRY OF THE PROBLEM
AND NUMBERS THE DEGREES OF FREEDOM
SUBROUTINE LAYOUT(X,Y,ICD,IX,JX,AREA,NE,NN,NVAR,NMAT,NDEG,NNODEL,
* NNSL,XLEN,NNSP,INEL,JNEL,KNEL,LNEL,JGR,COVER)
DIMENSION X(1),Y(1),ICD(1),IX(1),JX(1),AREA(1),XLEN(1)
NNN=NNODEL+2
NNS=NNSL+2
NNSP=NNSP+2
IF(JGR.EQ.1) READ(5,49) NELL,NELW,IT,IB,IS,XL,XW,D,DP
IF(JGR.EQ.1) CALL XYGRID(X,Y,XL,XW,D,DP,NELW,NELL,
* IX,NVAR,NN,IS,IT,IB)
DO 10 I=1,NN
I2=NVAR*I
I1=I2-NVAR+1
IF(JGR.EQ.0) READ(5,43) X(I),Y(I),(IX(J),J=I1,I2)
10 CONTINUE
IF(JGR.EQ.0) READ(5,43) XW,D
COVER=XW-D
IF(JGR.EQ.1) CALL ICOGR(NELL,NELW,IT,IB)
REWIND 1
REWIND 2
DO 11 I=1,NE
IF(JGR.EQ.0) READ(5,45) (ICD(J),J=1,NNN)
IF(JGR.EQ.1) READ(1) (ICD(J),J=1,NNN)
WRITE(4) (ICD(J),J=1,NNN)
N1=ICD(1)
N2=ICD(2)
N3=ICD(3)
X1=X(N1)
X2=X(N2)
X3=X(N3)
Y1=Y(N1)
Y2=Y(N2)
Y3=Y(N3)
AREA(I)=(X1*Y2+X2*Y3+X3*Y1-Y1*X2-Y2*X3-Y3*X1)/2. DO
11 CONTINUE
III=NE+1
JJJ=INEL+1
CALL SGEOM(III,INEL,ICD,NNS,XLEN,X,NE,JGR)
IF(INEL.NE.JNEL) CALL SGEOM(JJJ,JNEL,ICD,NNS,XLEN,X,NE,JGR)
KKK=JNEL+1
DO 15 JJ=KKK,LNEL
IF(JGR.EQ.0) READ(5,45) (ICD(J),J=1,NNP)
IF(JGR.EQ.1) READ(2) (ICD(J),J=1,NNP)
WRITE(4) (ICD(J),J=1,NNP)
15 CONTINUE
NMAT=NVAR*NN
NDEG=0
DO 12 I=1,NMAT
IF(IX(I)) 1,2,3
3 IF(IX(I)-1) 80,80,81
81 NDEG=NDEG+IX(I)
GO TO 82
80 NDEG=NDEG+1
82 JX(I)=NDEG

```

```

      GO TO 12
1   NDEG=NDEG+IX(I)+1
      JX(I)=NDEG
      GO TO 12
2   JX(I)=0
12  CONTINUE
43  FORMAT(2F10.0,6I3)
45  FORMAT(16I3)
49  FORMAT(5I5,4F10.0)
      RETURN
      END
*   SUBROUTINE BONDEL CALCULATES THE STIFFNESS MATRIX
*   AND LOAD VECTOR FOR THE GOODMAN JOINT ELEMENT
      SUBROUTINE BONDEL(S,U,XLEN,DIA,NBAR,IEL,FL,ILIN,JC,IBF,CF)
      DIMENSION S(8,8),U(1),XLEN(1),R(3),Q(3),FL(1),IBF(2,1)
      DATA R(1),R(2),R(3)/-.774597,0.,.774597/
      Q(1)=.555556
      Q(2)=.888889
      Q(3)=.555556
      S11=0.
      S31=0.
      S33=0.
      T1=0.
      T2=0.
      IF(IEL.EQ.1) Q(1)=1E10
      PD=ASIN(1.0)*DIA*NBAR*XLEN(IEL)*CF
      U1=U(7)-U(1)
      U2=U(5)-U(3)
      CALL PRESET(S,8,8)
      DO 10 I=1,3
      B1=.5*(1-R(I))
      B2=.5*(R(I)+1)
      VREL=B1*U1+B2*U2
      UREL=ABS(VREL)
      IF(UREL.GT..0012) VREL=VREL/UREL*.0012
      IF(UREL.GT..0012) UREL=.0012
      SK=PD*(1.95E6-4.7E9*UREL+4.19E12*UREL*UREL-1.32E15*(UREL)**3)
      S11=S11+Q(I)*B1*B1*SK
      S31=S31+Q(I)*B1*B2*SK
      S33=S33+Q(I)*B2*B2*SK
      IF(ILIN.EQ.0) GO TO 10
      IF(ILIN.GT.0.AND.JC.EQ.-1) GO TO 10
      IF(VREL.EQ.0) GO TO 10
      TS=VREL/UREL*(1.95E6*UREL-2.35E9*UREL**2+1.39E12*UREL**3-
      $.33E15*UREL**4)
      T1=T1+Q(I)*B1*TS
      T2=T2+Q(I)*B2*TS
10  CONTINUE
      S(1,1)=S11
      S(3,1)=S31
      S(3,1)=-S31
      S(7,1)=-S11
      S(3,3)=S33
      S(5,3)=-S33
      S(7,3)=-S33
      S(5,5)=S33
      S(7,5)=S31
      S(7,7)=S11
      IF(ILIN.EQ.0) GO TO 15
      IF(ILIN.GT.0.AND.JC.EQ.-1) GO TO 15

```

```

FL(7)=T1*PD
FL(5)=T2*PD
FL(3)=-FL(5)
FL(1)=-FL(7)
15 DO 20 I=1,7,2
DO 20 J=I,7,2
S(I,J)=S(J,I)
20 CONTINUE
30 RETURN
END
FUNCTION ESHR(TIME, TCREEP, TDRY, DELT, SHCDEF, TSH)
TIM=TIME-DELT
AA=226+TIM**1.336
ONE=.1286*DELT*TIM**(.336)/(AA**2)
BB=(226+TIM**1.336)*.336*TIM**(-.664)
TWO=.1286*.5*DELT*DELT*(BB-2.672*TIM**(.672))/(AA**3)
ESHR=ONE+TWO
RETURN
END
* SUBROUTINE CSRATE CALCULATES THE CREEP STRAIN RATE
* INCREMENTS. BAZANT AND PANULA'S EQUATION FORM IS
* USED
SUBROUTINE CSRATE(EQSIG, BCDEF, DCOEF, POWER, AN, TSH, CSR, DT, DCSR)
TWO=32.93+DT**(.9144)
CSR=3.39E-5*DT**(-.0856)/(TWO**2)*EQSIG
ONE=(32.93+DT**(.9144))*(-.0856)*DT**(-1.0856)
DCSR=3.39E-5*(ONE-1.8288*DT**(-.1712))/(TWO**3)*EQSIG
RETURN
END
* SUBROUTINE EXPAND PRINTS THE NODAL DISPLACEMENTS
SUBROUTINE EXPAND(AMODE, NAM, VV, JX, NDS, NVAR)
DIMENSION VV(1), AMODE(1), JX(1), DD(1)
DO 5 I=1, NAM
AMODE(I)=0.0
IF(JX(I).EQ.0) GO TO 5
AMODE(I)=VV(JX(I))
5 CONTINUE
WRITE(6,40)
DO 10 I=1, NDS
I2=NVAR*I
I1=I2-NVAR+1
WRITE(6,41) I, (AMODE(J), J=I1, I2)
10 CONTINUE
40 FORMAT(///, 5X, 'NODE', 9X, 'U-DISPL. ', 9X, 'V-DISPL. ', /)
41 FORMAT(I7, 8X, E12.6, 5X, E12.6)
RETURN
END
* SUBROUTINE SETUP PLACES THE ELEMENT STIFFNESS MATRIX
* AND LOAD VECTOR INTO THE GLOBAL STIFFNESS MATRIX
* AND LOAD VECTOR
SUBROUTINE SETUP(A, B, S, FL, NVEL, LJ, NVAR, LBAND)
DIMENSION A(1), B(1), S(8,8), FL(1), LJ(1)
DO 12 I=1, NVEL
LJR=LJ(I)
IF(LJR.EQ.0) GO TO 12
B(LJR)=B(LJR)+FL(I)
DO 11 J=I, NVEL
LJC=LJ(J)
IF(LJC.EQ.0) GO TO 11
IF(LJR-LJC) 9, 10, 10

```

```

10 K=(LJC-1)*LBAND+LJR
GO TO 13
9 K=(LJR-1)*LBAND+LJC
13 A(K)=A(K)+S(I, J)
11 CONTINUE
12 CONTINUE
RETURN
END
* SUBROUTINE BANDWH CALCULATES THE HALF BANDWIDTH
SUBROUTINE BANDWH(ICO, JX, LJ, NE, NVAR, LBAND, NNOD)
DIMENSION ICO(1), JX(1), LJ(1)
LBAND=0
NV2=2*NVAR
DO 3 I=1, NE
READ(4) (ICO(M), M=1, NNOD)
DO 4 J=1, NVAR
DO 4 K=1, NNOD
K1=(K-1)*NVAR
LJ(J+K1)=JX(NVAR*ICO(K)-NVAR+J)
4 CONTINUE
MAX=0
MIN=2000.
NV3=NVAR*NNOD
DO 8 J=1, NV3
IF(LJ(J).EQ.0) GO TO 8
IF(LJ(J)-MAX) 6, 6, 5
5 MAX=LJ(J)
6 IF(LJ(J)-MIN) 7, 8, 8
7 MIN=LJ(J)
8 CONTINUE
NB1=MAX-MIN
IF(NB1.GT.LBAND) LBAND=NB1
3 CONTINUE
RETURN
END
* SUBROUTINE PLACEZ TAKES CARE OF THE CONSTRAINED
* BOUNDARY CONDITIONS
SUBROUTINE PLACEZ(PP, C, CON, ICON, NCON, NN, LBAND)
DIMENSION C(1), CON(1), PP(1), ICON(1)
DO 18 I=1, NCON
I1=ICON(I)
I2=LBAND*(I1-1)+I1
LC1=I1-LBAND
IF(LC1.LE.0) LC1=1
LC2=I1+LBAND
IF(LC2.GT.NN) LC2=NN
DO 17 J=LC1, LC2
IF(I1-J) 9, 10, 10
10 IJ=LBAND*(J-1)+I1
GO TO 16
9 IJ=LBAND*(I1-1)+J
16 PP(J)=PP(J)-C(IJ)*CON(I)
17 C(IJ)=0. DO
18 CONTINUE
DO 25 I=1, NCON
I1=ICON(I)
I2=LBAND*(I1-1)+I1
C(I2)=1. EOB
PP(I1)=1. EOB*CON(I)
25 CONTINUE

```

```

RETURN
END
* SUBROUTINE BAND SOLVES THE SIMULTANEOUS LINEAR
* EQUATIONS AND CALCULATES THE NODAL DISPLACEMENTS
SUBROUTINE BAND(A, B, N, M, LT, DET)
DIMENSION A(1), B(1)
MM=M-1
NM=N*M
NM1=NM-MM
IF (LT.NE.1) GO TO 55
MP=M+1
KK=2
FAC=DET
A(1)=1./SQRT(A(1))
BIGL=A(1)
SML=A(1)
A(2)=A(2)*A(1)
A(MP)=1./SQRT(A(MP)-A(2)*A(2))
IF(A(MP).GT.BIGL)BIGL=A(MP)
IF(A(MP).LT.SML)SML=A(MP)
MP=MP+M
DO 62 J=MP, NM1, M
JP=J-MM
MZC=0
IF(KK.GE.M) GO TO 1
KK=KK+1
II=1
JC=1
1 KK=KK+M
II=KK-MM
JC=KK-MM
2 DO 65 I=KK, JP, MM
IF(A(I).EQ.0.)GO TO 64
GO TO 66
64 JC=JC+M
65 MZC=MZC+1
ASUM1=0.
GO TO 61
66 MMZC=MM*MZC
II=II+MZC
KM=KK+MMZC
A(KM)=A(KM)*A(JC)
IF(KM.GE.JP)GO TO 6
KJ=KM+MM
DO 5 I=KJ, JP, MM
ASUM2=0.
IM=I-MM
II=II+1
KI=II+MMZC
DO 7 K=KM, IM, MM
ASUM2=ASUM2+A(KI)*A(K)
7 KI=KI+MM
5 A(I)=(A(I)-ASUM2)*A(KI)
6 CONTINUE
ASUM1=0.
DO 4 K=KM, JP, MM
4 ASUM1=ASUM1+A(K)*A(K)
61 S=A(J)-ASUM1
IF(S.LT.0.)DET=S

```



```

GRAV=-AR*H*GR/3. DO
FL(2)=GRAV
FL(4)=GRAV
FL(6)=GRAV
11 IF (IB.EQ.0) GO TO 1000
XL=SQRT(((X(2)-X(1))*2)+((Y(2)-Y(1))*2))
XL=XL*H
READ(5,5) PX(1),PY(1),PX(2),PY(2),PX(3),PY(3)
IF (IB.EQ.2) GO TO 12
FL(1)=FL(1)+XL*(2. DO*PX(2)+PX(1))/6. DO
FL(2)=FL(2)+XL*(2. DO*PY(2)+PY(1))/6. DO
FL(3)=FL(3)+XL*(3. DO*PX(3)+PX(3))/6. DO
FL(4)=FL(4)+XL*(2. DO*PY(2)+PY(3))/6. DO
GO TO 1000
12 CONTINUE
5 FORMAT(6F10.0)
1000 RETURN
END
* SUBROUTINE BLMAT SETS THE KINEMATIC LARGE DISPLACEMENT
* MATRIX
SUBROUTINE BLMAT(BL,A,B,U,AL,BE,GA,DE,ILIN,JC)
DIMENSION BL(3,1),A(1),B(1),U(1)
IF (ILIN.EQ.0) GO TO 1
AL=B(1)*U(1)+B(2)*U(3)+B(3)*U(5)
BE=B(1)*U(2)+B(2)*U(4)+B(3)*U(6)
GA=A(1)*U(1)+A(2)*U(3)+A(3)*U(5)
DE=A(1)*U(2)+A(2)*U(4)+A(3)*U(6)
IF (JC) 1,2,1
2 AL=AL/2. DO
BE=BE/2. DO
GA=GA/2. DO
DE=DE/2. DO
1 BL(1,1)=AL*B(1)+B(1)
BL(1,2)=BE*B(1)
BL(1,3)=AL*B(2)+B(2)
BL(1,4)=BE*B(2)
BL(1,5)=AL*B(3)+B(3)
BL(1,6)=BE*B(3)
BL(2,1)=GA*A(1)
BL(2,2)=DE*A(1)+A(1)
BL(2,3)=GA*A(2)
BL(2,4)=DE*A(2)+A(2)
BL(2,5)=GA*A(3)
BL(2,6)=DE*A(3)+A(3)
BL(3,1)=GA*B(1)+AL*A(1)+A(1)
BL(3,3)=GA*B(2)+AL*A(2)+A(2)
BL(3,5)=GA*B(3)+AL*A(3)+A(3)
BL(3,2)=DE*B(1)+BE*A(1)+B(1)
BL(3,4)=DE*B(2)+BE*A(2)+B(2)
BL(3,6)=DE*B(3)+BE*A(3)+B(3)
RETURN
END
* SUBROUTINE CONST CALCULATES THE CONSTANTS FOR
* USE WITH BAZANT AND PANULA'S CREEP AND SHRINKAGE
* PREDICTION METHOD
SUBROUTINE CONST(BCOEF,DCOEF,POWER,AN,TSH,TCREEP,E,SHCOEF,TDRY
*,FC1,DENS)
READ*,FC,DENS,AC,AG,SC,WC,C,VS,RH,TDRY,TCREEP
SA=SC/AC
GS=AC/(SC*AG)

```

```

Z1=.00005*DENS*DENS*FC
Z2=1.7*Z1*Z1
EO=Z2/(Z2*.09+1.0)*1.0E6
X=2.1*AC/(SC**1.4)+.1*(FC**1.5)*(WC**333)*(AG**2.2)-4
IF(X.GT.4.0) AN=.12+.07*X**6/(5130+X**6)
IF(X.LE.4.0) AN=.12
AM=.2B+1/(FC*FC)
ALPHA=.025/WC
AN3=10**(-3*AN)
PHI1=.5/(AN3*(2B**(-AM)+ALPHA))
Z=(1.25*SQRT(AC)+.5*GS*GS)*((1+SC)/WC)**.333*SQRT(FC)-12
IF(Z.LT.0.0) ESU=330
IF(Z.GT.0.0) ESU=1210-880/(390*Z**(-4)+1)
C7=.125*WC*C-12
C1=C7*(.05+SQRT(6.3/TDRY))
TSH=1.6667*VS*VS/C1
E607=1+AN3*PHI1*(607**(-AM)+ALPHA)
ETSH=1+AN3*PHI1*(TDRY+TSH)**(-AM)+ALPHA)
ESHU=ESU*ETSH/E607
RHSH=1-RH**3
R=56000*(SA*FC)**.3*(GS**1.3)*(WC/ESU)**1.5-.85
IF(R.GT.0.0) PHID=.008+.027/(1+.7*R**(-1.4))
IF(R.LE.0.0) PHID=.008
PHID=PHID/SQRT(1+(TCREEP-TDRY)/(10*TSH))
CD=2.8-7.5*AN
RHCR=.98**1.5-RH**1.5
BCOEF=PHI1*AN*(TCREEP**(-AM)+ALPHA)/EO
DCOEF=10*PHID*TCREEP**(-AM/2.)*RHCR*ESHU*CD*AN*TSH/EO
SHCOEF=ESHU*RHSH*1.0E-6
POWER=CD*AN
FC1=1000.*FC
RETURN
END

```

```

* SUBROUTINE NONLINC CALCULATES THE ELEMENT STIFFNESS
* MATRIX FOR CRACKED CONCRETE ELEMENTS
SUBROUTINE NONLINC(S, SIG, A, CR1, AR, H, IS, IEL, ILIN, BL, ANG, NEL)
DIMENSION S(8, 8), SIG(800, 1), A(3), BL(3, 1), ANG(1), T(6, 6)
IF(IS.EQ.0) GO TO 100
EE=H*AR
DO 2 J=1, 6
DO 2 I=J, 6
T(I, J)=CR1*BL(2, J)*BL(2, I)
T(J, I)=T(I, J)
2 CONTINUE
IF(ILIN.EQ.0) GO TO 6
DO 3 I=1, 5, 2
DO 3 J=I, 5, 2
II=.5DO*(I+1)
JJ=.5DO*(J+1)
AK=A(II)*A(JJ)*SIG(IEL, 2)/(4.DO*AR)
T(J, I)=T(J, I)+AK
T(J+1, I+1)=T(J+1, I+1)+AK
T(I, J)=T(J, I)
T(I+1, J+1)=T(J+1, I+1)
3 CONTINUE
6 CO=COS(2*ANG(IEL))
SI=SIN(2*ANG(IEL))
DO 5 J=1, 5, 2
DO 5 I=J, 5, 2
S(I, J)=(.5DO*(T(I, J)+T(I+1, J+1))+.5DO*(T(I, J)-T(I+1, J+1))*CD

```